INTERNATIONAL THERMAL ENERGY AND ENVIRONMENT CONGRESS

PROCEEDINGS ITEEC 97

Volume 2

ITEEC 97
9 -12 June 1997, Marrakesh, Morocco

Edited by A. Mir, Z. Zrikem

The Organizing Committee of the International Thermal Energy and Environment Congress ITEEC 97 shall not be responsible for statements or opinions advanced in papers presented during the congress or in these Proceedings.

These proceedings can be obtained by sending 150 US$ to ITEEC.

ITEEC97
Ecole Superieure de Technologie
B.P. 33/S, Agadir, Maroc

Dépot legal 473 / 1997
ISBN 9981 - 143 - 00 - 6 (Two volumes)
9981 - 143 - 02 - 2 (Volume 2)

PREFACE

These are the proceedings of the International Thermal Energy and Environment Congress ITEEC97 held in Marrakech, Morocco from 9 to 12 June 1997.

This congress is intended to provide a platform for a North-South dialogue in the important field of thermal energy and environment by bringing together academics and scientists from northern and southern countries to exchange new ideas, experiences and research results. The congress covers the current status of thermal energy and environment, in particular heat and mass transfer in fluid and porous media, energy systems, buildings, renewable energies and environmental impact.

Four symposia are organized in conjunction with the technical sessions. These symposia focus on the followings themes : natural convection, building-energy and indoor environment, new energy technologies and environment.

World-renowned experts in thermal energy and environment are invited to open the technical sessions and symposia with keynotes in plenary sessions. These are followed by research papers presented in oral and poster sessions.

These two volumes bring together, keynotes papers and papers presented in the technical sessions and symposia. We hope that they serve as a useful reference material to all participants and to those who are not able to attend the congress.

A. Mir and Z. Zrikem
Chairmen

ORGANIZING COMMITEE OF THE
INTERNATIONAL THERMAL ENERGY AND ENVIRONMENT CONGRESS

Conference Chairmen

Prof. A. Mir : Director, Ecole Supérieure de Technologie d'Agadir, Morocco
Prof. Z. Zrikem : Faculty of Sciences Semlalia, Marrakech, Morocco

Symposia Chairmen

Prof. J.K. Platten : Université de Mons (Belgium)
Symposium on **Natural Convection**
Prof. Haghighat : Concordia University, Montreal (Canada**).**
Symposium on **Building - Energy and Indoor Environment**
Prof. V. Naso : University la Spienza, Roma (Italy),
Symposium on **New Energy Technologies**
Dr. M. Mansoor : Research Center for Environment, Munich (Germany)
Symposium on **Environment**

Program Chairman

Prof. Z. Zrikem : Faculty of Sciences Semlalia, Marrakech, Morocco

Congress Arrangements Chairman

Prof. A. Bennouna : Faculty of Sciences Semlalia, Marrakech, Morocco

This conference is hosted by :

University Cadi Ayyad,
Faculty of Sciences Semlalia, Marrakech, Morocco

GENERAL CONTENTS OF THE PROCEEDINGS

Volume 1

Volume 2

TABLE OF CONTENTS

Volume 1

Volume 2

ACKNOWLEDGEMENTS

The ITEEC97 Organizing Committee gratefully acknowledges the assistance and co-operation of University Ibnou Zohr, Agadir, University of Cadi Ayyad, Marrakech, Ecole Supérieure de Technologie, Agadir and Faculty of Sciences, Marrakech.

The Chairmen of the Symposia have worked hard to provide us with the best possible programs. We wish to thank them for their co-operation and patience

We also wish to express our depth of gratitude to the Chairmen and Co-chairmen of the technical sessions, who guarantee the technical quality of this congress.

We must not forget the authors, without whom none of this would be possible, we would like to express to them our deepest appreciation.

The ITEEC97 Organizing Committee wishes to thank the following companies and organizations for their contributions :

Société d'Equipement et de Diffusion Electronique (SEDEL), Casablanca, Morocco

ISES-Italy, co-organizer of the symposium on New Energy Technologies

The organizing committe

SYMPOSIUM ON BUILDING ENERGY AND INDOOR ENVIRONMENT

THERMAL COMFORT, INDOOR AIR QUALITY AND ENERGY CONSUMPTION STUDIES IN 12 OFFICE BUILDINGS

Fariborz Haghighat and Giovanna Donnini*

Centre for Building Studies, Concordia University, Montreal, Canada
***ADN Inc. Montreal, Canada**

STRACT:

The indoor air quality and thermal comfort were investigated in twelve mechanically ventilated dings. Measured parameters concerning the quality of indoor air included ventilation rate, centration of TVOC, CO_2, CO, RH, and formaldehyde. The thermal comfort parameters included m air, mean radiant, plane radiant asymmetry, and dew point temperatures, as well as air velocity turbulence intensity, etc. Monthly energy consumption data was also gathered for each building.

Ventilation performance, in terms of air flow rate and indoor air quality, was compared with Standard. The measured and calculated thermal environment results were also compared with the ndard and the Guideline.

INTRODUCTION

The quality of indoor air has become a major concern ever since efforts to reduce ventilation s in buildings started. It has long been recognized that the quality of indoor air should not be proved at the expense of higher energy consumption. However, good indoor air quality and rgy conservation practices can be compatible. To achieve a good indoor environment at minimum t, it is necessary to determine where IAQ, ventilation, and energy conservation are naturally in mpetition and where they can work together.

The ANSI/ASHRAE Standard 55-92 "Thermal environmental conditions for human occupancy" SHRAE, 1992) is used extensively in Canada, as a reference for comfort levels. As more and re studies of Canadian buildings in the cold climate are emerging, it is apparent that the measured ameters satisfy the comfort limits as set out by ASHRAE, yet it is found that less than 80% of occupants are satisfied (Haghighat et al. 1992). ANSI/ASHRAE Standard 55-92 is based almost rely on data from climate chamber studies performed in temperate climates. This perhaps lains the discrepancies between occupant satisfaction in a cold climate and satisfaction of workers temperate climate.

OUTDOOR WEATHER CONDITIONS AND BUILDING CHARACTERISTICS

Measurements were carried out at several workstations of 12 mechanically ventilated buildings. measurements were performed during normal occupancy. The investigated buildings vary greatly surface area (3000 to 68 000 m^2), in number of floors (2 to 25 storeys), in date of construction 45 to 1992), in type of HVAC system (free cooling CAV, double duct VAV), and in type of ant (police station, court house, private company).

The measurements included physical and chemical monitoring, and assessment of the percei indoor air quality, thermal comfort, etc. The chemical measurements included concentration TVOC, formaldehyde, CO_2, and CO. The physical measurements consisted in operative temperatu air temperature, relative humidity, air velocity and ventilation rate. The monthly energy consumpt of the building and the daily weather conditions were also recorded.

The mobile system collected concurrent physical data: air temperature, dew-point temperatu vapour pressure, globe temperature, radiant asymmetry, air velocity, turbulence, temperature of supply, air return, and room, illuminance, carbon monoxide, carbon dioxide, formaldehyde, vola organic compounds, and tracer gas decay. The transducers and measurement points were placed represent the immediate environment of the seated subjects.

3. RESULTS AND CONCLUSION

3.1 VENTILATION PERFORMANCE

Outdoor fresh air is needed to maintain acceptable indoor air quality. The outdoor fresh flow rate was measured using the decay tracer gas technique. The ventilation rate fell withi l/s/person, in building #5, and 93 l/s/person in building #4. Results also indicates that the ventilat rate in the majority of the buildings is much higher than the minimum 10 l/s/person recommen by the ASHRAE Standard 62-1989R.

3.2 INDOOR AIR CONTAMINANTS

The concentration of the following contaminants was measured during the heating and cool seasons: CO_2, formaldehyde, TVOC, and CO. The level of CO_2 concentration was lower than maximum permitted in the ASHRAE Standard, and was mainly between 450 and 650 ppm, in b seasons. In the investigated buildings, the CO_2 concentration was not a function of the ventilat rate; it is assumed that almost all the buildings were ventilated much higher than the ASHR Standard recommended.

The formaldehyde concentration in these buildings varied between 74 ug/m^3 in a large majo of buildings and 2190 ug/m^3 in one building (during both cooling and heating seasons). concentration levels were significantly different during the heating and cooling seasons. relationship was found between the ventilation rate and formaldehyde concentration during cooling season. A relationship between these parameters was observed during the heating seas the HCHO concentration decreased as the ventilation rate increased.

The TVOC concentration level deviated between 36 ug/m^3 in building #6 in summer to 2 ug/m^3 in the same building in winter, respectively. In some buildings, the variation of TVOC f one workstation to another was more than 100%. In general, no correlation was found between ventilation rate and TVOC concentration.

The CO concentration level was almost the same as the outdoor CO concentration within workstations and in all buildings.

THERMAL COMFORT

Detailed measurements of thermal comfort parameters were carried out at the exact physical tion of the occupant in the workstation. The air and globe temperatures, as well as air velocity turbulence, were measured at three heights (10, 60, 110 cm). The dew point temperature and our pressure were measured at one height (60 cm). Radiant asymmetry was also measured. This was used to calculate the environmental and comfort indices: operative temperature, mean ant temperature, effective temperature, predicted mean vote (PMV), predicted percentage of atisfied (PPD), and predicted percent dissatisfied due to draft (PD). Table 1 shows the statistical maries of the indoor climate measurements during the cooling and heating seasons, respectively.

Mean air and radiant temperatures, averaged across the three heights, generally fell within 21 28°C for the cooling season, and within 20 and 28°C for the heating season. The variation in individual building was very low; the standard deviation being less than 1°C. It was only from building to the next that a large difference was seen. Vertical air temperature gradients were, on rage, about 0.67°C/m in the occupied zone; which is within the Standard. Average relative idities fell within 30 and 62%, in the cooling season, and within 10 and 39%, in the heating on. Mean air speeds, averaged over the three heights, were quite low; they averaged 0.09 m/s and ged from 0.04 to 0.24 m/s during the cooling season, and averaged 0.08 m/s and ranged from 0.03 .29 m/s during the heating season. Similar variations were also observed from one workstation nother, within the same building. The maximum average air speed in the occupied zone is cified by the ASHRAE Standard 55-1992 as 0.15 m/s in heating season and 0.25 m/s in cooling son. This indicates that during the heating season, the air speed in some workstations exceeded ASHRAE limit. The turbulence intensities fell within 9 and 59% during the cooling season, and nd 66% during the heating season (average 32-33% for both seasons)

The ASHRAE Standard 55-1992 uses the operative temperature as the environmental parameter evaluating global thermal comfort. The Standard then defines a range of operative temperatures humidities that are acceptable to 80% or more of the occupants. This range is mainly applicable sedentary activity, 1.2 met, with normal winter clothing, 0.8-1.2 clo, or summer clothing, 0.6-0.8 The measured parameters were used to calculate the operative temperature using Chapter 13 of ASHRAE 1993 Fundamentals (ASHRAE, 1993), and the results were superimposed onto the ndard's comfort psychometric charts for both the heating and cooling seasons.

Data shows that only 63.4% of the measurements fall within the Standard's summer comfort e (cooling season). The remaining 33.3% fall to the left of the comfort zone (within cooler peratures). These percentages are based on the total amount sampled, and therefore is not an rage value. This means that in some buildings, there is less than 63.4% of the occupants that are py with their environment. Data Also indicates that during the heating season, only 26.9% of the surements fell within the winter comfort zone (heating). The remaining 73.1% fell below the °C dewpoint level indicating the difficulty in humidifying buildings in the cold climate. Again, se percentages are based on the total amount sampled, so one might expect worse numbers in ne buildings.

Table 2 shows a statistical summary of the thermal comfort indices for both seasons. On rage, operative temperature, ET*, and SET values fell within the 22 to 24°C range. The PMV ue fell within the -.02 to -.03 range; indicating marginally cooler-than-neutral conditions. The responding PPD ranged from 13.1 to 13.6%.

In evaluation of the operative temperature and defining the ASHRAE comfort zone for indo air studies, two assumptions are made: activity level and clothing value. To verify the validity the assumptions, the occupants were asked to identify their activity level up to one hour prior filling the questionnaire. On average, the activity level of 1.2 met was acceptable in both heating a cooling seasons. The clothing insulation of the occupant was evaluated using the garment valu published in ASHRAE Standard 55-1992. The intrinsic clothing value averaged 0.62 clo (males) a 0.53 clo (females) in the summer (about 16% higher than the 0.5 clo assumed in the Standar averaged 0.93 clo (males) and 0.81 clo (female) in the winter (about 3% lower than the 0.9 assumed in the Standard).

The garment clo values of the occupants were then corrected by adding the chair clo valu The correction value was proportional to the amount of chair surface area in contact with the bo (chair type). This modification increased the average level by 0.22 clo (males) and 0.09 (females) in the summer and 0.26 clo (males) and 0.14 clo (females) in the winter; increasing insulation values to 0.84 clo (males) and 0.62 clo (females) in the summer and 1.19 clo (males) a 0.95 clo (females) in the winter. The clothing insulation values were much higher (about 0.11 c for the males than for the females, in both seasons. This difference was even greater when the eff of chairs was included (about 0.23 clo).

Some of the thermal environmental and comfort indices were re-evaluated by including chair insulation values to the clothing values. The new indices are shown as the last four rows Table 2. This translates into a 1.2 to 1.3°C increase in SET, and a 0.2 to 0.3% increase in PM index, that corresponds to a 2.0 to 2.4% decrease in PPD index.

3.4 ENERGY PERFORMANCE

In mechanically ventilated buildings, the energy required to heat, cool, condition, and move air amounts to from 30% up to 50% of the total building energy consumption. It is therefore common perception that energy saving will result in deterioration of indoor air. Data shows t energy cost varies from building to building. The average total energy cost per gross air- condition area fell between 0.92 to 6.4 $/m^2/year. Data also indicates no apparent correlation between ventilation rate and total energy cost. There are many reasons for this incoherent result.

The energy required for ventilation is only part of the total energy consumption; the ot consumptions include conduction losses through the building envelope, lighting, elevators, off equipment (computers, fax machines, etc). The investigated buildings also used a wide variety HVAC system types, and energy conservation measures such as heat recovery systems. As well, t used a variety of energy sources: electricity, gas, oil, etc. It was not possible to differentiate actual amount of energy used solely for the ventilation from the rest of the consumption.

4. REFERENCE

ASHRAE 1992, ANSI/ASHRAE Standard 55-1992, Thermal Environmental Conditions Human Occupancy. Atlanta: American Society of Heating, Refrigerating, and Air condition Engineers, Inc. USA.

Haghighat, F., Donnini, G. and D'Addario, R. (1992) "Relationship Between Occupa Discomfort as Perceived and as Measured Objectively", Indoor Environment; 112-118.

Measured indoor air parameters

		Summer													Winter											
	building	1	2	3	4	5	6	7	8	9	10	11	12	TOT	1	2	3	4	5	6	7	8	9	10	11	TOT
	sample size	40	39	40	41	44	41	40	31	40	40	40	6	445	39	38	39	41	44	40	41	30	40	39	40	43
air temperature (C)	mean	23.3	23.3	22.7	24.0	25.1	23.4	23.1	26.4	23.7	25.5	23.4	23.5	23.9	22.9	23.2	23.2	22.7	23.1	22.8	23.2	22.7	23.7	22.2	23.3	23.0
(average of 3 heights)	standard deviation	0.7	0.8	0.5	0.6	0.7	0.7	0.5	0.7	0.7	1.0	0.8	0.6	1.3	0.4	1.0	0.5	0.5	0.7	0.6	0.8	1.0	0.7	1.0	0.7	0.8
	minimum	21.5	21.2	21.7	21.7	23.4	21.7	22.1	24.6	22.1	23.3	21.9	22.6	21.2	21.9	21.1	21.9	21.3	21.7	21.2	21.0	21.3	22.2	20.3	21.4	20.3
	maximum	24.7	25.3	23.4	24.9	26.5	25.1	24.3	27.5	25.2	27.4	25.1	24.3	27.5	23.9	25.1	24.2	23.7	24.6	23.8	26.3	24.6	24.9	23.7	24.5	26.3
mean radiant	mean	22.9	22.5	22.0	23.4	24.8	22.7	22.6	25.3	23.0	24.8	23.0	22.7	23.3	22.7	22.6	22.5	21.5	22.4	21.8	22.2	21.8	22.6	21.5	22.9	22.2
temperature (C)	standard deviation	1.0	0.8	0.4	0.5	0.6	0.6	0.5	0.6	0.6	0.9	1.0	0.7	1.2	1.2	0.9	0.5	0.5	0.6	0.5	0.7	0.9	0.6	1.0	0.5	0.9
(calculated)	minimum	20.9	20.7	21.2	22.3	23.4	21.5	21.6	23.6	21.6	23.0	21.7	22.0	20.7	21.6	20.8	21.2	19.8	21.2	20.7	20.1	20.2	20.8	19.5	21.4	19.5
(average of 3 heights)	maximum	26.7	24.4	23.1	24.1	25.8	25.1	23.7	26.4	24.5	26.5	27.1	23.6	27.1	28.3	24.9	23.6	22.4	23.8	22.8	23.7	23.7	23.1	23.3	23.8	28.3
plane radiant	mean	1.4	0.6	1.0	0.6	0.8	0.6	0.9	0.7	0.6	1.3	1.5	0.9	0.9	1.2	1.2	0.6	1.0	1.2	0.7	1.2	0.9	1.4	1.5	0.8	1.1
asymmetry (C)	standard deviation	1.5	0.5	0.7	0.7	0.8	0.5	0.7	0.4	0.4	1.4	1.9	1.0	1.0	1.4	1.6	0.4	1.0	1.0	0.5	1.0	0.7	1.1	1.4	0.6	1.1
(above 1.1 m)	minimum	0.0	0.0	0.0	0.0	0.0	0.0	0.0	0.0	0.1	0.0	0.0	0.3	0.0	0.0	0.0	0.0	0.0	0.0	0.0	0.0	0.1	0.0	0.0	0.1	0.0
	maximum	6.0	2.1	3.3	4.3	3.1	2.2	2.5	1.5	1.6	5.3	10.3	2.9	10.3	5.9	10.0	1.5	3.9	4.2	2.2	4.1	3.0	4.0	5.7	2.6	10.0
dew point	mean	8.9	8.9	10.3	12.5	13.8	8.9	14.7	11.9	10.2	10.4	9.9	10.2	11.3	6.5	2.5	1.4	1.4	5.5	3.9	0.7	5.6	6.2	1.2	5.1	3.6
temperature (C)	standard deviation	1.0	2.2	0.4	1.3	0.8	1.0	0.3	1.4	0.5	1.3	0.6	0.2	2.3	2.2	2.0	0.8	0.6	2.3	0.6	0.5	1.6	1.3	0.8	0.9	3.5
(at 0.6 m)	minimum	7.5	5.4	13.0	9.9	12.5	7.1	14.0	10.2	9.5	9.0	9.3	10.0	5.4	1.3	0.3	0.2	0.1	0.3	2.4	0.1	0.8	3.9	0.1	2.1	0.1
	maximum	10.2	12.5	14.8	14.8	15.4	11.9	15.2	15.1	11.0	12.0	11.3	10.5	15.4	9.1	5.8	3.2	2.7	8.8	5.1	2.0	7.8	8.9	4.6	6.7	9.1
relative humidity (%)	mean	39.5	39.7	56.7	48.3	49.2	39.3	58.7	40.2	42.1	38.6	42.1	42.5	45.0	16.5	17.8	23.5	19.5	13.7	28.8	22.4	32.7	12.3	20.8	30.5	21.4
(calculated)	standard deviation	3.6	5.3	2.0	4.3	2.7	2.8	1.5	3.7	1.6	4.5	3.1	1.5	7.6	8.0	3.0	1.2	1.0	2.8	1.2	1.4	3.5	1.0	1.2	1.7	7.0
	minimum	33.0	29.5	53.5	39.5	45.0	34.3	54.7	36.3	37.2	32.3	37.7	40.3	29.5	10.0	11.7	21.5	16.9	10.0	26.0	19.9	21.5	9.7	17.3	26.3	9.7
	maximum	45.3	47.8	62.2	55.5	54.0	52.2	61.4	49.3	44.6	45.7	50.4	44.8	62.2	31.5	23.2	26.7	22.9	20.7	31.8	25.9	39.2	14.0	23.3	34.8	39.2
vapor pressure (kPa)	mean	1.1	1.2	1.6	1.5	1.6	1.1	1.7	1.4	1.2	1.3	1.2	1.2	1.4	0.5	0.5	0.7	0.5	0.4	0.8	0.6	0.9	0.4	0.6	0.9	0.6
(at 0.6 m)	standard deviation	0.1	0.2	0.0	0.1	0.1	0.1	0.0	0.1	0.0	0.1	0.1	0.0	0.2	0.2	0.1	0.0	0.0	0.1	0.0	0.0	0.1	0.0	0.0	0.1	0.2
	minimum	1.0	0.9	1.5	1.2	1.5	1.0	1.6	1.2	1.2	1.1	1.2	1.2	0.9	0.3	0.3	0.6	0.5	0.3	0.7	0.6	0.6	0.3	0.4	0.7	0.3
	maximum	1.3	1.5	1.7	1.7	1.8	1.4	1.7	1.7	1.3	1.4	1.3	1.3	1.8	0.9	0.7	0.8	0.6	0.6	0.9	0.7	1.1	0.4	0.7	1.0	1.1
air velocity (m/s)	mean	0.10	0.11	0.09	0.08	0.11	0.08	0.08	0.07	0.09	0.08	0.09	0.09	0.09	0.10	0.11	0.09	0.06	0.08	0.07	0.08	0.07	0.08	0.07	0.09	0.08
(average of 3 heights)	standard deviation	0.03	0.03	0.02	0.03	0.02	0.03	0.02	0.01	0.02	0.02	0.02	0.03	0.03	0.03	0.05	0.03	0.01	0.02	0.02	0.04	0.03	0.03	0.03	0.03	0.03
	minimum	0.06	0.06	0.05	0.05	0.06	0.05	0.04	0.05	0.06	0.05	0.06	0.06	0.04	0.06	0.05	0.05	0.05	0.05	0.04	0.05	0.04	0.03	0.04	0.05	0.03
	maximum	0.21	0.22	0.14	0.24	0.16	0.19	0.11	0.11	0.13	0.14	0.14	0.13	0.24	0.17	0.24	0.20	0.10	0.12	0.12	0.29	0.16	0.15	0.16	0.19	0.29
turbulence intensity (%)	mean	31.6	33.1	31.2	32.0	30.6	30.0	33.6	33.5	34.3	33.0	32.1	34.5	32.6	33.0	32.5	29.3	29.6	31.3	30.8	32.0	34.9	30.9	33.4	31.4	31.8
(calculated)	standard deviation	5.7	5.8	4.7	8.5	5.3	6.0	6.0	7.0	7.3	6.8	4.8	7.9	6.4	5.6	5.5	4.6	5.5	4.8	6.3	7.1	8.4	9.1	9.2	4.9	6.8
(average of 3 heights)	minimum	21.0	22.0	23.0	9.0	22.0	20.0	20.0	23.0	23.0	20.0	23.0	23.0	9.0	18.0	21.0	21.0	20.0	21.0	16.0	12.0	19.0	5.0	18.0	21.0	5.0
	maximum	49.0	41.0	44.0	55.0	45.0	45.0	49.0	49.0	59.0	56.0	44.0	46.0	59.0	44.0	44.0	44.0	42.0	42.0	46.0	48.0	52.0	54.0	65.0	46.0	65.0

Statistical summary of calculated indoor climatic and thermal comfort indices

		Summer													Winter											
	Building	1	2	3	4	5	6	7	8	9	10	11	12	TOT	1	2	3	4	5	6	7	8	9	10	11	TOT
	sample size	40	35	40	41	44	41	40	31	40	40	40	6	445	39	38	39	41	44	40	41	30	40	39	40	431
operative temperature (C)	mean	23.1	22.9	22.3	22.7	24.9	23.1	22.5	25.5	23.3	25.1	23.2	23.1	23.6	22.8	22.9	22.9	22.1	22.8	22.3	22.7	22.3	23.2	21.9	23.1	22.8
	standard deviation	0.8	0.8	0.4	0.5	0.6	0.6	0.5	0.8	0.6	0.9	0.9	0.6	1.2	0.7	0.9	0.5	0.5	0.6	0.5	0.7	1.0	0.6	1.0	0.6	0.8
	minimum	21.3	21.0	21.4	22.2	23.5	21.7	21.9	24.1	21.8	23.2	21.9	22.3	21.0	21.9	21.1	21.6	20.5	21.5	21.1	20.5	20.9	22.0	19.9	21.5	19.9
	maximum	25.6	24.6	23.1	24.5	26.1	25.1	24.0	26.3	24.9	26.9	25.6	23.9	26.9	25.9	25.0	23.8	23.0	24.2	23.3	23.9	24.2	24.3	23.0	24.1	25.9
ET* (C)	mean	23.0	22.9	22.4	23.6	24.9	22.9	22.9	25.5	23.2	24.9	23.1	23.0	23.6	22.2	22.2	22.3	21.6	22.1	21.9	22.1	22.0	22.4	21.4	22.7	22.1
	standard deviation	0.8	0.8	0.4	0.6	0.6	0.6	0.5	0.8	0.6	0.8	0.8	0.6	1.2	0.8	0.9	0.5	0.5	0.6	0.5	0.7	0.9	0.7	0.9	0.6	0.8
	minimum	21.2	20.9	21.6	22.2	23.5	21.6	22.0	23.7	21.7	23.1	21.9	22.2	20.9	20.9	20.4	21.3	20.2	20.1	20.9	20.2	20.6	20.1	19.5	21.3	19.5
	maximum	25.6	24.5	23.2	24.4	26.5	25.0	24.1	26.5	24.8	26.5	25.7	23.7	26.6	24.8	24.5	23.6	22.6	23.7	22.9	23.6	23.8	23.7	22.9	23.8	23.8
SET (C)	mean	23.3	23.1	23.0	23.0	24.0	23.1	22.7	25.6	23.5	24.3	23.5	24.0	23.6	24.6	25.0	25.0	23.6	24.3	24.1	24.1	23.6	24.5	24.5	25.0	24.4
	standard deviation	1.3	2.0	2.3	1.1	1.2	2.3	1.7	1.7	2.0	1.4	1.5	1.9	1.9	1.8	2.4	2.1	2.1	2.1	1.9	1.9	2.2	2.3	2.1	2.5	2.3
	minimum	20.8	19.4	20.2	21.2	21.9	19.6	20.1	22.9	19.8	21.0	20.4	21.9	19.4	21.0	20.5	20.8	20.0	21.0	21.2	20.7	19.8	20.7	20.7	18.9	18.9
	maximum	27.2	29.2	28.6	25.8	27.4	30.4	27.7	30.8	29.2	28.1	26.7	27.1	30.8	28.1	29.8	29.7	27.7	29.4	29.8	29.0	29.4	30.5	29.3	30.4	30.5
DISC (from 2-node)	mean	-0.1	-0.1	0.0	-0.1	0.0	-0.1	-0.1	0.2	0.0	0.0	-0.1	0.0	0.0	0.1	0.2	0.1	-0.1	0.0	0.0	0.0	0.0	0.1	0.0	0.2	0.1
	standard deviation	0.2	0.3	0.3	0.1	0.2	0.3	0.2	0.4	0.3	0.2	0.1	0.2	0.2	0.3	0.4	0.3	0.2	0.3	0.3	0.3	0.3	0.4	0.3	0.5	0.3
	minimum	-0.3	-0.4	-0.3	-0.3	-0.2	-0.5	-0.4	-0.2	-0.4	-0.2	-0.3	-0.2	-0.5	-0.3	-0.3	-0.3	-0.4	-0.4	-0.2	-0.4	-0.4	-0.3	-0.3	-0.6	-0.6
	maximum	0.6	1.1	0.8	0.1	0.6	1.4	0.7	1.6	1.0	0.8	0.4	0.5	1.6	0.8	1.3	1.1	0.6	1.1	1.3	1.0	1.2	1.5	1.1	1.5	1.5
PMVF	mean	-0.4	-0.4	-0.4	-0.4	-0.1	-0.5	-0.4	0.1	-0.4	0.0	-0.3	-0.2	-0.3	-0.2	-0.1	+0.1	-0.5	-0.3	-0.3	-0.3	-0.3	-0.3	-0.3	-0.1	-0.2
	standard deviation	0.5	0.6	0.6	0.4	0.4	0.7	0.5	0.6	0.6	0.5	0.5	0.4	0.6	0.5	0.6	0.6	0.6	0.6	0.5	0.6	0.6	0.6	0.6	0.7	0.6
	minimum	-1.7	-2.2	-1.5	-1.3	-1.5	-2.1	-1.9	-0.9	-2.0	-1.0	-1.5	-0.7	-2.2	-1.6	-1.9	-1.6	-1.9	-1.5	-1.2	-1.6	-1.9	-1.4	-1.5	-2.7	-2.7
	maximum	0.5	0.7	0.7	0.4	0.7	0.9	0.8	1.2	0.9	0.9	0.5	0.4	1.2	0.7	0.9	0.7	0.6	0.7	0.7	0.8	0.9	0.8	0.9	0.9	0.5
PPDF (%)	mean	11.3	15.2	15.7	11.0	8.7	18.0	13.5	11.6	15.0	9.8	12.3	8.8	13.1	11.7	12.9	12.0	17.6	13.8	12.4	13.5	14.6	13.9	12.7	14.6	13.6
	standard deviation	12.8	16.4	12.5	8.7	6.6	20.1	12.2	7.9	14.5	5.7	10.9	3.9	12.5	9.8	13.6	10.6	16.7	11.7	8.4	11.7	10.5	9.7	10.2	15.7	12.4
	minimum	5.0	5.0	5.0	5.0	5.0	5.0	5.0	5.0	5.0	5.0	5.0	5.0	5.0	5.0	5.0	5.0	5.0	5.0	5.0	5.0	5.0	5.0	5.0	5.0	5.0
	maximum	60.0	84.0	93.0	42.0	48.0	81.0	68.0	33.0	74.0	34.0	55.0	14.0	84.0	55.0	71.0	56.0	70.0	51.0	35.0	58.0	73.0	46.0	51.0	97.0	97.0
predicted dradught dissatisfaction (%)	mean	7.5	9.2	8.4	5.0	6.6	11.5	9.4	5.3	9.4	4.3	8.0	3.2	8.1	8.0	8.5	6.3	2.7	5.0	5.3	5.0	5.3	5.9	4.7	9.0	5.3
	standard deviation	9.1	4.7	2.5	3.5	2.6	3.7	1.9	1.7	1.9	2.7	2.3	2.9	3.5	3.1	5.4	3.8	2.1	2.8	3.1	3.8	3.8	3.0	3.8	3.2	3.8
	minimum	2.3	2.2	3.0	0.0	1.8	0.0	2.4	0.0	2.1	0.0	0.0	0.0	0.0	2.5	0.0	0.0	0.0	0.0	0.0	0.0	0.0	0.0	0.0	0.0	0.0
	maximum	17.6	26.3	11.8	15.3	12.9	16.8	9.8	7.9	9.9	11.3	12.1	6.1	26.3	16.3	23.5	16.1	8.0	10.9	10.5	20.2	15.7	14.1	16.0	16.9	20.2
SET (C) (including chair insulation)	mean	24.5	24.3	24.5	24.2	25.1	24.4	23.9	26.7	24.5	25.5	24.7	24.5	24.7	26.9	26.2	26.6	24.9	25.5	25.3	25.1	25.3	25.6	26.1	26.1	25.7
	standard deviation	2.1	2.4	2.9	1.3	1.5	2.7	2.1	3.0	2.4	1.7	1.6	1.9	2.3	1.9	2.7	2.3	2.1	2.3	2.2	2.2	2.3	2.4	2.2	2.7	2.3
	minimum	20.8	20.4	20.4	21.8	21.9	19.6	20.1	22.9	19.5	21.3	21.8	21.8	19.3	21.0	20.5	22.4	21.4	21.4	21.6	20.7	21.2	21.6	22.4	20.3	20.0
	maximum	28.7	31.1	31.0	27.2	28.6	32.2	30.5	30.8	31.2	30.2	28.6	27.1	32.2	30.5	31.2	31.3	29.3	30.9	31.4	30.6	31.6	32.1	33.8	31.6	33.8
DISC (from 2-node) (including chair insulation)	mean	0.1	0.1	0.1	0.0	0.1	0.1	0.0	0.4	0.1	0.2	0.1	0.1	0.1	0.2	0.4	0.4	0.1	0.2	0.2	0.1	0.2	0.2	0.3	0.4	0.3
	standard deviation	0.3	0.4	0.5	0.1	0.3	0.4	0.3	0.5	0.5	0.3	0.3	0.3	0.4	0.4	0.5	0.5	0.4	0.4	0.4	0.4	0.5	0.5	0.5	0.6	0.5
	minimum	-0.5	-0.3	-0.3	-0.2	-0.2	-0.5	-0.4	-0.2	-0.4	-0.2	-0.2	-0.2	-0.5	-0.3	-0.3	-0.2	-0.3	-0.3	-0.2	-0.4	-0.3	-0.2	-0.2	-0.4	-0.4
	maximum	0.9	1.7	1.6	0.5	0.9	2.0	1.6	1.7	1.7	1.4	0.9	0.5	2.0	1.5	1.8	1.7	1.0	1.6	1.6	1.4	1.9	2.1	1.6	1.9	2.1
PMVF (including chair insulation)	mean	-0.1	-0.1	-0.1	-0.1	0.1	-0.2	-0.1	0.5	-0.1	0.2	-0.1	-0.1	0.0	0.1	0.1	0.2	-0.2	0.0	-0.1	-0.1	0.0	0.0	0.1	0.1	0.0
	standard deviation	0.5	0.6	0.6	0.3	0.4	0.7	0.5	0.5	0.6	0.4	0.4	0.4	0.5	0.5	0.6	0.5	0.5	0.5	0.5	0.6	0.5	0.5	0.5	0.6	0.5
	minimum	-1.4	-1.3	-1.0	-0.5	-1.3	-2.1	-1.5	-0.9	-2.0	-0.8	-1.1	-0.7	-2.1	-1.6	-1.9	-1.0	-1.3	-1.4	-1.0	-1.5	-1.4	-1.1	-1.0	-2.0	-2.0
	maximum	0.7	1.0	0.9	0.7	0.9	1.0	1.0	1.2	1.1	1.1	0.7	0.4	1.2	1.0	1.1	0.9	0.7	0.9	0.9	0.9	1.1	0.9	1.0	1.0	1.1
PPDF (%) (including chair insulation)	mean	10.8	12.6	11.6	7.5	8.6	14.2	10.9	15.0	12.9	10.2	9.1	8.0	11.1	10.2	13.1	10.7	11.6	11.2	9.9	12.0	10.9	10.9	9.7	13.4	11.2
	standard deviation	8.1	9.9	6.3	3.9	6.5	15.0	12.3	9.7	15.9	6.0	5.6	3.2	9.5	9.8	13.7	5.2	8.3	8.3	5.6	11.1	9.9	6.5	5.6	12.4	9.1
	minimum	5.0	5.0	5.0	5.0	5.0	5.0	5.0	5.0	5.0	5.0	5.0	5.0	5.0	5.0	5.0	5.0	5.0	5.0	5.0	5.0	5.0	5.0	5.0	5.0	5.0
	maximum	47.0	41.0	27.0	18.0	40.0	79.0	68.0	37.0	74.0	31.0	28.0	14.0	79.0	55.0	71.0	26.0	41.0	48.0	25.0	58.0	43.0	26.0	26.0	79.0	79.0

A User Friendly Computer-Aided Thermal Design Tool Utilizing Transfer Functions

Ali Malkawi, Ph.D.
John Wambaugh
College of Architecture and Urban Planning
The University of Michigan
2000 Bonisteel Blvd.
Ann Arbor, MI 48109
U.S.A

ostract:

A user friendly computer-aided thermal design tool that helps rchitects optimize energy use in building has been developed. his tool assists architects in refining their individual design pproaches to reduce energy consumption and increase thermal erformance of buildings using multi-expert systems. The tool llows the user to run a simulation based on the Transfer Function ethod utilizing a new module that allows easy wall and roof efinitions and Transfer Function retrieval. This module has a ser-friendly Graphical Interface that constitutes a front-end or a wall and roof transfer function coefficient database. It is n easily operated tool that allows the user to quickly retrieve he transfer functions for almost any combination of wall or roof aterials to run a thermal simulation.

Introduction:

Computer applications in the design of the building envelope nclude simulation and optimization using quantitative and recent nowledge-based techniques. Thermal simulation applications that re used for detailed analysis require experts to interpret and se. These models are not appropriate for providing aid to the rchitect within the design process due to their complexity. Their nput data is constructed in a format that requires numerous etails, and their output data requires expert knowledge to valuate, ref.(1).

Accurate simulation of a proposed building design without orrect data is impossible. However, the many variables required or consideration in good simulation often become tedious and orce researchers to spend valuable time consulting tables and erforming repetitive calculations. Experiments show that by liminating the focus upon the extreme conditions of climate for nergy design or monthly energy consumption levels, and by rienting toward detailed analysis, the designer gains a deeper nderstanding of the choices available in the design of the uilding envelope, ref.(2). Generalities associated with pproximate simulation methodologies prevent design guidance for pecific design problems and optimal design solutions, as well as or the prediction of exact thermal design locations. Experiments ndicate that poor understanding of heating and cooling control

and load performance often results when approximation such as peak loads, is the only consideration, ref. (3). In addition, methods using approximation can lead to wrong conclusions, ref. (4).

In recent years our research team has developed an intelligent architectural computer aided thermal system. The system utilizes the Transfer Function Method for thermal simulation integrated with multi-expert systems for its problem detection and advice. Transfer function method was first introduced by Stephenson and Mitalas, ref. (5,6). This procedure is based on response factors and the interplay of heat exchange between various surfaces and sources of heat gain, ref. (7). Transfer functions are based on two concepts: the conduction transfer factors (CTF) and the weighting factors (WF). The CTF are used to describe the heat flux at the inside wall, roof, partition, ceiling or floor as a function of previous values of the heat flux and previous values of inside and outside temperatures, ref.(8). The WF are used to translate the zone heat gain into cooling loads, ref.(9). These functions are derived mainly from response factors. These response factors are defined as an "infinite series that relates a current variable to past values of other variables at discrete time intervals. A transfer function converts the theoretically infinite set of response factors into a finite number of terms that multiply both past values of the variable of interest and past values of other variables", ref.(8).

Currently, the system's database structure and its relation to the interface is being redesigned. This is done in order to allow the user to simulate the building early in the design process and to overcome the problems of TFM complexity. The tool eliminates the tedious task of finding Transfer Functions for the building's walls and roof and allows the user to quickly define the problem and run a simulation. The goal of this new module is to integrate the detail of wall and roof transfer function coefficients with the existing system in a manner that could be quickly understood and easily manipulated. This paper describes an overview of the intelligent computer aided thermal system. It discusses the transfer function coefficients module integrated with the system in detail. Its search method, database structure and its links to the overall system are described.

2. Overall System Description:

Recently a project that focused on the relationship between detailed thermal analysis and guidance advice and criticism was initiated, ref.(10,11). To design the system, a detailed thermal analysis module was developed. The module is integrated with intelligent agents (artificial intelligence computational methods) that reason about the simulation outcome and provide diagnostics (criticism) and advice to solve potential problems. The system allows users to evaluate, critique and optimize energy use and design in buildings. The system is based on a hierarchical representation of building elements in the simulation mode to establish a well-defined output, taking into consideration

ossible element interactions and conflicts. This changing output ccording to the building design is used to build associations ith the inference process and related knowledge sources. The nference process is used to optimize the building energy design y providing criticism and advice. The criticism and advice are onducted based on problem detection and their locations using rtificial intelligence uncertain reasoning, heuristics and search ethods. Their framework utilizes a model that facilitates ynamic multi-expert system interaction and conflict avoidance ithin problem solving. Because of its open architecture, the ystem can simulate individual processes and test their outcome n an individual basis or as a combination with others, figure 1).

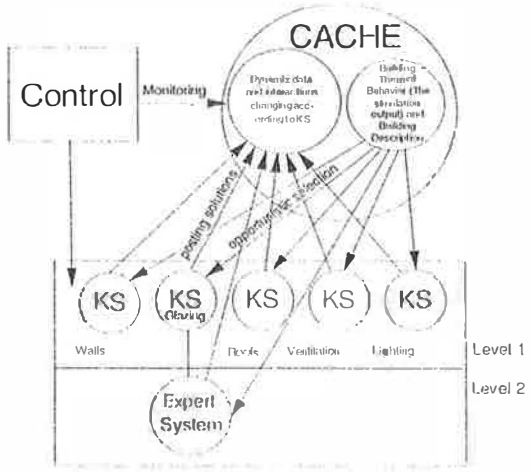

Figure 1. The dynamic multi-expert system interaction model.

The system uses the Transfer Function Method for its thermal nalysis where its output is later used by the expert systems to rovide problem detection and advice. Currently, the system's latabase structure and its association with both the interface and he thermal simulation engine has been redesigned. The new tool ntegrates the details of wall and roof transfer function oefficients with the existing system in a manner that can be used arly in the design process due to its simplicity.

.1. The Wall and Roof TF Tool:

The tool has a user-friendly Graphical User Interface that onstitutes a front-end for a wall and roof transfer function oefficient database. It is an easily operated tool that allows he user to quickly retrieve the transfer functions for almost any ombination of wall or roof materials. The tool manipulates data rom databases consisting of two components. The first component s a traditional table of wall/roof transfer function coefficients s determined by the layer sequence of the wall. While this table

has long been available, only with this tool is it easily accessible in a form that can immediately input the necessary variables into a computer simulation. The second component is a new table that abstracts the first traditional table in a way conducive to modern computer searches. It is the second table that allows the user to work efficiently.

The abstract table contains a single, numerical entry for each wall or roof for every possible component in a wall or roof's layer sequence. The entries reflect the amount of the given material, as determined by thickness, in the wall. For components with negligible thickness, such as finish, the entry is a simple logic bit -- either zero or one. The abstract table can be easily manipulated by computer software to determine relevant entries in the traditional table of transfer functions.

The actual implementation of the new roof and wall transfer function database front- end was achieved with the use of two different search methods. When the user first starts the front-end, they are presented with all the information necessary to retrieve the transfer functions they need in one easy-to-understand screen. On one side of the screen is a list of all the entries in the traditional table of wall or roof transfer functions. On the other side is a list of all the components possibly present in those entries, figure (2). Using a mouse, the user can select whether or not the roof or wall they are simulating contains certain components. He or she has the choice of excluding all entries with a material (such as wood or concrete), including only entries containing a certain material, or including entries regardless of the component's presence. Each time a new criterion is entered, it is applied to the abstract form of the transfer function coefficients table, and the computer can quickly eliminate all those entries that do not match from the list of walls or roofs. In this manner, the user can, in a matter of seconds, narrow the list of entries in the table to a few choices that can be represented graphically and closely correspond to the wall or roof the user wishes to simulate. Thus, it is possible to simulate building designs very early, even if the user only has partial information about the walls or roofs to be simulated (for instance, he or she may only know that they want a wall containing wood and no concrete).

Once the list of possible wall or roof makeups has been shortened to a few entries, the user can then apply the second search option. Concrete and insulation are materials present in almost all walls or roofs, but in widely varying quantities. Therefore, the software allows the user to rank the list of entries by the quantity (either from high to low or from low to high) of concrete and/or insulation in each entry's layer sequence. The choice best matching the user's specifications is then ranked first in the list of choices, preventing the need for the tedious task of thoroughly examining the entries for one matching the proposed wall or roof. Both searches are made possible by the new, abstracted form of the wall functions table that is quickly searched every time criteria is changed to generate an up to date list.

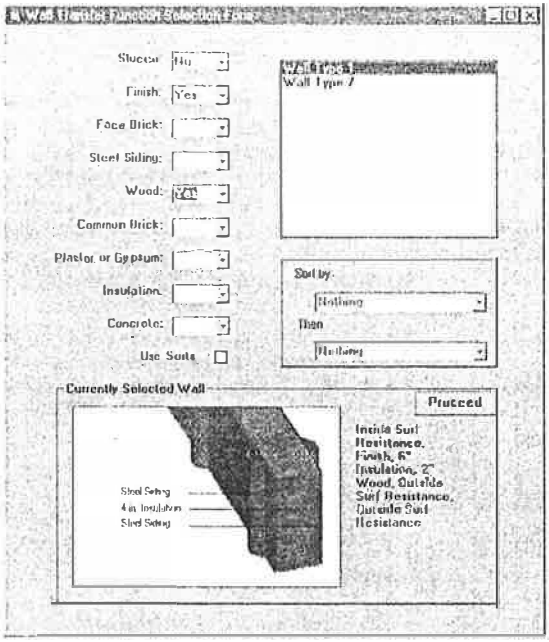

Figure 2. The interface of the Wall and Roof TF Tool.

Because the abstract table allows for rapid, frequent searches, the user discovers immediately if he or she has specified a set of criteria not matched by any entry in the traditional transfer function coefficient tables and can then undo the last selection they made. This is superior to other database schemes that do not refine their searches after each criterion is entered, and thus require users confronted with negative search results to reexamine all the criteria entered. As a module to an existing building simulation system, it allows users to achieve accuracy in an unprecedented fashion that does not require the user to have an in-depth familiarity with transfer functions. It allows the user to rapidly and easily locate the precise transfer function coefficients he or she needs for his or her simulations, and enter them without the danger of data entry errors. Additionally, the ease with which a user can change the wall or roof composition in his or her simulation, allows for rapid and easy simulation to be conducted. For example, by changing the amount of insulation in a simulated wall from two inches to four inches, the user can quickly see how this seemingly minor change can affect the building as a whole. Before, making this same change would have required a great deal of time and effort. Now it can be done with a few clicks of the mouse.

3. Conclusions:

Previous computer systems handling transfer functions required an in-depth familiarity with matters that should be incidental to valuable building simulation research. The tool developed allows the user to rapidly and easily locate the precise transfer functions he or she needs for his or her simulations, and enter them without the danger of data entry errors. New entries can be added and old entries updated with extreme ease to allow for expansion and revision. As a module to existing building simulation, the tool allows users to achieve excellent accuracy in an unprecedented fashion early in the design process. This new tool is another step forward in integrating accurate information into existing and forthcoming building simulations.

4. References:

(1)DOE 2.1 - Department of Energy Simulation Program, Users Manual "DOE 2.1" Los Alamos, New Mexico: 1980.

(2)Zdepski, M.S. "Architectural Diversity Through Climate-Responsive Architecture," Exterior Envelopes of Buildings III Prc of ASHRAE/DOE/BTECC Conference 1985; Florida, 2-5 December: 1409-1413

(3)Hittle, D.C. "Energy Analysis in an HVAC Design Course," ASHRAE Transactions 1989; Vol.95, Pt.1:1174-1177

(4)Shaviv, E. and Peleg, U.J. "A Knowledge-Based System for the Schematic Design of Passive Solar Buildings," ASHRAE Transactions 1990; Vol.96, Pt.2:557-561.

(5)Stephenson, D.G. and Mitalas, G.P. "Cooling Load Calculations by Thermal Response Factor Method," ASHRAE Transactions Vol. 73, Pt.I, 1967.

(6)Mitalas, G.P. "Calculating Cooling Load Caused By Lights," ASHRAE Journal 1973; June: 37-40.

(7)Romine, T.B., Jr. "Cooling Load Calculation: Art or Science?," ASHRAE Journal 1992, January: 14-24.

(8)McQuiston, F.C. and Spitler, J.D. "Cooling and Heating Load Calculation Manual," 2nd ed. Atlanta: American Society of Heating, Refrigerating and Air Conditioning Engineers, Inc., 1992.

(9) Sowell, E.F. and Chiles, D.C. "Zone Descriptions and Response Characterization for CLF/CLTD Calculations," ASHRAE Transactions 1984; Vol.91, Pt.2A:179-200.

(10) Malkawi, A. "An Approach to Rigorous Intelligent Computer-Aided Systems: Architectural Thermal Design". Proceedings of the 7th International Conference on Systems Research, Informatics and Cybernetics. August 15-21, 1994. Baden -Baden, Germany.

(11) Malkawi, A. "Simulation and Reasoning: Intelligent Building Thermal Problem Detection", Proceedings of the 4th International Building Simulation Conference, August 14-16, 1995, Madison, Wisconsin. 176:182

RECENT DEVELOPMENTS IN US LIGHTING REGULATION FOR ENERGY EFFICIENCY

Mohamed Boubekri, Ph.D.
School of Architecture, University of Illinois
611 Taft Dr., Temple Buell Hall # 117
Champaign, IL 61820, USA

ABSTRACT

In the latest National Energy Policy Act (EPACT) of 1992, several energy efficiency programs have been enacted. Within the field of illumination, these programs included lamp standards, testing procedures, lamp labelling, luminaire testing and information procedure and energy consumption standards. Many of the programs have not taken effect until 1995. This paper describes some of these programs and the implementation of these new lighting efficiency regulations.

INTRODUCTION

The latest National Energy Policy Act became law on October 1992 after passing both houses of US Senate and US Congress. It was initiated and designed as a response to growing concerns about America's increasing dependence on imported oil (1). US domestic energy Policy continued to decline throughout the 70's and 80's but the reliance on foreign oil rose to nearly 50% of US consumption. The several Middle-East crises ranging from the 1973 oil crisis to Desert Storm war of 1990 forced US politicians to respond in a comprehensive manner to the potentially severe problems that the country could face some day.

EPACT1992 (2) affects all users and manufacturers of electric lighting equipment and/or energy. It impacts the manufacturing and utilization of electric motors, transformers luminaires, and lamps. It establishes minimum efficiency standards for incandescent and fluorescent lamps of certain types. Lamps not meeting these standards are no longer available since November 1995 as specified in the Act. Facilities not using inefficient lamps need, therefore, to change their lamp technology which could consist of simply changing the lamp type to a more radical change such as installing a completely new lighting system.

LIGHTING SYSTEM PERFORMANCE STANDARDS

EPACT 1992 addresses energy performance standards for new construction of public and assisted housing, single family and multifamily residential housing (other than manufactured homes)

subject to mortgage insured under the National Housing Act . These must meet the Council of American Builders Officials (CABO) energy code of 1992. A provision in the Act states that no later than 2 years after the date of enactment of EPACT '92, each state was required to certify to the Secretary of Energy that it has reviewed the provisions of its residential building code regarding energy efficiency and made a determination as to whether to revise such residential building code provisions to meet or exceed the Council of American Building Official (CABO) code of 1992.

The requirements for the commercial buildings were to meet the American Society for Heating Refrigerating and Air Conditioning Engineers (ASHRAE) and the Illuminating Society of North America (IESNA), ASHRAE/IESNA 90.1-1989 Standard (5) or any successor standards and t states were asked to comply with these standards no later than two years after the enactment of EPACT 1992. On June 28, 1995 ASHRAE and IESNA have completed the revision of the previous standard to the new one ASHRAE/IESNA 90.1-89R. DOE is providing assistance to states for implementation and monitoring their compliance with EPACT upgrades.

As in the previous standard, the new one is based on calculation of both interior and exterior power allowances (ILPA and ELPA respectively). The actual connected power should be equa or less than the maximum allowed ILPA or ELPA. trade-offs are allowed within each of the interior lighting budget or exterior lighting budget but not between them.

Specification for Lighting Power Density

The lighting Power Density (Watts /square meter or square foot) prescribes a maximum power consumption level per unit area either per building type or per space function type. The buildin LPDs are based on the weighted average LPD values of the space function and the typical areas of those functions typically found in that particular type of building. Overall building LPD value vary according to the total lighted area of the building and tend to decrease as the lighted area o the building increases.

Space LPD values are more specific and relate to the function of each space. Previous LPDs were based on a room cavity ratio of 1 and were adjusted using an area factor (AF) which accounts for the space lighted area and the ceiling height. The new LPD values are generally lower than the previous standard because they take into consideration the most recent efficient lighting technologies.

The Interior Lighting Power Allowance may be calculated using the Total Building Area Metho or the Space Function Method. The calculation procedures have not changed between the two versions of the standards.

The Building Area Method calculates the entire ILPA based on the allowable lighting power density for that building type. The lighting power density varies according to the type of buildin and the total lighted area of the building. The larger the building, the smaller the LPD.

Table 1. A Sample of Recommended Power adjustment Factors (Reference 5)

Automatic Control Device (s)	Power Adjustment Factor (PAF
Daylight Sensing Controls, continuous dimming	0.30
DS, multiple step dimming	0.20
DS, On/Off	0.10
DS, continuous dimming and programmable timing	0.35
DS, multiple step dimming and programmable timing	0.25
DS, On/Off and programmable timing and lumen maintenance	0.40
Occupancy sensor	0.30
Occupancy sensor and DS, continuous dimming	0.40

Space Function Method calculates the lighting power budget based on the power allowance for each space and the area of each space in relation to the building. The interior lighting power allowance and the exterior lighting power allowance are separate. Trade-offs are allowed within ILPA or ELPA but not between them.

The two calculations methods are not all that much different from the Building Area Method. The only major difference is that power adjustment factors can be used for each space to calculate the adjusted power allowance based on whether that particular space uses some special energy saving lighting controls or not as indicated in Table 1.

LABELLING AND EFFICIENCY REQUIREMENTS

In terms of lamp technology, the 1992 EPACT specifically addresses general service incandescent lamps, incandescent reflector lamps (R), Ellipsoidal Reflector (ER) lamps and Parabolic Aluminized Reflector (PAR) lamps, , straight, "U" shaped , and compact fluorescent lamps and high intensity discharge (HID) lamps (3). EPACT now prohibits the manufacture or importation of certain within these categories (4).

General Service Incandescent Lamps

The products included are the medium base tungsten-halogen lamps 115-130 volts, 30 watts and above, used for general service lamps applications. Traffic signal, street lighting, transportation, stage and studio, industrial heating, reprographic, medical, colored, shatter resistant, decorative, showcase and appliance lamps incandescent lamps are excluded from labelling and efficiency standardization.

Under EPACT '92, the US federal Trade Commission (FTC) is the agency required to design labelling program for all lamps included in the new Act (4). The deadline enforced was 15 May 1995 for most lamps except for incandescent group for which the deadline was extended to

December 1995. All products included within EPACT must meet labelling requirements, namely lamp packages display lumen output, lamp wattage, and rated lamp life. For lamps operating at other voltage than the US standard 120 volts, they must be listed for their operating voltage as well as for the US standard one.

The labeling is intended to help consumer select high energy efficiency products to meet their needs. Similar labeling requirements are now enacted for medium-base compact fluorescent lamps, which emphasizes the relative cost of energy for these commonly lamp types encouraging more use of efficient light sources.

Incandescent Reflector Lamps

The products included within this category of lamps are medium-base reflector R and PAR shaped lamps, 115-130 volts, 40 watts and above, with a diameter not exceeding 2.75 inches. Exempted products are the specialized lamps such as traffic signal, streetlighting, transportation, stage and studio, industrial, heating reprographic, medical, scientific, decorative, showcase, colored, shatter resistant, appliance, lamps, rough/vibration service, lamps with bases other than E26, ER and BR bulb shapes R20 or smaller and low voltage lamps. Performance data must mee or exceed minimum efficacy limits. Table 2 indicates the minimum efficacy (lumen/watt) standard that reflector lamps need to meet or exceed.

Table 2. EPACT 1992 minimum efficacies for projector lamps

Nominal Lamp Wattage	Minimum Average lamp Efficacy (LPW)
40 - 50	10.5
51 - 66	11
67 - 85	12.5
86 - 115	14
116 - 155	14.5
>155	15

Lamps not meeting the above prescribed efficacy values cannot be manufactured after October 31, 1995. Lamps that do not employ halogen capsule technology will not meet the minimum efficacy standards, thus are now eliminated. In this list we find some popular and often used lamp such as most R30, R40, and incandescent PAR30 and PAR38 lamps.

General Service Fluorescent Lamps

According to EPACT, general fluorescent lamps need to meet or exceed mandatory minimum lamp efficacies and Color Rendering Index (CRI). Table 3 shows these efficacy and CRI limits according to lamp type and nominal wattage. All regular 2400 mm and 2400 mm high-output manufactured after April 30, 1994 were subjected to these requirements. U-shaped 1200 mm and 600 mm lamps must meet efficacy requirements after November 01, 1995. Colored fluorescent lamps are exempt from these requirements, but the DOE proposes that a CRI values no less than 80 must be met. All other lamps falling within the categories as shown in Table 3 and do not meet the requirements could not be manufactured as of October 31, 1995. Product exempted are lamps with a CRI of 82 or greater, plant growth, cold temperature, colored, impact resistant, reflectorized, reprographic or UV radiation lamps.

These standards have eliminated full-wattage lamps that use the lower-cost halophosphors, thereby, encouraging the use of reduced wattage or lamp using more efficacious rare earth-phosphors.

Table 3. Efficacy and CRI requirements for general services fluorescent lamps

Fluorescent Lamp Type	Nominal Lamp Wattage	Minimum CRI	Minimum Average Lamp Efficacy (LPW)
2 ft U	>35 <35	69 45	68 64
4 ft Med bi-pin	>35 <35	69 45	75 75
8 ft high output	>100 <100	69 45	80 80
8 ft slimline	>65 <65	69 45	80 80

High Intensity Discharge Lamps

There are no specific guidelines under EPACT 1992, but the Department of Energy (DOE) was required to prescribe efficiency standards if they are warranted. in other words. if they would result in significant savings and are economically feasible. If DOE determines that such standards are needed, they will be effective by October 1999.

CONCLUSION

The revised ASHRAE/IESNA standard 90.1-89R is comprehensive energy efficiency standard dealing with several energy consumption sources in commercial and residential building that mor than 3 stories. This revised standard has gone an extensive public review and is a culmination of the work of several committees. In the area of building illumination, the new standard includes several clauses dealing with lamp standards, testing procedures, lamp labelling, luminaire testing and information procedure and energy consumption. Because of the new standard, a number of very popular lamps can no longer be manufactured in the US because they don't meet any longer the newest energy efficiency standards. The new standard reflects most recent advances in light fixture technology and the constantly developing field of lighting.

REFERENCES

1. Johnston B. J., Energy Policy Act of 1992 - Forward Statement, Public law, 102nd Congress, Report 102-1018, US Government Printing Office, Washington DC 1992.

2. U.S. House of Representatives, Energy Policy Act of 1992, Public law, 102nd Congress, Report 102-1018, US Government Printing Office, Washington DC 1992.

3. Pacific Gas and Energy of California, "The 1992 Energy Policy Act", Pacific Gas and Energy Document

4. Atkinson B. et al. "US Lighting Regulation: 1995 Update", Proceedings of 3rd Europear Conference on Energy-Efficient Lighting", University of New-castle Upon Tyne, June 18 25, 1995

5. ASHRAE and IESNA, "ASHRAE/IES Standard 90.1-1989: Energy Efficient Design of New Buildings Except Low-Rise Residential Buildings." Co-Sponsored Document by IESNA and ASHRAE, 1989

International Collaboration within the IEA Energy Conservation in Buildings and Community Systems Programme

Sherif Barakat, Ph.D.
Institute for Research in Construction
National Research Council of Canada
Ottawa, Canada, K1A OR6

ostract

Collaboration on energy technology research and development through the ernational Energy Agency (IEA) contributes to the economic development, energy curity and environmental protection objectives of Member countries.

The IEA Energy Technology Collaboration Programme provides a framework for perts to work co-operatively and share results. The benefits typically include sharing sts, pooling resources, and avoiding unproductive research paths. Further, participants e able to spread the risks associated with the choice of research priorities. The tcomes of collaboration enable the research and development objectives of national ergy technology programmes to be better achieved at a lower cost.

This paper introduces one of the IEA collaborative programme on Energy nservation in Buildings and Community Systems programme (ECBCS) and highlights e achievements of a number of its collaborative projects.

THE INTERNATIONAL ENERGY AGENCY

The International Energy Agency (IEA) is an autonomous body which was established November 1974 within the framework of the Organization for Economic Cooperation d Development (OECD). Its purpose is to implement an International Energy ogramme. It carries out a comprehensive programme of energy cooperation among 23 OECD's 24 member countries, and allows for the participation of non-member untries.

The challenges the IEA member countries face in the energy sector have evolved er the past two decades. Energy security remains a primary goal. But in recent years ere has been increasing awareness of the significance, for energy policy and energy curity, of two further factors: concern over the environmental impact of energy-related tivities and the growing globalization of energy issues, as countries' economies and ergy markets become increasingly interdependent but nevertheless different in terms energy sources, price etc.

e objectives of the IEA are:

- to improve the world's energy supply and demand structure by developing alternative energy sources and increasing the efficiency of energy use
- to encourage collaboration among member countries in energy research, and technology development and demonstration

- to ensure that environmental considerations are taken into account in the formulation of energy policy
- to maintain and improve a system for coping with oil disruptions
- to operate a permanent information system on the oil market and other sources of energy
- to maintain cooperative relations with non-member countries and international organizations

1.1 Organization of the Collaboration Programme

IEA energy technology activities are set up under simple contractual arrangements called Implementing Agreements. The Implementing Agreement provides the legal mechanism for establishing the commitments of the participants, the management structure to guide the activity, and the distribution of the benefits derived from the co-operative work.

There are currently 41 active IEA Implementing Agreements covering fossil fuels technologies, renewable energy technologies, efficient energy end-use technologies, fusion technology and energy technology information centres. Research expenditures of more than $100M (US) per annum are coordinated, providing substantial cost savings.

A provision for non IEA-Member countries to participate in Agreements as Associate Participants was introduced in 1992. The Republic of Korea, the Russian Federation, Poland, Israel, Brazil, Venezuela and China have become Associate Participants in a number of Implementing Agreements.

The Implementing Agreements are managed by Executive Committees made up of experts nominated by the participating countries. The various activities of each Implementing Agreement are set out in separate Annexes and are managed on a day to day basis by an Operating Agent. The Implementing Agreements are monitored by technical and policy experts who represent Member countries on the IEA Governing Board, Committee on Energy Research and Technology (CERT), and three Working Parties on specific technology areas. All resources for projects are supplied by the Participants rather than by the IEA. The resources are provided by Participants contributing financial resources (cost-sharing) or by Participants devoting specified resources to the agreed work programme (task-sharing).

2. ENERGY CONSERVATION IN BUILDING AND COMMUNITY SYSTEMS

Approximately one third of primary energy is consumed in non industrial buildings, such as dwellings, offices, hospitals and schools where it is needed for thermal conditioning, lighting and the operation of appliances. The percentage of the total energy used in non industrial buildings varies from 30 to 50% depending on the country. Exceptions are countries without heavy industries; such as Denmark and The Netherlands where the energy used in the built environment is estimated to vary from 50 to 70%.

Hence this sector represents a major contributor to fossil fuel use and carbon dioxide production. Following uncertainties in energy supply and recent concern over the risk of global warming, many countries have now introduced target values for energy savings in buildings. Overall, these are aimed at reducing energy consumption by between 15-30%

o achieve such aims, international co-operation in which research activities and nowledge can be shared is seen as an essential.

In recognition of the significance of energy use in buildings, the International Energy gency (IEA) has established an Implementing Agreement on Energy Conservation in uildings and Community Systems (ECBCS). This is aimed at initiating research and roviding an international focus for building energy efficiency. Tasks are directed at eneric energy saving technologies and activities that support their application in practice. esults are also used both nationally and internationally to develop relevant standards nd guidelines.

Member organizations of the ECBCS are drawn from a total of 21 Countries and the uropean Commission. The designation by governments of a number of private rganizations, as well as universities and government laboratories, as contracting parties ave provided a broader range of expertise to tackle the projects in the different echnology areas than would have been the case if participation was restricted to overnments. Participation in any particular programme of research is optional and most ommonly takes the form of a 'task shared' Annex in which each participant commits an greed level of effort. Typically an Annex will operate for a four year period. ccasionally, an Annex may be jointly funded, in which case a single institution receives unding from participants to undertake a given task.

Overall control of the programme is maintained by an Executive Committee, which not nly monitors existing projects but identifies new areas where collaborative effort may be eneficial. The Executive Committee ensures all projects fit into a predetermined trategy without unnecessary overlap or duplication but with effective liaison and ommunication.

.1 Programme Objectives:

eneral objective of the BCS Implementing Agreement is to facilitate and to accelerate ntroduction of new and improved energy conservation and environmentally sustainable echnologies into buildings and community systems. In order to achieve that both echnical and non-technical goals are defined. Specific objectives of the BCS R&D rogramme are:

- to support the development of generic energy conservation technologies within international collaboration
- to support technology transfer to industry and to other end-users by dissemination of information, through demonstration projects and case studies and through attracting direct industry participation
- to contribute to the development of international standards, test methods, measuring techniques and evaluation/assessment methods
- to remove technical and to some extend also non-technical obstacles to the penetration of new advancements in energy conservation technologies
- to encourage non-Member countries to participate in BCS activities by inviting their industries which are recognized in the specific area of the Annex, to accelerate the introduction of energy efficient technologies in these countries.

The work of the BCS programme covers a large number of areas, including: design ools (early-stage, LCC-analysis, etc.), community planning tools, system engineering, uilding automation and energy management systems, advanced technical systems ighting, envelope, HVAC systems, heat recovery), operational technologies, advanced

building materials and components, indoor air quality and ventilation; energy retrofitting, and integration of energy conservation and renewable energy technologies.

The R&D activities cover both new and existing buildings, residential and office/commercial buildings, even though main emphasis is on improving the energy-efficiency of the existing building stock because of the declining trend in new construction.

2.2 Activities of the Buildings and Community Systems Program:

Since the start of the Agreement in 1977, the Executive Committee has initiated 34 collaborative projects (Annexes) with 25 of them completed and reported. The work addressed the main R&D areas reaffirmed as part of the Strategy Plan. These projects resulted in a large number of reports with results ranging from international state-of-the-art review to design guidelines, to validated simulation models and energy analysis tools.

To enhance the dissemination of the program results, the ExCo encourages participation of industry in collaborative projects, it publishes a semi-annual Newsletter, publicizes the work on an Internet World Wide Web page (www.ecbcs.org), and encourages presentation of the results at relevant national and international conferences.

Description of all annexes and a list of resulting publications are available on the Web page. Some of the main R&D areas and annexes addressing these areas are summarized below. More details are sometimes given on some annexes to illustrate particular achievements.

2.2.1 Energy Management and Control Systems

The implementation of building energy management and control systems can result in a considerable reduction in energy use. Efforts have concentrated on providing guidelines for selecting suitable systems (Annex 16), the development and assessment of building HVAC emulation tools (Annexes 10, 17 and 30) and of diagnostic and fault detection techniques (Annexes 25 and 34).

Annex 16 examined the functions of a number of existing monitoring and control systems, how these worked in various countries and climates and the cost reductions that resulted from system implementation. Sensor types and installations were assessed, a number of buildings fitted with computerized energy management systems were inspected to gain experience with different applications and experiences were also collected through interviews with manufacturers, consultants and property managers. Examples indicated that investment in computerized energy management and control systems can result in 15-30% energy saving, depending on operating strategy.

While Annex 16 primary task was to examine existing systems, the purpose of Annex 17 was to develop the algorithms used in the control systems. The options for better control were demonstrated by means of simulations using different operating strategies. Two simulation software packages were used: TRNSYS and HVACSIM, and emulators were developed and implemented at six different sites. Comparisons have also been made between various emulators (e.g. for the operation of the boiler, cooling system, cooling tower, supply and return air fans) and results were in most cases within 5%. The work indicated that emulators can be used to inspect or examine the hardware and software of the control system, assess the structure, control strategies and algorithms, fine-tune the default or pre-set values and train operating personnel.

2.2 Development and Evaluation of Design Tools

Several annexes have been devoted to the development and application of design ols including thermal simulation (Annexes 10 and 21). Several models have been veloped and/or assessed, many of which are in the public domain. The work of Annex (in collaboration with Task 12 of the Solar Heating and Cooling program) has resulted a comprehensive method to test and help correct computer-based energy analysis odels. This work has been accepted by national accreditation bodies and is leading to tter design and assessment of energy efficient buildings.

Effective energy reduction is dependent on improving the energy efficiency of the ilding stock without compromising occupant comfort or building integrity and durability pecially in relation to moisture accumulation. Efforts have been dedicated to veloping computer prediction models and design guidelines for building envelope stems (Annexes 14, 19 and 24). Annex 14 objective was to provide architects, building vners and practitioners with better knowledge and understanding of the physical ckground of the phenomena of condensation, including material characteristics and tical conditions for mold growth. Also to provide better computational models, taking eat, air and moisture in account in predicting surface condensation and potential lutions to avoid it. Design and practice guidelines were produced and presented in one the final reports.

Motivated by the work of Annex 14 and the fact that national building codes and andards continued to treat the subject of combined heat, air and moisture performance a very elementary way, 14 countries have joined in Annex 24 to improve the derstanding of heat, air and moisture transport in new and retrofitted envelope parts d to analyze the consequences of thermal and hygric performance on durability. The nnex resulted in the most comprehensive compilation of computer models and material operty data. It also defined the concept of Indoor Climate Class with the governing arameter as the indoor-outdoor vapour pressure excess, to classify the hygrothermal ress on the envelope. Finally, the consequences for energy consumption of enthalpy ow, latent heat release and moisture content were quantified in exemplary practical ases. Parasitic airflow was highlighted as a major cause of unwanted extra losses and oisture accumulation. Examples of effects on durability were also given for cases of ological and chemical attacks and mechanical degradation.

2.3 Ventilation and Indoor Air Quality

It is estimated that 30% or more of space conditioning load (heating and cooling) of a uilding is in the departing air stream. Therefore, in addition to impacting the indoor air uality, ventilation has an important energy implication. ECBCS program has oncentrated on understanding the role of ventilation and evaluating ventilation systems. tudies have focused on energy efficient ventilation strategies and methods for predicting r flow patterns (annexes 20, 23 and 26). Other aspects include evaluating the impact of r infiltration on ventilation and energy performance and the use of ventilation heat covery systems (Annexes 8, 9, 18 and 27). Information on air related aspects is sseminated through the Air Infiltration and Ventilation Centre (AIVC or Annex 5).

Annex 20 was formed to evaluate the performance of single- and multi-zone air and ontaminant flow simulation techniques and to establish their viability as design tools. The valuation was done through a number of simulation exercises covering free, forced and ixed convection cases as well as a displacement ventilation case. This also provided a

methodology and data sets for future work. Computational fluid dynamics (CFD) codes were found to predict room air movement with sufficient realism to be of use to design practice, however significant skill and experience are still required to use such codes. The work also identified three areas needing of further development, modeling of supply air jets, turbulence and thermal wall functions. In the area of multi-zone modelling, experts of Annex 20 developed a number of algorithms including flow through large openings and single sided ventilation, inhabitant behaviour (use of doors and windows), air flow-driven contaminants and multi-room ventilation efficiency. These development were now incorporated into simulation code COMIS developed in Annex 23.

Experiences of Annex 20 were also extended to Annex 26, to provide design guidanc on the application of air flow simulation tools for understanding ventilation in large enclosures such as shopping malls, atria, airport terminals and covered theaters and stadiums. Each of these presents enormous design challenges in relation to heating and cooling loads, the provision of good indoor air quality and protection against fire and smoke movement. The annex developed new methods that have provided new guidanc on the operation and applicability of CFD models. "Simple" analysis tools were developed for basic engineering application. These included the "flow element" technique in which the flow field is predicted by individually analyzing each flow element, i.e. jets, plumes, boundary layer flow, etc. In addition, a simplified measurement procedure to evaluate building air leakage has been devised, and existing infra-red photography methods have been adapted to map surface temperatures inside spaces that can only be viewed from oblique angles. CFD predictions have been compared with measured results and demonstrated to predict the flow and thermal patterns to a reasonable degree of accuracy including coping with the complexities of radiative exchange. Various developments of Annex 26 were incorporated into a "tool kit" aimed a assisting the practitioner to achieve proper flow pattern control for energy efficient ventilation.

2.2.4 Advanced Building Materials and Systems

Developments in window technologies, to improve the thermal insulation value as wel as the use of natural daylight and passive heating and cooling techniques, have a considerable impact on energy efficiency of buildings. These technologies are developed and assessed in various annexes on windows (Annex 12), daylighting (Annex 29) and Low energy cooling (Annex 28). Combined with these are prediction methods and a variety of new materials and energy efficient systems for use in buildings.

2.2.5 Community Systems Energy Planning

Widespread implementation of energy conserving technologies and measures depends on the scale of penetration. Various projects are aimed at developing community wide strategies or local area planning. Activities are concentrating on the development of planning tools and implementation strategies that optimizes the energy use within a whole community (Annexes 22 and 33). This involves the co-operation of local authorities willing to participate in the use of proper planning tools as part of an international case study approach.

2.2.6 The Future Building Forum

An important part of the ECBCS program is the Future Building Forum - 2025. This is aimed at identifying long-term energy, environmental, economic and technical issues and assessing their impact on future buildings. The Forum also monitors technological

vances appropriate to building science and defines research priorities based on
nerging technologies that will ensure that buildings contribute to a sustainable society
the year 2025 and beyond. The direction of the FBF is maintained through regular
rkshops and expert meetings; six workshops on various subjects were held to-date
oceeding available through the AIVC). The FBF Organizing Committee includes
presentatives from all building-related IEA Implementing Agreements including: District
eating and Cooling, Heat Pumps, Energy Storage and Solar Heating and Cooling.

2.7 New Activities:

Several new Annexes have recently been established each aimed at improving the
plication of knowledge to practice. These activities include:

Energy Related Environmental Impact of Building - Annex 31

e main intention of this project is to document and develop techniques that can be
ed to analyze how energy use in buildings impacts on the interior, local, regional and
bal environments. The planed work covers: documentation of methods and data;
alysis; demonstration; and information transfer.

The project will be centered around life cycle analysis combined with the impact of the
rastructure associated with building and the energy chains involved in delivering energy
buildings.

Integral Building Envelope Performance Analysis - Annex 32

is activity is aimed at the optimization of the building envelope to achieve energy
ficiency combined with a good indoor environment. Two main tasks are proposed to
velop appropriate methodology for performance analysis and to establish case studies
assist in improving and demonstrating optimization methods. These studies will
corporate new construction, renovation, laboratory tests and full scale demonstration.

Advanced Local Area Planning - Annex 33

ajor effect has recently been undertaken in several countries to develop local energy
anning concepts (LEP) into a tool for the integrated planning of entire communities.
is combines knowledge at the "microscopic" or individual building design level with
stem analysis at the "macroscopic" or community level. Not only is modern day LEP
ncerned with minimizing the cost of energy supply but also in integrating demand and
pply side measures with environmental requirements and the planning and decision
ocess.

There is now an enormous diversity of planning tools which are available to the
anner, however a wide gap still exists between available techniques and there
plication in current practice. The objective of annex 33 is to close this gap by
oducing tools to support practical application.

Computer Aided Fault Detection and Diagnosis - Annex 34

recent study has indicated that 20-30% energy savings in commercial buildings is
hievable by re-commissioning of the HVAC systems to rectify faulty operation. Current
rategies do not explicitly optimize performance and cannot respond to the occurrence of
ults which cause performance to deteriorate. The objective of this Annex is to work with
ntrol manufacturers, industrial partners and/or building owners and operators to
monstrate the benefit of computer aided fault detection and diagnostic systems.
ethods will be incorporated either in stand alone "PC" based systems or incorporated
ithin a future generation of "smart" building control systems.

3. Summary

Since 1977, the IEA Buildings and Community Systems program of collaborative research has significantly contributed to the knowledge and expertise on efficient energy use in buildings. The outcomes of the collaboration have enabled the research and development objectives of national energy technology programmes in participating countries to be better achieved at a lower cost and a very high quality.

4. Bibliography

(1) IEA, International Collaboration, Energy Technology and R&D, The International Energy Agency, Paris, France, 1995.

(2) IEA, International Energy Technology Collaboration: Benefits and Achievements, The International Energy Agency, Paris, France, 1996.

(3) Energy Conservation in Buildings and Community Systems (BCS) - Strategy Play 1994-1997, IEA, Paris, France, 1994.

Boundary Layer Control by Characteristic Length Manipulation

D. Michelle Addington
Harvard University Graduate School of Design
48 Quincy Street
Cambridge, MA 02138 USA

Abstract

Computational fluid dynamics offers the unprecedented opportunity to explore the discrete behavior of air, but the majority of simulations have been devoted to large scale models with high momentum air supplies. Small scale CFD modeling of the boundary layer, however, reveals that heat transfer from a given thermal source can be significantly altered if the characteristic length which drives convective transport is shifted. This shifting can occur simply by changing the location and/or orientation of the cold sink, without changing any physical parameters of the thermal source. FIDAP, a finite element code, was used to investigate the impact of characteristic length on boundary layer heat transfer, and preliminary results indicate that orientation has a far greater impact on characteristic length than previously assumed. As a result, discrete control of the boundary layer heat transfer is achievable and may be an ideal application of MEMS technology.

Nomenclature

Ra	Rayleigh number
Nu	Nusselt number
Pr	Prandtl number
g	gravitational acceleration
β	volumetric expansion coefficient
ΔT	temperature difference between hot and cold isothermal surfaces
L	length of isothermal surface
L_c	characteristic length
ν	kinematic viscosity
α	thermal diffusivity
μ	viscosity
ρ	density
h	heat transfer coefficient
k	thermal conductivity
C_p	specific heat

1. Introduction

Computational fluid dynamics (CFD) and Microelectromechanical systems (MEMS) can complement each other ideally, the former enabling a means to characterize discrete behaviors in air, and the latter providing the ability to act at a discrete level. These two fields, however, are developing independently of each other. CFD investigations in building air behavior have tended to focus either on the evaluation of existing systems in typical room scenarios or on the investigation of specialized applications such as laboratory facilities and double walls. MEMS development has been carried forth almost exclusively by microelectronics researchers, and their vision for future applications considers the deployment of MEMS only in conjunction with more efficient energy conversion, i.e. so as to provide direct personal cooling or to replace the plant in a building. Coupling these two fields, however, requires discretization at sub-millimeter dimensions, which is irreconcilable with the length scales associated with normal room dimensions. By removing the *prima facie* high velocity air diffuser from the room behavior, one can consider that the air phenomena present are essentially independent behaviors that interact with the room air through their respective boundary layers. As such, individual phenomena can be explored accurately at length scales relevant to their boundary layers and, therefore, without the severe computational penalties imposed by room size models. The isolation of phenomena and the

associated investigation at small length scales can then enable the characterization of the flow variables, and thus the subsequent determination of the parameters for directly controlling the phenomena.

The proposition that discrete thermal phenomena in a space can be controlled locally and directly is, of course, not new; the microelectronics industry has been actively developing strategies for discrete thermal management for over two decades. The application of this approach to room air behavior, however, seems to be a *non sequitur* for two reasons: (1) the quiescent ambient, considered as an infinite thermal sink in microelectronics cooling, must be controlled within prescribed conditions in building environments, and (2) the high velocity air discharge of typical HVAC systems introduces length scales on the order of room dimensions, superseding any small length scale behavior. By shifting the focus from analysis of existing system responses to analysis of existing thermal inputs, which generally induce buoyant behavior, the high velocity diffuser, and thus its resultant mixed core flow, is no longer a requisite element. The elimination of the dominant mixing behavior should result in an aerodynamically quasi-calm core environment and therefore the thermal inputs can behave as individual bounded phenomena [1]. Indeed, the growing success of displacement ventilation strategies demonstrates that discrete buoyant behaviors can maintain their autonomy if mixing flows are suppressed [2, 3]. More difficult to discard, however, is the first condition which requires the maintenance of a given quiescent ambient. Notwithstanding the economy and contaminant removal efficacy of displacement ventilation systems, they still can not produce the ambient control typified by high velocity induced mixing. It is for this condition that the inclusion of MEMS holds the most promise. The fundamental premise of the author's research is that individual thermal behaviors can be mitigated *before* they affect the ambient conditions, if appropriate action is taken to control heat transfer across the boundary layer. MEMS will eventually enable the local and necessarily discrete interactions along the boundary layer for this control. The key initial step, then, is to begin to determine the relevant variables for controlling heat transfer from a *given* thermal input.

2. The Governing Variables

Thermal behaviors typically produced in rooms can be characterized either as bounded convection, such as induced by surfaces and windows which contain thermal gradients, or unbounded convection, such as induced by people, computers, luminaires, etc. Both types of convection are buoyantly driven and their flows are thus governed by the Rayleigh number, which expresses the balance between the driving buoyancy force and the diffusive processes retarding the motion resulting from that force:

$$Ra = \frac{g\,\beta\,\Delta T\,L^3}{\nu\alpha} \qquad (1)$$

The heat transfer from buoyantly driven convection is governed by the Nusselt number which is defined as the ratio of the heat transport due to buoyancy to the purely diffusive transport resulting only from the temperature gradient:

$$Nu = \frac{h\,L}{k} \qquad (2)$$

Within this relationship, the heat transfer coefficient, h, is dependent upon the specific flow characteristics, and thus is typically empirically derived. When the Nusselt number is equal to one, heat transfer is purely by conduction. Unfortunately such general conclusions can not be made regarding convection and there are numerous formulations for the local Nusselt number, most of which are in a form similar to $Nu_x = f_1\,(Pr)\,Ra_x$ where Pr is the Prandtl number (0.71 for air) and the function f_1 is empirically derived [4].There are distinct formulations for each given flow description, as well as modifications depending upon the flow regime. The complexity of determining the Nusselt number, and thus the local heat transfer, has led many room air modelers to substitute wall functions rather than suffer the computational penalty necessary for direct determination [5]. While adequate for estimating the overall heat transfer, wall functions are not sufficient for accurate characterization of boundary layer flow. Therefore, with the exception of h, all of the variables for determining the Nusselt and Rayleigh numbers are generally considered as givens, in that for a known thermal input in a particular space, the temperatures, length and properties are all prescribed.

3. The Characteristic Length

In natural convection scenarios, however, the characteristic length is not always representative of the same dimension. Depending on the flow description, the characteristic length may be equal to the height of a vertical isothermal surface or the square root of the area of a horizontal surface [6]. In addition, if isothermal vertical surfaces are closely spaced, the characteristic length reverts to the horizontal spacing, and particularly interesting relationships emerge if surfaces are tilted [7]. Microelectronics cooling strategies depend heavily on the management of characteristic length to maximize heat transfer to the ambient environment. The key element determining the resulting characteristic length is the relative location of the cold sink. In conventional HVAC systems, there are two types of cold sinks; the first is produced by the enthalpic sponge of the supply air and the second is the chiller, both of which have no length relationship with a specific room thermal input. By accepting the premise that MEMS will eventually allow local placement of discrete sinks, then there is the potential to manipulate the effective characteristic length of any given thermal behavior in a room. As such, the governing Rayleigh number and the resulting boundary heat transfer coefficient can then be manipulated to control the heat transfer.

4. Numerical Modeling

The initial investigation into the possible determinants of characteristic length was carried out numerically, using the commercially available CFD code FIDAP. FIDAP 7.5 is a sophisticated finite element package that is little used for building simulations, because of its complexities, but is routinely used for the simulation of microelectronic heat transfer. Two basic models were developed. The first model acted as the simulation validation and was based on the classic numerical benchmark for natural convection [8]. In addition, it served as the baseline determination of the relationship between the dimensionless Rayleigh and Nusselt numbers as driven by the characteristic length. The second model was dimensioned, and was developed to explore the relationship between cold sink location and heat transfer. This relationship has been expressed as an "effective" characteristic length, in that as the cold sink location relative to the thermal input shifts, the characteristic length which determines the Rayleigh and Nusselt numbers will shift even as the dimensions are unchanged. The boundary conditions for both models are shown in Figure 1.

The first model is a square cavity with isothermal vertical surfaces and adiabatic horizontal surfaces. As it is non-dimensional, the input physical properties are replaced with the following parametric values:

$$\rho = \sqrt{\frac{\mathrm{Ra}}{\mathrm{Pr}}}$$

$$c_p = \mathrm{Pr}$$

$$\mu = g = \beta = k = 1$$

For air, with a constant Prandtl number, the Rayleigh number is the only variable influencing convective behavior inside of the cavity, and assuming that the input temperatures are given, then the characteristic length is the only variable driving the Rayleigh number. An order of magnitude comparison of Rayleigh numbers, from 10^3 to 10^8, was carried out not only to demonstrate the non-linear relationship between characteristic length and the Nusselt number, but also to determine the Nusselt number profiles across the boundary of the heated wall. For the higher Rayleigh number simulations, a finer mesh was used in the numerical model along the boundaries (with first node points located 0.4 mm from the boundary).

The second model is also a square cavity, but with embedded plates acting as the isothermal surfaces. All of the input variables are fixed---dimensions, temperatures and physical properties--- and only the location of the isothermal plates is varied in each case (see Fig. (2) for plate orientation). A fine mesh model allows direct determination of the heat transfer coefficient, and if the Nusselt number is held constant for the cases then the following relationship must exist between the heat transfer coefficient and the characteristic length among the different cases:

$$\frac{h_i}{h_j} = \frac{L_j}{L_i}$$

Using this relationship with the actual input conditions would then produce an "effective characteristic length as relative to the normative characteristic length represented by the benchmar case orientation (indicated by the subscript *i*). This effective length supplants the actual surfac dimension or spacing that is typically assumed for this value. The effective Rayleigh number ca then be determined for each orientation.

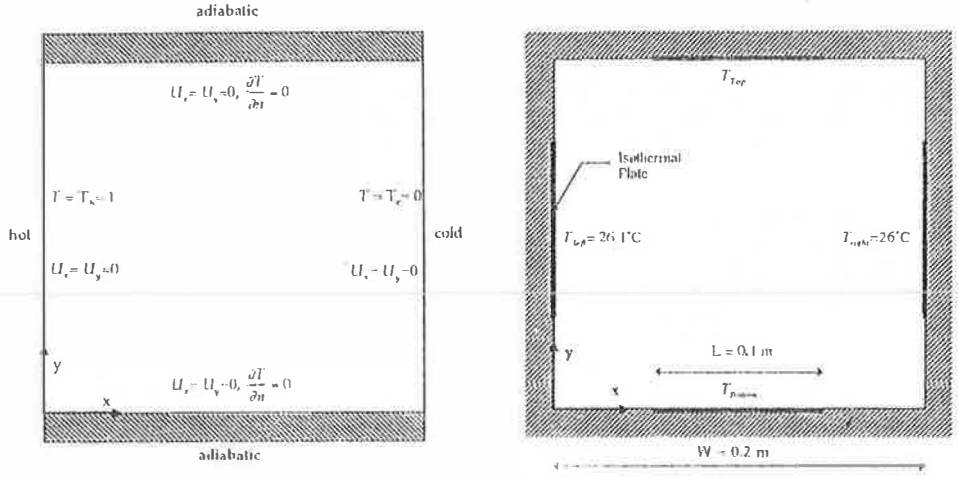

Figure 1: Boundary conditions of dimensionless model(left) and dimensioned model (right)

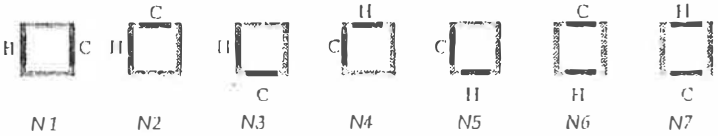

Figure 2: Isothermal plate orientations for dimensioned model simulations

5. Simulation Results

The results for the first model are summarized in Table (1). The purely diffusive case, Ra=10^3, is considered to be the baseline with all dimensions normalized to one. By forcing th isothermal temperatures to remain constant, then each successive order of magnitude increase i Rayleigh number can only be achieved by increasing the characteristic length by a factor of $10^{1/}$ The ratio L_c / L_i, then, simply represents the relationship of the characteristic length of the highe Rayleigh number cases to the diffusive case. The Nusselt number in the table represents th average of the local Nusselt numbers along the height of the hot isothermal boundary. Fig. (3 compares the plots of the local Nusselt number profiles for all the cases.

Ra	10^3	10^4	10^5	10^6	10^7	10^8
L_c / L_i	1	2.15	4.64	10	21.5	46.4
Nu	1.11	2.25	4.56	9.13	15.82	27.56

Table 1

As boundary layer flow becomes established at Rayleigh numbers above 10^5, the gradient of the local Nusselt number profile becomes more pronounced. If the Nusselt number is also plotted across the boundary layer rather than only along it, the gradient disappears at increasingly closer distances to the boundary as the Rayleigh number increases (at $Ra=10^8$, the gradient becomes flat at a distance of 0.018 x L from the boundary).

The results for the second model are summarized in Table (2). The first three cases—N1, N2 and N3—are simulated with a vertical isothermal warm surface, and the remaining cases are for a horizontal placement. The benchmark case, N1, is considered to be the baseline, and therefore the ratio L_j/L_1 represents the relationship of the normative characteristic length for each case to that of the base case, as determined from the average heat transfer coefficients; whereas L_{eff}/L is the calculated, or apparent, characteristic length for each case in relationship to the actual dimension. The effective Rayleigh number can then be determined using L_{eff}.

	N1	N2	N3	N4	N5	N6	N7
h_{avg}	0.077	0.0828	0.0495	0.053	0.0795	0.0245	0.0187
L_j/L_1	1.0	0.93	1.56	1.45	0.97	3.14	4.12
L_{eff}/L	1.0	1.075	0.64	0.69	1.03	0.318	0.243
Ra_{eff}	9.2×10^4	1.1×10^5	2.4×10^4	3×10^4	1×10^5	2.9×10^3	1.3×10^3

Table 2

Two orders of magnitude separate the highest Rayleigh number case from the lowest, which is an additional order beyond what the literature predicts [9]. Figure (4) compares the plots of the local heat transfer coefficients along the boundary (calculated at nodes .009 m from the heated surface) for the two groups of cases. As one would expect, when both the warm surface and cold sink are oriented horizontally, as occurs in N6 and N7, then boundary layer flow, and thus heat transfer, is suppressed.

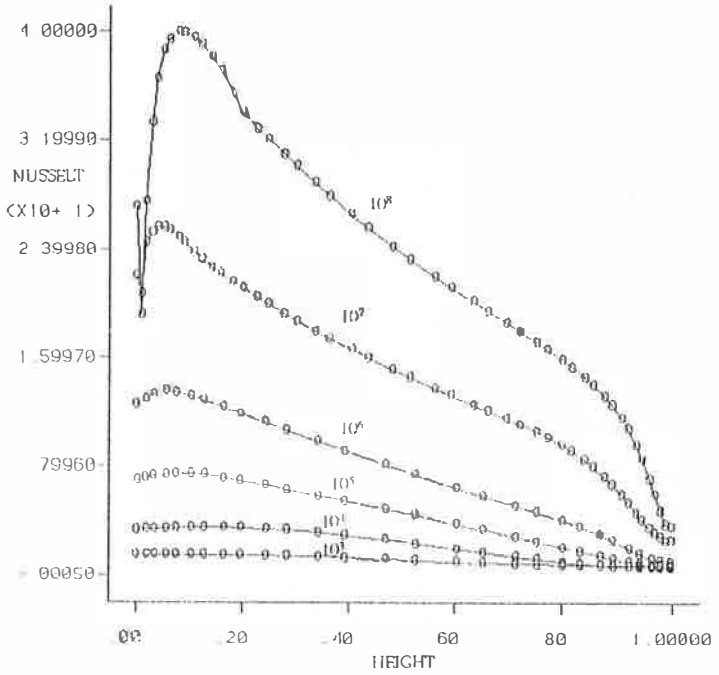

Figure 3: Local Nusselt number profiles for Rayleigh numbers 10^3 to 10^8

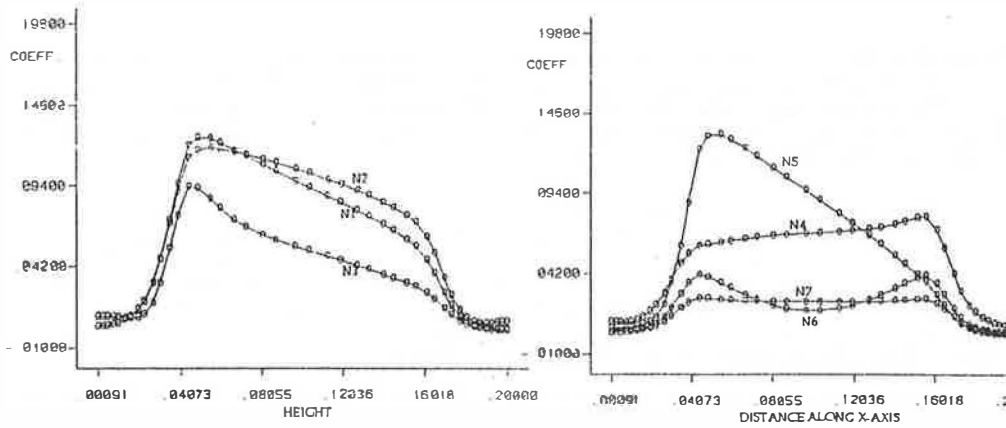

N cases with vertical heated plate

N cases with horizontal heated plate

Figure 4: Local Nusselt number profiles for cases with vertical (left) and horizontal (right) sources

6. Conclusions

The cases discussed in this paper were chosen to demonstrate the potential impact of characteristic length manipulation to alter boundary heat transfer. The author concedes that a substantial amount of verification work must take place before any substantive conclusions can be drawn. In addition, further simulation studies need to be carried out to determine the limiting factors which may impact the allowable spacing between source and sink and thus reduce the boundary layer interaction. Nevertheless, it is clear that thermal phenomena can be controlled locally and directly by shifting the "effective" characteristic length, even if none of the dimensions or parameters of the thermal input are in themselves altered. As an example, if a window that is 1 m. high by .5 m. wide is rotated 90° then the heat transfer can be reduced in half, even as the total surface area remains unchanged. Judicious placement of the cold sink can significantly change not only the effective characteristic length, but also the gradient of the heat transfer coefficient, indicating that the potential exists to selectively manage heat transfer at discrete locations. Although one can apply the results of this work to surfaces of any size, MEMS affords the greatest flexibility in placement. The author's current work in modeling point sources and sinks with slip flow boundaries is investigating the potential of discrete placements to manage local transport of particles, and initial studies have shown that very small interventions near boundary layers can significantly redirect particle momentum and deposition.

References

(1) Popiolek, Z., 1993, "Buoyant Plume in the Process of Ventilation—Heat and Momentum Turbulent Diffusion," Proc. Annex-26 Expert Meeting, Poitiers, France.

(2) Cooper, P., and Linden, P.F., 1996, "Natural ventilation of an enclosure containing two buoyancy sources," *J. of Fluid Mech.*, Vol. 311.

(3) Ostrach, S., 1988, "Natural Convection in Enclosures," *J. of Heat Transfer*, Vol. 110.

(4) Gebhart, B., Jaluria, Y., Mahajan, R., and Sammakia, B., 1988, *Buoyancy-Induced Flows and Transport*, Hemisphere Publishing Corp., Washington.

(5) Yuan, X., Moser, A., and Suter, P., 1993, "Wall functions for numerical simulation of turbulent natural convection along vertical plates," *Int. J. of Heat Mass Transfer*, Vol. 36

(6) Leal, L. G., 1992, *Laminar Flow and Convective Transport Processes*, Butterworth-Heinemann, Boston.

(7) Incropera, F. P., 1988, "Convection Heat Transfer in Electronic Equipment Cooling," *J. of Heat Transfer*, Vol. 110.

(8) FIDAP, 1993, *FIDAP 7.0 Examples Manual*, Fluid Dynamics International, Evanston.

(9) Yovanovich, M. M., and Jafapur, K., 1993, "Bounds on Laminar Natural Convection from Isothermal Disks and Finite Plates of Arbitrary Shape for all Orientations and Prandtl Numbers," *Fundamentals of Natural Convection*, ASME HTD, Vol. 264

Guidelines for Ventilation During the Repairing Process of Ship-Hull in an VLCC

Kong HC, H Sun, Xu WQ, Koh CN
Singapore Productivity and Standards Board
1 Science Park Drive, Singapore 118221

ABSTRACT

During the repairing process of the ship hull of a very large crude carrier (VLCC), large amount of smoke, heat and harmful gases are generated. In order to improve the productivity of the workers, their health condition and safety, ventilation is needed to have better indoor air quality. A new ventilation system is proposed which basically transfers fresh air from the deck (top) to the bottom of the ship-hull via an air duct and then spread to the entire ship hull by an air-distributor before being sucked out at the deck. A set of design and usage guidelines for this ventilation system was prepared for the convenience of engineers' use. It caters for ship hulls of different dimensions and the number of air-distributors, supply and suction fans to be used. It is important that in order to achieve maximum ventilation efficiency, due to different physical characteristic for different ship hull, correct configuration must be selected from the guidelines.

1. INTRODUCTION

1.1 During the repairing process of the ship hull of a very large crude carrier (VLCC), large amount of smoke, heat and harmful gases are generated. From experimental analysis, smoke and dust are the main harmful substances produced. In order to improve the productivity of the workers and their safety, the ship hull needs to be ventilated. The main purpose of this ventilation is therefore to reduce the level of smoke and dust concentration to an acceptable and safe level. At present, there is no any international standards for ship-repairing ventilation. With reference to the present ship-building ventilation (Japan) standards, the acceptable smoke and dust concentration level is 3 mg/m^3.

1.2 The ship hull repairing has the following characteristics:

a. The ship hull is very large;
b. a number of harmful substances are generated;
c. the repairing locations are not fixed;
d. the amount of repair required at each location is not fixed;
e. the internal construction of the ship-hull is complex;
f. the number of openings on the deck are limited;
g. the repair duration is short (from one week to one month);
h. the ventilation system needs to be dismantled after the repairing works.

1.3 With the above characteristics, the following ventilation system has been designed (see Fig. (1)).

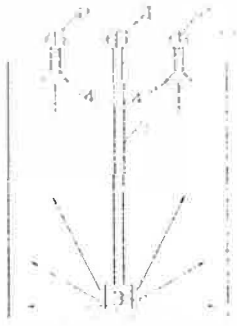

1. air supply pump
2. air suction pump
3. air-distributor
4. suction hoods
5. air duct

Figure 1: Air flow pattern of the ventilation system

Fresh air is supplied from the deck by air supply pump 1, via air duct 5 to the air-distributor 3 at the bottom of the ship-hull. The air is then spread through the entire ship-hull by the air distributor before being sucked out via suction hood 4 by air suction pump 2 to the atmosphere. The above proposal can be referred to as "all-directional, global ventilation using the push-pull and upward moving displacement method".

This configuration has several advantages:

a. The displacement type of ventilation not only conforms to the construction characteristic of the ship hull, it also follows an upward-flowing flow pattern. This aids the process o removing the harmful substances in the hull while reducing the risk of explosions.

b. The different elevated-angled supply of air reduces the amount of circulation whil raising ventilation efficiency and saving energy.

c. The ventilation system is simple (Fig. (1)) making the task of assembling / dismantlin easy. Thus it is suitable for short duration works such as ship repair.

d. The jet of air from the air distributor is able to supply air to the working zones improvin the working conditions.

2. DESIGN PROCEDURES OF THE VENTILATION SYSTEM

2.1 Determination of the Air-Flow Rate

2.1.1 According to the dimensions of the ship-hull, the layout and number of the air distributors are chosen. From there, the air flow rate L_1 is determined. For example, dimensio of ship hull already known $l \times w \times h = 40m \times 20m \times 20m$. From Table 7, two air-distributors ar required with air flow rate $L_1 = 2 \times 13000 = 26000 m^3/h$.

2.1.2 According to the allowable smoke and dust concentration level, the air flow rate L_2 i calculated.

$$L_2 = \frac{M}{C_2} \bullet K$$

where: K is the safety factor, taking K = 4.

C_2 is the allowable smoke and dust concentration level, taking $C_2 = 3 mg/m^3$.

M is the rate of generation of smoke and dust i.e. $M = n_c m_c + n_w m_w$

n_c, n_w are the number of workers doing cutting and welding respectively.

m_c, m_w are rates of generation of smoke and dust due to cutting and weldin respectively. (see Table (1), ref.(1)).

Table 1: Rates of generation of smoke and dust due to cutting and welding

Experiment No.		1	2	3	4	Average
m_c (mg/s/torch)	heavy rusting	0.16	0.20	0.26	0.17	0.20
m_w (mg/s/torch)	no rust	0.13	0.12	0.07	-	0.11

1.3 Lastly, by comparing L_1 and L_2, the larger air flow rate is chosen.

2 *Precautions and Treatments to be Taken when Setting up the System*

2.1 Flexible plastic tubings are used as the ducts. Due to its flexibility, special precautions d treatments are needed when the duct passes through the deck opening, when bending is quired and when the duct needs to be joined either to one another or to the air-distributor.

For the portion from the fan exhaust to the deck opening of the ship hull (Fig. (2)), the duct should be made of rigid material to reduce the pressure loss due to any acute bending.

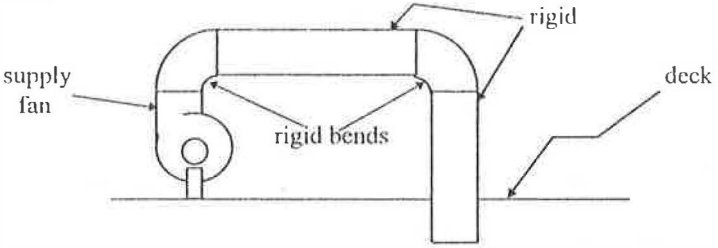

Figure 2: Portion from the fan exhaust to the deck opening of the ship hull.

At the joint of the duct and entrance of the air distributor, the vertical angle, α, between the duct and the air distributor must be less than 15° (i.e. $\alpha < 15°$). This is to prevent a lobe-sided distribution of air to the air-distributor.

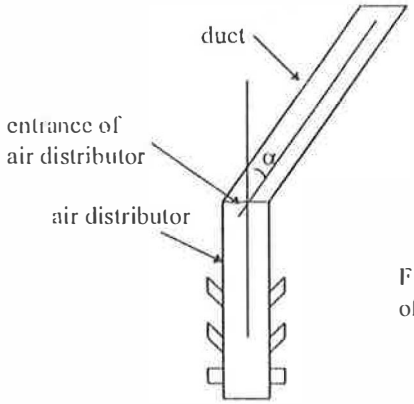

Figure 3: Joint of the duct and entrance of the air distributor.

2.2 The duct diameter should not be less than ϕ400mm. This is because smaller diameter ould result in higher resistance and cause a pressure rise.

2.3 At the exhaust, there **should not** be any gap between the suction pump and the deck ening. This is to prevent any short circuit of the air flow which would affect the effectiveness d efficiency of the suction pump. If any gap does exist, it should be properly sealed.

Not Correct

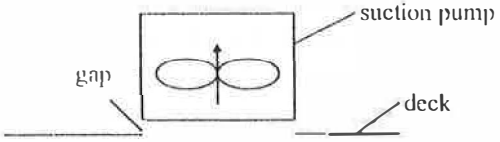

Correct

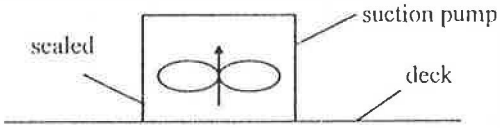

Figure 4: No gap should be between the suction pump and the deck opening.

2.3 *Determination of the resistance of the duct and air distributor*

2.3.1 Some of the resistances for different flow rates are listed in Table (2) whereby the tota resistance of the system can be calculated as follows:

Total resistance = Frictional loss + Local loss + Air distributor resistance.

Table 2: AD400 ventilation system internal resistance for different air flow rate.

Air flow rate (m^3/h)	Frictional loss per unit length (Pa/m)	Frictional loss* (Pa)	Local loss@ (Pa)	ξ_{AD}+ (total pr./ dyn. pr.)	Resistance of air distributor (Pa)	System total resistance (Pa)
6000	4.0	120	60	5	530	710
7000	5.0	1500	75	5	720	945
8000	6.0	180	90	5	940	1210
9000	8.0	240	120	5	1190	1550
10000	10.0	300	150	5	1470	1920
11000	11.5	345	173	5	1770	2288
12000	13.0	390	195	5	2110	2695
13000	15.0	450	225	5	2480	3155

* duct diameter = 0.4m + obtained experimentally

duct length = 30m @ local loss is taken as 0.5 times of frictional loss

2.4 *Selection of fan*

From Table (2), with reference to the air flow rate and total resistance, the fan is selected

2.5 *Determination of layout and number of air distributor in the ship hull*

2.5.1 Fig. (5) shows the different layouts and arrangements of the air distributor(s) for differer ship hull sizes. This is for selection and reference during the designing process.

5.2 The largest length that will be discussed here is 40m. The ratio for the ship hull dimension is $l : w : h = 1 : (0.5\text{-}1.0) : 0.5$.

5.3 In the Fig. (5), "O" represents the air distributor. The recommended air distributor is Model AD400 (i.e. the entrance pipe diameter of ϕ400mm). The air flow rate has a range of 6,000-14,000 m^3/h.

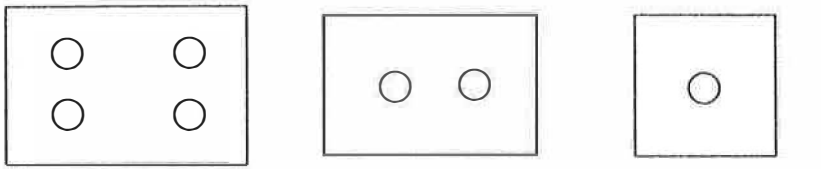

(a) Four AD required (b) Two AD required (c) One AD required

Figure 5: Plan view of position of the air distributors (AD) in the ship hull when different number of AD are required.

5.4 The relationship between the air flow rate and the distance reach by the jet of the air distributor is governed by the equation (ref.(2))

$$\frac{v_s}{v_o} = \frac{0.48}{\frac{as}{d_o} + 0.147}$$

Table 3: Relationship between the air flow rate and distance reach by the jet of air distributor

Air flow rate (m^3/h)	9000	10000	11000	12000	13000
Velocity at the nozzle v_o (m/s)	21.7	24.1	26.5	28.9	31.3
Distance, s, reach by the jet (m)	6.8	7.6	8.3	9.1	9.9
Remarks	Taking: Final axial velocity v_s = 1.5 m/s Turbulence coefficient a = 0.09 Number of nozzles = 18 (of 0.08 x 0.08 m) Equivalent diameter, d_o, of nozzle = 0.09m				

5.5 The suction rate at the exhaust is determined by the number of openings available on the deck and the exhaust rate **must be equal** to the supply rate.

5.6 Some of the recommended supply flow rates and the number of air distributors to be used are shown in Tables (4) to (7).

Table 4: $\frac{l}{w} = 1.0$

Ship hull's l (m) x w (m)		30 x 30	25 x 25	20 x 20	15 x 15
No. of air distributor AD (unit)	13,000 m^3/h/AD			1	
	12,000 m^3/h/AD				
	11,000 m^3/h/AD				
	10,000 m^3/h/AD	4			1
	9,000 m^3/h/AD		4		

Table 5: $\frac{l}{w} = 1.2$

Ship hull's l (m) x w (m)		40 x 33	35 x 29	30 x 25	25 x 21
No. of air distributor AD (unit)	13,000 m^3/h/AD	4			
	12,000 m^3/h/AD		4		
	11,000 m^3/h/AD				
	10,000 m^3/h/AD			4	
	9,000 m^3/h/AD				4

Table 6: $\frac{l}{w} = 1.6$

Ship hull's l (m) x w (m)		40 x 25	35 x 22	30 x 18	25 x 16
No. of air distributor AD (unit)	13,000 m^3/h/AD	4			
	12,000 m^3/h/AD		4	2	
	11,000 m^3/h/AD				2
	10,000 m^3/h/AD				
	9,000 m^3/h/AD				

Table 7: $\frac{l}{w} = 2.0$

Ship hull's l (m) x w (m)		40 x 20	35 x 18	30 x 15	25 x 13
No. of air distributor AD (unit)	13,000 m^3/h/AD	2			
	12,000 m^3/h/AD		2		
	11,000 m^3/h/AD				
	10,000 m^3/h/AD			2	
	9,000 m^3/h/AD				2

3. ACKNOWLEDGEMENT

We would like to take this opportunity to express our greatest appreciation and thanks to National Science & Technology Board of Singapore (NSTB), Jurong Shipyards Limited (JSL) management and staff and all those who have helped in one way or another to the success of this project.

4. REFERENCES

(1) Xu WQ, Sun QQ, H Sun, etc, "Ventilation Study of Very Large Crude Carrier (VLCC) During Ship Repair", The 2nd Int'l Symposium on HVAC, Tsinghua-HVAC '95, Beijing, China, Vol. 2, 25-27 Sept 95.

(2) V.V. Baturin, "Fundamentals of Industrial Ventilation", Pergamon Press Ltd, Headington Hill Hall, Oxford U.K. (1972).

(3) Xu WQ, Sun HC, Sun QQ, etc, "Investigation of Air Flow Pattern of the Ventilation System in the Repair Process of VLCC", The 7th Int'l Conf. on Indoor Air Quality and Climate, Indoor Air '96, Nagoya, Japan, 21-26 July 1996.

(4) Xu WQ, Sun HC, Sun QQ, etc, "Design and Study on Three Dimensional Jet Air Distributor", The 7th Int'l Conf. on Indoor Air Quality and Climate, Indoor Air '96, Nagoya, Japan, 21-26 July 1996.

Feasibility Study of Applying The Cool Thermal Energy Storage for Department Store

Chutchawan Tantakitti, Ph.D
Associate Professor

Santichai Leeyutthanont[+]
Graduate Student

Mechanical Engineering Department
Faculty of Engineering
Chiang Mai University
Chiangmai 50200
THAILAND

Abstract

950 buildings in Thailand have to be charged with the time-of-day rate, about 120 buildings re the department store where the cooling load demand during on-peak period is 20-30 % of he building demand. The cool thermal energy storage can be substituted this demand. The detail audit had been conducted in the department store for 15 days. DOE2.1 E program has been used for the simulation and the results are verified. After that, 3 cases of TES operation types, namely full-storage, partail-storage and demand-limit storage with 10 hours charging period and combined with the ice-harvester and ice-on-coil are studied . The results show that he ice harvester with demand-limit storage and 10 hours charging can drop 657.4 kW of peak nd save $US 58,295 of electricity with the investment of $US 611,616. It has 9.08 years payback period and 8.88 % EIRR. Further study also shows that 20 hours charging associated with demand-limit storage and ice-harvester gets even better results. The utility saving is $US 61,120 with the investment of $US 324,768. This gives 5.94 years payback period and 16.96 % EIRR.

1. Introduction

The time of day rate (TOD) has been applied to 950 buildings (1) in Thailand. The demand charges are $US 0.0, 2.52 and 12.2 for off-peak (9.30 PM. - 8.00 AM.), partial-peak (8.00 AM.- 6.30 PM.) and on-peak (6.30 PM.-9.30 PM.) respectively. The energy charge is $US 0.0428/kWh flat rate. Also,these buildings have to be under the Energy Promotion and Conservation Act 1991. That means, from January 1996 they have to do a preliminary energy audit in 6 months to find the potentials of energy conservation measures and detail audit afterward. Some expenses will be supported by the Department of Energy Development and Promotion (DEDP). At the same time, the Electric Generation Association of Thailand (EGAT) also launches the Demand Side Managemnet (DSM) Program, purposely, not only to save energy but also to improve the system's load factor. The saving measures are, namely, replaced 20 and 40 Watt by 18 and 36 Watt fluorescent lamp, high efficiency refrigerator and air-conditioning and installed the cool thermal energy storage (TES). Hopefully that these will shift the power peak to off-peak period. This paper show the potential of using TES in the department store.

2. Detail Energy Audit

5 storey department store has been in the operation since 1992. There are 42,184 sq.m. utilized area with 38,494 sq.m. air-conditioning space. The working hour is from 10.00 AM. - 10.00 PM. everyday.

Building Function *Underground floor*- supermarket and food center. *1st-3rd floor*- department store and shopping center. *4th floor* - playground, theater and shops.

Building Structure *Floor* - 3 m. height floor-to-floor, 30 cm. thick reinforced concrete topping with marble, except machine room. *Wall* - 2 layers of 10 cm. brick with air gap in between. *Roof*- 30 cm. thick reinforced concrete top with waterproof materials. *Window*- 8 and 10 mm. thick single-glassed clear, stick wth film.

Space load 3,205 x 36 Watt and 1,356 x 18 Watt recessed fluorescent lamps, 2,618 x 9 Watt compact bulbs with external ballast, 1,330 x 50 Watt halogen lamps, lighting density of 1.1, 1.7 and 2.2 W/sq.ft for plaza shops and food center respectively. Infiltration 0.04, 0.05 and 0.08 airchanges/hr. for plaza, offices and the food center, respectively.

HVAC System Temperature setpoint = 76 °F, outside air 7 CFM/person.

Chillers 5 x 500 TR water cool, Hermatic centrifugal chiller with energy input ratio of 0.1764 at ASHRAE standard and 10 % part load ratio.

3. Verification

The input for DOE2.1 E (2) had been written and simulated with 1994 Chiangmai TRY format weather data. The results, such as chiller consumptions and chiller pumps, monthly peak demand and energy consumptions, had been compared with the actual ones. The difference is less than 8 %, so the input is good enough to represent the building performance.

4. Cool Thermal Energy Storage

Since the building has been installed with normal chillers. Ice thermal energy storage with plate heat exchanger is selected due to less space need and complication. The ice-harvester and ice-on-coil (external melt) which 3-type of operations, namely full-storage, partial-storage (one chiller as base load) and demand-limit, are studied.

Storage sizing To find the storage size of each operation types, hourly cooling load of that peroid are summed up. 12,700, 6,675 and 3,315 Ton-hours are the sizes of full-storage, partial-storage and demand-limit respectively.

Icemaking machine sizing Dividing the storage's size with daily operating hours will get the size of icemaking machine. For all operation types, the operating hours are 10 hours (10.00 PM.-8.00 AM.). For the ice-on-coil due to ice formation on the outside causes the insulation effect , sothat, the machine's size is 10 % larger than the ice-harvester.

TES investment The cost for TES system are from I.T.C. Co.,Ltd (3) and Temp Tech Engineering Co.,Ltd (4).

5. Results and Discussion

5.1 10 Hours Charging System

Effect on Peak Demand - Monthly peak demand of each period (PP. - partial-peak, OP - on-peak) except off-peak (OF.P.) for an ice-harvester and ice-on-coil are considered. For partial storage, since one chiller operates as base load. The demand will increase from full storage case, but the demand is still less than basecase because only one chiller operates in this period. For demand limit, the demand on a partial-peak will be the same as a basecase due to the same operation. Except the on-peak period, the demand will be the same as full storage case. Both the ice-harvester and ice-on-coil show the same result on the demand drops.

Effect on Monthly Energy Comsumption - Monthly energy consumption of 3 cases using the ice-harvester are studied. With TES, monthly energy consumption is no doubt increased due to lower COP of the system and also waterpumps are added. As comparing between these two types, the ice-on-coil type consumes more energy than the ice-harvester type due to increasing the insulation effect of ice formed around the tubes.

Electric Tariff Figure 1(a) illustrates the tariff of each system. With the ice-harvester, total electric tariff is less than basecase because the decrease in peak demand cost is more than the increase in energy cost. Figure 1(b) shows for the ice-on-coil case. As comparing between the ice-harvester and ice-on-coil, the energy cost of the ice-harvester is less than the ice-on-coil. Because, even both systems have the same drop in peak demand but the ice-on-coil consumes more energy than the ice-harvester. Considering all cases, the demand limit case with the ice-harvester is the least electric cost.

Economic Interest Rate of Return (EIRR) and Pay Back Period (PBP)

To calculate the EIRR and PBP the following inputs are applied, the investment , the saving , the conversion factor for equipment = 0.88349, the conversion factor for labor = 1, the electricity cost 0.074 $US/kW-hr., the inflation 6.5%, the inflation for energy = 1% to 1999 A.D.and 4.5% from 2000 A.D., the equipment life 16 years.

Table 1(a), (b) show the EIRR and PBP for each cases of the ice-harvester and ice-on-coil. The demand limit case with the ice-harvester is the best based on of the EIRR and PBP.

Since, the ice-harvester, with 10 hours charging (22.00 - 08.00 hrs.) and 4 hours discharging (18.00 - 22.00 hrs.), shows the best selection for investment.

By looking carefully to this system, it is interesting to find out if the charging hours is extended to 20 hours. This way, the ice-making machine size will be reduced to half of 10 hours charging, therefore, the investment decreases. But, since the ice-making machine has to run on the partial-peak period, sothat the cost of demand on partial-peak increases. However, the cost of demand charge on partial-peak is only 2.52 $US/kW., possible the EIRR and payback period are better.

5.2 20 Hours Charging System with Demand Limit

Since, both the ice-harvester and ice-on-coil are considered at the beginning, sothat both cases will be analyzed for this case. DOE 2.1E Program cannot simulate on this case due to the limit of program. Therefore, the new procedure is applied, based on the following assumptions. *For the ice-harvester* - The average kW/TR of chiller at chiller-mode and ice-mode are 0.76 and 1.27, respectively. *For the ice-on-coil* - The calculation is the same as Ice-

Harvester except the average kW/TR at ice mode is 1.56. Table 2 shows the energy consumption of both cases.

Electric Tariff The electric tariff consists of two parts namely energy cost and demand cost. The energy cost is obtained from multiplied the energy consumption in Table 2 by 0.0428 $US/kW-hr. The demand cost is obtained by added the partial-peak demand increase with the partial-peak on the base case as shown in Figure 2 and multiplied with 2.52 $US/kW. The sum of these two costs is yearly electric cost of both systems.

Investment The investment for the ice-harvester and ice-on-coil are $US 324,768 and 666,555 respectively.

EIRR and Pay Back Period Table 3 compares the results of both systems. The best selection is the ice-harvester with 20 hours charging because the EIRR and PBP are 16.96 % and 5.94 years. If considering between 10 hours and 20 hours charge with the ice-harvester system. It is found that 20 hours charge ice-harvester gives better EIRR and PBP (16.96 %, 5.94 years) than 10 hours charge (8.88 %, 9.08 years).

6. Conclusion

This department store has the potential to install the ice-harvester which the details are: Ice-making machine 166 TR-Ice-mode with 20 hours charging, ice storage tank 5 x 5 x 13.3 m^3 (3315 Ton-hr.), heat exchanger 1100 TR at ΔT 5 °C. Total investment are $US 324,768. EIRR = 16.96 %. Payback Period = 5.94 years. This study does not include the concrete work.

Reference

1. "Feasibility study for Control Buildings in Thailand", Department of Energy Development and Promotion, Ministry of Science, Technology and Environment, August 1995.
2. "Micro-DOE2.1E", ERG/Acrosoft International Inc., CO 80127, USA.
3. I.T.C. Co.,Ltd, 20/103 Soi Soonkarnkha, Sukhaphiban 3, Ramkhamhaeng Rd., Bangkapi, Bangkok, 10240,Thailand.
4. Temp Tech Engineering Co.,Ltd., 65/300 Moo 6 Ekachai Rd., Bangbon, Bangkhuntien, Bangkok 10150, Thailland.

Table 1(a) Results of EIRR and PBP of Ice-Harvester (10 hours)

	Full Storage System	Partial Storage System	Demand-Limit System
Investment ($US)	2,281,560	1,194,084	611,616
Saving ($US)	25,980	17,694	58,295
EIRR (%)	-	-	8.88
Payback Period (Years)	unprofitable	unprofitable	9.08

Table 1 (b) Results of EIRR and PBP of Ice-on-Coil (10 hours)

	Full Storage System	Partial Storage System	Demand-Limit System
Investment ($US)	3,101,782	1,608,065	811,490
Saving ($US)	-11,049	5,100	49,217
EIRR (%)	-	-	2.75
Payback Period (Years)	unprofitable	unprofitable	13.29

Table 2 Yearly Energy Consumption of 20 hours (kWh)

	Base Case	Ice Harvester	Ice-On-Coil
Total	10,657,446	11,021,690	11,228,809

Table 3 Results of EIRR and PBP (20 hours)

	Ice Harvester	Ice-On-Coil
Investment ($US)	324,768	666,555
Saving ($US)	51,120	40,020
EIRR (%)	16.96	2.28
Payback Period (Years)	5.94	13.70

Figure 1 (a) Tariff of Ice-Harvester

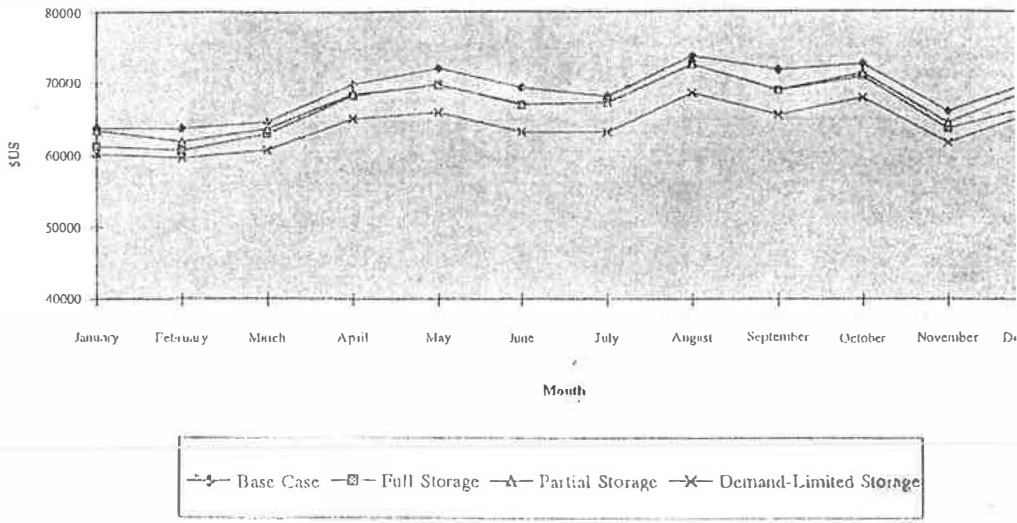

Figure 1 (b) Tariff of Ice-on-Coil

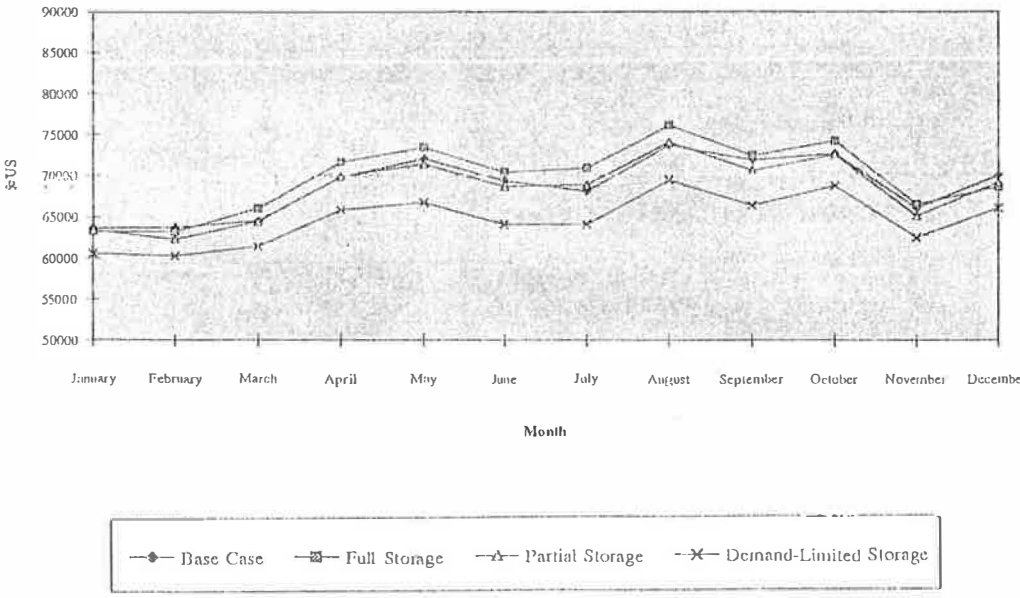

Demand-Limit Thermal Energy Storage for Commercial Buildings

Chutchawan Tantakitti, Ph.D.
Associate Professor
Mechanical Engineering Department
Faculty of Engineering
Chiang Mai University
Chiangmai 50200
THAILAND

Abstract

950 buildings (192 hotels, 69 hospitals, 395 offices and 297 other) in Thailand have to be charged with the time-of-day rate. The cool thermal energy storage can be substituted this demand. The detail audit had been conducted in 3 types of buildings, namely office, hotel and hospital for 15 days. Preliminary analysis shows that changing the light fixture, decreasing the peak demand and improving the coefficient of performance of chillers have the energy conservation opportunity . The electricity cost savings are $US/year 18,016, 84,000 and 10,420 with the investment of $US 9,000, 487,560 and 13,630 for the office, hotel and hospital respectively. Afterthat, DOE2.1 E program has been used for the simulation and the results are verified. The demand-limit storage with 10 and 20 hours charging period and combined with the ice-harvester and ice-on-coil are studied . The results show that the ice-harvester is the best investment for all buildings. Both charging hours can reduce the power peak on the on-peak period by 447.5 kW for the office, 678.2 kW for the hotel and 262.3 kW for the hospital on the peak month. For the office, 20 hours charging hours is the best with the investment of $US 254,880 and the saving of $US 36,665 sothat it has 8.9 years payback period and 9.08 % EIRR . For the hotel and hospital, 10 hours charging period is the best due to 24 hours working of the building. The investment is $US 420,550 and $US 146,520 and the saving is $US 54,590 and $US 22,000 for the hotel and hospital respectively. Considering on the economic, 7.0 years payback period and 13.62 % EIRR is for the hotel, and 7.1 years payback period and 13.06 % EIRR for the hospital.

1. Introduction

The time of day rate (TOD) has been applied to 953 buildings (1), (192 hotels, 69 hospitals, 395 offices and 297 other) in Thailand. The demand charges are $US 0.0, 2.52 and 12.2 for off-peak (9.30 PM. - 8.00 AM.), partial-peak (8.00 AM.- 6.30 PM.) and on-peak (6.30 PM.-9.30 PM.) respectively. The energy charge is $US/kWh 0.0428 flat rate. Also,these buildings have to be under the Energy Promotion and Conservation Act 1991. That means, from January 1996, they have to do a preliminary energy audit in 6 months to find the potentials of energy conservation measures and detail audit afterward. Some expenses will be supported by the Department of Energy Development and Promotion (DEDP). At the same time, the Electric Generation Association of Thailand (EGAT) also launches the Demand Side Managemnet (DSM) Program, purposely not only save energy and also improve the system's load factor. The measures are namely, replaced 20 and 40 Watt by 18 and 36 Watt fluorescent lamp, high efficiency refrigerator and air-conditioning and installed the cool thermal energy storage (TES). Hopefully, that these will shift the power peak to off-peak period. This paper shows the potential of using TES in the office, hotel and hospital.

2. Detail Energy Audit

Three types of buildings had been detailly audited which can be described as follow,

Office -11-storey building and 6-storey parking lot have been in the operation since 1986. There are 37,184 sq.m. utilized area with 19,602 sq.m. air-conditioning space. The working hour is 12 hours.

Building Function *Ground - floor* - lobby, security office, store and contorl room. *1nd- floor* accounting. *2nd - floor* financial and computor rooms. *3rd- floor* Oversea service. *4th- floor* loan office. *5th - floor* training center, library and nursing. *6th-8th - floor* banking office. *9th - floor* garantee department. *10th-11th - floor* offices.

Building Structure *Floor* - 3.5 m. height for the ground floor, 5 m. for 1st- floor, 4.0 m. height floor-to-floor for the rest , 16 cm. thick reinforced concrete for ground floor. The rest is 12 cm. *Wall* - 10 cm. brick except underground floor using 10 cm. thick reinforced concrete. *Roof*- 10 cm.thick reinforced concrete top with waterproof materials and insulation. *Window*- 6 and 12 mm. thick clear and tinted single-glassed .

Space load 36 watt recessed fluorescent lamps, 341 x 60 Watt and 92 x 100 Watt incandescent lamp, lighting density of 0.4 W/sq.ft . Infiltration 0.3 and 0.06 airchanges/hr. for office when on and off, respectively.

HVAC System Temperature setpoint = 74 °F, outside air 7 CFM/person.

Chillers 2 x 275 TR and 1 x 550 TR water-cool, open centrifugal chillers with energy input ratio of 0.22 at ASHRAE standard and 10 % part load ratio.

Hotel -5-storey building have been in the operation since 1984. There are 40,545 sq.m. utilized area with 36,467 sq.m. air-conditioning space. The working hour is 24 hours.

Building Function *Underground - floor* - laundry and locker room. *Ground floor* ballroom, pantry, restaurant, kitchen, store room, machine room and parking lot. *1nd- floor* meeting room, shops, ballroom, restaurant, guestroom and lobby lounge. *2nd - floor* guestroom. *3rd- 5th - floor* guestroom.

Building Structure *Floor* - 3.0 m. height floor-to-floor upper covered with rubberpad or carpet, only the lobby is covered by marble. 20 cm. thick reinforced concrete for underground floor. *Wall* - 15 cm. thick reinforced concrete. *Roof*- 15 cm.thick reinforced concrete top with waterproof materials and insulation. *Window*- 6, 12 and 20 mm. clear and tinted thick single-glassed.

Space load 40 watt recessed fluorescent lamps, 569 x 60 Watt and 2,219 x 100 Watt incandescent lamp, lighting density of 1.0, 1.5 and 2.5 W/sq.ft for guestroom, restaurant and ballroom respectively. Infiltration 0.05 airchanges/hr. for guestroom and 0.1 for the rest.

HVAC System Temperature setpoint = 74 °F, outside air 7 CFM/person.

Chillers 3 x 350 TR water-cool, screw compressor chillers with energy input ratio of 0.24 at ASHRAE standard and 10 % part load ratio.

Hospital - 12-storey hospital has been in the operation since 1990. There are 30,460 sq.m. utilized area with 22,914 sq.m. air-conditioning space. The working hour is 24 hours.

Building Function *Underground floor*- reception, lobby, emergency, X-ray ultrasound, office, accounting, pharmacy, parking lot and machine rooms. *2nd- floor* dental, infront, blood store, kitchen and parking lot. *3rd- floor* drug store, office, store, resturant and parking lot. *4th-5th-floor* patient wards, conference room, administration and parking lot. *6th-12th-floor* patient wards. *Roof-floor* machine room and main distribution board.

Building Structure *Floor* - 2.3 m. height for basement, 4.25 m. for ground floor and 1st-floor, 3 m. height floor-to-floor for the rest , 25 cm. thick reinforced concrete for 1st and 2nd floor. The rest is 30 cm. *Wall* - 10 cm. brick except underground up to 2nd floor using 10 cm. thick reinforced concrete. *Roof*- 25 cm.thick reinforced concrete top with waterproof materials and insulation. *Window*- 6 and 12 mm. clear and tinted thick single-glassed.

Space load 3,676 x 36 Watt and 819 x 18 Watt recessed fluorescent lamps, 265 x 60 Watt incandescent lamp, lighting density of 2.0, 1.5 and 1.0 W/sq.ft for out patient, resturant and patient wards respectively. Infiltration 0.04, 0.24, 0.3 and 0.06 airchanges/hr. for out patient, patient ward, office when on and off, respectively.

HVAC System Temperature setpoint = 74 °F, outside air 7 CFM/person.

Chillers 4 x 160 TR air-cool, reciprocating chillers with energy input ratio of 0.21 at ASHRAE standard and 25 % part load ratio.

3. Verification

The input for DOE2.1 E (2) program had been written and simulated with available TRY format weather data. The results, such as chiller consumptions and chiller pumps, monthly peak demand and energy consumptions, had been compared with the actual ones. The difference are less than 10 %, so the inputs are good enough to represent the building performance.

4. Cool Thermal Energy Storage

Since the buildings have been installed with normal chillers. Ice thermal energy storage with plate heat exchanger is selected due to less space need and complication. From Tantakitti C and Leeyutthanont S (3) , the demand-limit storage is the best for the Thailand utility rate, sothat the ice-harvester and ice-on-coil (external melt) with the demand-limit, are studied.

Storage sizing To find the storage size that enough for the on-peak hour, hourly cooling load of that peroid are summed up. 2,600, 1,000 and 1,350 Ton-hours are the sizes of demand-limit for office, hotel and hospital, respectively.

Icemaking machine sizing Dividing the storage's size with daily operating hours (10 or 20 hours) will get the size of icemaking machine. For the ice-on-coil due to ice formation on the outside causes the insulation effect , sothat, the machine's size is 10 % larger than the ice-harvester.

TES investment The cost of TES system are from I.T.C. Co.,Ltd. (3) and Temp Tech Engineering Co.,Ltd. (4) .

5. Results and Discussion

Effect on Peak Demand For demand limit storage, the demand on a partial-peak will be the same as the basecase due to the same operation no matter what kind of operation and ice storage. Except for the on-peak period, the demand will be dropped. Both the ice-harvester and ice-on-coil show the same results on the demand drops. Sothat, Figure 4 only shows the comparison of maximun monthly peak demand of the on-peak period for the ice-harvester and ice-on-coil.

Effect on Yearly Energy Comsumption Table 1 compares yearly energy consumption of 3 building's types using the ice-harvester and ice-on-coil. With TES, yearly energy consumption is, no doubt, increased due to lower COP of the system and also waterpumps are added. As comparing between these two types, the ice-on-coil type consumes more energy than the ice-harvester type due to increasing the insulation effect of ice formed around the tubes.

Electric Tariff Table 2 illustrates the tariff of each system. With the ice-harvester, total electric tariff is less than basecase because the decrease in peak demand cost is more than the increase in energy cost. As comparing between the ice-harvester and ice-on-coil, the energy cost of the ice-harvester is less than the ice-on-coil. Because, even both systems have the same drop in peak demand but the ice-on-coil consumes more energy than the ice-harvester due to ice formation on the tube.

Considering all cases, the demand limit case with the ice-harvester is the least electric cost. For the office, 20 hours charging period shows the best economic due to 12 hours working of building. For 24 hours working, such as the hotel and hospital, 10 hours charging is the best.

Economic Interest Rate of Return (EIRR) and Pay Back Period (PBP) To calculate the EIRR and PBP the following inputs are applied, namely the investment and saving, the conversion factor for equipment = 0.88349 , and for labor = 1, the electricity cost 0.074 $ US/kW-hr., the inflation 6.5%, the inflation for energy = 1% to 1999 A.D. and 4.5% from 2000 A.D. and the equipment life 16 years.

Table 3 shows the investment, saving, EIRR and PBP for each buildings of the ice-harvester and ice-on-coil. Based on of the EIRR and PBP, the demand limit case with the ice-harvester and 10 hours charging period is the best, except the office, 20 hours one is the most economic.

6. Conclusion

All buildings have the potential of installed the TES system which is the ice-harvester type and using heat exchanger to transfer the cooling load to the exist system. The preliminary systems are, ***Office***, 20 hours charging Ice-making machine 130 TR-Ice-mode, Ice storage tank 6 x 6 x 7.5 m^3. (2,600 Ton-hr.), Heat exchanger 830 TR at ΔT 5 °C., and etc. Total investment is $US 254,880. EIRR = 9.08 %. Payback Period = 8.9 years. ***Hotel***, 10 hours charging Ice-making machine, 89 TR-Ice-mode, Ice storage tank 6 x 6 x 10 m^3. (3,340 Ton-hr.), Heat exchanger 1000 TR at ΔT 5 °C., and etc. Total investment is $US 420,550. EIRR = 13.62 %. Payback Period = 7.0 years. ***Hospital***, 10 hours charging Ice-making machine, 135 TR-Ice-mode, Ice storage tank 6 x 6 x 4 m^3. (1,350 Ton-hr.), Heat exchanger 350 TR at ΔT 5 °C., and etc. Total investment is $US 146,520. EIRR = 13.43 %. Payback Period = 7.1 years. This study does not include the concrete work. For the implementation, more detail needs to re-audit and re-design.

Reference

1. "Feasibility study for Control Buildings in Thailand", Department of Energy Development and Promotion, August,1995.
2. "Micro-DOE2.1E", ERG/Acrosoft International Inc., CO 80127, USA.
3. Tantakitti C. and Leeyutthanont S. , "Feasibility Study of Applying The Cool Thermal Storage for Department Store", Mechanical Engineering Department , Faculty of Engineering, Chiangmai University, Chiang Mai, 50200, Thailand.
4. I.T.C. Co.,Ltd, 20/103 Soi Soonkarnkha, Sukhaphiban 3, Ramkhamhaeng Rd., Bangkapi, Bangkok, 10240,Thailand.
5. Temp Tech Engineering Co.,Ltd., 65/300 Moo 6 Ekachai Rd., Bangbon, Bangkhuntien, Bangkok 10150, Thailland.

Table 1 Yearly Energy Consumption (kW-Hr)

	Office	Hotel	Hospital
Basecase	4,973,276	9,475,194	4,220,086
Ice-Harvester			
- 10 Hours	5,272,353	10,042,317	4,418,046
- 20 Hours	5,265,511	No Run	No Run
Ice-on-Coil			
- 10 Hours	5,313,209	10,070,673	4,437,842
- 20 Hours	5,275,089	No Run	No Run

Table 2 Yearly Tariff ($US)

	Office	Hotel	Hospital
Basecase	393,068	614,745	273,314
Ice-Harvester			
- 10 Hours	256,403	560,155	251,320
- 20 Hours	360,800	No Run	No Run
Ice-on-Coil			
- 10 Hours	358,153	561,368	252,170
- 20 Hours	361,844	No Run	No Run

Table 3 Results of EIRR and Payback Period

	Office (20 Hours)		Hotel (10 Hours)		Hospital (10 Hours)	
	Ice-on-Coil	Ice-Harvester	Ice-on-Coil	Ice-Harvester	Ice-on-Coil	Ice-Harvester
Invester ($ US)	537,000	254,880	622,700	420,550	222,695	146,520
Saving ($ US)	31,224	36,665	53,290	54,590	21,145	22,000
EIRR (%)	-	9.08	7.23	13.62	6.01	13.06
Payback (Years)	-	8.9	8.2	7.0	10.7	7.1

Life Cycle Costing for Office and Commercial Buildings

SABAH ALKASS

Centre for Building Studies, Concordia University, Montreal, H3G 1M8, Canada

he paper emphasizes the importance of the "Life Cycle Costing" in building development. It so details the development of a quantitative life cycle costing model for the assessment of nancial feasibility of building projects at the preliminary design stage. The model handles most chnical data and financial factors which are required to determine the life cycle costs and conomic feasibility of proposed buildings, with basic, minimum input. Three assessment factors re calculated : present worth, annual worth and savings-investment ratio. To have a better nderstanding of the process a real life case study is considered. The alternatives are: extend the xisting facility or build a new one. Expenses are estimated in both cases, it consists of : Capital osts which includes construction, real estate and interim financing costs, and Operational Costs, hich includes warehouse efficiency, transport efficiency, energy, maintenance, major repairs, ecurity and taxes costs.

NTRODUCTION

he cost of a building over its lifetime includes first a series of initial expenses including urchase of land, design fees, construction costs etc., paid as capital costs. This is followed by nnual expenditures on operation and maintenance as well as occupancy costs such as municipal ates, management and administrative charges.

ecisions in the building industry at the design phase have traditionally been based on a omparison of initial capital costs. The main reason for employing this decision method is ecause of its simplicity and the general feeling that the lowest capital cost option will also be he lowest total cost option.

his is no longer the case. Figure 1 illustrates the life cycle cost commitment for a typical office acility[1]. In this figure, operation and maintenance costs, which are incurred either annually or at eriodic intervals over the life of the facility, account for 58% of the total life cycle costs, and are ius greater than the capital costs, which are incurred at the initial construction stage. Fig. 2 hows similar results for life cycle costs for two office buildings in Canada. It can thus be seen hat the long-term costs can far outweigh initial capital costs, and should therefore be considered eriously when taking decisions with respect to the design of office buildings.

ife Cycle Costing (LCC) is a step forward in building economics, it deals with the costs endured uring the effective life of a project. In most construction projects, detailed studies are carried out o provide precise estimates for the conception and implementation, without really considering he after-the-fact costs. Life cycle costing includes the initial costs, all subsequent expected costs or operation and maintenance and a disposal value. As life cycle costing covers a long period of

time, the time-value of money should be accurately weighed. The cost estimate for LCC is usually based on actual prices and then adjusted by cost indices, to cover prices escalation. However the forecast of LCC is still a major difficulty in the process for its unforeseeable factors. Life cycle costing technique is used whenever a decision must be made on a project that requires substantial operating and maintenance costs.

This paper attempts to clarify the use of LCC analysis in the real work environment. A real life case study identifies the most appropriate decision to be taken when considering either to renovate / extend an existing warehouse or to construct a new one. The method adopted in performing the comparative analysis was to use the differential cost comparison, which consequently produced a cash flow directly identifying savings and expenses. The real identities of the parties involved in the case study were not designated for confidential reasons.

LIFE CYCLE COSTING AT THE PRELIMINARY DESIGN STAGE

Life cycle costing enables the economic assessment of competing design alternatives considering all significant cost items of ownership over the projected life, expressed in equivalent dollars[2].

While initial costs are clear and visible at an early stage, long-term costs are not. Estimating the life cycle cost of a building at the preliminary design stage is important because in the building industry, the earliest decisions tend to establish boundaries for the later ones. It has been suggested[3] that although the expenditure during design is comparatively small, decisions and commitments made during this phase have a big influence on what later expenditures will actually be. Typically, about 75%-95% of the total life cycle costs of a building are thus locked in by the time the working drawings are prepared. Figure 2 shows that it is in the preliminary design phase that the decision maker can greatly influence the total life cycle cost[3]. Therefore, if an estimate of the total life cycle cost is available at an early design stage, cost reducing modifications are relatively easy to make; once the project goes into construction, the opportunity to influence the total project cost diminishes greatly.

There have been a number of specific studies on life cycle costing, but their concepts and results cannot be generalized to different categories of buildings. Bromilow and Pawsey[4] have described the theoretical background for a life cycle cost model by using data relating to a 30-year old university building. Neely and Neathammer[5] have presented several different maintenance life cycle data bases developed by the U.S. Army Construction Engineering Research laboratory to assist in life cycle cost analysis. Computer-aided procedures to evaluate the financial feasibility of construction projects have existed for some time, but their use has frequently been cumbersome, requiring too much data. FINFEAS program developed by Tucker[6] is a software for modeling the life cycle cost of a building project with extensive user input.

Very little research has been reported on the estimation of life cycle costs of buildings at the preliminary design stage, and there is hardly any software available which could perform this job with simple and minimum user's input. One such attempt is the creation of a prototype expert system for predicting the cost-time profiles of major construction elements to produce an estimate at an early design phase in the life of a school building construction project[7].

aroughout the building industry, there is now an appreciation that computers (particularly icrocomputers) can be of considerable assistance in evaluating the financial requirements of ıilding projects. A computer model[8] called LCC-O (**L**ife **C**ycle **C**osting of **O**ffice Buildings) ıs been developed that addresses these issues at the preliminary design stage of an office ıilding project. LCC-O is written in C and implemented in TURBO C 2.0 in a DOS ıvironment. The system has been expanded to accommodate for other decision such as selecting etween two alternatives, i.e., renovate a facility or build a new one. This new feature has been sted against a real case study.

IFE CYCLE COST MODEL

. comprehensive cost model is useful at the early stages of decision making to identify the elative importance of each life cycle cost category. All relevant cash flows are established over ıe entire life of the building, from project commencement to the end of its useful economic life. 'he measure of return, i.e., present value, which signifies the economic worth of an investment, ; derived from the cash flows. This helps in comparing facilities with different lives or differing roportions between the initial and operating costs.

ife cycle cost categories

he following major life cycle cost cash flows have been considered:

- Capital costs
  - Land
  - Financing
  - Actual construction costs (site-work, structural, HVAC, electrical and mechanical)
  - Design fees
  - Refrigeration equipment costs
  - Contingencies.
- Operation costs (annual)
  - Energy (electricity, gas, fuel-oil)
  - Cleaning (wages, supplies, contract services, trash removal)
  - Security/grounds maintenance (wages, supplies, contract services for security and grounds maintenance)
  - Administrative (wages for personnel, legal/consultant fees related to managing property, general office expenses, supplies etc.)
  - Taxes/Insurance (real estate tax, building insurance etc.)
- Repair and maintenance costs (annual)
  - Includes expenses on contract services for maintenance of elevator, HVAC, electrical, structural, roof, plumbing, fire/life safety equipment, supplies and wages
- Salvage value
  - Resale value of land plus scrap value of building (may be negative if demolition is required)
- Income (annual)
  - Income generated from all renewable space.
  - Warehouse efficiency
  - Transportation efficiency

Figure 3 shows schematically the life cycle cost model for office buildings used in LCC-O.

THE CASE STUDY

"Food Inc." (the real name of the company is left out for confidentiality) is the largest food retailer in Quebec, with more than 200 stores and distribution centres located in province of Quebec, " Food Inc. has recently purchased from "Good Food Ltd." 65 stores located in the Montreal area. However, these stores used to be serviced by Good Food's warehouses in Ontario. Therefore, Food Inc. needs to expand its warehousing capacity in the Montreal area. Two alternatives have been identified by Food's Inc. managers: 1) extend and renovate the existing warehouse, or 2) sell the existing warehouse and build a new one that will handle the existing and newly purchased stores.

Information on the case study was input into the model and its output is summarized in table 1.

TABLE 1 INCREMENTAL OPERATIONAL COST SUMMARY

Start-Up	Year 1	+ $ 10 000		(saving)
Warehouse Efficiency	Annual	+ $ 469 000		(saving)
Transport Efficiency	Annual	- $ 180 000		(expense)
Energy	Year 1-5	+ $ 36 000	+	(saving)
	Year 6-20	$ 31 000		(saving)
Maintenance	Annual	+ $ 27 000		(saving)
Major Repairs	Year 5	+ $ 496 000	+	(saving)
	Year 15	$ 36 000		(saving)
Taxes	Annual	- $ 21 000		(expense)

Recommendations

Reference to the comparative analysis section of this chapter, both monetary and non-monetary considerations have to be accounted for.

An incremental cash flow and present worth figure were calculated for the new facility compare to the existing facility. These were performed on an incremental basis as there were no revenue values and the objective was to represent the cash flow in terms of savings and expenses. It can be seen that the cash flow after tax on an annual worth basis for 20 years is a positive value for a major part of the cash flow. This indicates that by choosing the alternative of constructing the new warehouse, savings would be generated annually. Also, the present worth saving at MARR 12% was $1,865,550. Therefore, by settling on the new warehouse alternative, Food Inc. is better off in the long run. According to the sensitivity analysis in, which tested for a volume of business of 75% and 50%, Food Inc. will still be better off. The present value savings at 75% of expected business volume is $1,595,716 and at 50% of the expected business volume is $1,325,882. Therefore, at a relatively bad forecast, Food Inc. is still better off. It must be noted that the present worth figures are on an incremental basis, i.e. the positive sign indicates a saving.

Conclusions

After implementing the real-life case study to the recommended theoretical section of this project, it may be concluded that each study tends to employ different factors which would allow the main comparative decision to be taken.

: most important factor in arriving to a valid comparison is that time and accurate sideration should be devoted to identifying the various factors which contribute to capital and rational costs.

verify the validity of a decision, sensitivity analysis need to be made on the factors which uld alter the dollar figures and are directly liable to change with business volumes due to ctuation in the economy.

nay be concluded that decision makers on viability comparative studies can take effective vantage in identifying the factors that need to be considered in their studies.

so, a proposed expansion of the project is recommended in the case where revenues are urately provided or forecasted providing a clearer overview of the subject.

FERENCES

1. R. Flanagan, G. Norman, J. Meadows and G. Robinson, *Life Cycle Costing, Theory and practice*, BSP Professional Books, U.K., 1989.
2. A. J. Dell'Isola and S. J. Kirk, *Life Cycle Costing for Design Professionals*, Mc Graw-Hill Book Co., N.Y., U.S.A., 1981
3. General Accounting Office,"Computer-Aided Building Design", *U.S. Department of Commerce*, Washington D.C., Report PB 283 306, 1978.
4. F. J. Bromilow, and M. R. Pawsey, "Life Cycle Cost of University Buildings", *Construction Management and Economics* 5 (1987).
5. E. S. Neely Jr. and R. Neathammer, "Life-Cycle Maintenance Cost by Facility Use", *Journal of Construction Engineering and Management* 117(2) (1991).
6. S. N. Tucker, "Computer User Manual for Program FINFEAS - A program for modelling the Life Cycle Costs of a Building Project", *CSIRO Division of Building Research*, Australia, 1985.
7. J. Christian, "Data Acquisition and Expert Knowledge Elicitation for Expert Systems in Construction", in Applications of Artificial Intelligence in Engineering VI (edited by G. Rzevski and R. A. Adey). Computational Mechanics, Southampton and Elsevier Applied Science, London, U.K., 1991.
8. A. Khanduri, C. Bedard and S. Alkass, 1996 "Assessing Office Building Life Cycle Costs At Preliminary Design Stage", Structural Engineering Review, Vol. 8, No. 2/3, pp. 105-114.

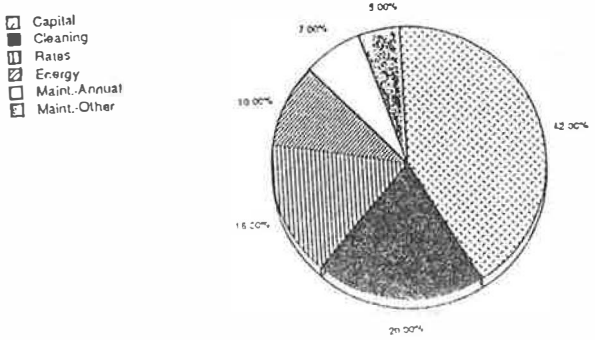

Fig. 1 Office building life cycle costs

employment of heat recovery systems, utilisation of renewable energy and the use of building energy control systems. In winter, energy consumption in offices may be reduced by lowering the indoor air temperature, hence reducing heating costs. More recent field studies (2), (3) have shown that optimum satisfaction with the thermal environment in office buildings can be achieved at a lower temperature than that obtained under laboratory based conditions, which is the basis of ISO 7730 (4).

In this paper, the thermal environment and the air quality in naturally-ventilated office rooms are studied. The thermal environment in the rooms is compared with predictions using Fanger's thermal comfort criterion. Generally, thermal comfort was achieved at a lower room temperature than that predicted by Fanger and as a result the potential of energy saving in winter is investigated in the paper.

2. METHOD

This investigation has been carried out by means of physical measurements combined with a subjective assessment of the indoor environment in five naturally ventilated office rooms (denoted as rooms A, B, C, D and E). The offices are situated in the FURS building at the University of Reading. Rooms A, B, C, and D are staff offices and room E accommodates several computer workstations. Rooms A and B which are situated in the north wing of the building are built of one concrete external wall and three concrete brick walls connected to other rooms. Each of the two rooms are connected to the north corridor via hinged wooden doors. There are two small and one large weatherstripped double-hung aluminium frame windows in the north facade of room A and room B respectively. Room C is located between south and north corridors which connects the south and north wings. The walls separating the room and the corridors are glazed while the other walls are made of concrete bricks. There is a small axial fan in the north facade near the ceiling for supplying air into the room. Room D and room E have similar structures to room A and room B respectively but are both situated in the south wing and connected to the south corridor. Rooms A, C and D are heated by hot water radiators in cold seasons. In room B there is a full-width convector under the window in addition to hot water radiators. Room E is heated by a convector of the same type as that for room B under the window in the south wall. During hot days a rotating fan was used in some of the tests. The investigation lasted for 14 months in 1991/92. Tests were conducted in winter (1991) in room A, early spring (1992) in room B, late spring in room C, summer in room D and in winter (1992) in room E.

2.1 Measurements

During an experimental test the indoor air velocity, turbulence intensity and air temperature were measured continuously using thermal anemometers (DANTEC Multi-channel Flow Analyser type 54N10). Measurements were taken at points 0.1m (foot/ankle level), 0.6m (centre of gravity of a seated person) and 1.1m (neck/head level of a seated person) above the floor. The plane radiant temperature and indoor air humidity were measured using an indoor climate analyser (Bruel & Kjaer type 1213). Thermal comfort indices (PMV and PPD) were measured using a comfort meter (Bruel & Kjaer type 1212). A CO_2 gas analyser was used for the measurement

of indoor CO_2 concentrations.

The air change rate was determined using the concentration decay method with an infra-red gas analyser. A portable fan was employed to ensure a good mixing of tracer gas (isobutane) and air in the rooms for a few minutes after injecting the gas. The wind speed was measured with three vane cup anemometers and the wind direction with a wind anemometer mounted on the top of the building (about 5m above the roof). The outdoor air temperature and humidity were measured using a copper-constantan thermocouple (radiation shielded) and a hand-held humidity meter respectively.

2.2 Subjective assessment

A subjective assessment was undertaken simultaneously with the physical measurements. The assessment of the thermal environment was based on the occupants' vote on the thermal sensation and air movement in the offices under various outdoor and indoor conditions and different arrangements of window and door openings. This assessment was based on judgements at head and foot levels as well as for overall comfort. The indoor air quality was assessed according to the impressions of odour and freshness of air. A seven-point thermal sensation scale was used to evaluate thermal sensation and five-point scale to rate the impressions of comfort with regard to air movement, odour intensity and air freshness. The rating scales for these thermal environment and air quality indices are shown in Table 1.

RESULTS AND DISCUSSION

A summary of the results for physical measurements of room environment is presented in Table 2. These measured results are discussed together with those from the subjective evaluation as follows.

3.1.Room environment

The Physical parameters describing the room environment, except for the air change rate, were obtained for every test. Figures 1 to 3 show the distributions of mean air velocity, turbulence intensity and mean air temperature at head level, foot level and overall (mean of three heights) respectively.

The air velocity in these rooms was usually below 0.17 m/s when the windows and doors were closed and fans were not in operation. Velocities above 0.17 m/s resulted either from the provision of an additional fan used in warm days in room D or from opening windows in rooms C, D and E. It is shown in Figure 1 that the air velocity at foot level was usually higher than that at head level, especially in rooms B and D which have a ceiling level higher than that of the other three rooms.

The turbulence intensity data is presented in Figure 2. The values were between low and moderate for room A but between moderate and high in the other four rooms (Table 2).

The indoor air temperature results are plotted in Figure 3. The temperature changed from day to day during the course of measurement due to the fluctuations of outdoor temperature, air change rate and heat loss or gain from the rooms and due to opening the windows or doors. In some tests overheating was observed during mild outdoor climates. Temperatures much higher than 26°C were due to the solar heat gain from the partly opened south window of room D in the summer. It can be seen in Table 2 that the air temperature at head level is higher than that at foot level with a mean vertical temperature difference of 1.7K.

The measured plane radiant temperature, and hence the calculated mean radiant temperature, were generally lower than the mean air temperature for all rooms except for room C where there was no external wall exposed to the cold ambient. The average difference between the mean air temperature and mean radiant temperature for all the tests was within 1K.

The relative humidity in the room throughout the test period was normally within the comfort limits, ranging from 40% to 55%. On some occasions it dropped to slight below 40%.

The air change rate was determined for most of the tests in rooms A, B, D and E. However, only one test was carried out for room C because the ventilating fan was always on during occupancy and the air change rate was assumed to be constant.

3.2 Subjective evaluation

Figures 4 to 6 present the distributions of votes over the measured space during the time of measurement. The results are those for thermal sensation, air movement, odour intensity and air freshness.

3.2.1 Thermal sensation

As shown in Figure 4, the mean thermal sensation was on the warm side of the neutral point. However, the measured PMV values, which were obtained from Fanger's comfort equation for the corresponding tests were close to the neutral point for most of the test conditions. This suggests that Fanger's equation underestimates the thermal impressions and under-values the deviations of the impressions from neutrality. This may be due to three main reasons. One is the assumption of steady state conditions used in the derivation of Fanger's equation. Another is the over-simplification of the metabolic rates of the occupants. The occupants rarely sat quietly in the rooms for a long period, say more than one hour, without engaging in some activity or movement. The metabolic rate was however taken constant as 1.2 met in the calculation of PMV due to the difficulty of predicting its exact value. The third reason is the sensitivity of PMV to the thermal resistance of clothing (clo value). In laboratory experiments, the clo values are consistent whereas in field tests the clothing levels vary with individual occupants and time.

The thermal sensation was found to be dependent on the air temperature and velocity in room A. The effect of air velocity was however insignificant for other rooms

probably because of insufficient data collected for each subject or too high an indoor air temperature to be compensated for by a small increment of air velocity. The regression equation for the termal sensation (TS) at head level, foot level and overall for the rooms against mean air temperature (T in ^{0}C) and, for room A, velocity (V in m/s) can be expressed as follows:

$$TS = a\,T - b\sqrt{V} - c \qquad (1)$$

where a, b and c are constants whose values are dependent on the room environment.

In Figure 7, the occupant's thermal sensation responses are presented as a function of mean air temperature. The PMV lines predicted from Fanger's equation are also presented for comparison (assuming a metabolic rate of 1.2 met and clo values between 0.8 and 1.0 and using the average values of the measured air velocity and radiant temperature for the corresponding rooms). Note that a PMV line is theoretically not a straight line but because the curvature is very small, then the error caused by linerising the curve is negligible in the region close to the comfort temperature. From Figure 7 a neutral temperature i.e. T for TS = 0, can be obtained. The neutral temperature can also be predicted from Fanger's comfort equation. The neutral temperatures calculated from the above equation and from Fanger's equation together with the difference in neutral temperature between them are shown in Table 2.

It can be seen from Table 2 that Fanger's equation overpredicts the neutrality for the rooms except room C. The reasons for this were mentioned above, which seems to confirm the findings of Schiller, et al. (2) and Brager (3). They found that the predicted neutral temperature was on average 2.4K higher than that measured for 304 office workers in 10 buildings. In addition, Figure 7 indicates that the data lines from the present investigation are steeper than those given by Fanger's equation, suggesting the occupants are more sensitive to changes of air temperature. This fact was also observed by Fishman and Pimbert (5) whose field study showed that the gradient of their data curve deviated from Fanger's equation particularly at temperatures above 24^{0}C. Furthermore, they found that Fanger's comfort equation predicted the neutral temperature 0.6K higher than that obtained from the field survey, which was attributed to their incorrect estimation of the subjects' clothing.

If according to Fanger's definition the central three categories of the thermal sensation scale were regarded as an indication of an acceptable state for thermal comfort whereas the votes outside these central categories were considered to represent dissatisfaction with the thermal state, the results suggest that about one third of the responses were dissatisfied with the thermal environment whether for the head, foot or the overall impression. Most of the dissatisfaction that occurred in rooms A, B and E when the windows and doors were closed was caused by overheating, which could be avoided by window opening or by controlling the heat output from the emitters and hence reducing the heating costs with the help of a thermostat or a weather compensated heating system. For room C however these measures were not adequate because the emitter was already turned off during the test period. Although in the latter period of tests, a window was opened on the roof, the room was still

uncomfortably warm in most days. The roof window was effective in reducing the indoor temperature only when the outside was windy such that cooler outdoor air would be blown into the room. A possible way to decrease the indoor temperature in cold seasons is to introduce air directly from the outside of the building rather than from the corridor, using the existing ventilating fan. Due to its location a comfortable thermal environment is difficult to achieve in room D in hot sunny summer days unless it is mechanically ventilated or air conditioned.

3.2.2. Air movement

Figure 5 shows that the overall impression of the air movement was on the side of being stagnant. For room A when a window and/or the door were partly opened, the impression of air movement shifted to being slightly draughty. The main cause of the draught was considered to be low temperature as air velocity and turbulence intensity were not very high.

Figure 5 also indicates that the overall impression of air movement is similar to that felt at head level, i.e. when the head feels stagnant the overall response of the air movement will be stagnation. This is also true for draught. In these tests the feet were more sensitive to air temperature but less sensitive to air velocity than the head.

3.2.3. Odour intensity

Odour was detectable in most cases see Figure 6. However, no satisfactory correlation between odour intensity and CO_2 level or air change rate could be established. In some cases, when the CO_2 level was low, or the air change rate was high, odour was still perceivable while in other cases when the CO_2 level was higher than 1000 ppm the odour intensity was not detectable. This seems to suggest that there were other pollution sources such as building materials or furnishings which could be more significant than the odour emission from the occupants. The judgement could also be affected by fatigue of the olfactory sense due to long term exposure to the pollutants.

3.2.4 Air freshness

Figure 6 also shows that the rating of air freshness was in general slightly stuffy. The assessment of odour intensity and air freshness shows that the air change rate is not a good indicator of indoor air quality since the air reaching the breathing zone could be contaminated as a result of poor mixing in the room.

4. ENERGY SAVING POTENTIAL

Since the neutral temperature given by Fanger's equation is higher than that found from field measurements, energy can be saved by decreasing the room temperature. The potential for energy savings is described here.

In most office buildings, heat losses in cold seasons are mainly due to conduction and ventilation. These heat losses are proportional to the temperature difference between

indoors and outdoors (T_i - T_0). Thus, for a comfort temperature based on laboratory models, the amount of heat loss, q_l, is

$$q_l \propto (T_{il} - T_0)$$

and for the comfort temperature which is based on the field measurements, the heat loss, q_f, is

$$q_f \propto (T_{if} - T_0)$$

where T_{il} and T_{if} are the required room temperatures predicted from the laboratory model of Fanger and from the field measurements respectively.

The amount of energy saving is then

$$(q_l - q_f) \propto (T_{il} - T_{if})$$

Hence the ratio of energy saving based on the room temperature recommended by the current standards is

$$(q_l - q_f)/q_l = (T_{il} - T_{if})/(T_{il} - T_0) \qquad (2)$$

In the UK, the average outdoor temperature during the heating season, T_0, is about 6^0C and for the whole year is 10^0C. Assuming the room temperature predicted for neutrality is 22.6^0C, the ratio of energy saving is obtained for several differences between predicted and measured neutral temperatures and this is given in Table 3.

It is seen that lowering the room temperature by 1K represents about 6% reduction in space heating energy for $T_0 = 6^0$C. For a temperature reduction of 1.1K, the maximum value measured in this investigation, the potential of energy saving is 6.6%. To take full advantage of this saving, it is necessary to control the heat supply to an office by installing an individually adjustable thermostat or by using a personalised environmental system.

CONCLUSIONS

The results show that in naturally ventilated office rooms the air velocity at foot level is generally higher than that at head level. The turbulence intensity in the room however does not seem to correlate with the air velocity. The CO_2 concentration does not represent a good indicator of the sensation of freshness in the rooms. This was attributed to the poor mixing of outdoor air with room air in naturally ventilated rooms.

From the present investigation, it seems that the thermal models based on laboratory tests at steady state conditions can not accurately predict the thermal environment for naturally ventilated offices where the conditions are transient and where the occupants invariably change their activities. For the cases investigated, Fanger's equation for thermal comfort generally overpredicts the neutral temperature and under-predicts the

comfort requirement when the air temperature deviates from neutrality.

Heating energy can also be saved by lowering the room temperature from the currently recommended values by, for example, ISO 7730(4) without compromising the thermal comfort. Besides, a lower indoor temperature can reduce the occupants' complaints about the feeling of stuffiness.

REFERENCES

1. P.O.Fanger, Thermal Comfort - Analysis and Applications in Environmental Engineering, Robert E. Krieger Publishing Company, Florida, 1982.

2. G.E.Schiller, E.A.Arens, F.S.Bauman, C.Benton, M. Fountain and T.Doherty, A field study of thermal environments and comfort in office buildings, ASHRAE Trans, 1988, 94 (2), 280-308.

3. G.S.Brager, Using laboratory-based models to predict comfort in office buildings, ASHRAE Journal, April 2992, 44-49.

4. ISO 7730, Moderate thermal environments - Determination of the PMV and PPD indices and specification of the conditions for thermal comfort, International Organisation for Standardisation, 1984.

5. D.S. Fishman and S.L.Pimbert, Responses to the thermal environment in offices, Building Services and Environmental Engineer, January 1979, 10-11.

Table 1. Rating scales for thermal sensation (TS), air movement (AM), odour intensity (OI) and air freshness (AF).

RATING	TS	AM	OI	AF
- 3	cold			
- 2	cool	too draughty	not detectable	very fresh
- 1	slightly cool	draughty	slight	fresh
0	neutral	acceptable	moderate	neutral
1	slightly warm	stagnant	strong	slightly stuffy
2	warm	very stagnant	very strong	stuffy
3	hot			

Table 3. Energy savings during the UK heating season due to a lower room temperature.

$(T_{a'} - T_a)$ (K)	$(q_h - q_h)/q_h$ (%)
0.5	3.0
1.0	6.0
1.1	6.6
2.0	2.0

Table 2. Physical and thermal properties of room environment.

Room No.	A	B	C	D	E	ABCDE*
Dimension (m)						
Length	5.4	11.6	4.2	4.4	7.6	
Width	2.3	2.9	3.5	2.3	2.4	
Height	2.6	3.4	2.6	2.6	3.4	
Effective volume+ (m^3)	29.3	108.2	37.5	25.0	62.0	
Normal occupants	1	3	2	1	3$	
Average air change rate (h^{-1})	0.86	0.86	7.60	3.03	3.81	
Average air supply rate (l/s per person)	7.0	8.6	36.9	21.0	21.9	
Mean air velocity (m/s)						
Head level	0.059	0.071	0.098	0.063	0.066	0.071
Foot level	0.064	0.100	0.111	0.086	0.130	0.095
Overall	0.060	0.082	0.099	0.067	0.098	0.080
Turbulence intensity (%)						
Head level	39.4	59.2	43.8	38.6	47.8	44.5
Foot level	28.7	44.4	34.0	33.0	28.1	32.9
Overall	34.7	54.3	41.2	37.1	39.6	40.3
Mean air temperature (°C)						
Head level	23.1	23.8	25.7	27.1	23.1	24.5
Foot level	21.4	21.7	24.5	25.0	21.7	22.8
Overall	22.4	22.9	25.1	26.2	22.4	23.7
Difference between air temperature and radiant temperature (K)	0.6	0.7	-0.7	0.6	0.7	0.5
Relative humidity (%)	45.8	45.7	42.9	47.6	45.5	45.5
Measured neutral temperature (°C)						
Head level	22.4	22.4	23.2	22.8	21.1	21.7
Foot level	21.4	20.4	21.1	22.1	21.0	21.0
Overall	22.0	21.7	22.5	22.7	21.4	21.7
Predicted neutral temperature from Fanger's equation (°C)#	22.8	22.8	22.3	22.9	21.4	22.6
Difference between predicted and measured neutral temperature (K)	0.8	1.1	-0.2	0.2	0.0	0.9

Notes: * average of the data for rooms A, B, C, D and E

+ the volume excluding the space occupied by obstacles

$ the occupants are not the normal office users

based on 0.8 clo and 1.5met for rooms A,B,C and D, 1.0 clo and 1.2met for room E, 0.83 clo and 1.4met for all rooms

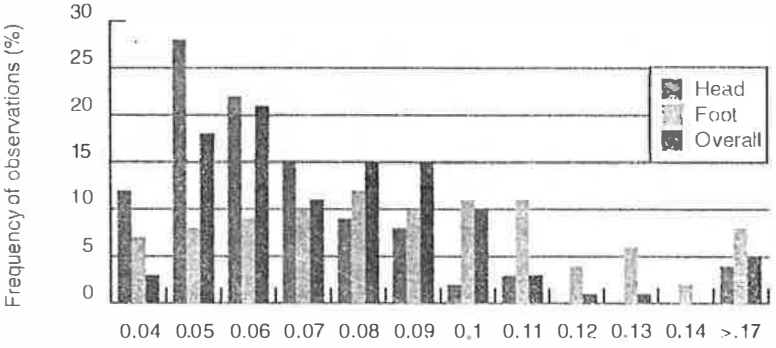

Fig 1 Frequency distribution of mean air velocity

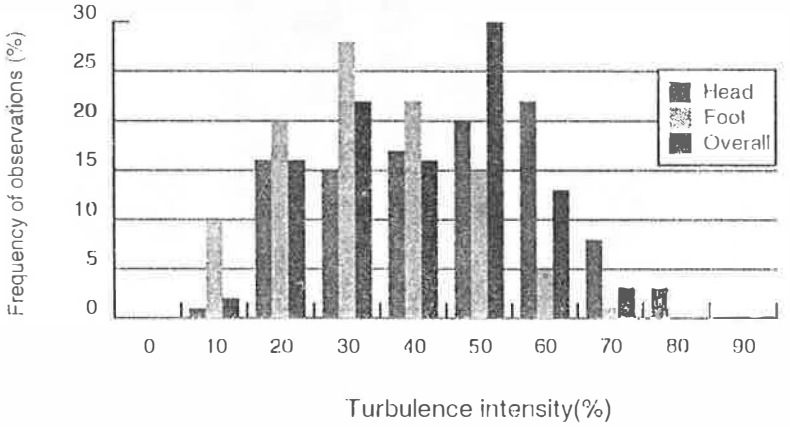

Fig 2 Frequency distribution of turbulence intensity

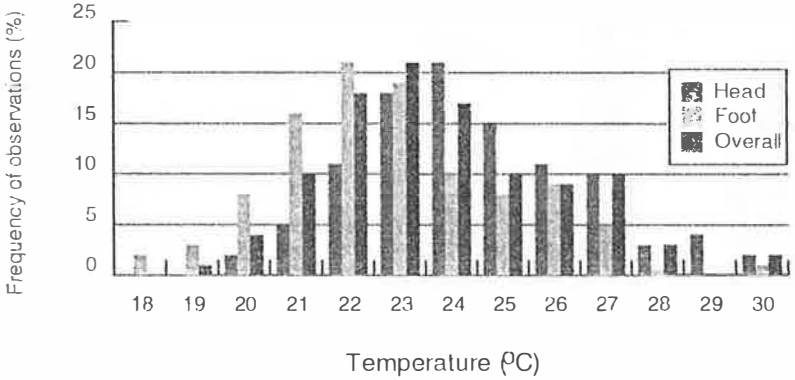

Fig 3 Frequency distribution of mean air temperature

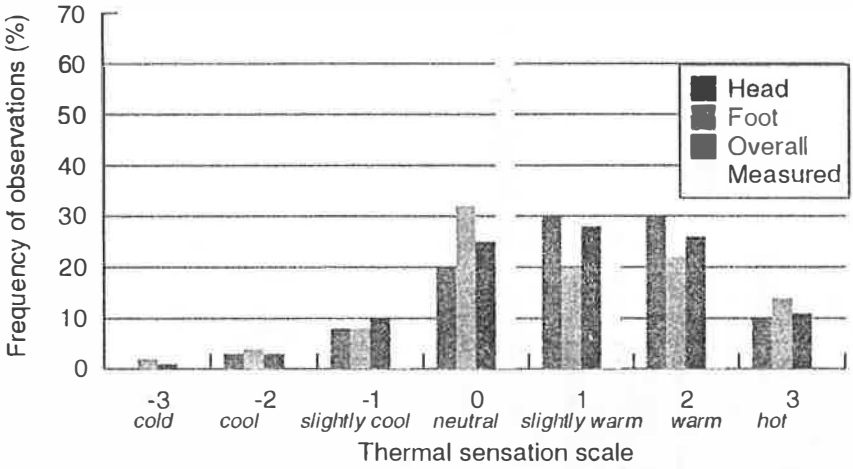

Fig 4 Frequency distribution of thermal sensation vote

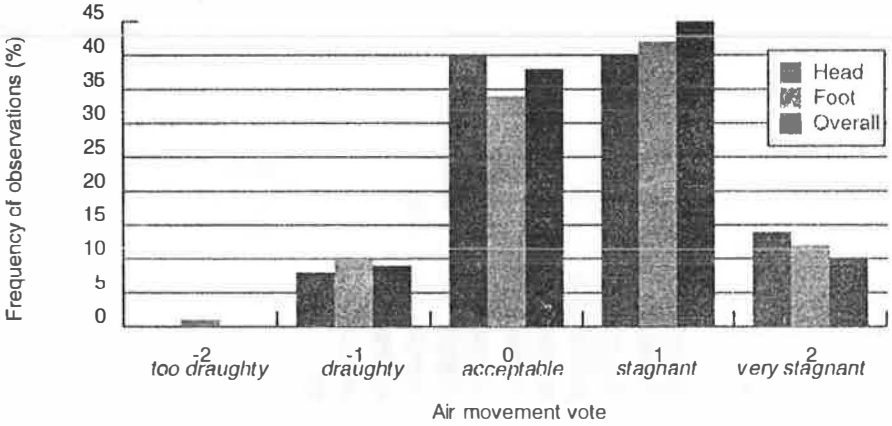

Fig 5 Frequency distribution of air movement scale

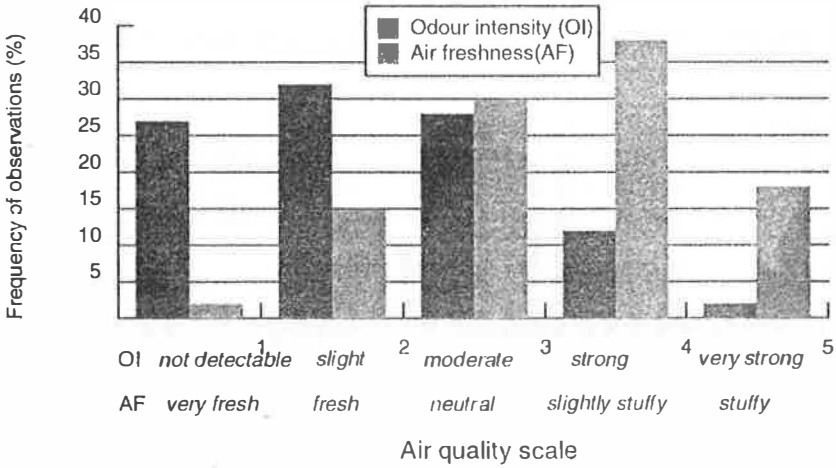

Fig 6 Frequency distribution of air quality votes

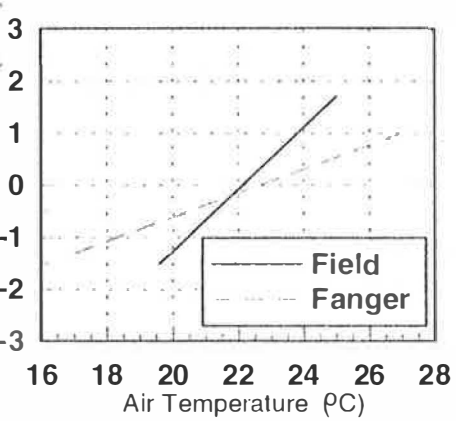

(a) Room A

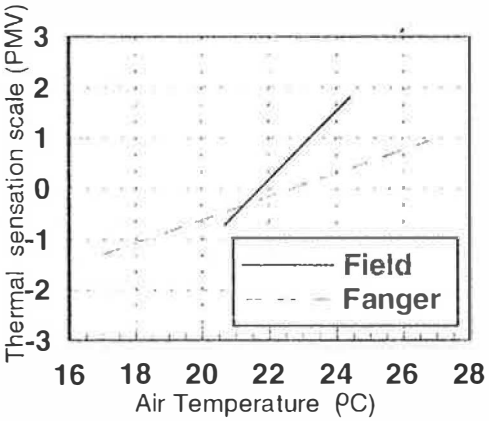

(b) Room B

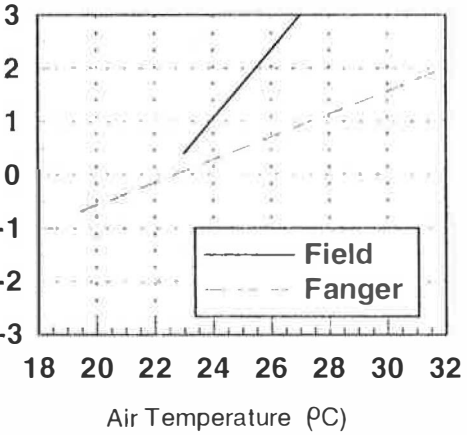

(c) Room C

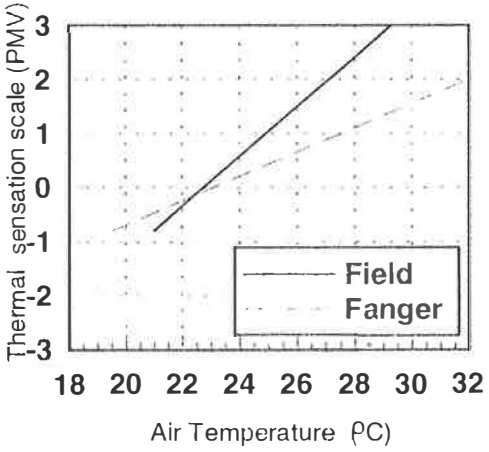

(d) Room D

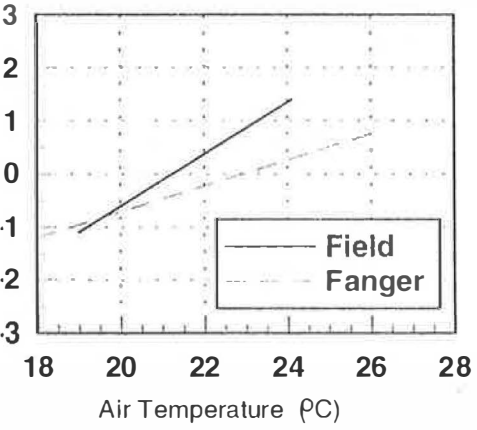

(e) Room E

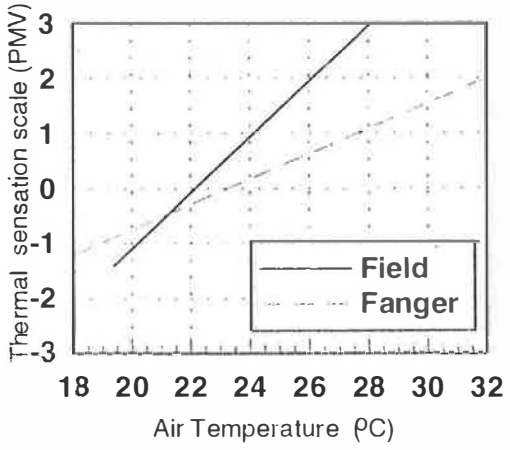

(f) Room A to E

Fig 7 Effect of air temperature on thermal sensation

Effect of Surface Heat Transfer Coefficients on the Thermal Environment in Rooms

A. Hatton and H.B. Awbi
Department of Construction Management & Engineering
The University of Reading
UK

Abstract

Convective heat transfer coefficients (chtc's) presently used in building thermal models have in most cases, been based upon experiments for small free edge heating plates. Recent researc has shown that in some cases there can be up to a 300% difference between chtc's used i building thermal models. This could lead to some inconsistency between the predictions mad by different building thermal models for the same thermal conditions in a room or a building.

This paper uses a test case based on solar heating of the internal surfaces of a room in building using a building thermal model. A range of chtc values are used to predict th environment in the room (such as surface and air temperatures and comfort conditions) for th cases when the floor, the ceiling or a wall is heated by the sun. Included amongst this selectio of chtc's were the chtc values recently measured by the authors for the heated surfaces of a enclosure.

1. Introduction

Surface convective heat transfer coefficients (chtc's) are an integral part of building therma models. However, there is no really accurate chtc that can be used in every thermal model. Th most common chtc's currently utilised in building thermal models, are those found in th ASHRAE Handbook [1], CIBSE Guide [2] and the rather elaborate formula by Alamdari an Hammond [3]. However, these coefficients have all been based upon experiments using small free edge heating plates. Recent work by the authors [4] has shown that the chtc's for a heate surface in a room are influenced by the conditions in the room such as the addition of a fa producing a wall jet over a heated surface and also the temperatures of the other surfaces in th room. These factors were not taken into account in the free-edge heating plate experiment reported in the literature.

It is clear that the surface chtc provides an important thermal link between the mass of th building and the air volume. Therefore in practice it has an influence on room temperatur control and thermal comfort in buildings.

In a study of thermal models by K Lomas [5], in which 4 chtc values were used within th thermal models ESP and HTB2 it was found that the estimated annual heating energy deman varied by around 27% depending on the chtc used. Also when the two thermal models teste were implemented with the same chtc one produced an estimated annual heating energy deman within 1% of the other model. This suggests that to provide consistency in the results, one set o

ccurate chtc's should be used in all models. However, that paper also states that the choice of htc had little impact on the peak daily air temperature predictions.

The authors have carried out extensive experimental work in a test chamber to produce ccurate chtc's for use in building thermal models. They also showed that one expression for htc for a surface will not always describe the real heat transfer from the surface particularly if ixed convection is being modelled.

This paper presents the results of a number of simulations which have been carried out to ompare predictions made using three chtc's; the ASHRAE equations, CIBSE's constant values nd the authors values in the building thermal model "ROOM". Although a popular choice of htc, Alamdari and Hammond's equation was not considered due to it's complexity and could ot be directly entered into the "ROOM" input data (see Section 2).

2. Thermal model simulations

The building thermal model "ROOM" was used to carry out the simulations required to predict PMV values in a room.

To assess the importance of the chtc's on thermal comfort, a test case was needed that would nvolve heating the floor, ceiling and wall of a room. The test case would also have to be ealistic. The heating of the surface would require the sun falling over it and so three scenarios were devised to allow solar heating on each surface. However, a number of specifications were common to each scenario. These were a well insulated room of dimensions 6m x 6m x 4m high having a low thermal capacity (U value of each surface = 0.3). The room was divided into 14 surfaces and was simulated in each of the 3 scenarios. The site position was also common to each scenario; this was London (latitude = 51.7°N). To keep an average air temperature between 21-25°C the air change rate and the supply air temperature needed to be specified for each test and these are described below.

Scenario 1 . 'Solar patches on a ceiling - internal light shelf, Fig (1)'.

Using "ROOM" nine surfaces represented the ceiling and 5 other surfaces represented the rest of the room. A single glazed window was allocated to the west wall and a reflective shelf positioned on the inside of the window. Two tests were carried out for this set-up, one for the month of July and the other for February. The air change rate was set to 5 ach at a supply emperature 19°C for July, and 1.5 ach and a temperature of 22°C for February.

Scenario 2. 'Solar patches on a floor'

In this case 9 surfaces were allocated to the floor. The west wall now became a whole window with no reflective shelf. Two tests were carried out for this set-up, one for the month of July and the other for February. The air change rate was set to 10 ach and the supply air temperature 10°C for July, and 1.5 ach and a temperature of 15°C for February.

Scenario 3. 'Solar patches on a wall'

Nine surfaces were allocated to the east wall. The window on the west wall was set high up o this wall. One test was carried out for this set-up for the month of December, because the su shone only on the east wall during a winter month. The air change rate was set to 1.5 ach and th air temperature to 21°C.

The chtc for each surface was determined by entering a value for the coefficients a & b in th equation:

$$h_c = a(\Delta T)^b$$

where h_c = convective heat transfer coefficient, W/m²K
ΔT = surface to air temperature difference, K
and a and b are the coefficients.

For each of the three scenario's "ROOM" was run using the chtc's in Table (1).

Table 1. Chtc's used in "ROOM" for the simulations

	The authors chtc's.	ASHRAE equations.	CIBSE constant values.
Wall:	$h_{cn} = \frac{1.82}{D^{0.121}}(\Delta T)^{0.293}$	$Nu = 0.12(Gr)^{1/3}$	3.0
Floor:	$h_{cn} = \frac{2.18}{D^{0.076}}(\Delta T)^{0.308}$	$Nu = 0.12(Gr)^{1/3}$	4.3
Ceiling:	$h_{cn} = \frac{0.7}{D^{0.6}}(\Delta T)^{0.133}$	$Nu = 0.22(Gr)^{1/4}$	1.5

As ventilation has been used in each simulation it was useful to make some assumptions as t the position and size of the inlet to evaluate a mixed convection heat transfer coefficient for th surface directly under the influence of the jet. For the sun patches on the ceiling in the month o July (scenario 1, summer case) an inlet was assumed to be at the top of one of the walls so as t allow a jet to spread over the ceiling. In this case the authors chtc for a jet acting over a ceilin was used for the ceiling chtc in the "ROOM" input data. However, the natural convection chtc' were entered for the remaining surfaces of the room.

The same applied to the tests with the sun patch on the floor for the month of July (scenario 2 summer case). The inlet was assumed to be at the base of a wall so the jet acts over the floo The chtc for a jet acting over a floor was used as the floor chtc in the "ROOM" input data, bu the natural convection chtc's were entered for the remaining surfaces of the room.

The comfort predictions were made for a plane at 0.6m from the floor (seated level) for ligh office work activity and light office wear clothing. The PMV values were then plotted for eac case and presented in the results.

5. Results

In Fig. (2) the results show that the PMV values are quite close with small differences in the PMV values occurring between about 11:00 and 14:00 hrs. It should be mentioned however that the ceiling sun patches only heat a small area of the ceiling. As the simulation is carried out for a summer month, a high ventilation rate is required resulting in a considerable air movement. Therefore, in such cases, natural convection expressions may not be suitable for calculating the heat transfer from the room surfaces.

In Fig. (3) one can see that the 3 sets of PMV results are again close. In this case the ventilation rate is low as a winter month was simulated but the sun patches on the ceiling again only cover a small area. Therefore the natural convective heat transfer from the ceiling is small and has little effect on the comfort in the room.

As mentioned in section 2 the plane at which comfort is calculated was at seated level (0.6m). Heat gain by natural convection from the ceiling would probably have a greater effect on the PMV values at a plane closer to the ceiling. Although this would not be a typical situation.

From Fig. (4) it can be seen that the difference between the PMV values for a heated floor are slightly higher than those for the cases with the sun patches on the ceiling. One reason for this could be that as the whole of the west wall is glazed in this case, then the sun patch on the floor covers a much larger area than in scenario 1 were the sun patch is on part of the ceiling. However, there is a high ventilation rate in this case (section 2) which suggests that heat convection will be dominated by forced convection.

The winter simulation for the sun patches on the floor produces the results shown in Fig. (5). In this case a much lower ventilation rate was used than the summer simulation and as a large area of the floor was heated by the sun patch we can say that natural convection has a greater effect on the comfort in the room. This can be seen in the figure by a greater difference in the PMV values predicted using the present values and the CIBSE chtc's than in the earlier simulations. The difference between the results from ASHRAE's and the present chtc's is much smaller.

Figure (6) shows that the PMV values calculated using the present chtc's are close to those obtained using the CIBSE chtc's early in the day. However, later on in the day the present values are closer to the ASHRAE values. The sun patches on the wall in this case covered only a small area thus the natural convective heat transfer to the room is small. Therefore, the difference in the chtc's has a little effect on comfort in the room for this case.

A point to mention regarding all these results is that during the winter simulations the solar gain is much lower than during the summer simulations.

Figure (7) shows the PMV results obtained using the authors' mixed convection coefficients for a heated ceiling compared to those predicted using natural convective coefficients. The PMV values obtained using the natural convective chtc's are higher than those obtained using the mixed convection values between 13:00-17:00 hours but are lower between 10:00-13:00 hours.

The comfort results in Fig. (8) show that the PMV values predicted using the natural convectio chtc's are higher than those calculated using the mixed convection chtc's.

4. Conclusion

From the results we can conclude that when natural convection dominates the heat transfe from the room surfaces, the chtc value used has a significant influence in predicting the comfor levels in a room. However, in many of the test cases considered natural convection did no dominate the heat transfer from the room surfaces because the solar heated area was small an the ventilation rate was high.

It was shown that natural convection chtc's generally produce greater PMV values in a roon compared to those using mixed chtc's. Although the heat transfer from room surfaces is greate with mixed convection the effect of air velocity on PMV is more dominant, thus producing lowe PMV's.

The significance of these findings to users and developers of building thermal models is tha consideration should be given to using the correct chtc in the model. For more realistic simulations, accurate chtc's, such as those given in Table 1, should be used in building therma models when natural convection is dominant and mixed convection coefficients should be use when a room is ventilated.

5. Acknowledgement

The Engineering and Physical Sciences Research Council, UK is supporting this work unde Grant Reference GR/J47606. The authors acknowledges Arup Research and Development fo providing their ROOM program for this work.

6. References

1. ASHRAE. 1993. ASHRAE Fundamentals, American Society of Heating Refrigeration and Air-conditioning Engineers, Inc., Atlanta, USA.
2. CIBSE. 1979 and 1986. CIBSE Guide, Section A5 and A9, Chartered Institute of Building Services Engineers, London.
3. Alamdari, F. and Hammond, GP . 1983. Improved correlation's for Buoyancy-driven convection in rooms, Building Serv. Eng. Res. Technol., Vol.4, No.3, pp106-112.
4. Hatton, A. and Awbi, H. 1996. Heat transfer from room surfaces, Proc. of ROOMVENT '96, vol 2, pp 395-402, Yokohama, Japan.
5. Lomas, K.J. 1995. The U.K applicability study: an evaluation of thermal simulation programs for passive solar house design, Building and Environment, Vol.31, No.3, pp. 197-206.

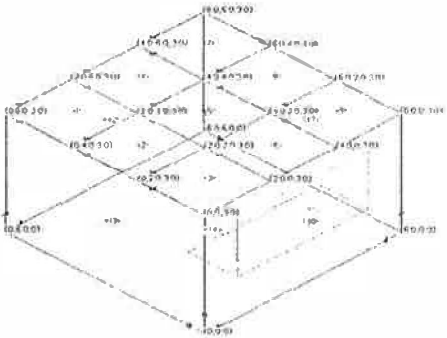

Figure 1. Selected room for scenario 1.

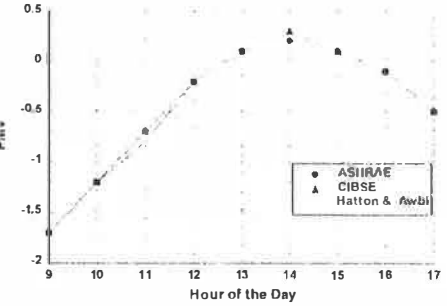

Figure 2. Comparison of PMV values predicted for a room with sun patches on the ceiling in the month of July.

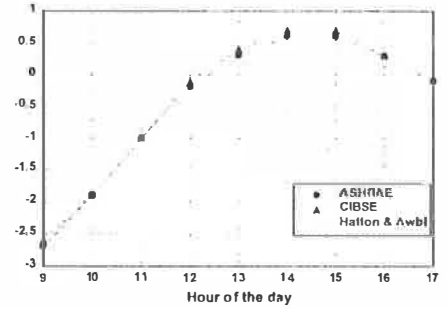

Figure 3. Comparison of PMV values predicted for a room with sun patches on the ceiling in the month of February.

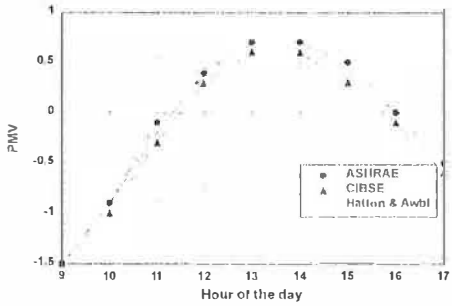

Figure 4. Comparison of PMV values predicted for a room with sun patches on the floor in the month of July.

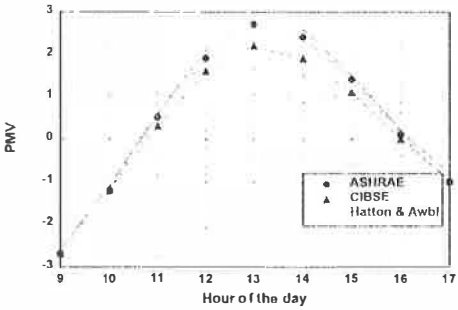

Figure 5. Comparison of PMV values predicted for a room with sun patches on the floor in the month of February.

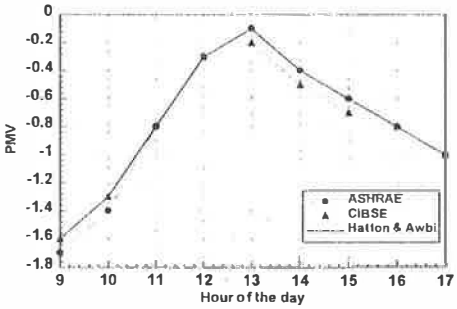

Figure 6. Comparison of PMV values predicted for a room with sun patches on the east wall in the month of December.

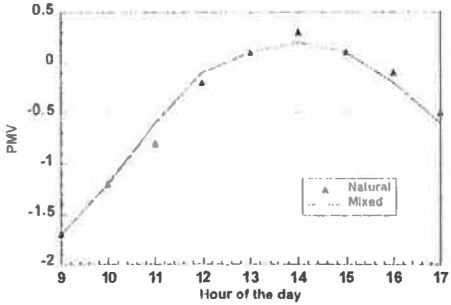

Figure 7. Comparison of PMV values predicted using mixed and natural chtc's for a room with sun patches on the ceiling in the month of July.

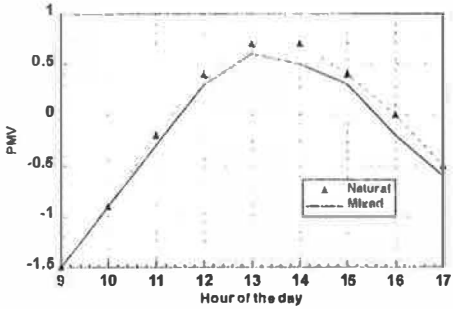

Figure 8. Comparison of PMV values predicted using mixed and natural chtc's for a room with sun patches on the floor in the month of July.

DYNAMICS OF AIR POLLUTION CONTROL FOR AN OBSTRUCTED ENCLOSURE

H.R. Hamidzadeh and F. Delfanian
Mechanical Engineering Department
South Dakota State University
Brookings, South Dakota 57007, USA

RACT

A dynamic model for prediction of pollution in an obstructed osure has been developed. The mathematical model is based on led lumped parameter modeling of total volume of enclosure. The e space representation is established to compute time response of ution in the system. The computed results have been verified by paring with results of an established model based on computational d dynamics. The effects of incoming pollution from outside, uced indoor pollution from sources, and percentage of recirculated have been investigated. The developed model considers maximum ewable indoor pollution and determines the required incoming flow in terms of percentage of recirculated air. As results of these ysis a design guidelines for determination of optimum flow rate and lement time versus percentage of recirculated air are presented.

INTRODUCTION

An accurate determination of the indoor air pollution and the tilation systems is often expected when designing a building. refore, a knowledge of the amount of pollution at all times and the uired fresh air supply has been of practical importance as well as of theoretical interest. The problem of dynamic response of the indoor lution has been studied by several investigators. In most analyses tribution characteristics of air ventilation system and air quality trol have been considered on the basis of computational fluid amics (CFD).

The other alternative approach is the lumped parameter method, also led the macroscopic model. In this technique, the whole enclosed ume can be divided into a number of sub-volumes. The time variation continuation in sub-volumes can be formulated based upon continuity nciples. The approach, due to ease of analysis, is very versatile in diction of pollution concentration in different regions and its persion.

Attention has been confined in subsequent publications to obtain erical solutions for prediction of pollution in an obstructed losure. For extensive literature review see references (1), (2), In these analyses, the time variation of indoor pollution has been dicted using models based on computational fluid dynamics. Although se models are expected to provide accurate solutions, they require essive computational time, and in most cases they are limited to ple cases.

$$q\,C_2 = V_3\,\dot{C}_3 + q\,C_3 - S_3 \qquad (1.c$$

$$q\,C_3 = V_4\,\dot{C}_4 + q\,C_4 \quad S_4 \qquad (1.c$$

$$q\,C_4 = V_5\,\dot{C}_5 + q\,C_5 - S_5 \qquad (1.e$$

$$q\,C_5 = V_6\,\dot{C}_6 + q\,C_6 - S_6 \qquad (1.$$

Where q is the steady state flow rate, P is the percentage recirculation, and S_i is the generated polutant in the i^{th} cont volume. Also, the state space model will be given by the follow equation.

$$\{\dot{C}\} = [A]\{C\} + [G]\{S\} + [B]\,C_{in} \qquad ($$

where

$$\{\dot{C}\} = \frac{d}{dt}\{C\} \qquad ($$

{C} is the concentration vector representing pollutant concentration all control volumes. [A] is the state matrix, [B] is the input matr [G] is the source matrix, {S} is the pollution generated for e control volume, C_{in} is the input pollution of the fresh air. The amo of contaminated concentration as a function of time are determined solving eqn.(2) using Matlab programming.

3. VALIDITY OF THE SIMULATED MODEL

The lumped parameter model is compared with available data for similar geometry of the system. In this case for a specific flow r of 0.004 m^3/s time variation of concentrated pollutant at each cont volume were determined and are presented in Fig.(2). For comparis recirculation source, and incoming pollutant are not considered. A 1 initial condition for pollutant concentration at each control volume assumed. The mean computed concentration from this case is compa with those determined using computational fluid dynamics (2). comparison indicates that for the first fifteen minutes excell agreement is achieved. However, for a longer period the results dive from each other. This comparison is presented in Fig.(3) It believed that due to very low incoming flow rate (natural ventilati the computational model provides better accuracy because of distribution of pollutant concentration within each control volu Nevertheless, authors trust that at high flow rates (forced ventilati

Among the investigators who have contributed to this area, Yamamoto al., (4) have presented a direct solution to a multizone indoor taminant distribution model. They provided an analytical tool to uate problems of indoor air quality and analyzed pollutant migration the building.

This paper presents mathematical formulation of a lumped parameter el for obstructed enclosure. The validity of the presented model is ained and excellent agreement is established by comparing the ained results with the available data based on computational fluid amics. Also, the effect of percentage of recirculated air on time ponse of pollution concentration at different regions for given flow e has been studied. In addition, the design chart relating the imum required flow rate and the settlement time for maximum allowable lution concentration versus the amount of recirculated air for ious height of obstacle have been determined.

STATE-SPACE SIMULATION

The physical system being considered is an enclosure with a tition. A portion of the exhausted air is being recirculated and ed to the supplied fresh air. The system includes a pollution source certain regions. Figure (1) depicts the schematic drawing of the el and the sub-volumes considered for the analysis. Average centration for the i^{th} control volume is presented by C_i and V_i pectively. The govrning equations, conservation of mass, for trol volumes are given in eqn.(1).

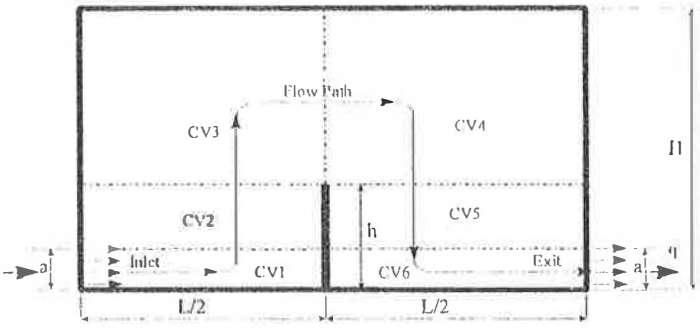

Figure 1. Schematic model for the obstructed enclosure
(H = 2.5 m, L = 4 m, h = 1 m, a = 0.2 m)

$$\frac{}{0}\ [(100-P)C_{in} + PC_6]\ q = V_1\dot{C}_1 + q\,C_1 + S_1 \qquad (1.a)$$

$$_1 = V_2\,\dot{C}_2 + q\,C_2 - S_2 \qquad (1.b)$$

better agreement can be achieved.

4. EFFECT OF RECIRCULATION ON POLLUTANT DISPERSION

Assuming that the level of pollutant entering the consider enclosure, and indoor sources is zero the dispersion of pollutant each control volume for a constant 5 air change pr hour (ACH) we determined. A typical dispersion curve for 20% recirculation (P = 2 is illustrated in Fig.(4). The results indicate that concentration every control volume decays rapidly except in the first control volu for certain time. As it is shown when concentration in this volu reduces to the level of recirculation, the slope of the dispersion wi be momentarily reduced by a considerable amount.

5. DESIGN REQUIREMENTS FOR INDOOR AIR QUALITY CONTROL

The required minimum air flow rates for different percentages recirculation as well as settlement time for maximum allowab concentration are investigated. In the analysis, CO_2 is considered be the only pollutant substance. The maximum allowable 1000 ppm in t enclosure, as recommended by ASHRAE (5), is assumed. In addition, concentration of 345 ppm for incoming fresh air was considered. The ti response for each control volume for an optimum flow rate at a specif recirculation percentage is computed and is presented in Fig.(5). provide design guide-lines, variation of optimum flow rate for (99% allowed pollutant is illustrated in Fig.(6).

6. CONCLUSION

A lumped parameter dynamic model for determination of polluti concentration at different region of an obstructed enclosure introduced. This model is capable of considering the effect recirculation, and possible pollutant sources within the enclosure The computed results compared well with the available results obtain using computational fluid dynamic. The model was used to predict t optimum required flow rate for a set maximum allowable pollutant in t enclosure.

7. REFERENCES

1. Bejan, A.,Lage, J. L., and Anderson, R, 1991, "Efficiency transient contaminant removal from a slot ventilated enclosure Int. J. Heat Mass Transfer, Vol. 34 pp 2603-2615.

2. Delfanian, F., 1995, "Infiltration and obstructed ventilati effects on indoor air movement and pollutant removal", Ph. Dissertation, North Dakota State University.

3. Rieder, W., and Delfanian, F., 1991, "Simulation of airbo pollutant levels and infiltration flows in an enclosure", J, So Energy Engineering, Vol. 113, pp 236-243.

4. Yamamoto, T., Owen, M. K., Ensor, D. S., Sparks, L. E., Damle, S., Lawless, P. A., 1989, "Fast direct solution methods multizone indoor model", Building systems: Room Air and Contaminant Distribution, ASHRAE publication.

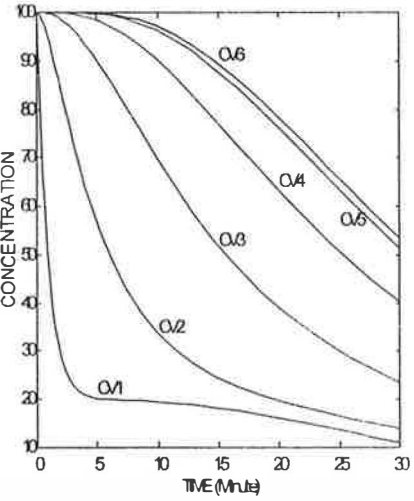

Figure 2. Pollutant concentration for control volumes

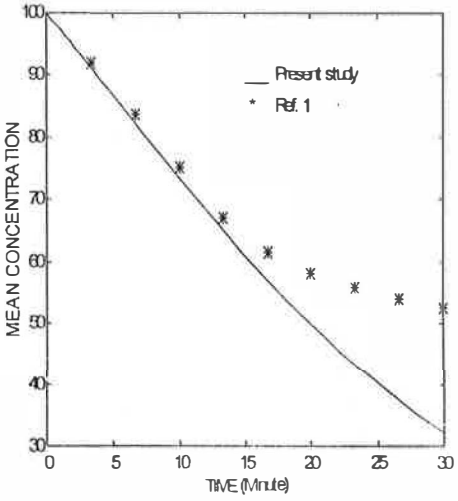

Figure 3. Comparisson of present results with those of Reffrence(2)

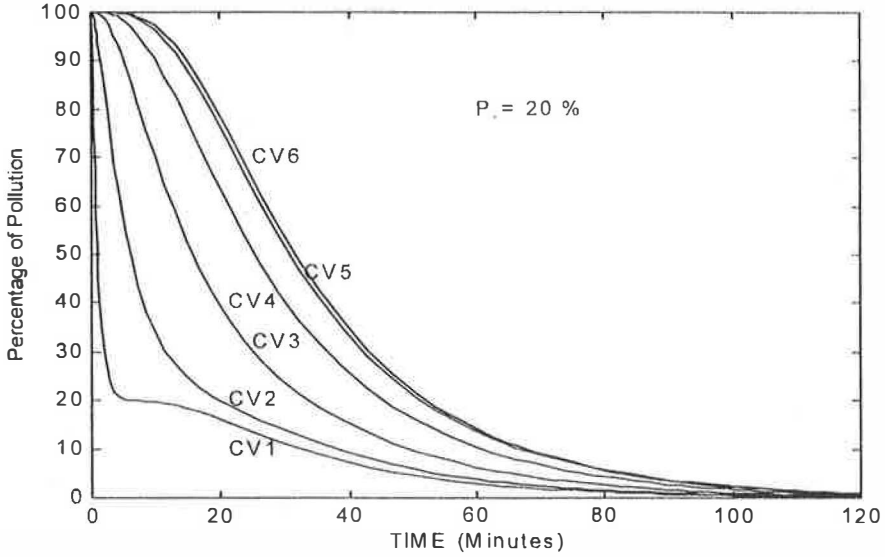

Figure 4. Pollutant disperssion curves for control volumes with 20% air recirculation

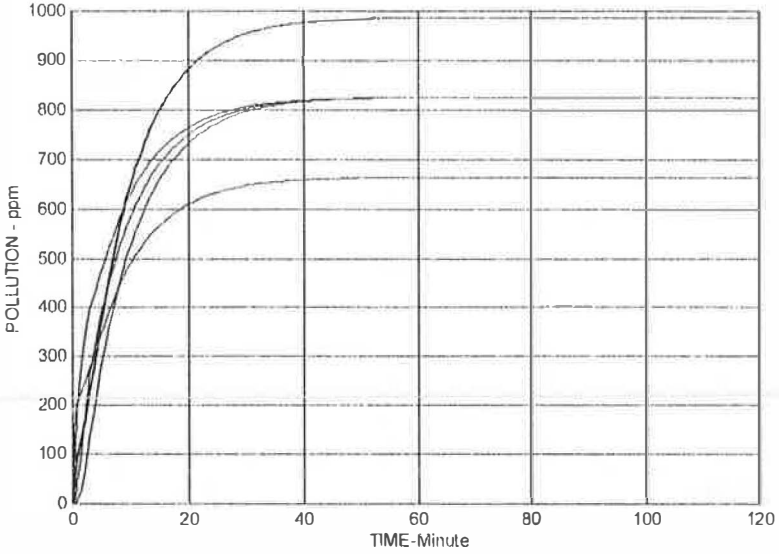

Fig. 5. Time response of pollutant in each control volume for 50% air recirculation

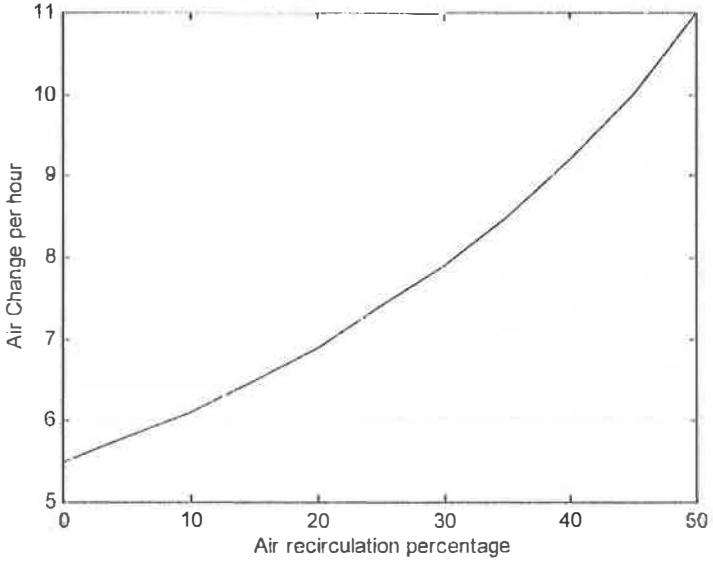

Fig. 6. Optimum required ACH versus the percentage of air recirculation

CLIMATIC CONDITIONING OF BUILDINGS IN MAGHREB CONTEXT: HYDRAULIC FLOOR FOR COOLING AND SOLAR HEATING

A. MOKHTARI*, H. KAZEOUI*, Y. BOUKEZZI*, L. KADI*, G. ACHARD**

Laboratoire de Thermique du Bâtiment, Institut de Génie Civil, USTO, B.P. 1505 El Menaouer, 31000 Oran, Algérie.
* Laboratoire de Génie Civil et Habitat, ESIGEC, Université de Savoie, 73376 LE BOURGET DU LAC, France.

ABSTRACT Considering the generous availability of solar energy in Algeria, one can expect good performances of solar heating by using Direct Solar Heating Floors. The additional advantage of such a heating system is that the same floor hydraulic loop could be used for heating and cooling. In this study, the performance of such systems has been analyzed, using the TRNSYS simulation tool. Results for an Algerian climate show the influence of the main sizing parameters and indicate that a large fraction of heating needs could be covered by solar energy. When cooling is considered, an important decrease in resultant temperature can be acheived with a relatively elevated fluid inlet temperature.

ntroduction

The technique of floor heating obtained these last years a excess of importance. The main dvantages of this technique are related to the low temperature of the heat source due to the high urface of emission a high degree of thermal comfort and as the performance of heating floor is ccordingly more elevated if the temperature of fluid is lower [1], the utilisation of the solar nergy ameliorate then considerably the conditions of comfort. The Solar Direct Heating Floor DSHF) is the most recent technique of heating by the sun, it was developed in French for year 980 by the Superior School of Engineers of Marseille (ESIM) and since made proof of implicity, of comfort and of economy of energy.

The use of low temperatures (about 40°C) in heating mode brought professionals to imagine working in summer comfort with water sent at about 18°C. Then, the cooling floor owes its xistence to the heating by the floor. This system, heating and cooling floor, allows to assure a limatic conditioning during the extremes of both summer and winter.

This study is intended to give a modelling of the behaviour of an experimental cell which is eing acheived at Oran in Algeria.

Description of the direct solar heating floor

The principle of the direct solar heating floor is of circulating directly in a network of pipes rowned in the floor a fluid heated by some solar collectors without using the intermediate torage tanks. The floor is then an element of the building structure and an element of storage. he system thus obtained offers many advantages with regard to the classic systems of solar eating on the plan of costs, of the liability [2].

In the modelisation of the heating floor, we choose the utilisation of TRNSYS software, ecause its flexibility, its modular structure and the importance of its domain of application. The eat transfer by conduction is treated by a convolution model: method of « Z-transform » oefficients for the walls and method of CTF [3] for the floor, the both being derived from the

method of thermal response factors. The following assumptions were interjected in order to simplify the calculations:

- the temperature of fluid is supposed the same in all the points of the loop, it is the arithmetic average between entry and exit temperatures,
- the thermal properties of the heating floor are supposed independent of the temperature,
- there are not thermal losses on the periphery of floor,
- the conduction transfer is supposed bidimensionnel and the study is limited to a half right section by reason of symmetry offered by the disposition of heating pipes.

The coupling of the heating floor with the building is achieved via the equivalent temperature of floor and the conduction flux in the slab [3]. This flux is calculated in the heating floor module of TRNSYS software with the assuption of high and low equivalent temperature of floor known treated. It is then like a variable of entrance of building module of TRNSYS which gives a new value of the equivalent temperatures in return. This process is then repeated until the convergence.

Simulation of the experimental DSHF system at USTO

The simulated building represents an experimental cell in progress of realisation at the Institute of Civil Engineering of the University of Sciences and Technology of Oran (USTO, Algeria) and composed two rooms of same dimension which only one is equipped of DSHF. The global surface is of 40 m2. The experience has for objective of testing and of knowing the behaviour of DSHF in the Algerian climatic conditions. Concerning the solar installation, we used a heating slab of reinforced concrete (10 cm) where the network of pipes is put directly on 4 cm of insulating material (polystyrene). The solar collectors are of 4 m2 area are installed on the roof and tilted 45° to the south. A derivation toward a hot water tank is foreseen in order to valorise the maximum of the solar energy (in summer) which will assure the pre-heating of the Domestic Hot Water (DHW), a daily volume of 150 l is delivered to the users at a temperature of 60°C.

The auxiliary system is considered like a system completely independent of the DSHF, it will bring the quantity of necessary energy in order to maintain the interior temperature to its required value which is fixed at 18°C. Note that we study in this article only the room equipped with DSHF supposed in contact, with outside, by all its wall., the case of floor in contact by its inferior surface with a sanitary cavity is also considered.

Hourly meteorological data were used for the simulations. The following measured variables at Oran (latitude 35,03°N) were considered for the specific year of 1992: - the external ambiant temperature; - the direct and diffuse components of solar flow; - the wind speed and direction; - the temperature of sky; - the temperature of cold water.

The incidence of two parameters on the energetic performance of the solar installation is studied in this article: solar collectors area and thickness of the heating slab.

We could note that the reduction of the thickness of the heating slab accompanies a reduction of energetic performances of solar system. Indeed, in analysing the economy* of heating energy (ECO HEA) brought by every slab (Fig. 1), we note that it is accordingly more elevated when the thickness is big. This is due to the fact that when the thickness is reduced (reduced energy storage), the energy which is given up is badly used. Knowing that the quantity of energy given to the floor is practically the same when its thickness varies, this energy is directly given up to the ambiance with a delay time and a deadening function of thickness of the slab. In analysing now the total economy brought by the solar installation (heating and DHW), we will say that it is noticeably the same for all the slabs (Fig. 1), because the absence of the regulation limited the quantity of energy given to the floor.

* The economy of energy is the difference between the energy requirements before and after introduction of solar installation devised by the energy requirements without solar installation.

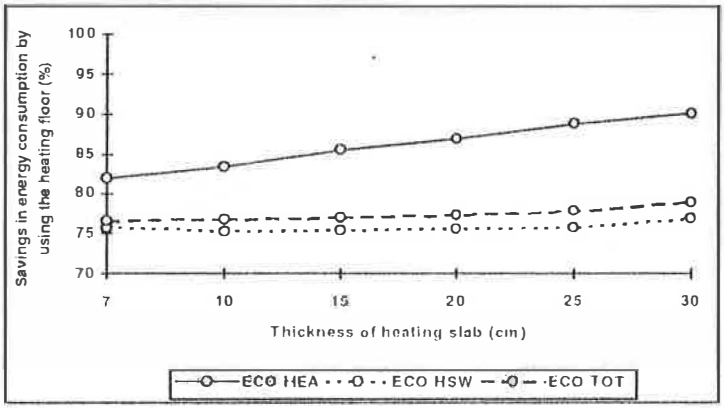

Fig. 1: Influence of the heating floor thickness on the savings in energy consumption.

n summary figure, we could note that

the reduction of performance** of heating for the slab of 07 cm is of 9% with regard to the slab f 30 cm. This is only of 7% for the slab of 10 cm.

the reduction of global performance is of 3.5% for the slab of 07 cm with regard to the slab of 0 cm and only of 3% for the slab of 10 cm. This mean that by reducing the thickness of more ıan 50%, the reduction of energetic performance is only of 3%.

The utilisation of an important thickness is not necessary, a heating slab of 10 cm will be an ıteresting compromise on condition to see the consequences of the use of this slab thickness on ıe comfort conditions.

In following the evolution of the interior temperature and surface floor temperature (Fig. 2), ve note that a maximum of interior average temperature of 25.5°C and 28.3°C at the surface are btained in the month of November. With such temperatures, we could affirm that some ıtolerable overheats are felt in addition to the temperature of surface of floor which exceed 28°C, mit of surface temperature of heating floors. With a slab of 30 cm, some sensations of verheating are also felt because we note a maximum interior average temperature of 24.5°C and 7.3°C at surface.

We conclude therefore that a slab of 10 cm with 4 m2 of collectors leads necessarily to some verheats that we must avoid. The solution is of supplying the DSHF with a system of regulation 3] which:

cuts the circulation of fluid as soon as the temperature of fluid returning from heating floor xceed a limit value (TRET) that we fixed at 25°C,

allows again the circulation of fluid as soon as its temperature is inferior to TRET-ΔT (ΔT is set) 2°C) and if the temperature of fluid coming out from collectors is inferior to a critical value 50°C).

igure (3) allows to compare the levels of interior temperatures obtained before and after ıtroducing the regulation system. We note that the levels of temperatures obtained with ıtroducing the regulator are less elevated than those obtained without this system. We note that ıe interior maximal temperature decreases from 25.5 to 20.7°C and the temperature of surface om 28.2 to 21.8°C.

* The reduction of performance is the difference of economies brought by the heating slabs of 30 cm and (e) of ickness devised by the economy of energy brought by the slab of 30 cm

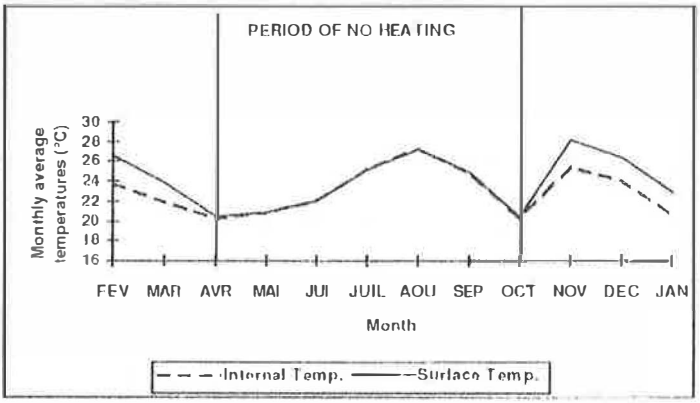

Fig. 2: Yearly evolution of the monthly averages of floor surface and internal ambiant temperatures. Slab of 10 cm and 4m2 of solar collectors at Oran (lat. 35°N).

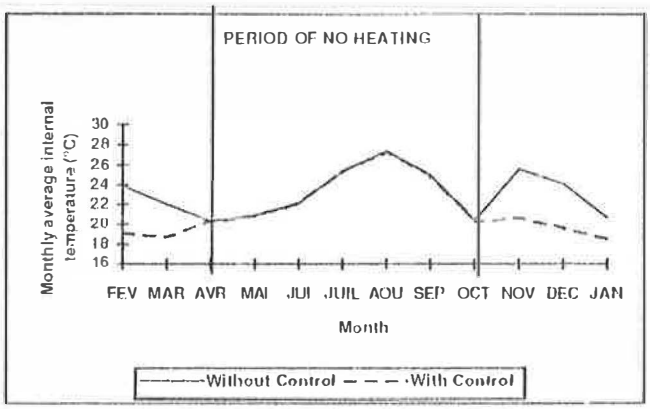

Fig. 3: Influence of the control on fluid return temperature on the yearly evolution of the internal ambiant temperature. Slab of 10 cm and 4m2 of solar collectors at Oran (lat. 35°N).

The introduction of a control system on fluid return temperature leads to an improvement of comfort. It is however important to analyse its influence on the energetic performances of the DSHF. We note that the energetic performance for the heating falls with the introduction of regulation system. However, this reduction accompanies an increase of performance for the DHW precesses system which and an increase of global performance for the two (Fig. 4). This is due to the fact of introducing the regulator, limits the quantity of energy given up to the heating floor. The energy no valorised is thus exploited in the DHW tank contrarily to the case of the absence of the regulation where this energy contributed to create some overheats when the DHW tank had again some needs.

Concerning the collectors area, we could see that an important collectors area reduces considerably the auxiliary energy for the two processes, heating and DHW. This phenomenon is caused by the fact that in increasing the area of collectors, we increase the quantity of energy given to the heating slab and to the DHW tank. So, the economy of energy brought by the solar installation is accordingly dimmer than the area of collectors is least (Fig. 5). It seems important to note that the utilisation of 2 m2 of collectors (10% of the area of heating floor) generates an

economy of energy of about 60%, so an economy superior to the one generated by 20% of collectors in French climate. In order to satisfy 45 to 50% of economy only, as in France, we say that a ratio (collectors area on heating floor area) of 8 to 10% is widely sufficient in Algerian climate. We are going to see now if this area (2 m2) could be used without the system of regulation. For this purpose, we are interested us to a sequence that we found very unfavourable on the plan of overheats: 1 to November 10, the hottest week in the period of heating of the year 1992, where we analysed the daily evolution of the interior temperature and the floor surface (Fig. 6).

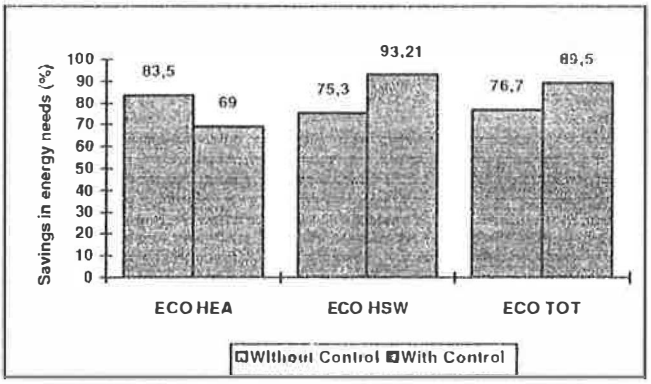

Fig. 4: Influence of the control on fluid return temperature on the yearly evolution of energy (heating and hot water) savings. Slab of 10 cm and 4m2 of solar collectors at Oran (lat. 35°N).

We can note that a surface of 2 m2 of collectors could be used without fearing the risk of overheats since the interior temperature never exceed 23°C and the surface temperature 24,5°C. But, like the climatic data are variable, we could not avoid the very sunny periods. In this case, it is more prudent of foreseeing a system of regulation allowing to avoid all risk of overheats whatever the area of collectors used.

We choose the utilisation of 4 m2 of collectors (20% of the area of heating floor) in order to have the maximum of the solar energy and minimise the auxiliary energy.

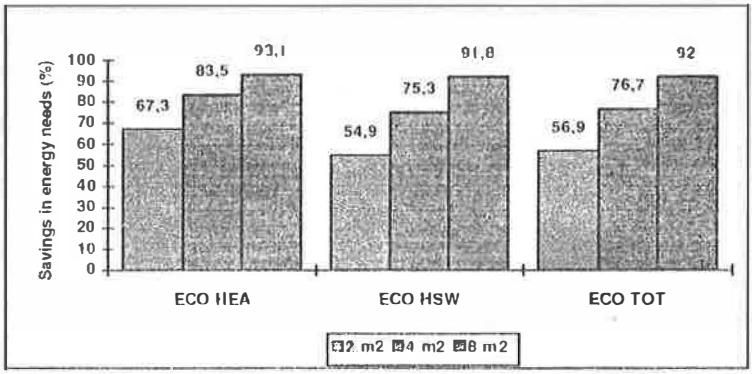

Fig. 5: Influence of solar collector area on the yearly savings on energy needs. Slab of 10 cm at Oran (lat. 35°N).

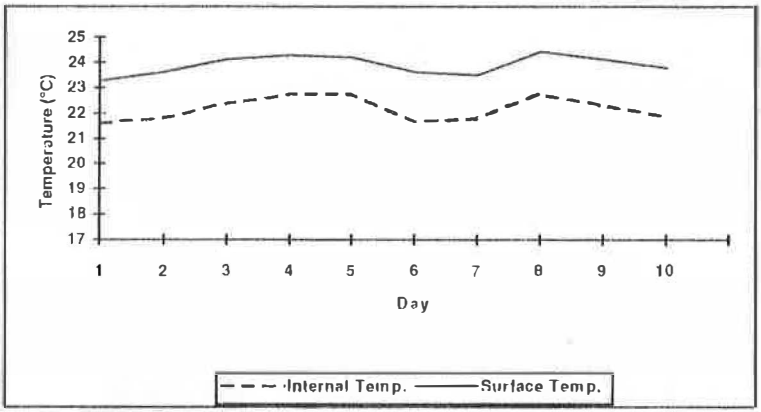

Fig. 6: Evolution of the internal ambiant and floor surface temperatures for the hotest decade in the year. Slab of 10 cm and 2m2 of solar collectors at Oran (lat. 35°N).

Simulation of the hydraulic floor system for cooling

In this case, we use some relative data to the direct solar heating floor installed. It is a matter of heating floor conception (composition, thickness and modelisation) and the hypotheses returning there. The lonely difference resides in the absence of collectors :instead of feeding the floor by collectors, another source called "cold source" takes place at once it is needed. The installation depends on cold source. Nevertheless, some difficulties impose as for its choice. Face to this problem, we suppose in our case to have a constant cold departure temperature.

As a matter of fact, our work is based essentially on the possibility of cooling with on hydraulic circuit in the floor of the room in Algerian climate. This, we have used the software of thermal design TRNSYS under Mediterranean climate (Oran).

The main problem intervening to the level of working of cooling floor is tied to the problem of condensation [4]. As a matter of fact, a too low surface floor temperature could lead to condensation on the floor. It is advisable to regulate the entrance fluid temperature in the slab starting from a limited temperature (dew temperature Dt). This last is determined thinks to air psychometric chart. Other comfort conditions must also be fulfilled. - the surface floor temperature (Sft) must be upper than 18.3°c [5] in order to avoid the sensations of cold weather to the feet, - the dry resulting temperature (Drt) must be located between 22°c and 25°c. The physiological comfort of human body is defined by that temperature. Henceforth, we define the summer comfort by: the absence of condensation and thermal ourly simulations were achieved in order to study the condensation and the thermal comfort. In order to analyse the problem of condensation, the day of August 05th is considered (Fig. 7). We consider separately two entrance temperature of fluid, 19 and 21°c. Concurrently to this analysis, we study the thermal comfort. The phenomenon of condensation is accentuated for an entrance temperature of 19°c.The dew temperature are elevated of about 23°c. The risk of condensation is diminished with an entrance temperature of 21°c, however, it is not eliminated. We find this risk at 3h in the morning. A higher entrance temperature, of about 22°c, will separate this problem. Globally, we could say that the criterion of comfort was respected : - a surface floor temperature upper than 21°c; - the dry resulting temperature does not exceed 25°c. Nevertheless, in order to avoid the problems tied to the condensation during all the period of cooling, we must augment the entrance temperature of fluid in the floor (a maximum of 22°c).

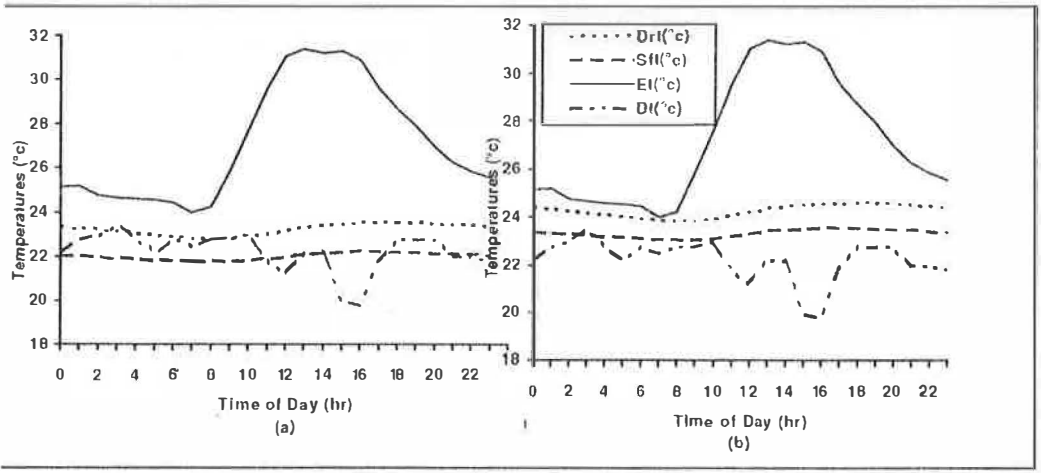

Fig. 7: Influence of fluid inlet temperature on the daily evolution of cell temperatures. External ambiant temperature (Et) is also represented. (a) Inlet temp.= 19°C; (b) Inlet temp.= 21°C.

Conclusion

The simulations achieved to the course of this work showed that the utilisation of the technique of Direct Solar heating Floor in an Algerian climate is very promising. The energy requirements covered by the solar are of 90% about the total needs of building with a ratio of collecting of 0.2 and of 60% with a ratio of 0.1 only. This mean that the ratio of collecting is diminished and the energetic performances are improved with regard to the climate of France 40 to 50% with a ratio of 0.2). We also showed that the utilisation of a thin slab (10 cm) reduces only to 3% the energetic performances with regard to 30 cm of thickness (slab advocated by ESIM) provided that this must be supplied with a system of regulation which avers indispensable whatever the thickness of heating slab and the area of solar collectors used. The influence of other different parameters must be studied before analysing economically this technique comparing to the other techniques of traditional heating. Also the theoretical study of cooling floor achieved in climatic cell in Oran put in evidence that the process could in actual fact give satisfaction in matter of cooling of the ambience, a lowering air and dry resulting temperatures of 4°c is possible with an entrance temperature of water relatively elevated, of some 22°c. The temperature of water must be chosen in function of : thermal comfort and risks of condensation.

References

[1] T. Cabirol et D. Roux, "Chauffage de l'habitat et énergie solaire.", Edisud, 1984.

[2] D. Roux, D. Mandineau et M. Chateauminoix, "Calcul des planchers solaires directs.", Edisud, 1983.

[3] P. Papillon, "Contribution à l'amélioration de la technique du plancher solaire direct. Analyse de la solution " Dalles minces " et gestion optimisée du chauffage d'appoint.", Thèse de Doctorat, Université de Savoie, 1992.

[4] E. Michel, "Les installations de rafraîchissement par le sol.", Revue Promoclim, Tome 25, n°2, mars/avril 1994.

[5] O. Fanger, "Les exigences du confort thermique", 2ème congrès ICBEM, Ames, Iowa, 1983.

ASSESSMENT OF OPTIMUM WINDOW GLAZING IN TEMPERATE CLIMATE IN TERMS OF SOLAR AIR TEMPERATURE

Kohei ONO*, Akihito OZAKI*, Takashi SUGAI*, Dai Morita**

*Department of Architecture, Faculty of Engineering, Fukuoka University
Nanakuma 8-19-1, Jounan-ku, Fukuoka, 814-80
Tel : +81-92-871-6631, Fax : +81-92-865-3109

** Department of Construction, Faculty of Engineering, University of Ryukyus
Senbaru 1 Nishiharacho, Okinawa

ABSTRACT

The effects of thermal performance of glazing and building structure on air conditioning load of dwelling house are analyzed in Fukuoka Japan. Then, guide line of optimum window glazing unit using SAT as regional index in temperate climate is proposed. The adequacy is shown by the relation of SAT to simulated heating and cooling load of one room model with a south window. At the simulation, effective solar heat gain in winter is counted in connection with thermal performance of building structure. By SAT-Glazing relation maps, it is shown that Low-E double glazing unit is adaptable through year over the wide area of SAT in Japan.

1. INTRODUCTION

Optimum thermal performance of window glazing for dwelling houses in temperate climate should be designed so as to save both of heating load in winter and cooling load in summer. Window performance is determined by two elements of thermal insulation and sun shading. The thermal insulation is generally accepted to be desirable because it contributes to reduction of heat transfer caused by temperature difference between indoor and outdoor. However, if the air and wall temperature of indoor are higher than those of outdoor in summer, such condition is often appears at night, thermally insulated window is disadvantage for saving cooling load. Sun shading contributes to reduction of cooling load, but possibly increases heating load because of retaining of indoor heat. In addition to such seasonally contradictory effects of window performance, the regional difference of outdoor temperature and solar radiation intensity makes the required thermal load different. Thermal performance of building structure, particularly thermal capacity, is another important factor to change the amount and balance of heating and cooling load. Such complicated relations are discussed on the basis of numerical simulation of heat flow through 10 kinds of glazing and thermal loads of dwelling house which has the glazing

Table 1 Thermal and Optical Performance of Glazing (Normal Incident Angle)

	Kinds of Glazing									
	(1)	(2)	(3)	(4)	(5)	(6)	(7)	(8)	(9)	(10)
Solar Heat Gain Coefficient	0.87	0.77	0.51	0.44	0.77	0.52	0.43	0.41	0.31	0.29
Solar Heat Transmittance [kcal/m²h℃]	5.1	2.9	2.2	2.2	2.6	1.4	1.4	1.5	2.7	2.3
Visible Ray Transmittance	0.90	0.82	0.68	0.68	0.82	0.68	0.68	0.30	0.27	0.27

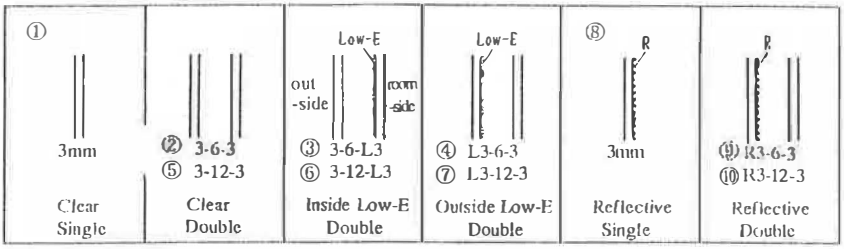

Figure 1 Specifications of Glazing Units

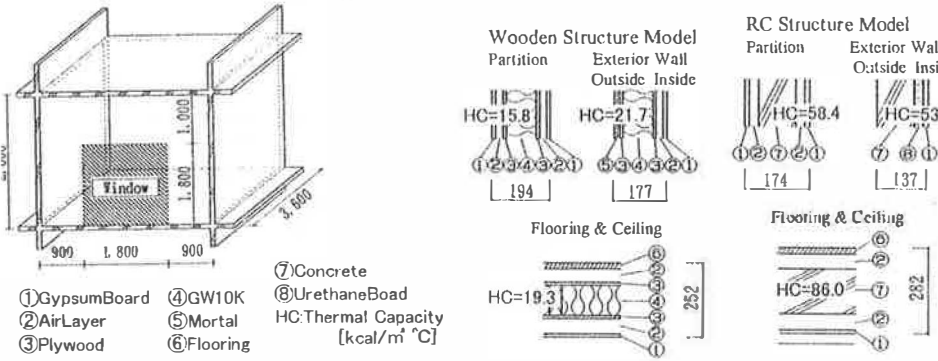

Figure 2 One Room Model of Multiple-Layer Dwelling House and the Wall Structure

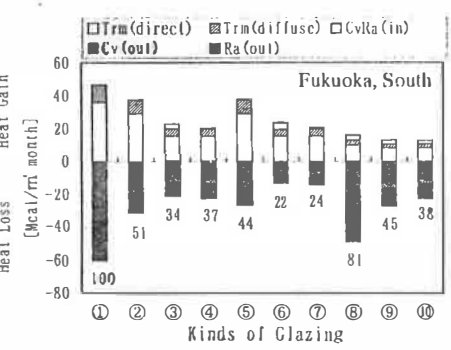

Figure 3 Heat Flow through Glazing in February

Remarks in Figure 3,5 :
Trm: Transmittance of direct or diffuse solar radiation.
Cv, Ra:Convection and Radiation heat flow between room and room-side pane surface.
Figures in Figure 3～6 show the rate to glazing No.①

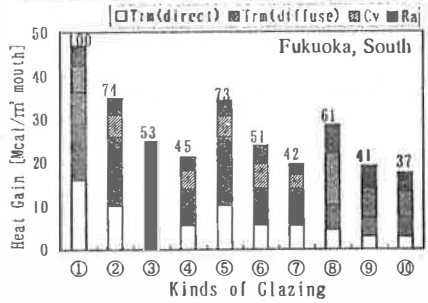

Figure 5 Heat Flow through Glazing in August

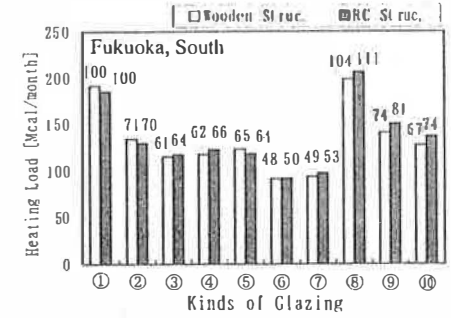

Figure 4 Heating load of Wooden and RC Model

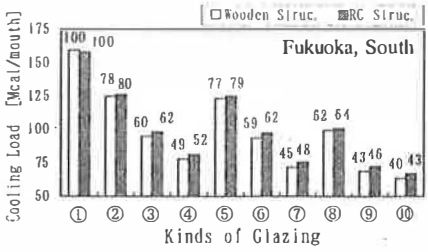

Figure 6 Cooling Load of Wooden and RC Model

unit facing south in Fukuoka Japan. Then, the authors propose the method of assessmen of optimum window glazing unit by region in terms of SAT (Solar Air Temperature) a the the climate index, overall expression of outdoor air temperature and solar radiatio intensity. The adequacy is shown by the relation of heating and cooling load to SAT of 1 cities through longitudinal location in Japan. Here, the effective solar heat gain throug glazing, the part of solar heat gain which rises the room temperature to the setting poin (22℃), is counted as the contribution to heating load reduction. Then, SAT- Glazin relation maps are given for wooden and RC structure.

2. CONDITIONS OF NUMERICAL SIMULATION

2.1 Simulation Method

Simulation program for room temperature fluctuation and thermal load, THERB[1~2], i used. Time-varying of surface heat transfer coefficient, long wave radiation balanc among indoor surfaces, solar radiation incident-angle-dependency of glazing therma performance and multiple reflections of transparent solar radiation among indoor surface are strictly dealt in the program. Non-stationary or stationary linear equilibrium equatio is applied to heat flow calculation through opaque wall or glazing, respectively.

2.2 Housing Model and Conditions for Simulation

The specifications of selected glazing units and the thermal performance are shown i Table 1 and Figure 1. No.③ and ⑥ are insulation type of Low-E glazing unit with Low-E film coated on room-side pane, and ④ and ⑦ are sun-shading type with Low-E film o outside pane. Figure 2 shows one room model of multiple-layer dwelling house wit wooden and RC structure which has a south window. Temperature of adjoining rooms i dealt with the same as objective room. Standard-Climate-Data of 18 regions by SHASE [3] is used as outdoor climate. Room temperature is set at 22℃ constant in winter (February) or under 26℃ in summer (August).

3. RESULT AND DISCUSSION

3.1 Influence of Glazing and Building Thermal Performance on Air Conditioning Load

Figure 3 shows the heat flow through glazing and the ratios of each glazing to singl clear pane glazing (No.①) in February. The heat loss is consisted of convection an radiation from room to inside pane surface, and the heat gain is mainly of solar radiatio transmittance. The former is considered to convert directly into heating load, while, som extent of the latter contributes to the reduction of heating load. The amount is the effectiv solar heat gain which rises the room temperature to the setting point (22℃) depending o the thermal performance of building structure. Figure 4 shows heating load calculated o the consideration of the effective solar heat gain and the ratios to single clear pane glazin for wooden and RC structure. On the comparison of two figures, the difference of ratio among glazing units of heating loads of wooden and RC model is much smaller than tha of heat loss through glazing. This means the substantial contribution of solar heat gain o heating load reduction for all glazing units. In Figure 4, heating load of RC structure wit the high thermal capacity is larger than that of wooden structure in case sun shading typ glazing (No.④, ⑦~⑩) is used.

Figure 5 shows the heat gain through glazing and the ratios in August. Both of direc and diffuse solar transmittance are remarkably reduced in case of Low-E and reflective glazing units. The heat gain is considered to convert directly into cooling load. Figure 6 shows the cooling loads of wooden and RC structure. The difference of ratios among glazing units of cooling loads of wooden and RC model is smaller than that of heat gain

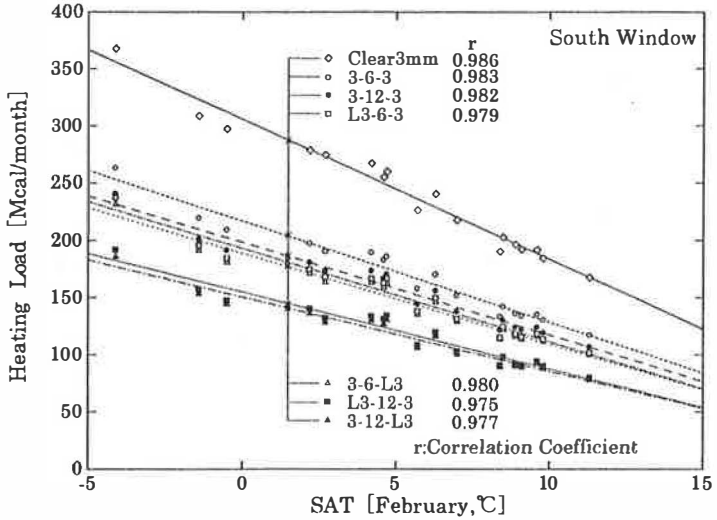

Figure 7 Relation of Heating Load to SAT by Glazing (Wooden Structure Model)

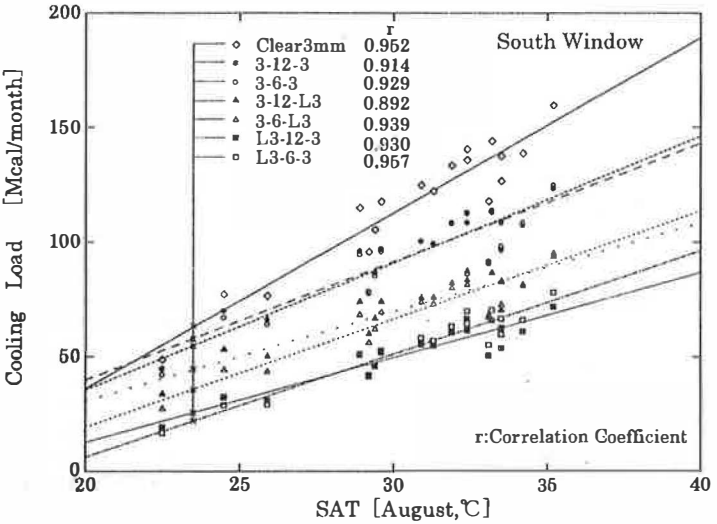

Figure 8 Relation of Cooling Load to SAT by Glazing (Wooden Structure Model)

Table 2 Linear Correlation Coefficient of Thermal Load to SAT and Air Temperature

Glazing	①	②	③	④	⑤	⑥	⑦	⑧	⑨	⑩
Cooling Load to SAT	0.952	0.929	0.939	0.957	0.914	0.892	0.930	0.982	0.978	0.975
to Outdoor Air Temp.	0.915	0.887	0.898	0.924	0.868	0.840	0.889	0.961	0.956	0.953
Heating Load to SAT	0.986	0.983	0.980	0.979	0.982	0.977	0.975	0.986	0.982	0.980
to Outdoor Air Temp.	0.967	0.964	0.961	0.960	0.963	0.958	0.956	0.966	0.962	0.960

(Wooden Structure Model)

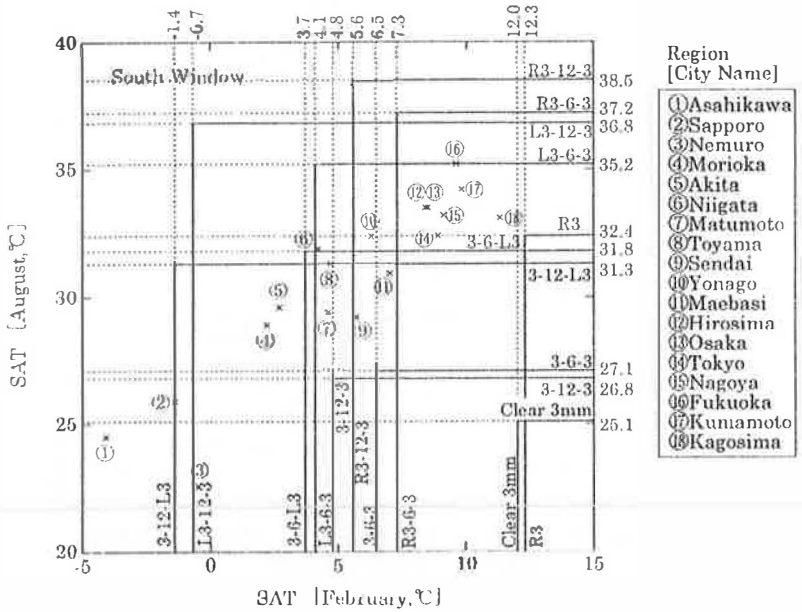

Figure 9 Guideline of Regionally Adaptable Glazing in terms of SAT (Wooden Model)

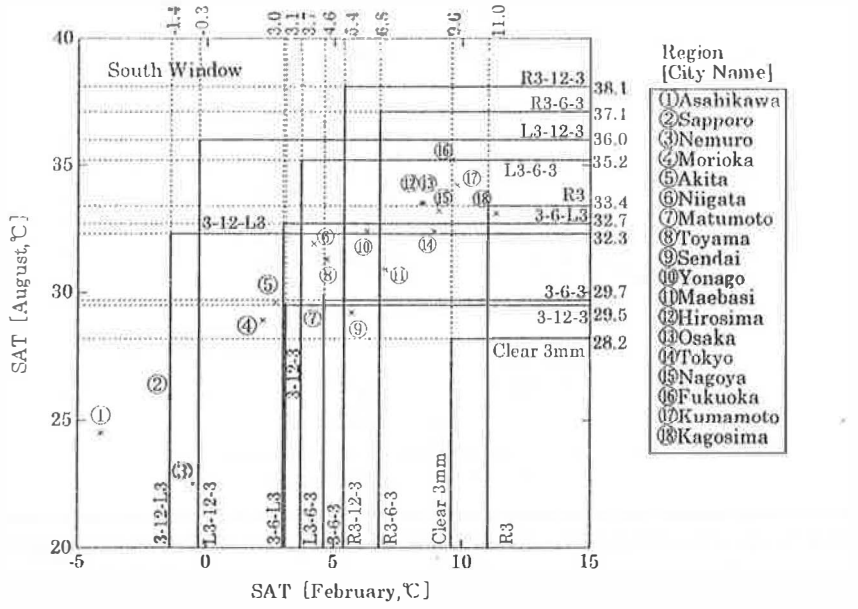

Allowable Area in Figure9, 10 : winter ; right side part of vertical line for each glazing
summer ; under-part of horizontal line for each glazing
through year ; rectagular part satisfying both of above

Figure 10 Guideline of Regionally Adaptable Glazing in terms of SAT (RC Model)

hrough glazing, particularly in case of glazing with high insulation performance (No.③ ⑥). This indicates the retaining effect of indoor heat by the insulation performance of glazing. In Figure 6, cooling loads of RC structure with the high thermal capacity are lightly lager than those of wooden structure for all glazing units except single clear pane No.①). Summarizing on summer, sun shading effect of glazing on cooling load reduction s diminished to some extent by insulation performance of glazing and heat storage of building structure.

3.2 Correlation of SAT to Heating and Cooling Loads

Figure 7, 8 show relations of heating and cooling load of wooden structure to 18 egions' SAT by glazing. Table 2 shows that the values of linear correlation coefficient vith SAT are higher than those with outdoor air temperature in all cases. The values of cooling load to air temperature is comparatively low especially in high insulation type glazing (No.⑤⑥). This causes by that cooling load is primary depend on solar radiation ntensity but not on air temperature, although higher the air temperature, larger the cooling oad. Therefore, the linear correlation with SAT, which equivalent solar air temperature is dded to air temperature, gives substantially improved results. We can conclude the propriety of using SAT as climate index for selecting optimum window gazing units.

3.3 The Relation between Allowable Area by SAT and Glazing

Here, we set a guideline of allowable heating load consumption in winter for all regions as the amount less than the heating load of Sapporo (the main city in cold region) in case glazing 3-12-L3 is used. As for in summer, we set it as the cooling load of Fukuoka showing the highest SAT in 18 cities in August in case of L3-6-3 is used. Glazing 3-12-L3 satisfies the insulation performance in coldest region in Japan by the Energy Conservation Standard, while, L3-6-3 has been assessed to be the most suitable grade both for insulation and sun shading performance in Fukuoka by our previous study[1].

On such bases, the adaptable area for each glazing in terms of SAT of winter (February) and summer (August) is presented as Figure 9 combining Figure 7 and 8. Figure 10 is the map for RC structure by the same procedure. Some of useful information from the maps are obtained as follows:

(1) There is no through-year adaptable city for clear double glazing units (3-12-3) in case of wooden structure, while there are two cities in case of RC structure.
(2) Sun shading type Low-E glazing unit (L3-6-3) is adaptable for wide area of 13 of 18 cities through year.
(3) Heat reflective single glazing (R3) is adaptable where the priority is given to cooling load saving under the climate of high SAT in summer and not so low SAT in winter(city ⑱ in case of RC structure).
(4) In Tokyo or Fukuoka, four kinds of glazing (L3-6-3, L3-12-3, R3-6-3, R3-12-3) are adaptable through year.

4. CONCLUSION

Propriety of using SAT as climate index for selection of optimum south window glazing was shown. By this guideline, complicated effects of glazing performance of solar heat transmittance and shading on thermal load consumption could be reasonably dealt with. Furthermore, it was clarified that Low-E glazing unit, particularly sun shading type, has the adaptability throughout wide area in temperate climate of Japan.

REFERENCES

[1] Kohei ONO, etc. (Milan, 1995), Proceedings of Healthy Buildings '95. vol.1, pp. 317-322
[2] Kohei ONO, etc. (1996), J. Archit. Plann. Environ. Eng., AIJ, No.483, pp. 33-42
[3] Published by The Society of Heating, Air-conditioning and Sanitary Engineering of Japan

Energy and environmental audit of buildings: an indirect evaluation

D. Barbieri[†], A. Nucara[†], M. Pietrafesa[†§], G. Rizzo[††]

[†] Dipartimento di Elettronica e Matematica Applicata, Università di Reggio Calabria.
Via E. Cuzzocrea, 48. 89128 Reggio Calabria, Italy.
[††] Dipartimento di Energetica ed Applicazioni di Fisica, Università di Palermo.
Viale delle Scienze. 90128 Palermo, Italy.

Abstract

A simple indirect way of performing energy and environmental auditing of buildings is here presented. It is based on the proper application of a recently released Italian standard aimed at the energy saving in climatisation of buildings. Its structure, that can be easily turned into a computerised frame, enables such standard to be employed as a complete analysis tool for predicting the thermal behaviour of buildings. By means of the application of this model, the effectiveness of the adopted technical solutions can be usefully ranked in terms of saved energy for climatisation purposes. Another relevant feature of the method is the possibility of getting environment related information, in terms of amount of released CO_2, resulting from the use of the selected equipment. An application to a simple building module, located in a southern Italian town, is also presented.

1. Introduction

Building energy auditing represents one of the best known procedures which allow to achieve information about the energy performance of a dwelling. Above all it is very useful in verifying the energy savings resulting from retrofit measures and in detecting occasional or systematic occurrences of high energy consumption.

Many auditing tools are currently available to technicians. They can belong to the highly sophisticated simulation models like, for example, DOE (1) or ESP (2), that provide estimates of energy consumption on the basis of the knowledge of thermal and physical characteristics of buildings and equipment, along with information concerning local climatic data. Other tools can also refer to the so-called energy signature procedures, like PRISM (3), that predict the building energy consumption by means of a proper regression curve (generally linear) of the heating energy demand versus the outside temperature. Alternatively, some manual methods can also be employed, mainly referring to energy inspection procedures (4).

However, at present, building auditing represents a very time and work spending operation, due to the complexity of the above mentioned available tools, at any level of detail. On the contrary, technicians do require easier methods, in order of getting fast information about the consequences of the adopted design choices, even at a rough stage of precision.

In the recent years, several domestic technical rules have been released by most of the industrialised countries, with the aim of promote energy saving in the climatisation of buildings.

§ author to whom all correspondence should be addressed

Many of these rules need a computerised frame and allow the thermal analysis of buildings to be performed with an enough detailed level. As that, this kind of models can be directly adopted like auditing tools, since they are capable of providing almost the same range of results. A newly released Italian rule can be assumed as a typical example of such kind of methods. It can be easier operated in comparison with the classic auditing methods. In addition, as it will be emphasised in the following, the method can be also utilised for drawing environmental information concerning the consequences resulting from the working of the HVAC system.

As a matter of fact, the new awareness concerning the environmental implications of the use of energy at urban scale, strongly affects the structure of the standards that are nowadays to be compiled. Most of these standards are now so comprehensive and well defined that they can be used, not only for checking the law-related compatibility of the design choices, but directly as working tools for selecting layout and plans.

2. Using an Italian standard as a computation tool

The recent Italian law n° 10/1991 (5), for example, released in the aim of accomplishing the national energy plan (PEN), candidates itself like a prominent one in the European context, with respect to the energy use for climatisation of buildings. It, in fact, could be directly employed for design procedures, referring to the envelope and to the HVAC system of a given building. This law in fact, rejecting the older approaches that only estimated the heating loss through the building envelope, makes use of a limitation to the energy demand of the system, defined by the building and the heating and air-conditioning equipment. The method relies on a global energy balance, taking into account different contributions (primary energy used in the HVAC plant, solar radiation, internal loads) and various types of heat losses (transmission and ventilation through the building, losses of the HVAC system due to the separate steps of production, regulation, distribution and emission of the required heat).

The rule assumes as reference parameters the "normalised energy demand" of the building, FEN (kJ/m^3 DD), and the "global mean seasonal efficiency", η_g, to both of which limit values are imposed. An accurate analysis of several complex energy issues is also involved in the procedure, like the estimation of the solar gains and the detailed treatment of the components of the climatisation system, among other things.

These features obviously ask for the use of a computerised procedure. A comprehensive nomenclature of the several parameters involved in the procedure is given in the following Table (1). Figs. (1) and (2) illustrate the logical sequence and the calculating operations to be accomplished in order of getting the final energy parameters that characterise the selected building, that is the normalised energy demand, FEN, and the global mean seasonal efficiency, η_g. Obviously these parameters can be directly adopted as energy auditing indexes.

Table 1. Nomenclature of the symbols used through the procedure

Pn: useful power of the heater; **Cd**: heat loss volume coefficient; **V**: building volume; **DD**: degree days; **n**: number of hourly air changes; **I**: average solar irradiance on an horizontal surface; **a**: thermal internal gains; Q_f: demand of primary energy required by the HVAC system; Q_c: primary energy required for the thermal conversion in the furnace; Q_e: primary energy corresponding to the electric consumption of the auxiliary systems; Q_p: thermal energy generated by the HVAC system; Q_{aux}: thermal energy transmitted from auxiliary systems; Q_{bu}: electric energy required by the burner; Q_{po}: electric energy required by the circulating pump; η_{tu}: useful thermal efficiency; η_{sen}: Italian electric

board efficiency; Q_u: useful energy demand; Q_{uws}: useful energy demand in the actual working duty cycle (non continuous); Q_L: overall heat losses by transmission and ventilation; Q_{Se}: thermal energy due to the solar radiation absorbed by the opaque surfaces; Q_{Si}: thermal energy due to the solar radiation falling on the glazed surfaces; Q_I: thermal energy due to the internal gains; Q_T: thermal energy exchanged by transmission with the outdoor environment; Q_G: thermal energy exchanged by transmission with the ground; Q_V: thermal energy exchanged by ventilation and infiltration; Q_U: thermal energy exchanged by transmission and ventilation with adjacent non-heated confined environments; Q_A: thermal energy exchanged by transmission and ventilation with zones characterised by a constant (and known) value of the air temperature; N: number of days in a month; H_x: heat loss coefficient; $\Delta\theta_x$: difference of temperature between the interested elements or thermal zones; H_K: overall thermal losses coefficient; η_h: efficiency of the HVAC system; η_d: efficiency of the distribution system; η_e: efficiency of the regulation system; η_e: efficiency of the heating elements; η_u: utilisation factor of heat gains; F_{il}: reduction factor of the transmission heat losses (depending on the intermittent working regime); F_{ig}: reduction factor of the thermal energy due to the solar radiation and the internal heat gains (depending on the intermittent working regime); k: coefficient taking into account the working profiles; $q_{s,j}$: overall daily irradiance on the surfaces with j exposition; $A_{e,j}$: equivalent area of the surfaces with j exposition.

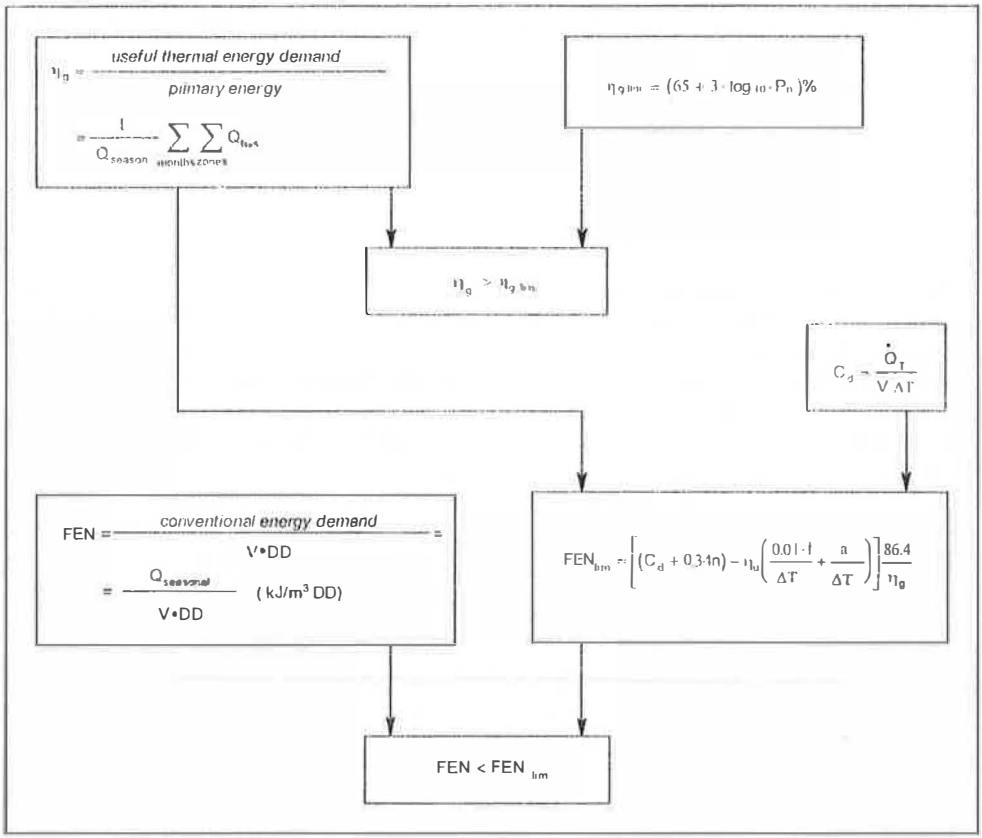

Fig. 1 Procedure for the computation of the energy parameters for the auditing process.

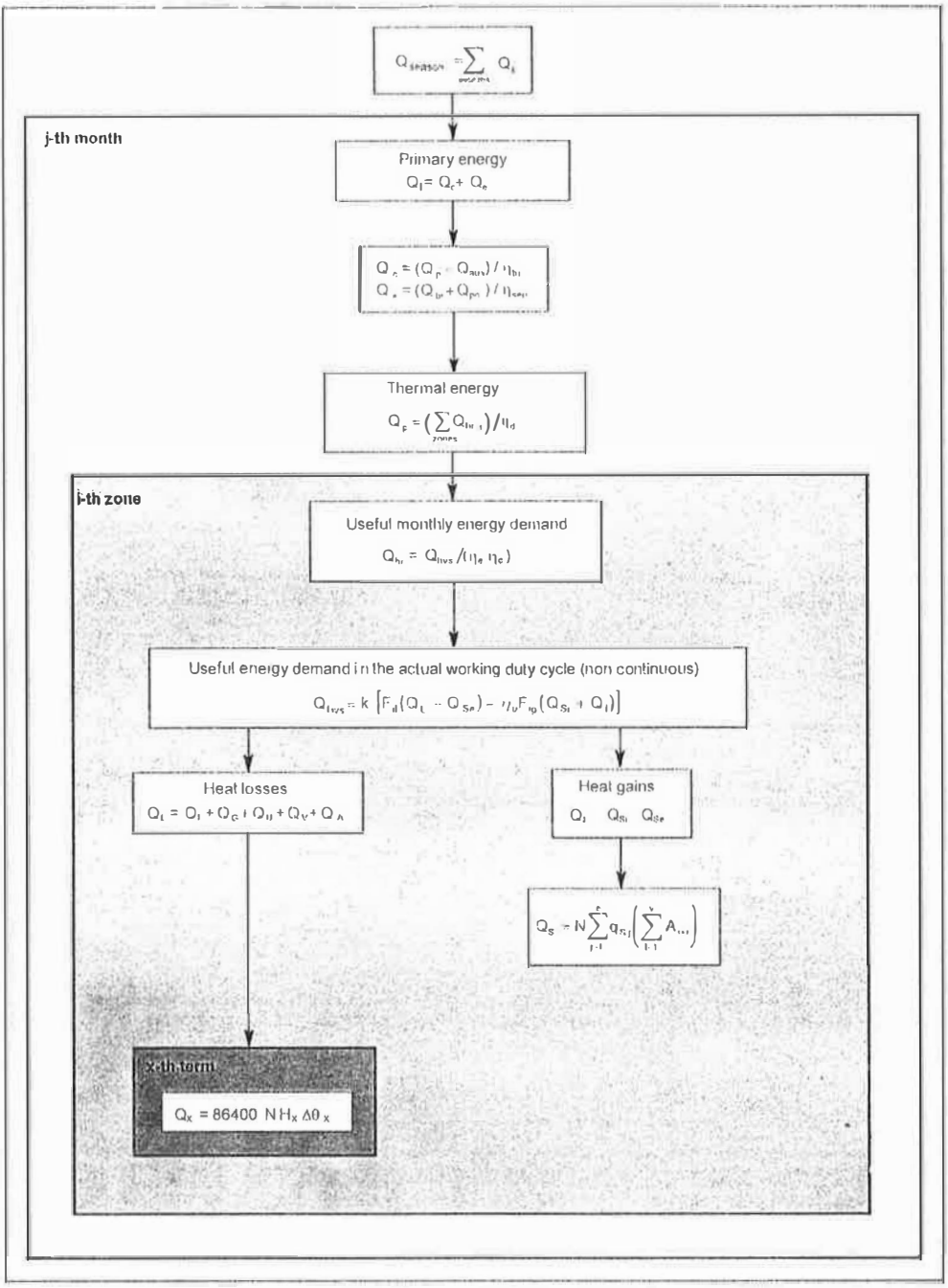

Fig. 2 Detailed sequence of the algorithms involved in the audit method.

3. An application

Using a commercially available electronic sheet, the Italian standard is here managed as a fully comprehensive design tool for a whole system represented by the envelope and the heating, ventilating and air conditioning equipment. As selecting parameters, we assume here both the seasonal energy demand, $Q_{seasonal}$, and the environmental suitability of the design choices. With this aim and in order of showing the feasibility of the method, a very simple building is here adopted, for which the energy demand required for the climatisation and the released amount of CO_2 from the heating plant are computed.

The simulated building is a simple parallelepiped module (4x5x3 m^3) supposed to be located in the climatic condition of Palermo, Italy (38°3 north latitude, 751 DD): both mean monthly temperatures and mean monthly solar irradiance can be assumed as typical of the whole Mediterranean area, as it is reported in Table (2) for the heating period. All external surfaces of the envelope are supposed to face the outdoor condition, while the indoor temperature is set at 20°C; the ventilation rates are set at 0.5 changes per hour, according to the Italian rule. Some main thermal features of the envelope are also reported in Table (3).

Table 2. Main climatic parameters for the heating season of Palermo

	Outdoor temperature (°C)	Solar irradiance on south surface (MJ/m^2)	Solar irradiance on horizontal surface (MJ/m^2)
January	11.1	11.9	7.7
February	11.6	13.8	11.1
March	13.1	13.1	15.7
December	12.6	11.0	6.9

Table 3. Thermal characteristics of the building module.

	Vertical surfaces	Floor	Ceiling	West window	East door
Overall transmittance (W/m^2K)	0.85	1.00	0.90	4.50	3.00
Linear transmittance of the related thermal bridges (W/mK)	0.135	0.010	0.010	0.150	0.150

After all the calculation described in Figs. (1) and (2) has taken place, the most relevant results for the given building, to be assumed as auditing information, can be split into two different categories, that are respectively related to energy and environment issues.

As representative parameters of the energy performance of the building we adopt here the whole seasonal average efficiency of the heating plant, η_g, and the normalised energy demand, FEN. As representative parameters of the environmental performance of the building we select the primary seasonal energy demand, Q (directly linked to the amount of fossil fuel and electricity required by the heating plant) and the quantity of carbon dioxide released through the heating period of time. These parameters are labels that feature the building and are considered as the most relevant indexes in order of auditing the building, by means of the indirect way here introduced. Table (4) reports the profile of the simulated building, both in terms of energy and environmental issues.

Table 4. Energy and environmental labels of the selected building.

Energy profile	
Average efficiency of the heating plant, η_g	0.71
Normalised energy demand, FEN (kJ/m³/DD)	117.73
Environmental profile	
Primary seasonal energy demand, Q (MJ)	5305
primary energy required for thermal conversion, Q_c (MJ)	5125
primary energy corresponding to the electric consumption of the auxiliary systems, Q_e (MJ)	180
CO_2 released (kgC)	114.2

The total amount of released carbon dioxide is evaluated by means of the emission factor computed through the whole cycle of the pertinent fuel (7). In the hypothesis of oil (or any oil derivative) employed as fuel for the furnace heating plant, the corresponding emission factor to be adopted is 21.52 gC/MJ.

4. Conclusions

An indirect method, based on the application of an energy saving standard, has been proposed for a quickly auditing of buildings. The method, implemented on a commercially available electronic sheet, can be usefully employed in the early stages of the thermal analyses, when general information about the performances of buildings are required. It only needs data referring to the thermal characteristics of the envelope, to the features of the HVAC system and to the climatic site.

Another relevant characteristic of the procedure is the possibility of obtaining information about the environmental impact of the building (at least in terms of greenhouse gas released), once that the heating plant and the used fuel are defined.

The final result of the method is a table where the energy and the environmental profiles of the building are reported by means of four relevant parameters.

5. References

(1) DOE2 Reference Manual. Rep. LBL-8706, Revision 2. Lawrence Berkeley Laboratory, Berkeley, CA, 1981.

(2) J. Clarke, D. Mc Lean. ESP: A Building and Plant Energy Simulation System, Version 6.2. Adam Hilger Ltd., 1987.

(3) M. Fels. PRISM: An Introduction. *Energy Build.*, 9, 1986.

(4) G. Fracastoro, M. Masoero. Manuale dell'Energy Auditing - Consiglio Nazionale delle Ricerche *in conjunction with* International Energy Agency (Annex XI): Energy Conservation in Buildings and Comunity Systems Programme, Torino, 1990 (*in italian*).

(5) GURI Legge 9 gennaio 1991, n. 10, "Norme per l'attuazione del piano energetico nazionale in materia di uso razionale dell'energia, di risparmio energetico e di sviluppo delle fonti rinnovabili di energia". Supplemento ordinario alla GAZZETTA UFFICIALE, Serie generale - n.13, 1991 (*in italian*).

(6) D. Barbieri, A. Nucara, M. Pietrafesa, G. Rizzo: Advanced energy saving loads in the building sector: the Italian case. *Proceedings of the* PLEA 96 - Building & Urban Renewal, 289-294, Louvain-La-Neuve, 1996.

(7) D. Barbieri, F. Morabito, A. Nucara, M. Pietrafesa: Role of car materials recycling in mitigating global warming effects. *Proceedings of the* III International Congress "Energy, Environment and Technological Innovation", Vol. I, pp. 153-157, Caracas, 1995.

INFLUENCE OF RADIATION HEAT TRANSFER ON SPACE HEATING AND COOLING LOADS

S. Hokoi, Ph.D.* , M.Matsumoto, Ph.D.**
* Department of Architecture and Environmental Design, Kyoto Univ., Sakyo, Kyoto 606, Japan
** Department of Environmental Design, Osaka Sangyo Univ., Nakakakiuchi, Daito 574, Japan.

ABSTRACT

The influence that radiant heat transfer has on space heating and cooling load is investigated based on the fundamental equation of radiation inter-reflection. The analysis shows that in a space with a uniform enclosure, even when each wall has a different emissivity and different adjacent outdoor temperature, the radiative heat transfer has no net effect on space heating load. In this case, only the convective component of the combined convection-radiation coefficient of heat transfer should be used in the calculation of heating load. Example calculations show that there would arise a significant discrepancy between an accurate space heating load and a value obtained through the use of the combined coefficient of heat transfer. Also shown is that a peak load error of more than 80 % might be possible at the warming-up period of intermittent heating if the combined surface coefficient is used.

1. INTRODUCTION

Usually the combined surface coefficient of heat transfer consisting of convective and radiant components is used to calculate space heating and cooling load and/or room air temperature. To obtain reliable results, however, convective and radiative heat transfer must be dealt with separately. This involves a calculation of a surface-by-surface conductive, convective and radiative heat balance for each room surface and a convective heat balance for the room air[1]. In particular, a complicated equation of inter-reflection must be solved for the radiative heat transfer. The computational algorithms[5][6][7] and simplification of the treatment[2][4] have been proposed and investigated from a practical point of view. Among others, Hutchinson[4] re-examined the standard value of the radiant fraction of heat transfer through the air film adjacent to the inside surfaces of walls, floor and ceiling. Through the analysis of the cubic room enclosed by a uniform construction and external air with a uniform temperature, he showed that a significant reduction of the equivalent film coefficient for radiant transfer is possible.

In this paper, the influences of radiation heat transfer between room surfaces on space heating and cooling load, room air temperature are studied for a better understanding of the radiant heat transfer process. The intent of the present paper is to re-examine the radiant fraction of heat transfer, and the importance of inter-reflection of radiative heat transfer under a transient condition will be stressed.

2. FUNDAMENTAL EQUATIONS

Following are the fundamental equations used in this paper.

(1) Heat Balance of Room Air Enclosed by Surface S

$$c\sigma V\frac{dt_a}{dt} = c\sigma Vn[t_{ov}(t) - t_a(t)] + \int_A h_c(s)[t_i(s,t) - t_a(t)]ds + Q(t) \qquad (1)$$

where,

$t_a(t)$: room air temperature [℃], c : air specific heat [J/kgK], σ : air density [kg/m^3],
$t_{ov}(t)$: outdoor temperature related to air exchange [℃], n : air exchange rate [1/s],
$h_c(s)$: convective heat transfer coefficient at interior surface [W/m^{2}K], V : room volume [m^3],
Q(t) : heat input by the air-conditioning system and internal heat source at time t [W],
A : inner surface area of walls [m^2], s : position at the inside surface of wall,
$t_i(s, t)$: inner surface temperature of wall at time t [℃], t : time [s].

(2) Heat Balance at the Inner Surface of Wall

$$h_c(s)[t_a(t) - t_i(s, t)] + q(s, t) = -\lambda \frac{\partial t_w}{\partial x} \tag{2}$$

where, q(s, t) : net radiative heat flux absorbed by wall [W/m^2],
λ : thermal conductivity of wall material [W/mK], t_w : wall temperature [℃].

One-dimensional heat flow through the wall is assumed here. Eq. (2) reduces to the following form at steady state :

$$h_c(s)[t_a - t_i(s)] + q(s) = \frac{1}{r(s)}[t_i(s) - t_o(s)] \tag{3}$$

where, $t_o(s, t)$: outdoor temperature [℃], r(s) : thermal resistance from inner surface to outdoor.

(3) Long-Wave Radiative Heat Transfer between Room Surfaces

If every surface is assumed to be completely diffusive, the equation expressing the radiation inter-reflection is given as,

$$G(s, t) = \int_A \varepsilon(s')E_b(s', t)F(ss')ds' + \int_A [1 - \varepsilon(s')]G(s', t)F(ss')ds' \tag{4}$$

where, G(s, t): irradiation [W/m^2], $\varepsilon(s)$: emissivity of inner surface of wall [-],
F(ss')ds : shape factor, $E_b(s, t)$: emissive power of a blackbody [W/m^2].

(4) Net Radiative Heat Flux Absorbed by Wall

$$q(s, t) = \varepsilon(s)[G(s, t) - E_b(s, t)] \tag{5}$$

(5) Sum of the Net Radiative Heat Flux

By making use of Eqs. (4) and (5), the following equation can be derived:

$$\int_A q(s, t)ds = 0 \tag{6}$$

3. INFLUENCE OF RADIATIVE HEAT TRANSFER ON SPACE HEATING AND COOLING LOAD IN THE CASE OF UNIFORM WALL RESISTANCE

A space enclosed by walls with uniform thermal resistance and convective film coefficient is considered in this section. Under the assumption of uniform thermal properties, the characteristics of radiative heat transfer between walls can be understood easily as will be seen later. First, the steady state is examined. Next, non-steady state conditions are dealt with.

3.1. Space Heating Load at a Steady State

With regard to space heating load and room air temperature, the following relationship is valid : The net effect of radiative heat transfer on the space heating load is 0. Therefore, a convective film coefficient must be used instead of the combined convection-radiation coefficient of heat transfer in the calculation of space heating load and room air temperature.

This can be explained as follows (see Fig. 1) : The influence that radiation inter-reflection has on the heat transfer process on a wall surface is equivalent to the surface heat generation with the magnitude of net absorbed radiative heat flux q(s, t). A part of this heat flows outward through the wall, and the rest flows into the room through the inside air film. The sum of the outward heat fluxes over all enclosures is the heating load caused by the radiative heat transfer. The outward heat flux is determined by the ratio of thermal resistances, one from the surface to the outside air and the

other from the surface to the room air (interior film resistance). Since this ratio is assumed here to be constant at each wall, the sum of the outward heat flux remains constant no matter how nonuniformly the surface heat generation may be distributed. Furthermore the sum of this equivalent surface heat generation is 0 because the sum of the net absorbed heat caused by radiation over all surfaces is 0 (Eq. (6)). Therefore, the sum of the outward heat flux caused by radiation is also 0.

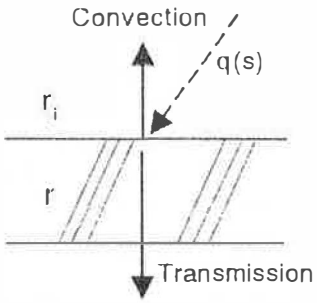

Figure 1 Graph illustrating the separation of absorbed heat into convective and transmitted fluxes

This proof requires no assumptions on the external air temperature distribution, surface emissivity and its frequency characteristics and the linearization of radiative heat transfer. Thus, the statement given at the beginning of this section is valid even in the following situations :

(1) surrounding external temperatures are different from wall to wall,
(2) emissivities are different from wall to wall,
(3) nonlinear dependence of radiation on surface temperature (4th power law) is taken into account,
(4) the dependence of radiation on wavelength is also taken into account.

Also by making use of this result, some insight into the validity of using the combined convection plus radiation surface coefficient of heat transfer and its adjusted value for practical use can be obtained. The fact that the convective film coefficient (conventional value of 2.3 to 3.5) should be used in a building with a uniform resistance means the overestimation of heating load when predicted by the usual thermal calculation with the combined surface coefficient (the conventional value of which is 9.3).

3.2. Space Heating Load at Non-Steady State

The conclusion obtained in section 3.1. has its equivalent under the transient state. That is, the net effect of radiation heat transfer under non-steady state is 0 if the thermal properties of the wall and the convective heat transfer coefficient is uniform along the enclosure[3]. This relationship is valid even if the surrounding external temperatures and their emissivities are different from wall to wall.

4. NUMERICAL EXAMPLES

4.1. Objectives

Since the results in section 3 are valid only at a space surrounded by a uniform enclosure, it is necessary to examine how far these can be applied to an actual situation with non-uniform enclosures. Here, by comparing the heating loads of a simple room obtained by the following three methods of thermal calculation, the importance of the radiative heat transfer is investigated.

(1) Radiation heat transfer is calculated exactly by taking account of inter-reflection,
(2) heating load is calculated by making use of the conventional method of thermal calculation where the combined surface coefficient is used, and
(3) the same method is used as (2) except that only the convective surface coefficient is used.

4.2. Method of Numerical Analysis and a Room Analyzed

The fundamental equations used here are Eqs. (1) through (5) and the nonsteady heat conduction equation. For the numerical computation, each wall and glazing is divided into rectangular cells (2 $\times$ 2 in the following example). Furthermore wall depths are divided into several slices for finite difference calculation. Explicit finite difference method is used to solve one-dimensional heat

onduction equation.

The room shown in Fig. 2 was analyzed. It as dimensions $5 \times 3 \times 3$ m^3 and the walls and lazing face the outside (or the next room). The vall is 14 cm thick RC (thermal conductivity 1.6 W/mK) and the glazing is 3 mm thick glass thermal conductivity 0.79 W/mK). Outdoor air nd setpoint room air temperatures are 0℃ and 0℃, respectively. The convective, radiant and he combined surface coefficients of heat ransfer were set at 4.6, 4.6 and 9.3 (W/m^{2}K), espectively. Here a constant value of 4.6 is nerely given to the radiant coefficient h_r. A value close to this is often used as a standard value for design purposes in Japan.

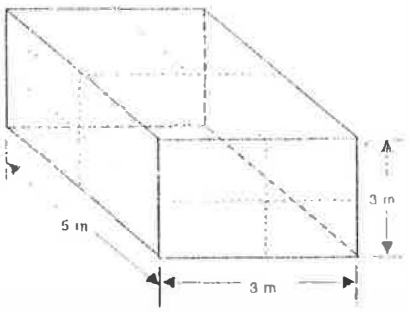

Fig.2 Schematics of room employed in simulation Broken lines denote the cell partition.

4.3. Results and Discussions

Fig. 3 shows the time history of heating load where only one-fourth of the wall with 5×3 m^2 rea is glazed. In this calculation, the initial temperatures were all set at 0 ℃ and the room air emperature was raised to 20℃ at time $t \geq 0$. Solid line denotes the heating load where the adiation inter-reflection is taken into consideration (hereafter called an exact solution) and the broken line shows the result of the usual thermal calculation with the conventional combined surface coefficient of 9.3 (hereafter called conventional coefficient solution). The upper figure shows the heating loads and the lower one shows the percentage deviation from the exact solution. The results of conventional thermal calculation with convective film coefficient (called a convective solution) denoted by chain lines are almost coincident with the exact solutions.

After 30 hours when a steady state is almost achieved, the conventional coefficient solution is 6.1 (kW) compared with exact solution 3.4 (kW) and overestimates by 46 %. The difference is larger than 80 % at the beginning of air-conditioning and remains still large with 65 % even after 2 hours, which is much larger than the steady state error of 46 %. As shown in this figure, just after the change of room air temperature, the ratio of the heating loads obtained by using the combined and convective coefficients is close to the ratio of their values $(h_c+h_r)/h_c = 9.3/4.6 = 2$, since the initial temperatures of all enclosures except for the window are set at 0℃.

Fig. 4 shows the result where a wall with a surface area of 5×3 m^2 is glazed and the wall opposite to the glazing is a non-adiabatic partition wall. The air temperature of the neighboring room adjacent to this partition wall was set equal to the room air temperature being analyzed. There is more non-uniformity of thermal properties of the enclosing walls in this situation than in the former example, thus the deviation of the convective solution from the exact one may be expected to become larger. The errors of the conventional coefficient solution at steady state and at the beginning of the air conditioning are 50 % and 80 %, respectively. On the other hand, the error of the convective solution is negative in this case and takes its maximum value of about - 1.8 % at the steady state. This discrepancy is not so large from a practical point of view. Furthermore, since an error at the starting time of the air conditioning is also negligible, it can be said that the simple conventional method of thermal analysis using the convective film coefficient instead of the conventional combined one is practical where the degree of non-uniformity of the enclosure is not larger than the present example.

5. DISCUSSIONS

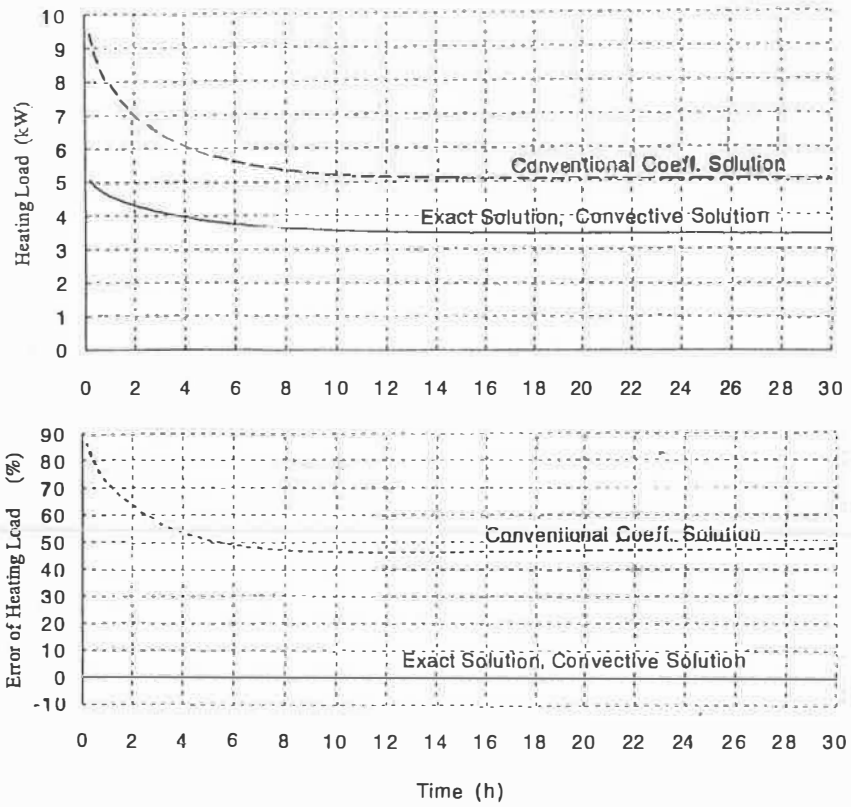

Figure 3 Comparison of heating loads

One-fourth of an external wall is glazed. The upper figure shows the heating load (kW) and the lower the discrepancy from the exact value (%).

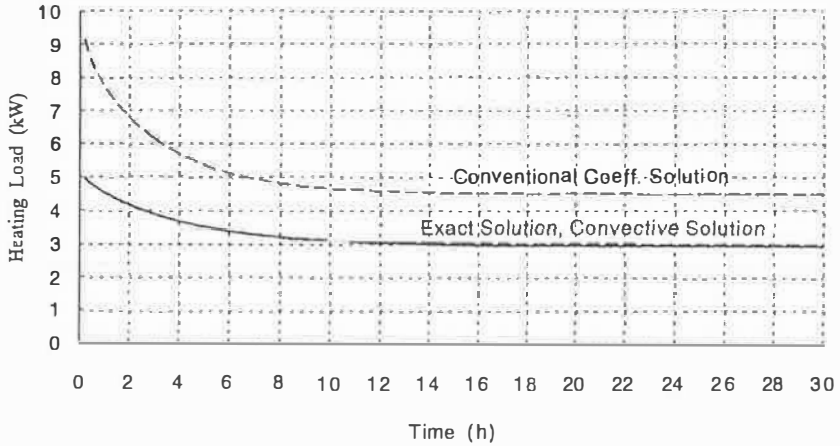

Figure 4 Comparison of heating loads

One external wall is entirely glazed and the opposite wall is a partition.

Although the situation where a convective film coefficient should be used instead of the ombined surface coefficient of heat transfer has been investigated so far, it must be noted that this not always the case and there are several situations where the usual combined surface coefficient ust be used. The following comments seem appropriate with regard to this point.

Consider a room whose internal walls are all adiabatic. The external temperature is assumed igher than the room air temperature (cooling case). By exchanging radiation with exterior walls, ie adiabatic walls have a net radiation gain so that they will have a temperature above the room air mperature, thus supporting convection to the room air from other than the exterior walls. Thus, ie "film" coefficient must be increased by some amount to account for this radiative effect epending on the relative size of the transmission walls and adiabatic walls. In the case of a very nall transmitting wall area, the temperature increase of the internal walls is also very small thus ading to the result that the internal wall temperature almost equals the room air temperature. The ppropriate radiant coefficient in this case is the standard one.

In the case of a multi-room space, it is not possible to obtain an exact heating load by using a onvective film coefficient. Consider a partition wall that separates two symmetrical rooms. Here ie boundary condition at the center of the partition wall becomes adiabatic if the conditions of the djacent room are the same as the room of interest, which results to the infiniteness of equivalent ermal resistance of the partition wall. Since the thermal resistances of the other walls are usually nite, the condition of uniform resistance will not be satisfied.

. CONCLUSIONS

The influence of radiation inter-reflection on space heating and cooling load was investigated in is paper. The conclusions of this paper are summarized as follows :

1) Radiant heat transfer has no net effect on the space heating and cooling load if the thermal esistance of the enclosure is uniform. This means a convective film coefficient should be used nstead of the combined surface coefficient of heat transfer for the calculation of the space heating oad. This is valid even if the outside temperatures adjacent to the external walls are different from lace to place and the emissivities of wall surfaces are different from each other.

2) The possibility that the use of the conventional combined surface coefficient of heat transfer night give too large a value of heating load at steady state, up to 40 %, was shown by a simple heoretical analysis. Numerical examples showed that a space load error of more than 80 % might e possible at the starting time of the air-conditioning if the conventional combined surface oefficient of heat transfer is used.

3) It has been stressed that the inter-reflection of radiant heat transfer is important and the thermal nalysis with a convective film coefficient is effective under certain circumstances.

REFERENCES

) ASHRAE. 1993. ASHRAE handbook - 1993 fundamentals, pp.26.1-26.3. Atlanta : American Society of Heating, Refrigerating, and Air-Conditioning Engineers, Inc.

) Davies, M.G. 1978. On the basis of the environmental temperature procedures, Building and Environment, Vol.13, No. 1, pp.29-46.

) Hokoi, S. and M.Matsumoto. 1994. Influence of radiant heat transfer on heating load (in Japanese), Proc. of Kinki branch, Architectural Inst. of Japan, No.34, pp.201-204.

) Hutchinson, F.W. 1964. A rational re-evaluation of surface conductances for still air, ASHRAE Transactions, Vol.70, pp.105-109.

) Matsuo, Y. 1984. New architecture and building science series 10, Environmental Physics, Chapter 2. Thermal environment, (in Japanese), Shoukoku-sha.

) Nakamura, Y. 1975. Radiant heat transfer for calculation of the space heating load (in Japanese), Summaries of Technical Papers of Annual Meeting, Architect. Ins. of Japan, pp.341-342.

) Walton, G.N. 1980. A new algorithm for radiant interchange in room loads calculations, ASHRAE Transactions, Vol.86, part 2, pp.190-208.

PERIODIC HEAT FLOW THOUGH VENTILATED WALLS: THE INFLUENCE OF AIR-SPACE POSITION UPON ROOM TEMPERATURE

C.Bartoli, M.Ciampi, G.Tuoni

Dipartimento di Energetica, Universita' di Pisa, via Diotisalvi 2, 56126 Pisa (Italy)
Tel 39-50-569611 - Fax 39-50-569666

Abstract. The thermal behaviour of a room equipped with different types of ventilated walls and subject to external temperature oscillations is analyzed. The results obtained confirm that the types of ventilated walls, found in a previous study to be preferable from the energy point of view under steady-state conditions, exhibit acceptable behaviour also when such temperature oscillations are present.

1. Introduction.

Ventilated walls have been recently attracting a good deal of research attention because their potential applications to climate control affect both the energy saving and comfort of buildings. In another paper presented at this Congress (1), the Authors reported the results of a study on the energy behavior of a room equipped with four different types of ventilated walls of equal thermal resistance with three different ventilation schemes.

More precisely, the walls denominated as types 1 and 3 had a layer of insulating material between the air space and the outer face, while in walls 2 and 4 the same layer was positioned between the air space and the external wall face. Moreover, in walls 1 and 2 the thicker brick layer (therefore of higher thermal capacity) is included in the outer face, while in types 3 and 4 it is in the inner one. Regarding the ventilation schemes of the interspace-to-room system, in case A, all the airflow into the interspace, of thermal capacity c (i.e. the product of the air mass flow by its specific heat), is collected from the outside and is used to turnover the air in the room; in case B the turnover air, is introduced directly in the room, has thermal flow defined as g, and is later used to ventilate the wall at the moment of ejection; in the limit case Y, wall ventilation is effected using a large airflow that is independent of room-air turnover (c>>g); finally, also the reference case R of a non-ventilated wall (though with the same thermal resistance) is considered.

The energy analysis developed in (1) has suggested a good compromise to be the choice of wall 2, with ventilation A during winter and B during summer. This report deals with ventilated-walls under conditions of periodic heat flow by analyzing the same structures with varying external temperature, solar radiation and air-conditioning system power. Indeed, under non-steady-state conditions, the arrangement of air spaces in ventilated walls is determined, not only by the ratio z between the air-space-to-outside thermal resistance and overall wall thermal resistance, but also by the distribution of thermal capacities within the wall (2,3). Furthermore, ultimate solution of the problem will depend on the thermal characteristics of structures within the room. Regarding the analysis, the operations followed to derive the main relations used are outlined in the appendix (2).

2. Statement and solution of the problem

In the case in which thermal stress is a periodic function of time, with angular frequency ω nd period $\chi=\omega/2\pi$, it is also necessary to consider the room's internal structure (vertical and orizontal partitions), as it has a considerable influence. Complex thermal variations T_i of the oom can arise from temperature oscillations of the external air in the shade T_o, oscillations of he radiation component (T_e-T_o) of the sol-air external temperature, or from oscillations of the ower Q_s of the air-conditioning system (i.e. "equivalent temperature" Q_sR_i). We can thus write 2):

1) $$T_i = L_1 T_o + L_2\left(T_e - T_o\right) + L_3 Q_s R_i$$

which can yield the frequency spectrum of the room's thermal response. Eq.(1) is a linear unction completely characterized by the three parameters L_1, L_2, L_3 which are dimensionless, omplex quantities with modulus of one or less. Then, the actual trend of the inside temperature ersus time can be obtained by calculating the Fourier antitransform of Eq.(1):

$$T_i(\tau) = \frac{1}{2\pi}\sum_{j=-m}^{m} T_i(\omega_j)\cdot e^{i\omega_j\tau}$$

with m indicating the maximum number of harmonic functions present in the expansions of T_o, T_e and Q_s. For some harmonic components, the coefficients L_i (i=1,2,3) depend on the chosen entilation scheme, as well as the elements of the transfer matrices of the two faces of the entilated wall and those of the elements transfer matrices relative to the structural components vertical and horizontal partitions) which make up the room interior. Regarding the ventilation chemes R, A, B and Y; an expression for these coefficients is presented in the appendix.

On the basis of Eq. (1), it seems that situations where coefficients L_1 and L_2 are small in modulus are preferable; in this way room temperature is less influenced by sudden climatic hanges (variations in T_o and/or T_e-T_o). On the other hand, large values of L_3 seem preferable, in rder to be able to "correct" room temperature variations with limited use of the climate-control ystem. Eq.(1) is a generalization Eq.(1) from (1), to which it reduces under stationary onditions (ω-->0); under such conditions, only temperature differences must be present in Eq.(1), and so it must hold that $L_1=1$. In the particular case in which a constant temperature is mposed within the room ($T_i=0$), Eq.(1) takes the form:

$$Q_s R_i = -\frac{L_1}{L_3} T_o - \frac{L_2}{L_3}\left(T_e - T_o\right),$$

which quite similar to Eq.(1) of (1), and depends only on ratios (L_1/L_3) and (L_2/L_3). Even more articularly, for a passive room ($Q_s=0$), (3), without no air turnover (g=0), and a non-ventilated all, we can write: $L_1=L_2$ (see Appendix); then, from Eq.(1), we can deduce: $T_i = L_2 T_e$.

3. Numerical results.

As a sample application, we have considered a reference room of 3x4x4m, with a single xternal wall of $3x4m^2$, and volume of $48m^3$. The ventilated external wall is the same that is onsidered in (1), the inner structures are made up of a partition of light 0.08 cm brick with laster on both faces and by tile-lintel floors 0.20m thick; the air in room has been represented y a pure thermal capacity M (per surface unit of external wall) assumed to be $M=8.4$ kJ/m^{2}K. The geometric and thermo-physical characteristics of the materials have been reported in Table I f (1). Regarding the thermal conductivity and diffusivity of the tile-lintel floor, we have ssumed values of 0.80W/mK and $3.6\,10^{-6}$ m^2/s, respectively.

n contrast to the steady-state case, under oscillatory conditions, the reference case depends on wall type; so we actually should utilize four different reference cases, one for each wall type.

However, since wall types 1 and 2 and types 3 and 4 differ only in that the position of the insulating layer and interspace have been switched, and since these two layers are essentially resistive, with a very good approximation we can state: $1R \cong 2R$ and $3R \cong 4R$. More substantial differences exist between the first two types of walls (1, 2), as well as between types (3, 4), which differ in the placement of the 0.25m brick layer and the 0.08m light brick.

Figure 1 shows the curve of $|L_1|$ versus the period χ (in hours) for all examined cases, for an air-turnover rate of n=0.5. The values of $|L_1|$ for the reference case (R) and case B, for examined values of χ, depend very little on wall type and are very close to each other. Thus, the graph presents cases R and B by a single curve (bold). From figure 1, it can be seen that the values relative to case 2A (considered optimal for energy saving) result clearly lower than those of the reference case; thus insuring better control of room temperature in response to outside in-shade temperature variations during winter. From this point of view, during summer ventilation pattern B offers no great advantage with respect to the reference case; it is evident that case 2Y yields values smaller $|L_1|$ than case R only during short periods (χ<7.4 h).

Figure 2 plots $|L_2|$ as a function of χ, with n=0.5, for the various cases examined; it should be recalled that in case Y the L_2 value is always zero and the internal environment is completely dissociated from the effects of insolation. Now, consider the differences between the values of $|L_2|$ for ventilation scheme A and those for the corresponding reference cases: these are always positive and generally increase with rising χ. Instead, the $|L_2|$ for ventilation pattern B are all inferior to those of the corresponding reference cases. Here again, the difference between case B and corresponding reference case increases, albeit slightly, as a direct function of χ.

With regard to variations in the intensity of solar radiation, we can confirm that during summer (ventilation pattern B), only a small improvement is achieved with respect to the reference case, while a clear worsening, still relative to the reference, is evident during the winter (ventilation pattern A) but however, this produces limited effects, because of the poor insolation characterizing this season. As the air turnover rate increases, the trends of the curves representative of the various cases, do not change qualitatively. At constant χ, the values of $|L_1|$ and $|L_2|$ for any given wall and ventilation type increase as a function of n. As the air turnover rate increases, so does the influence on the interior thermal behavior of both the in-shade temperature and insolation. $|L_3|$ is relatively independent of wall type and adopted ventilation system, but depend considerably on the air turnover. Figure 3, presents $|L_3|$ as a function of χ, with n=0.5 and n=2, practically equivalent in all the cases considered here (case 1Y presents higher values, but is of limited importance here). As the air turnover rate increases, the value of $|L_3|$ decreases. The higher n is, the less sensitive is the room's thermal state to the action of the conditioning system; the difference between the L_3 values for n=0.5 and n=2 increases, though only slightly, as a function of χ.

Figures 4 and 5 plot the phase trend (in degrees) respectively for factor L_1 and L_2 as a function of period χ (in hours) relative to wall type 2, with n=0.5. Regarding figure 4, it is evident that the phase trend of L_1, in relation to configurations A and Y remains inferior to those of the reference case R, while the phase for configuration B practically coincides with that of case R.

The L_2 phase trend (Fig.5) is quite different (configuration Y has been excluded, because L_2=0): here the discontinuity in the curves is only apparent because of the effects of periodicity. The L_2 phase of configuration A results greater than that of the reference case, and the difference between the two phases, although particularly notable due to the high-order harmonics, remains

ensitive to the fundamental harmonic case (χ=24 hours). For example, for the case of χ=24 ours and in the reference case, there is a time delay of about 8 hours, while for configuration A his delay is about 10 hours. Such behavior must be considered positive, because it tends to shift he temperature peaks caused by variations in insolation towards the nighttime, when comfort equirements are minor.

inally, it is note-worthy that, for coefficient L_2, as well, the phase relative to configuration B is ery close to the reference case. The curves plotted in the previous figures do not change ualitatively with increases in the air turnover what can be seen is that phases L_1 and L_2 increase ppreciably with increasing n, for any given χ and configuration. The greater is the air turnover, he greater also is the time needed for variations in the in-shade air temperature and insolation to nake themselves felt within the room. The L_3 phase does not depend very much on ventilation attern and practically coincides with phase L_1 relative to the reference case. Phase L_3 increases vith increasing "n", reducing the promptness the conditoning system's effects.

. Conclusion.

The linear structure of the problem is such that, for any given configuration, room thermal ariations turn out to be linear combinations, suitably weighted by complex coefficients, of the xternal air temperature in the shade (coefficient L_1), the insolation (coefficient L_2) and the ower of the conditioning system (coefficient L_3), see relation Eq (1). For control of the interior emperature, situations are desirable in which coefficients L_1 and L_2 are "small" in modulus, but vith a "considerable" phase in order to limit and delay the influence of climatic changes on the nterior (temperature of external air in the shade and insolation effects). On the other hand, oefficient L_3 should be "high" in modulus, but "small" in phase, in order to render the action of he conditioning system more effective and prompt. The analysis performed reveals the requency spectrum of the moduli and phases of the above-mentioned coefficients regarding the our types of walls considered and the more suitable ventilation schemes for summer and vinter. In particular, regarding wall type 2, considered optimal with respect to energy saving 1), we have observed the following: that coefficient L_1 is practically the same as that of the eference case when considering the summer and ventilation pattern B; that for ventilation attern Y, the values of $|L_1|$ are lower than the reference case when considering solely scillation of short period, while the its phase turns out not much inferior to the reference case; hat in winter with (ventilation pattern A), wall type 2 is preferable to the reference case with espect to both $|L_1|$ and phase L_2; that coefficient L_3 is quite independent of wall type and entilation scheme for all the cases examined.

Thus, we can conclude that wall type 2, aside from being optimal with respect to energy consumption, also demonstrates behavior, which though not satisfying all requirements for nodulus and coefficient L_1 phase, is overall quite acceptable for the various examined ventilation atterns under periodic heat flow.

Appendix.

We would like provide a brief outline of the calculation of coefficients L_i (i = 1,2,3), defined mplicitly in Eq.(1). Through this appendix all quantities are relative to one unit of external wall urface. Let the 2x2 matrices with elements E_1, F_1, G_1, H_1 and E_2, F_2, G_2, H_2 be the transfer natrix belonging respectively to the external and internal wall faces. Each of these matrices will e calculated as the ordinate product of the transfer matrix of the single-layers making up the ace in question. The first and last of these layers will be considered a purely resistive type epresenting the thermal boundary resistance (2,4). In the following we use the definitions:

$$N=E_2F_1+F_2H_1, \qquad \sigma=N(cF_1F_2)^{-1}, \qquad \eta=(1-e^{-\sigma})/\sigma.$$

The internal part of the room is formed by P structural elements (vertical and horizontal partitions). In many cases, the a given inner wall of area Sn is symmetrical and separates spaces having the same temperature. In these cases, the surface passing through the middle of the wall can be considered to be adiabatic; thus only the half-wall facing the room results important for the thermal problem of room itself. So, if we define as g_n and h_n the third and the fourth elements of the transfer matrix relative to the n^{th} inner half-wall, and we represent the air and objects in room as a purely thermal capacity M, the influence of the room's internal structure is explained by elements of type (2,4):

$$\Lambda_0 = j\omega M + \sum' \frac{g_n}{h_n} v_n$$

where the summation must be extended to all internal p structures and v_n represents the ratio between the surfaces of the n^{th} structure and the external wall. Regarding the ventilation patterns examined in the work (R, A, B,Y), let us consider the following relations (2):

R: $\Lambda = g + \frac{1}{F_2}\left(H_2 - \frac{F_1}{N}\right) + \Lambda_0$, $L_1 = \frac{1}{\Lambda}\left(g + \frac{1}{N}\right)$; $L_2 = \frac{1}{\Lambda N}$; $L_3 = \frac{1}{\Lambda R_t}$

A: $\Lambda = g + \frac{1}{F_2}\left[H_2 + \frac{F_1}{N}(\eta - 1) - \eta\right] + \Lambda_0$

$L_1 = \frac{1}{\Lambda}\left[g + \frac{\eta(F_1 + F_2 - N)}{F_1 F_2} + \frac{1-\eta}{N}\right]$ $L_2 = \frac{1}{\Lambda}\left[\frac{\eta}{F_1} + \frac{1-\eta}{N}\right]$ $L_3 = \frac{1}{\Lambda R_t}$

B: $\Lambda = g + \frac{1}{F_2}\left[H_2 + \frac{F_1}{N}(\eta - 1) - \eta\right] + \Lambda_0$, $L_1 = \frac{1}{\Lambda}\left(g + \frac{1-\eta}{N}\right)$, $L_2 = \frac{1-\eta}{\Lambda N}$, $L_3 = \frac{1}{\Lambda R_t}$

Y: $\Lambda = g + \frac{H_2}{F_2} + \Lambda_0$, $L_1 = \frac{1}{\Lambda}\left(g + \frac{1}{F_2}\right)$; $L_2 = 0$; $L_3 = \frac{1}{\Lambda R_t}$

The stationary case can be obtained from the previous relations as the limit case for $\omega \to 0$, that is, the limit for low frequencies. It can be clearly seen that

$$N \to R_t, \qquad \Lambda_0 \to 0, \qquad \sigma \to [cR_t z(1-z)]^{-1}$$

and therefore

$E_1 = H_1 = 1$, $F_1 = zR_t$, $G_1 = 0$, $E_2 = H_2 = 1$, $F_2 = (1-z)Rt$, $G_2 = 0$

and, finally, through the expression for L_i shown above, we can easily obtain the limit-case expression of $\lambda_i = L_i(\omega \to 0)$, which obviously corresponds to those used in (1).

References

(1) - C.Bartoli, M.Ciampi, G.Tuoni, "Ventilated walls: air-space positioning and energy performance". Memory presented to ITEEC 97 Marrakesh 9-12 June 1997.

(2) - M. Ciampi, G. Tuoni, "Sul comportamento delle pareti ventilate in regime termico periodico stabilizzato". Work in press.

(3) - G. Tuoni, "Locali in regime termico periodico. Influenza delle strutture interne". La Termotecnica, n.1, pp.41-49, 1984.

(4) - M. Ciampi, G. Tuoni, "Sul comportamento termico degli ambienti con pareti in parte vetrate. Un modello di calcolo". La Termotecnica, n.9, pp. 51-61, 1985.

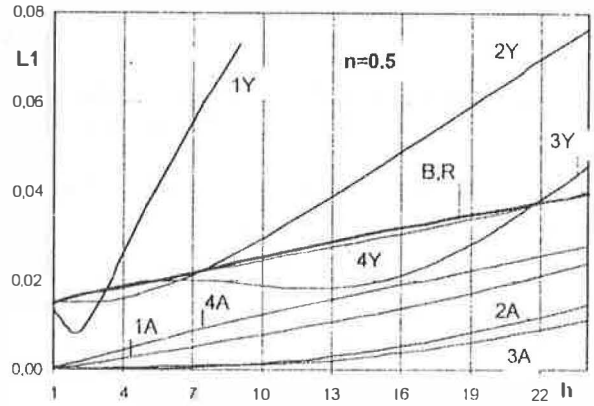

Fig. 1

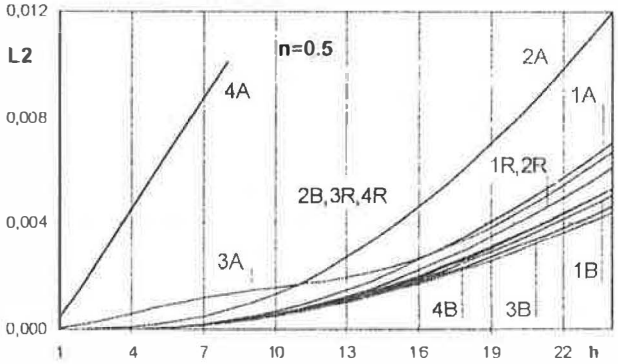

Fig. 2

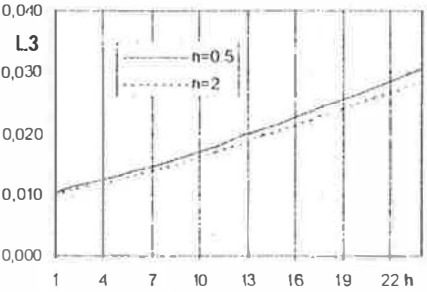

Fig.3

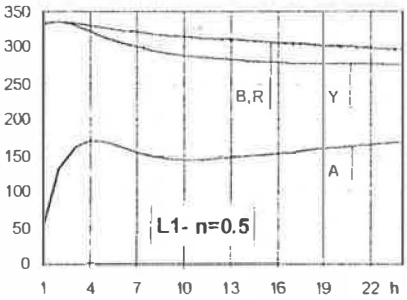

Fig.4

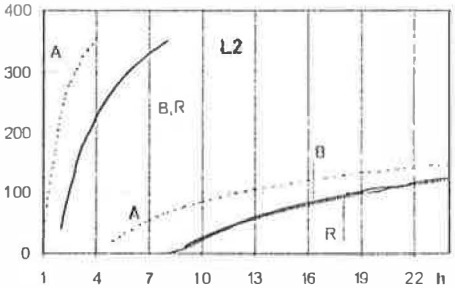

Fig.5

VENTILATED WALLS: AIR-SPACE POSITIONING AND ENERGY PERFORMANCE

C. Bartoli, M. Ciampi, G. Tuoni

Dipartimento di Energetica, Universita' di Pisa, via Diotisalvi 2, 56126 Pisa (Italy)
Tel 39-50-569611 - Fax 39-50-569666

Abstract: The energy behavior of walls having a ventilated air space is analyzed. Varying wall types and interspace arrangements are considered with the aim determining the configurations best-suited to the winter and summer seasons.

1. Introduction

Ventilated walls (double masonry walls whose interspace allows airflow) were initially designed to let humidity drain from the interspace. Later, resolving problems linked to air-conditioning and energy saving became the main goal of research (1-5). A recent study (1), analyzed the energy efficiency of different configurations of ventilated walls under steady-state conditions (including the case of a transparent external face exposed to sunlight) and arrived at three particularly efficient systems of interspace-to-room air circulation.

The present work examines the energy expenditure for climate control for the said three configurations, as well as for all possible arrangements of the air spaces. Although the arrangement minimizing energy varies, particularly according to the outside temperature and degree of insulation, it is nevertheless possible to find different configurations best-suited to the winter and summer seasons.

2. Statement and solution of the problem.

If $\overline{T}_0$ is the external air temperature in the shade, $\overline{T}_i$ the room temperature and $\overline{T}_e$ the well-known sol-air temperature defined as:

$$\overline{T}_e = \overline{T}_0 + a\overline{I}/\alpha_e$$

where a is the wall's solar-radiation absorption coefficient, I the radiation intensity, and α_e the external boundary surface heat transfer coefficient. The overstricken quantities denote average values over time (e.g. average monthly values).

Furthermore, let R_e and R_i be the thermal resistance between the interspace and the external and internal air, respectively, and $R_t = R_e + R_i$ the wall's overall thermal resistance. In the steady state, the interspace positioning within the wall is determined by the dimensionless parameter $z = R_e/R_t$ that represents the outward fraction of thermal resistance; obviously $0 \le z \le 1$.

The steady-state problem has been studied and the thermal power $\overline{Q}_s$ necessary for room conditioning calculated for all possible room-interspace air circulation schemes (1). If we neglect the contribution of irradiation inside the interspace, the results obtained by the previous authors may be summarized (with modifications in notation) by the relation:

$$\overline{Q}_s R_t = \frac{1}{\lambda_1}(\overline{T}_i - \overline{T}_0) - \frac{\lambda_2}{\lambda_1}(\overline{T}_e - \overline{T}_0) \qquad (1)$$

where coefficients λ_2 and λ_1 depend on the ventilation scheme and the properties of the ventilated wall through the quantities:

$$z, \qquad \gamma = gR_i, \qquad \sigma_0 = [z(1-z)\gamma, \qquad \eta = \left(1 - e^{-\sigma_0}\right) / \sigma_0$$

n which g is the thermal airflow into the room. Here, instead of g we will often utilize the number n= g/Vc', expressing the room air turnover, where V is the room volume and c' the specific heat of air per unit volume. Hereafter, we refer to thermal flow as the product of air mass flow by its specific heat. For our purposes, it is also useful to introduce the specific thermal requirement:

$$FTS = \frac{Q_s R_i}{\bar{T}_i - \bar{T}_0}$$

because we compare different walls with the same overall resistance and configurations in which all inward flow is new turnover air. We introduce the environment parameter ξ defined as:

$$\xi = \frac{\bar{T}_e - \bar{T}_0}{\bar{T}_i - \bar{T}_0}$$

which expresses the relationship between insulation effects and the inside-to-outside thermal gradient (in the absence of insulation $T_e = T_0$ and $\xi = 0$) [1]. Thus, Eq.(1) may be written as:

(2) $$FTS = \frac{1}{\lambda_3} - \frac{\lambda_2}{\lambda_3} \cdot \xi$$

So the specific thermal requirement FTS is a function of ratios $1/\lambda_3$ and λ_2/λ_3 and of the inside and outside thermal fields through the environment parameter ξ.

A critical parameter considered in the following analyses is called the performance parameter S. defined as:

$$S = \frac{Q_{inf} - Q_s}{Q_{inf}},$$

where Q_{inf} is the thermal power needed for room conditioning without a ventilated interspace, though with the same heat transfer coefficients. In what follows, this case will be adopted as a reference model, and shall be denoted by R. Obviously, if we compare walls having equal overall resistance, parameter S must also be defined in terms of specific thermal requirements.

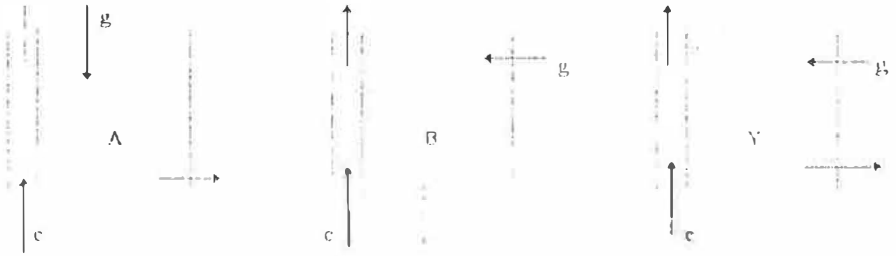

Fig.1. Ventilation patterns

For convenience, by winter season we refer to the period of the year during which $\bar{T}_0 \le \bar{T}_e \le \bar{T}_i$ ($0 \le \xi \le 1$), while summer is defined by $\bar{T}_i < \bar{T}_0 < \bar{T}_e$ ($\xi > 0$). During winter, at or very near midday the sun-air temperature for southern walls may reach peak values higher than the room temperature. Moreover, in general the average sun-air temperature value assures that parameter ξ is less than unity. As the analysis developed in (1) demonstrates, ventilation patterns A and B and borderline case Y are very important (see Fig 1). In case A we consider allowing all the interface air, taken from the outside at temperature $\bar{T}_0$, to enter into the room at thermal flow c as air turnover (c=g). In case B, all the stale air from the room at temperature $\bar{T}_i$ is ejected to the

interspace (c~g). At times it may he useful to eject to the outside all the air allowed to flowed into air space; if the interspace airflow is very high (c>>g), borderline case Y results, in which room's thermal behavior is independent of insolation. For such ventilation models, we have:

$$
\begin{aligned}
&\mathbf{R}: && \lambda_2 = \lambda_3 = \frac{1}{1+\gamma}, && FTS = 1+\gamma-\xi \\
&\mathbf{A}: && \lambda_2 = \frac{1+(\eta/z)-\eta}{1+\gamma-\eta}, \quad \lambda_3 = \frac{1}{1+\gamma-\eta}; && FTS = 1+\gamma-\eta-\left(1+\frac{\eta}{z}-\eta\right)\xi \\
&\mathbf{B}: && \lambda_2 = \frac{1-\eta}{1+\gamma-\eta}, \quad \lambda_3 = \frac{1}{1+\gamma-\eta}; && FTS = 1+\gamma-\eta-(1-\eta)\xi \\
&\mathbf{Y}: && \lambda_2 = 0, \quad \lambda_3 = \frac{1-z}{1+\gamma(1-z)}; && FTS = \frac{1}{1-z}+\gamma
\end{aligned}
\qquad (3)
$$

3. Numerical results.

We consider the very common case where the outer wall is made up of three layers of different materials: the first brick (L), the second light brick (Lg), the third in thermal insulation (Is); and the inner wall has two layers of plaster (In). The thermo-physical and geometric characteristics of the materials are reported in Table I (d thickeness of layers, k thermal conductivity and β thermal diffusivity). The assumed reference values for the internal and external boundary surface coefficients of heat transfer are 7.7 and 25 W/m^{2}K respectively, and that for the specific thermal resistance of the interspace 0.13 m^{2}K/W. We have considered a reference room of 3x4x4m with a single outer wall of 3x4m^2 and volume of 48 m^3.

Tab.I

Material	d (cm)	k (W/mK)	β 10^6 (m^2/s)
Bricks (L)	25	0.45	0.50
Light bricks (Lg)	8	0.35	0.58
Thermal insulation (Is)	5	0.054	2.8
Plaster (In)	1	0.70	0.44

The outer wall can assume four configurations depending on the order of the layers, with the constraint that the interspace (J) and insulation layers must be between the two brick layers. The arrangements are shown in figure 2 and numbered from 1 to 4 (insulation is represented by the shaded area, plaster layers are not drawn for clarity). More precisely, the layering for the different wall models are the following: In-L-Is-J-Lg-In, type 1; In-L-J-Is-Lg-In, type 2; In-Lg-Is-J-L-In, type 3; In-Lg-J-Is-L-In, type 4. Hereafter, for each wall type we will consider the three ventilation patterns specified above plus the reference one; thus yielding a total of 16 cases, each of which will be denoted by a number, indicating the outer wall type, and a letter (A, B, Y, R), for the ventilation pattern (e.g., 1A denotes the case of outer wall type 1 from figure 2 and ventilation pattern A). Under steady-state conditions we obviously have only one reference case (cases NR with N=1...4 are all equivalent) which will be indicated simply as R.

Figure 3 reports the FTS trend as a function of the environment parameter ξ for different possible cases and n=0.5. Figure 4 illustrates an enlarged detail of figure 3: E indicates the

tersection point of the straight lines corresponding to cases 4Λ and 2Λ; F the intersection of ases 3B and 4Y, and G the intersection of cases 2Λ and 3Λ. The graph shows that, with the xception of ventilation pattern Y, during winter ($0 \le \xi \le 1$) the ventilated wall is always preferable ver the non-ventilated one (case R); while during summer ($\xi < 1$) ventilation pattern B is always ore suitable. Ventilation patterns Λ and Y, on the other hand, may result superior for only a arrow range of values of ξ. More precisely, during the winter, for $0 \le \xi \le \xi_G$ ($\xi_G = 0.0350$), the ost suitable arrangement is 3Λ, while for $\xi_G \le \xi \le \xi_E$ ($\xi_E = 0.276$) it would be 2Λ, and for $\xi >$ it is 4Λ.

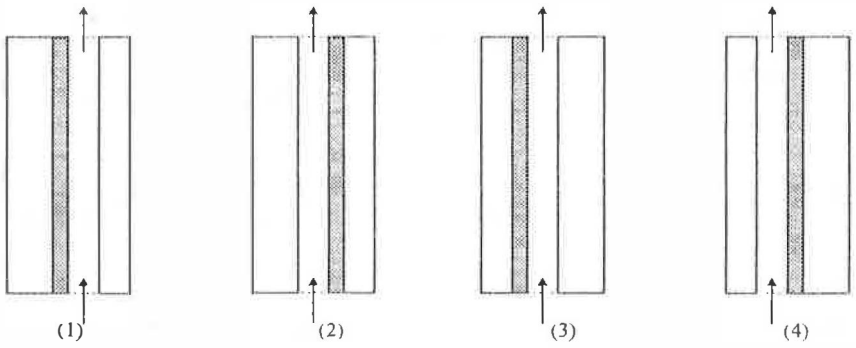

Fig.2. Outer wall configurations

uring the summer, for $\xi > \xi_F$ ($\xi_F = -0.795$) the most advantageous arrangement is 3B, whereas r $\xi < \xi_F$ it is 4Y.

the air turnover rate increases, the linear trends of the various cases do not change ialitatively. If n increases, the abscissas of points F, G and E decrease; in particular, for n=2, ξ_F -3.20, $\xi_G = 0.0122$, $\xi_E = 0.0811$; that is to say, as air turnover increases, so does the range of ξ ilues for which the case 4Λ yields better results during summer and case 3B is preferable in inter.

nally, it can be seen that the value of specific thermal requirement, FTS, concerning cases 4Λ id 2Λ (for $\xi > \xi_E$), those relating to cases 2Λ and 3Λ ($0 < \xi < \xi_E$), as well as, for $\xi < 0$, cases 3B id 2B and 2Yand 4Y, are very similar; all this lead the conclusion that in practice the best wall type 2 with ventilation pattern Λ in winter and ventilation pattern B or Y (for high insolation ilues) during summer.

gure 5 illustrates for wall type 2 alone the performance parameter S as a function of ξ, for =0.5 and n=2; it can be seen that with n=0.5 the curves for ventilation patterns B and Y tersect at $\xi = \xi_0 \cong -1.18$ (for n=2 the intersection would be occur at $\xi = \xi_1 = -3.98$). The graph veals that during winter, with ventilation pattern A, parameter S increases as ξ increases, and at for any given value of ξ, it decreases with increasing n. For n=0.5, parameter S varies from minimum value of roughly 13% at ξ=0 (no insolation), to a maximum of over 60%, for ξ=1, hich corresponds to insolation: $I = \alpha_e(\bar{T}_i - \bar{T}_0)/a$. In summer, for n=0.5, the most appropriate ntilation pattern would be B, if $\xi_0 \le \xi \le 0$, while if $\xi < \xi_0$, it would be Y. Parameter S increases ickly as ξ decreases, and at ξ=0 reaches a minimum, equal to about 13%. For n=2, except for ry high insolation values ($I > \alpha_e (\bar{T}_i - \bar{T}_e)\ \xi_1/a$), the most favorable pattern is B; again, rameter S increases as ξ decreases and reaches a minimum of 10% at ξ=0.

4. Conclusions

The practical case examined in this paper illustrates the design criterion for the arrangement of ventilated air space dealt with extensively in (1). Four different types of walls were studied, all with the same thermal resistance but differing values of parameter z. Clearly, from the practical point of view, the wall type must be fixed once and for all, while the ventilation pattern may be varied according to the climatic conditions (winter/ summer). The simplifications adopted allows the analysis to be performed through simple relations leading to easily-read graphical representations. In particular, of the walls studied, the best configuration results to be second, because it assures a suitable arrangement both in summer, when ventilation B (or Y for high insolation) is preferable, and in winter, when ventilation A is preferable. Energy savings over comparable non-ventilated walls are, in the worst-case scenario of no insulation at all, greater than 10%, and could easily attain values over 20-30% for any reasonable level of insolation.

References

(1) - M. Ciampi, G. Tuoni, "Sulle prestazioni energetiche delle pareti ventilate". La Termotecnica, n.3, pp.75-85, 1995.

(2) - M. Ciampi, G. Tuoni, "Sul comportamento delle pareti ventilate in regime termico periodico stabilizzato". Work in press.

(3) - F. Morselli, "*La radiazione solare e le pareti ventilate*". De Lettera, Milano, 1991.

(4) - E. Arquis, C. Langlais, S. Klarsfeld, J.P. Caltagirone, "Quelques aspects fondamentaux sur l'isolation dynamique". Revue Generale de Thermique, n. 256, pp. 321-327, 1983.

(5) - L. Gennai, N. Gucci, G. Tuoni, "Sul comportamento igrometrico delle coperture piane ventilate". La Termotecnica, n.8, pp. 89-95, 1996.

(6) - G. Tuoni, "Locali in regime termico periodico. Influenza delle strutture interne". La Termotecnica, n.1, pp.41-49, 1984.

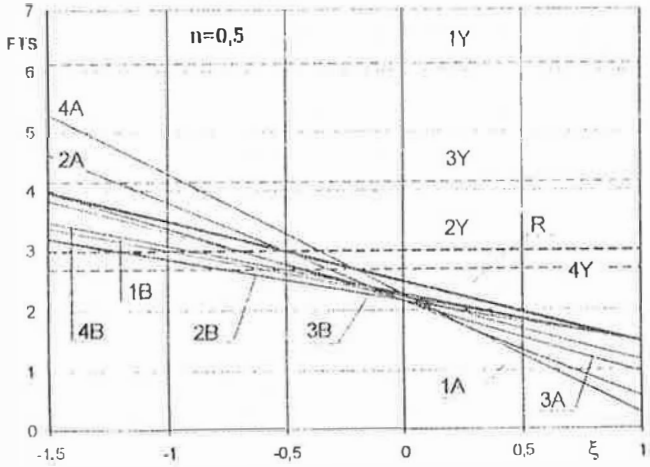

Fig.3

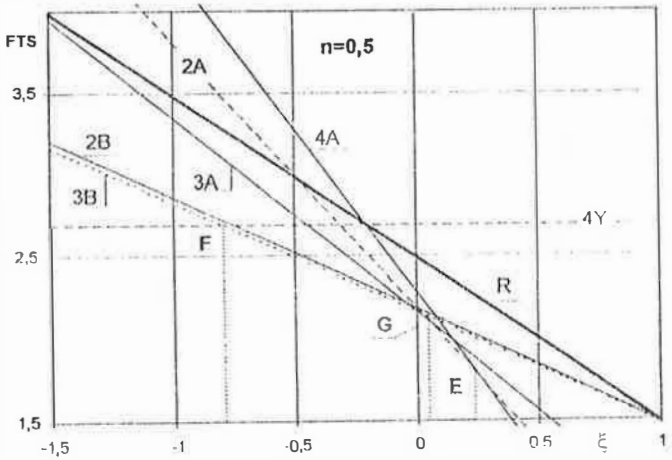

Fig.4

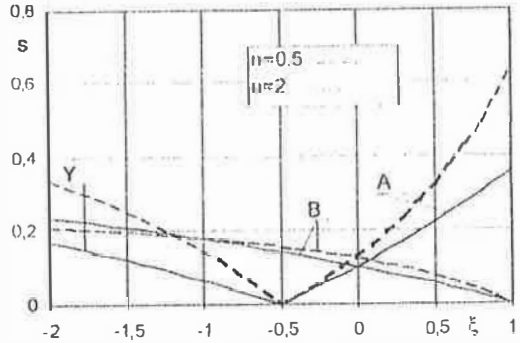

Fig.5

A SIMPLE COMPUTER CODE FOR ESTIMATING ENERGY LOAD IN BUILDINGS AS RESULT OF MECHANICAL VENTILATION

S. Vitale
ENEL S.p.A. - CRAM, Via Volta 1, 20093 Cologno Monzese (Milan), Italy
E-mail: vitale@cram.enel.it

Abstract

Mechanical ventilation in buildings requires appropriate systems for heating and cooling. The costs of energy demand represent a high percentage of the global costs for climatisation. As a part of a project concerning these subjects the development of a computer code for evaluating energy load due to mechani d ventilation in buildings is in progress.
The mathematical model is based on s plified equations to fit dynamically the psychometric curves. Inlet air flow rates are evaluated according to the more recent Italian regulations.
Energy amounts are calculated at hourly time-step taking into account time dependent operating conditions chosen by users such as: set-point temperatures, relative humidity, ventilation rates, use and occupancy of the rooms, scheduled time of operation. Meteo test reference years for the main Italian sites are used as default hourly climatic data.

1. Introduction

Within the frame of a research programme co-ordinated by ENEL Spa on air quality in non-industrial buildings, it was necessary to use an instrument for a quick estimation of thermal loads due to external air changes as a function of the expected climate trend, the choices made for running the systems, and the use of rooms. Literature already includes many softwares developed for this purpose, but their use is not always simple for non-expert users and the references to national regulations are not always up-dated. In order to have a product complying with our requirements, we are developing the "VELA" (Ventilation Load Analysis) code. Reference norms are the Italian ones and in particular refs. (1), (2), (3).

2. The mathematical model

In its present version, the code allows to dynamically estimate, with an hourly calculation cycle, the energy requirement arising from the treatment (heating/cooling and at the same time humidification/de-humidification) of external air by a central system, without taking into account thermal dispersal. For the calculation of humid air mass-enthalpy J (J/kg) of the dry air/steam mix, the formulation reported in ref. (4) was chosen, obtained by assuming, as is commonly done, that the value of air enthalpy at 0°C and $101.325*10^3$ Pa pressure, is equal to zero:

$$J = cp_a * T + 2490.7 *10^3 * X + cp_v * T * X \qquad (1)$$

wherein:

X	= air water content (kg/kg)
cp_a, cp_v	= specific air and water heat (J/kg K)
T	= air temperature (°C)

For air water content, the following equation may be adopted which, during the concerned interval, approaches the values that can be obtained from the psychometric curves, ref. (5), having fixed temperature a' umidity values:

$$X = U * 3.59 * 10^{-3} * \exp(0.0684 * T) / 100 \quad (2)$$

wherein U is the relative humidity.
Considering the subscripts i, e and r referred to internal, external and recirculating air respectively, the thermal load E (J) for the simulation period is determined as

$$E = \int_{t}^{t2} (M_i \cdot J_i - M_e \cdot J_e - M_r \cdot J_r) dt \quad (3)$$

Heating and humidification during winter and cooling and de-humidification during summer are the only air treatments taken into account.
The mass of internal air M_i (kg/s) treated during the time unit is expressed as

$$M_i = \rho * Q_o \quad (4)$$

ρ = air density (kg/m^3)
Q_o = air flow to be treated during the time unit (m^3/s)

In the field of air conditioning both air and steam may be considered as perfect gases and therefore for dry air, one obtains

$$\rho = 10333 / (29.27 * (T + 273.15)) \quad (5)$$

The air flow Q_o to be heated or cooled is calculated as follows:

$$Q_o = c_1 * Q_{op} * N \quad (6)$$

wherein
c_1 = altitude correction coefficient
Q_{op} = specific air flow per person (m^3/s)
N = reference crowding for design purposes

The correction coefficient c_1 is obtained by linear interpolation of the values of Table (1)

Table 1. Values of altitude correction coefficient

Altitude a.s.l. (m)	c_1 coefficient
0	1.00
500	1.06
1000	1.12
1500	1.18
2000	1.25

Lacking certain data on the N number of people permanently present in rooms, the following relation may be used:

$$N = N_s * S \quad (7)$$

N_s = crowding index per surface unit ($1/m^2$)
S = useful floor surface (m^2)

The surface S is estimated considering a conventional occupied volume V (m^3) as a room portion defined by the following surfaces:

- floor;
- a horizontal surface placed at a height of 1.80 m above the floor;
- vertical surfaces places at a distance of 0,60 m from each of the room walls or the apparatuses for environment climatisation

The values of Q_{op} and N_s (number of people present for design purposes per each square meter of useful floor surface) may markedly differ, according to the use destination of rooms. Table (2) shows some reference values:

Table 2. Reference values of specific air flow per person and crowding index

TYPE	Q_{op} ($10^{-3} m^3/s$)	N_s ($1/m^2$)
Individual offices	11	0.06
Open space offices	11	0.12
EDP centres	7	0.08
Meeting rooms(+)	10	0.60
Reading rooms-libraries(+)	5.5	0.30
Museums(+)	6	0.30
Living rooms, bedrooms	11	0.04

For rooms to be used for public entertainment or meetings, marked by (+) in the Table (2), instead of Q_{op} the Q_{ope} real flow is utilised, obtained as follows:

if $V / N \leq 15$ then $Q_{ope} = Q_{op}$ (8a)
else if $V / N \geq 45$ then $Q_{ope} = Q_{opmin}$ (8b)

wherein Q_{opemin} is the minimum air flow allowed, calculated according to the following Table (3):

Table 3. Values of minimum air flow allowed

Q_{op} ($10^{-3} m^3/s$)			Q_{opmin} ($10^{-3} m^3/s$)
up	to	7	4
7	to	10	5,5
10	to	12.5	7
over		12.5	8,5

Lastly, if $15 < V/N \leq 45$ one obtains

$$Q_{ope} = Q_{op} + ((Q_{opmin} - Q_{op}) / 30) * (-15 + V / N) \quad (8c)$$

3. Code use

The computer code is written in MS Visual Basic™ language and is composed of some masks with curtain menus for input preparation and for the graphic visualisation of the results. The following input data are required:

- Choice of a simulation site from a database of the standard years of the main Italian sites; utilised data include relative humidity, hourly temperatures and site altitude.
- Surfaces of rooms to be conditioned and their use destination, room crowding. According to use destination and expected crowding, the air flows are calculated in different manners. As an alternative to crowding data, already tabled indexes are proposed. These calculations are carried out according to what is provided by ref. (1).
- Subdivision of the period to be simulated into one or more heating, cooling or in-between season periods. The chosen minimum duration of each period must correspond to a week. Periods provided by ref. (3) are proposed by default depending on the climate zone of the site.
- For each period so determined the standard week must be defined, namely for each days of the week one must specify the hours when the system is running, which hours need not being consecutive, in relation with the particular needs of users.
- Choice of the temperature and relative humidity to be achieved by external air to be treated during heating or cooling periods.

When all of the required data have been defined, it is possible to start the computation phase or review and modify any defined input parameter, also by means of the use of a printout of the whole of the selected data and the diagrams of meteo data of the concerned site.

As output, the code provides in form of diagrams and tables, for the different use destinations and the various periods, the energy requirements of air treatment systems for heating, cooling and humidifying rooms. Data are recorded every hour and the possible visualisations range from those of daily trends to those concerning the whole year. Heating and cooling requirements as well as sensible and latent energy loads may be visualised also separately. For the purposes of the work session, the case can be filed and added to a reference database. Filed cases may be consulted quickly, as a short description is associated to the file name, and input data of the stored file may be utilised for new simulations, making therefore the loading phase easier.

4. Application example

The simulation concerned the computation of the thermal load of a central system, due to sensible and latent heat. Two identical buildings were chosen in Rome and in Milan. For the definition of running limits of thermal systems in winter, reference has been made to DPR 26 August 1993 no. 412, ref. (3). Input data are shown in the Table (4).

As the specific heat of dry air at the atmospheric pressure of $101.325*10^3$ Pa in the temperature interval from -40°C to 80°C ranges between 998.3 ÷ 1021.4 (J/kg K), a cp_a value equal to 1004,6 (J/kg K) was assumed. As specific heat of steam cp_v, the constant value 1925.6 (J/kg K) was adopted. Internal air recirculation is not considered.

In the calculation of the specific air flow per person Q_{op} and the reference crowding N, Eqs (7) and (8a) were used, as the $V/N \leq 15$ condition had taken place.

Diagrams show some results of the simulation. In particular, Figs. (1) and (2) show the monthly average temperature and relative humidity of external air for the two sites being examined. Thermal load trends for the various months of the year are shown in Fig. (3). It is possible to distinguish the heating, cooling and in-between season periods during which the system is not running.

Table 4. List of input data

Site	Milan and Rome
Surface assigned to offices	30 modules of 20 m^2
Surface assigned to meeting rooms	200 m^2
Surface assigned to EDP centres	100 m^2
Surface assigned to libraries	100 m^2
Room crowding	as per UNI 10339
Days of use of the system	Monday to Friday
Hours of working of the system	6:00a.m. to 7:00 p.m.
Winter and summer temperature set-point	22°C and 24°C
Winter and summer relative humidity set-point	50%
Duration of simulation	yearly
Duration of heating period	Milan: 15/10 - 15/4 Rome: 1/11 - 15/4
Duration of cooling period	15/6 - 15/9

5. Conclusions

The "VELA" code for the computation of energy consumption of HVAC systems in non-industrial buildings has been shortly summarised. In this first version the enthalpy differences ensuing from ventilation and humidification/de-humidification of external air are considered according to the Italian regulations in force. Further implementations shall concern the refinement of the evaluation of energy contributions, taking into account contributions such as the power required by fans and conditioning terminal units, the presence of possible heat recuperators, etc.

References

1. UNI 10339, "Air-conditioning systems for thermal comfort in buildings - General, classification and requirements - Offer, order and supply specifications" (1995).
2. Law 9 January 1991 no. 10, "Norms for the implementation of the National Energy Plan in view of a rational use of energy, energy saving and development of energy renewable sources". Gazzetta Ufficiale (1991).
3. DPR 26 August 1993, no. 412, "Regulations for the design, installation, running and maintenance of thermal systems of buildigs for the purpose of containing energy consumptions, in accordance with art. 4, sub-section 4, of law 9 January 1991, no. 10". Supplement to Gazzetta Ufficiale no. 242 of 14.10.1993.
4. C. Pizzetti, "Condizionamento dell'aria refrigerazione", Masson, 1980.
5. A. Briganti, "Il condizionamento dell'aria", Tecniche Nuove, 5th ed. (1995).
6. C. Rumor, G. Strohmenger "Riscaldamento, Ventilazione, Condizionamento, Recupero energetico, Impianti sanitari", Hoepli (1985).
7. F. Palmizi, "Vademecum del termotecnico", PEG (1992).

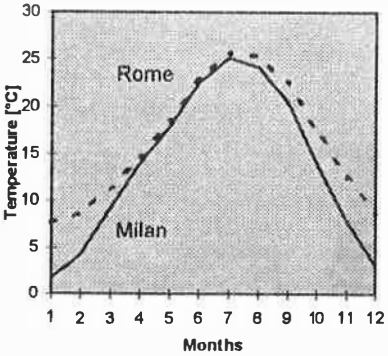

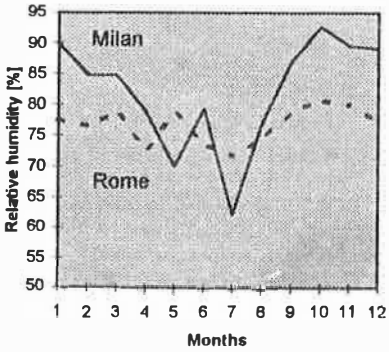

Figs. 1,2. Monthly average values of temperature and relative humidity for external air.

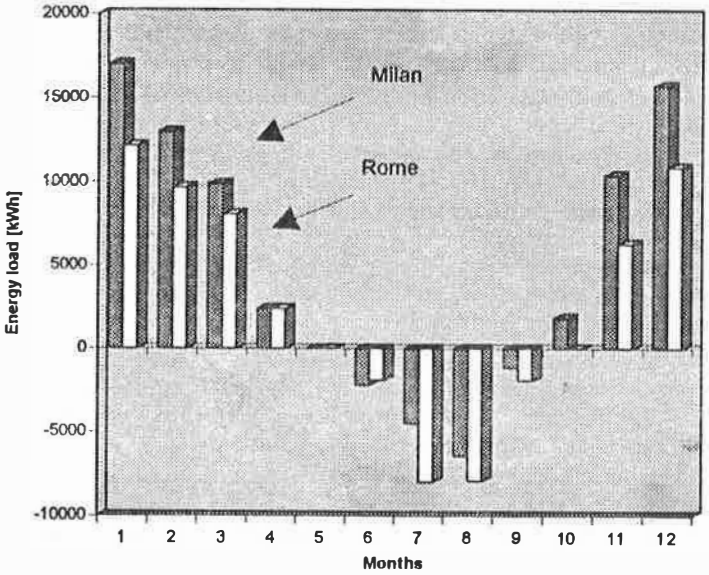

Fig. 3. Evolution of predicted global energy loads.

HOW CAN GLAZING IN WINDOWS INFLUENCE THE BUILDING ENERGY CONSUMPTION?

Juan C. Klainsek

Departamento de Construcción y Tecnología Arquitectónicas
E.T.S. de Arquitectura - Universidad Politécnica de Madrid
Av. Juan de Herrera, 4 - 28040 Madrid - Spain

ABSTRACT

Glazing is one of the parameters that most influences the building energy conservation, so it should be taken into consideration especially in non-residential buildings, since the surface of glass areas is very important in this typology. The aim of this paper is to analyse different glass area shapes as well as the influence they have on the energy consumption of a non-residential building. Horizontal glazing (with different heights) and vertical glazing (with the same area as the horizontal ones), separated by opaque areas are considered in a base case building. A traditional wall and a curtain-wall are also considered, and the different annual consumptions per surface unit are obtained in winter and summer.

1. INTRODUCTION

In non-residential buildings the thermal interactions between the structure of the building, the indoor air, the internal heat loads and the solar radiation result on fluctuations in heat surplus or deficit (4), so the building energy performance is particularly complex in this type of buildings. On the other hand, considering the fact that glazing is the weakest spot of building envelope from the point of view of thermal transfers, these transfers are more important than those which may take place through opaque areas, both in summer and winter. Although glazing plays such an important role in the local thermal condition passive control, it is usually treated at the design stage as if its only target was to visualize, illuminate or be just a composition element of the façades.

It is a fact that in many buildings, one third of the heat is lost only through the windows: the internal heat sources may balance these losses through the glazing (2), nevertheless a more realistic estimation of the thermal transmission through the window becomes a necessity if a proper design and a decreasing of heating and cooling energy consumption are to be achieved. On the other hand, the awareness exists that the theoretical basis of even the most sophisticated programs may not be totally appropriate for highly glazed areas, as it is the case of office buildings, for both the radiation transfer and the building structure interactions are extremely complex (5).

The Weighting Factor Method has been used in this paper (1). This method estimates the instantaneous sensible load with a simple, flexible technique, considering the parameters that

ffect the building energy flow. The Weighting Factor Method represents z-transfer functions 3) and it accounts for the parameters which affect the building flow; it also allows heat gains o be fixed at a constant temperature, from the physical description of the building, the nvironmental climate conditions and internal load profiles.

As it was stated above, glass areas have a great relevance, especially in the energy costs of commercial building, hence the effect of different glass shapes in a base case commercial uilding has been studied: horizontal continuous windows with variable height, and vertical iscontinuous windows with fixed height and variable width, so as they can have the same urface as the former ones.

.1 Base case building

A ten-floor office building located in Madrid is taken as a base case building in this paper; t has these characteristics: 40m x 26m floor; 37m height, which corresponds to a gross surface er floor of 1036 m², useful conditioned of 795 m². The location of this building is the most isadvantageous one because the largest façades look out into the east and west.

Months from November to March correspond to the winter season, all the others orresponding to the summer season.

In the estimations, a constant interior temperature of 20 °C and RH 50% in winter, and 25 °C and RH 55% in summer is taken into consideration; the exterior temperature is variable, so he calculations are carried out hourly.

With regard to the exterior conditions, meteorological variables are generated hourly from eliable meteorological data; on the other hand, an auxiliary programme has been used. Relating he daily starting data, the maximum and minimum temperature, the total daily irradiance on orizontal surface and the day absolute humidity at maximum temperature hour are considered.

The heat transmission coefficient of opaque areas (K-value): -horizontal- roof Kr=0.43 W/m².K, light color (cream); floor levels above open space Kf=0.66 W/m².K. -Vertical- raditional wall with seven layers and with a total thickness of 23.5 cm, with insulating material of 4 cm, 244.6 kg/m² and Kw=0.61 W/m².K, and a curtain-wall with four layers and a total hickness of 5.3 cm, an insulating material 5 cm thick 89.6 kg/m² and Kw=0.42 W/m².K, both nedium color (green and blue, bright red, light brown, wood and concrete). With regard to the metallic windows with different types of glass, which are studied in this paper, they are lescribed next.

Glazing having no shading devices, except the shadows cast by setback. The results of the energy consumption calculations are obtained per useful or net surface unit, and a free height of 2.80m in all floors is considered. The internal loads are fixed by: occupation 55 pers./floor; ventilation 2000 m³/h floor; illumination 7.95 kW/floor. The characteristics of the glazing considered in this paper are: colorless; insulating 6+6 mm with an air space 12 mm and 6 mm thick, and Kg=3.7 and 4.0 W/m².K respectively; single 6 mm with Kg=5.8 W/m².K. Each of his glazing is affected by its corresponding corrective coefficient of the solar gain factor (c.c.).

2. ANALYSIS OF RESULTS

The energy consumptions (e.c.) per conditioned surface in summer and winter for the base case building, with windows of different height, hw=1.00m, 1.10m, 1.20m, 1.30m, all of them round the perimeter of the building, are estimated. These glass areas are then transformed from continuous to discontinuous, with the same façade surface than the previous ones. In order to do this, the glazing height is: h=2.10m, from floors to lintels. This shape change done, taking as variable the external vertical opaque surfaces (traditional wall and curtain-wall), different e.c. are observed. These consumptions are achieved from different types of glazing with their codes into brackets, the first symbol for the continuous glazing and the second for the discontinuous one: 6+6 mm colorless insulating glass with a 12 mm air space (□) (▵); the same glass with a 6 mm air space (+) (x); 6 mm colorless single glass (◇) (▽).

When the e.c. values of each of these types of glazing are achieved, a regression line, obtained by the least square method, is adjusted, and in this way a line equation is obtained, representing the variation of these consumptions for glazing with a surface even smaller or bigger than that of the glazing considered in this paper.

In Tables 1, 2, 3 and 4 the e.c. corresponding to summer and winter with traditional walls and curtain-walls, insulating glazing with a gap of 12 mm, the four different heights and the transformed ones with the apostrophe, the equations and the medium variation are showed. In order to simplify, and just for the Tables, only values corresponding to 6+6 mm insulating glass, with a gap of 12 mm, are represented.

In Figures 1, 2, 3 and 4 the values obtained in summer and winter with a traditional wall and curtain-wall are studied. On the axis of ordinates in the diagrams, the consumptions per conditioned useful unit surface (kWh/year m²) are represented; on the abscissa axis, the four heights of continuous windows, which coincide in the same way with discontinuous shape-transformed windows with hw=2.10m, both cases having an equal glass area, are represented. In these Figures, not only the lines corresponding to the e.c. showed in the Tables for continuous rectangular horizontal windows, insulating glazing with a gap of 12 mm (□) and shape-transformed discontinuous windows, with the same glass (▵), are represented, but also those corresponding to insulating glazing, gap of 6 mm (+) (x), and single glazing (◇) (▽).

3. CONCLUSIONS

-The e.c. become higher if the glass areas are larger.
-There is a linear relation corresponding to a law as: e.c.=ax + b; this law is obtained from the different types of glazing shapes studied. In case there are no glass areas: b>o, for there is thermal transference even through opaque surfaces.
-The intervals of energy consumption for these shapes, depending on the three types of colorless glazing studied, in the summer season and with the traditional wall, vary from 0.92% to 0.78% with the curtain-wall the variation is from 0.39% to 0.3%. In the winter season, with traditional wall, between 0.18% to 0.16%; with the curtain-wall the difference is not significant.
In short, the energy consumptions are always higher in summer, if vertical discontinuous windows starting from the floor are used, than when the rectangular continuous ones of the same area are used. These energy consumptions can show an insignificant variation in winter, if the curtain-wall is considered.

. REFERENCES

1) *ASHRAE Handbook 1989 Fundamentals*. SI Edition. American Society, Refrigerating and Air Conditioning Engineers.

2) Braun, W. (1993). Glazed Façades and Energy Saving-a Contradiction?. International Symposium Energy Efficient Buildings, 397-402.

3) McKinley, A.D. and Mitalas, G.P. (1988). Room Thermal Transfer Functions, Computer Programs to Calculate Z-transfer Function Coefficients for Rooms. National Research Council of Canada, 1-3.

4) Nilsson, P.; Aronsson, S.; Jagemar, L. (1994). Energy-Efficient Retrofitting of Office Buildings. *Energy and Buildings, 21, N° 3*, 175-185.

5) Pfrommer P., Lomas K.J., Kupke Chr. (1994) Influence of Transmission Models for Special Glazing on the predicted Performance of Commercial Buildings. *Energy and Buildings, 21, N° 2*, 101-110.

Table 1. Energy consumptions in Summer with traditional wall

Shape	Height (m)	E.C.(kWh/y.m²)	Equation	Medium variation (%)
Horizontal	1.0	24.73	e.c. = 6.13x + 18.60	+0.78
	1.1	25.34		
	1.2	25.95		
	1.3	26.57		
Vertical	1.0'	24.96	e.c. = 5.93x + 19.03	
	1.1'	25.55		
	1.2'	26.14		
	1.3'	26.74		

Table 2. Energy consumptions in Summer with curtain wall

Shape	Height (m)	E.C.(kWh/y.m²)	Equation	Medium variation (%)
Horizontal	1.0	26.16	e.c. = 5.97x + 20.19	+0.30
	1.1	26.75		
	1.2	27.35		
	1.3	27.95		
Vertical	1.0'	26.24	e.c. = 6.0x + 20.24	
	1.1'	26.83		
	1.2'	27.43		
	1.3'	28.04		

Table 3. Energy consumptions in Winter with traditional wall

Shape	Height (m)	E.C.(kWh/y.m²)	Equation	Medium variation (%)
Horizontal	1.0	14.92	e.c. = 4.24x + 10.58	+0.16
	1.1	15.35		
	1.2	15.79		
	1.3	16.22		
Vertical	1.0'	14.94	e.c. = 4.40x + 10.54	
	1.1'	15.37		
	1.2'	15.81		
	1.3'	16.26		

Table 4. Energy consumptions in Winter with curtain wall

Shape	Height (m)	E.C.(kWh/y.m²)	Equation	Medium variation (%)
Horizontal	1.0	13.36	e.c. = 4.90x + 8.46	-0.05
	1.1	13.85		
	1.2	14.34		
	1.3	14.83		
Vertical	1.0'	13.35	e.c. = 4.93x + 8.42	
	1.1'	23.84		
	1.2'	14.33		
	1.3'	14.83		

GLASS AREAS (summer–traditional wall)

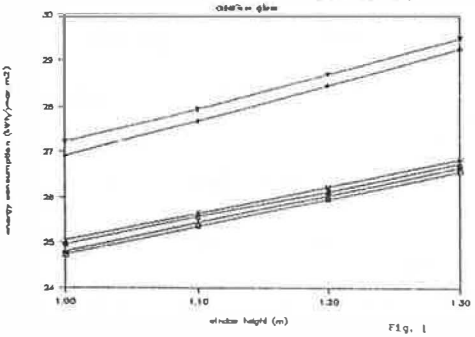

Fig. 1

GLASS AREAS (summer–curtain wall)

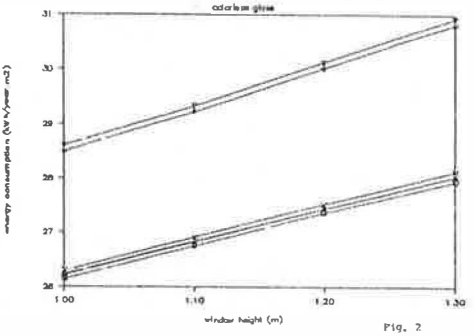

Fig. 2

GLASS AREAS (winter–traditional wall)

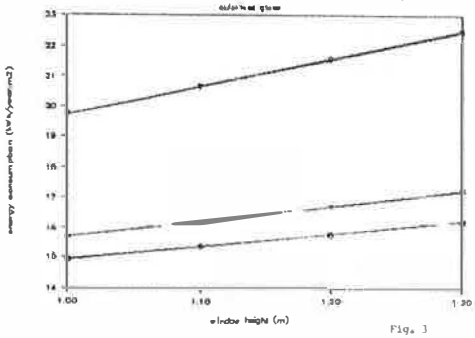

Fig. 3

GLASS AREAS (winter–curtain wall)

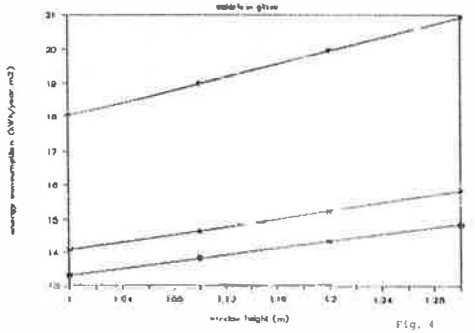

Fig. 4

An Experimental Study of a Thermoelectric Cooler System for the Airconditionnig in Building

Y. S. Yang *,I. S. Cho*, M. C. Chu*, Y.M. Park **Y.N.Lee***

*Active Solar Thermal Energy Lab., Korea Institute of Energy Research
71-2, Jangdong, yoosungku, Taejeon Korea

**Dept. of Mechancical Industry of Aju University, Suwon Korea

***Heat Transfer Research & Development, 1010 W. Lonnguist Blvd., Mt. Prospect, Illionois U. S. A.

Abstract

This project studied a new cooler system utilizing the Peltier effect for Building. The major objective of this study was to prove the baseline concept through experimental studies. The important results from this study included design and fabrication of a laboratory-scale cooling system. The cooling capacity of the TE-Cooler was 0.4 ton of refrigeration. The experimental testing system has been built to include a test chamber, heating element, circulation pump and cooling tower, and the instrumentation system included watt-hour meter, temperature sensor, hygrometer, flow meter, calorie meter and data acquisition system by the Hewlett-Packard and the TE Model TS-205 The preliminary testing results showed the system COPc of close to 0.4.

1. Introduction

Environmental pollution is becoming a greatest issue on earth as global energy demand increases. Particularly, carbon dioxide gas generated as a result of combustion of fossil fuels, depletion of ozone layer as a result of use of freon gas etc... are becoming cause of accelerated global warming. Thus, every country on earth will soon have to be regulated by an international agreement, " Green Round" , regarding consumption of fossil fuels. This paper reviews principles of thermoelectric heat pump and a power generator which respectively utilizes Peltier effect and Seebeck effect of thermoelectric semi-conductor materials and aims to develop a new cogeneration thermoelectric heat pump and a power generator utilizing "solar power as main source of heat". The paper reports on the design, fabrication and preliminary experimental results of an air-conditioning system.

2. Theory of thermoelectric technologies

2.1 Peltier Effect

Peltier effect was discovered in 1834 by Peltier, a French man. He found that when direct current is passed through a closed electrical circuit comprising two dissimilar materials, one of the two junctions become cold while the other becomes hot, indicating that the circuit works as a heat pump as shown in Fig. 1.

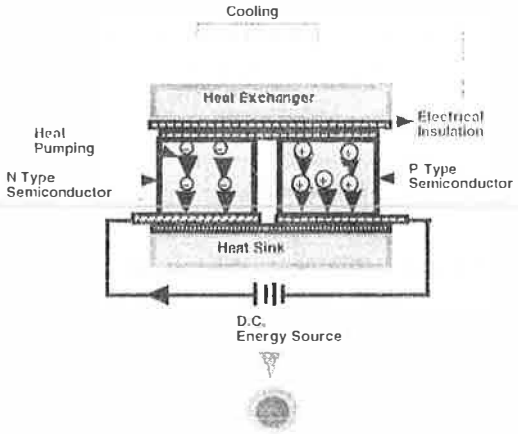

Fig. 1. Principle of Peltier effect and basic construction of Peltier cooler

Fig. 1 also shows the principles of a most elementary thermoelectric cooler comprising P-type and N-type semi-conductor materials. The N-type material has excess electrons while the P-type material has on the hand insufficient electrons while electrons originating from the cathode of the battery are flowing toward its anode through the two semi-conductors in the circuit, the excess electrons in the N-type material and the hole in the P-type material carries heat energy from the cold junction to hot junction (radiator). Thermal energy transported to the radiator is expressed by :

$$Qp = S \; I \; Tc$$

where

Qp = Peltier cooling effect (Watts)
S = Seebeck coefficient (volt/°c)
I = Electric current (amp)
Tc = Cold junction temperature (°c)

2.2 Seebeck Effect

Seebeck effect which has direct relationship with Peltier effect,was discovered in 1882 by Seebeck, a German, 12 years prior to the discovery of Peltier effect. Its principles, as explained in Fig.2, are as follows: when two junctions of an electric circuit comprising two semiconductor materials, P- and N-types are subjected to a temperature difference, an electromotive force is generated in the open circuit and an electrical current is available when the circuit is closed - phenomenon of Peltier effect in reverse. Physists explain this phenomenon as follows : When excess electrons at the hot junction of the N-type material are subjected to a high temperature, these electrons energizes on the average above the Fermi level in the energy level. These electrons in a higher energy level diffuse toward the low temperature junction in order to reduce energy level, resulting in a negative charging on cold junction while the hot junction becomes positively charged. In counter to the process of this electron diffusion flow toward the cold junction, a voltage is generated. On the other hand, in the P-type material where holes are carriers, the cold junction becomes positively charged while the hot junction negatively charged, resulting in power generation due to the electromotive force. Fig.2 schematically shows a case where solar heat is used a heat source.

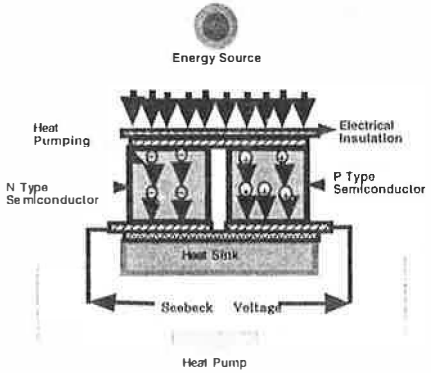

Fig. 2 Principle of Seebeck effect and example of solar thermoelectric power generator

3. System design and performance analysis

3.1 Modeling of air-conditioning system

In order to study on thermoelectric air-conditioning, an experimental air-conditioning system of 0.4 RT capacity has been

modeled as shown in Fig.3. An experimental prototype (Fig.4) was built for performance tests, where heat extracted from air at the cold side is first transferred to airr to be eventually dissipated to ambient air.

When electric power is connected to part 1 of the thermoelectric cooler, heat is extracted from the chamber air(Part1). The heat extracted plus energy input to drive the cooler is carried away by means of a circulating fancoil to be dissipated at the heat sink(Part2). Air flow meter measures flow rate of conditioning air in the chamber. A data acquisition system connecting with sensors for measuring air temperatures at various was to monitor data.

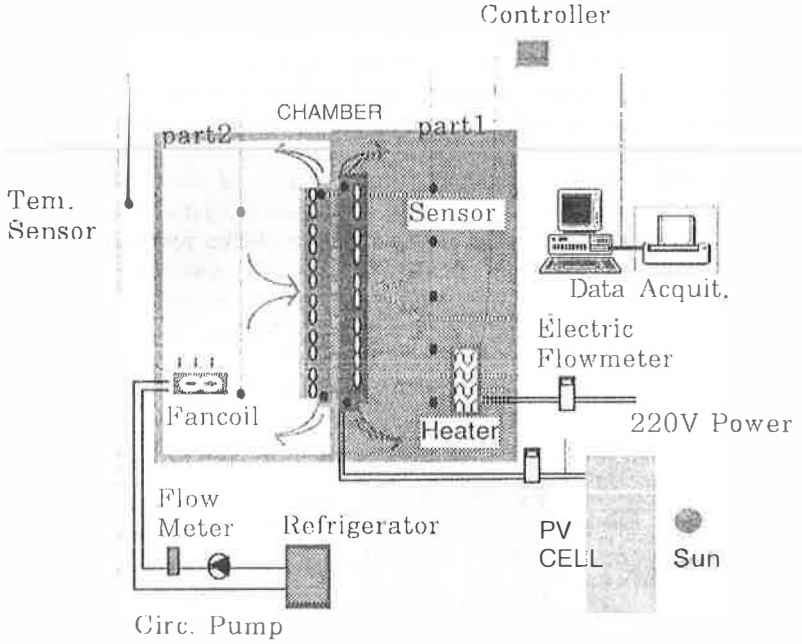

Fig.3 System diagram of Test cell of the Air to Air Cooler System 1.5 Kw

3.2 Constitution of experimental setup and performance analysis

As shown in Fig. 4, a thermally insulated chamber approximately of 2.88 cubic meter is installed in order to measure cooling capacity. The chamber contains an electric heater which is used to maintain the chamber temperature at constant temperature while heat is being extracted from the chamber air. To dissipate all the heat including heat input to the thermoelectric modules, a fan coil unit is installed in which a circulating water

pump carries heat to the coil to be dissipated there. T-type thermocouples are used to measure temperatures ; to measure electric power inputs to the thermoelectric modules and to the heater, power meter is used.

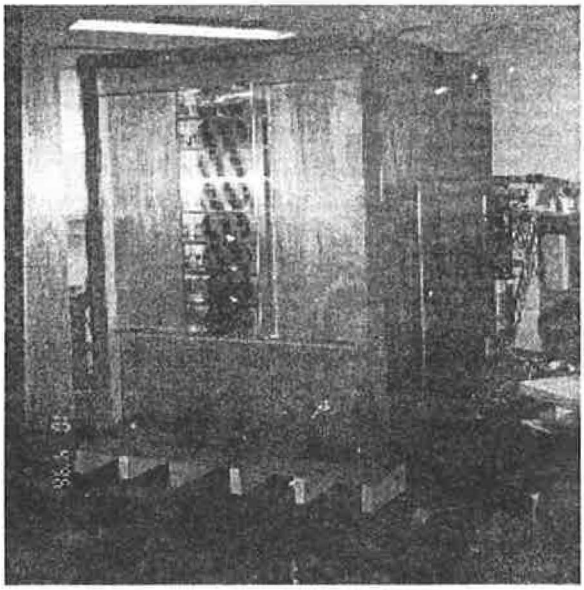

Fig. 4 Test Cell of TEC Cooler (KIER model : 0.4 RT)

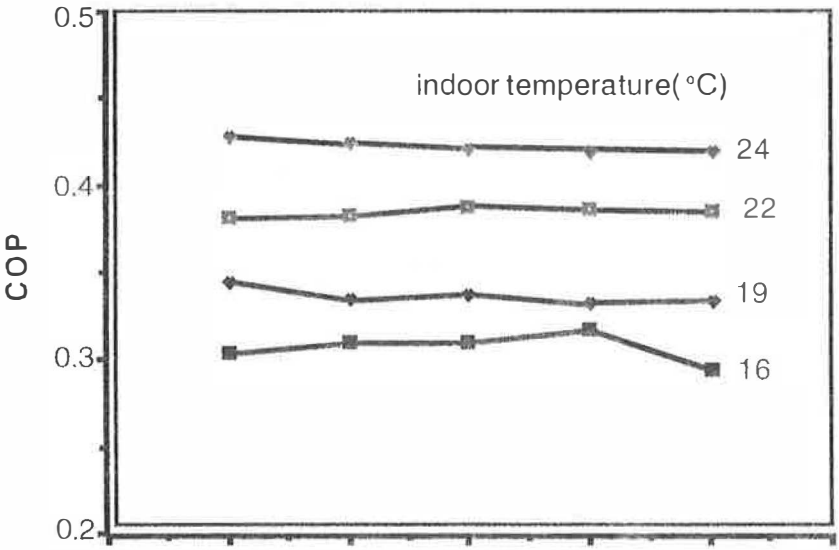

Fig. 5 COP Variation Depend on the Indoor Various Temperature

4. Conclusion

A prototype of an new air-conditioning system utilizing Peltier effect which is basic to thermoelectric technologies, has been designed and built for experimental studies. The experimental results show (fig. 5) that COP varies between 0.29 to 0.48, which supports the initial predicted system COP of the 0.4 RT unit. Thus, it is expected that a practical thermoelectric air-conditioning may be feasible via cascading modules, system design modifications, etc. This study also suggests that the present COP is substantially low compared to the conventional system. From the stand point of environmental protection, however, further studies are considered to be needed.

REFERENCE :

1. B. Mathiprakasam, P. Heenan, and D. DeMott, Development of a Small Thermoelectric Water Chiller for Medical Instrument Cooling, Proc.12th ICT,1993

2. R.J. Buist, Design and engineering of thermoelectric cooling devices, 10th ICT,1991

3. J.G. Stockholm, Reliability of thermolelectric cooling systems, 10th ICT,1991

4. Y.S. Yang ,Trends on the Thermoelectric conversion system, Journal of Air-conditioning and Refrigeration Engineering, Korea 1994

5. Y.S, Yang et al., A review on energy conservation and utilization technology by thermoelectric energy conversion systems., Energy R & D vol.16 1994

6. Y.S. Yang et Al., Development of Solar Thermoelectric Cogeneration System, Journal of The Korean Solar Energy Society, 1996.6

Natural ventilation efficiency in apartment and Reynolds analogy in a water channel

T. LIMAM, F. ALLARD
L.E.P.T.A.B Univ. Of La Rochelle
Av. Marillac F-17000 La Rochelle

Introduction: Within the frame of ALTENER/AIOLOS [1] programme of the European Community experiments have been carried out in order to study the efficiency of natural ventilation in a real apartment. In this study, through the experiments occurred during the last July and August, natural ventilation effects have been thrown into relief. The cooling effect induced by natural ventilation has been shown by the resultant temperature results and the efficiency coefficients enable us to show clearly the quality of natural ventilation in relation with the opening strategy. For the Reynolds analogy, the aim of study was to define an experimental protocol in order to visualise air flow patterns in naturally ventilated building.

I. Site characteristics and building description

«Porte Océane» is located just in front of the ocean. The building has a facade of white stone and glass so that every inhabitant get a fantastic view on the ocean. The south facade shows the searching for openings and transparency given by the integration of large windows and balconies. The local climate is typical of the temperate climate. In summer there's a quite large amplitude between night and day (11 - 12 °C in August). Nights temperatures are cool. This apartment has got the advantage to present a large balcony in front of the ocean. Inside of the apartment there' s one large room (26 m²) with a window (11.32 m²) like a loggia bay.

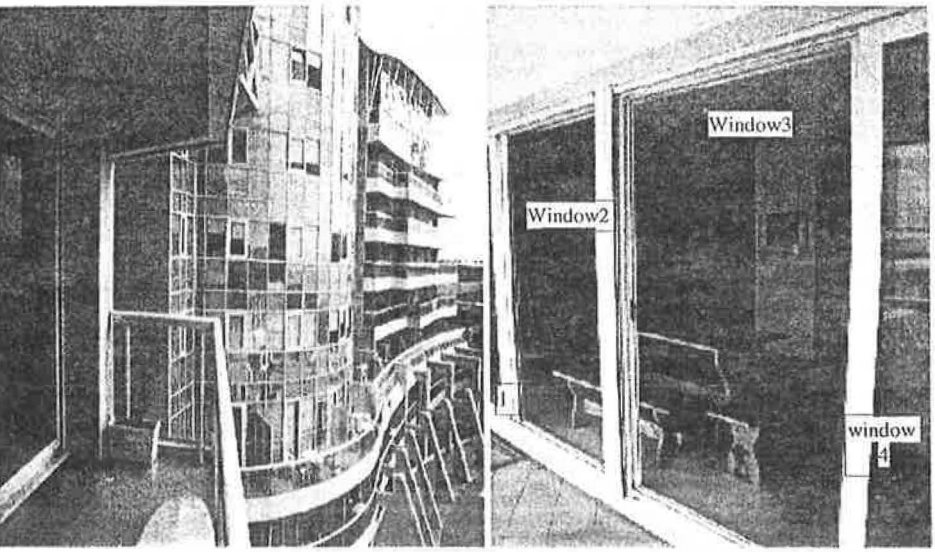

(a) (b)

Fig. 1 : (a) The apartment(5th floor of the building) (b)The window pane

The window pane is of 5.10 m width and is divided in 4 sliding sections of the same surface. It's striking to notice that the window is front of the ocean, it's suppose to have an important impact of natural ventilation if the window is opened. In the following experiments, CMV (Controlled Mechanical Ventilation) is closed or opened. CMV is a mechanical system which permits to exhaust pollutant in the kitchen, the bathroom and the toilet. It's located near the pollutant source, at the ceiling. When CMV is opened, it exhausts 0.7 volume per hour.

2. Weather characteristics during the experiments

Table (1) gives the wind characteristics (velocity and direction) for each experiment. The first one is measured in meter per second. The second one is measured in degree. 0 and 360 to the North, 90 to the East, 180 to the South and 270 to the West.

Experiment	n°	Wind Speed (m/s)	Wind Direction (deg.)	Configuration
July	1	2,5	50	Window3: opened CMV, Doors: closed
August	1	4	30	Window1, CMV: opened Doors: closed
	2	4	30	Window1, CMV, Doors: opened
	3	6	320	Window1&4, CMV: opened Doors: closed
	4	7	330	Window1&4, CMV: opened Doors: closed
	5	8	330	Window1&4, CMV, Doors: opened
	6	6,5	340	Window2&3, CMV: opened Doors: closed
	7	4	350	Window2&3, CMV, Doors: opened
	8	2,5	300	Window2&3, CMV, Doors: opened
	9	3,5	75	Window1, CMV: opened Doors: closed
	10	4	75	Window1,CMV, Doors: opened
	11	4	75	Window1,CMV, Doors: opened
	12	2	20	Window2&3, CMV: opened Doors: closed

Tab. 1 : The Configurations

3. Thermal behaviour of the building during summer

The experimental results are described in the two following parts, the first one shows the results of the July experiments and the second one analyses those of the 12 experiments carried out during the August period.

3.1 Cooling effect induced by natural ventilation : Our interest concerns especially the black bulb temperature. Indeed this temperature is the most representative to express the thermal sensation feeling of the user. As can be seen in the first graph, there's a 7 days period with the same exterior conditions. During the 3rd one, window 3 was opened. Fig. 2 shows that the black bulb temperature is lower when the window is opened, it's the direct effect of natural ventilation.

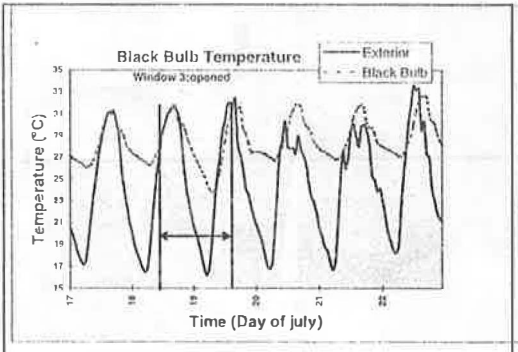

Fig. 2: July experiments results

An other important point is that the black bulb curve has an amplitude of 7 °C while this of the exterior has an amplitude of 15°C. In addition, there's a difference in phase of about 1 hour. That shows the apartment inertia effect, the apartment structure reduces and alters the important outdoor temperature oscillations. Indeed, the external walls are made of concrete blocks with an exterior insulation and the floor and the ceiling are made of concrete slab, so the apartment has a high inertia. It would be important to take this fact into consideration when the object of designing night ventilation for example.

3.2 Natural ventilation efficiency: The figure (3.a) shows the evolution (Decay Method) of concentration in the centre of the room. We observe an important decrease of concentration (ppm) which concerns the three cases of opening (window 1 opened, window 2&3 opened, window 1&4 opened). In each case of opening (surface of the opening is 2.83 m² or 5.66 m²); the decrease of SF6 is very quick, compared to the decrease concerning the permeability of the room.

The two following graphs (fig. 3.b and 3.c) show the CMV effect on the air renewal. When CMV is closed, the efficiency coefficients for the central point (61.78%) and kitchenette (60.81%) are the same (difference of only 1%). But when CMV is opened there's a drop of kitchenette efficiency coefficient, mostly 20% (the central one is 57%). This can be explained by the fact that the extraction opening is located in the Kitchenette ceiling. It's striking to notice that only central and kitchenette results have been reported in the graphs because on the one hand middle, east, west and ceiling comportment and on the other hand kitchenette and corridor are the same. As can be seen in figures 4.a and 4.b, for the same lapse of time (about 20 minutes), the double quantity of gas has disappeared when the windows 1 and 4 are opened (compared to the case of one opening window). Moreover the opening of two windows has lead to have a good air renewal, so there was not an accumulation at the ceiling.

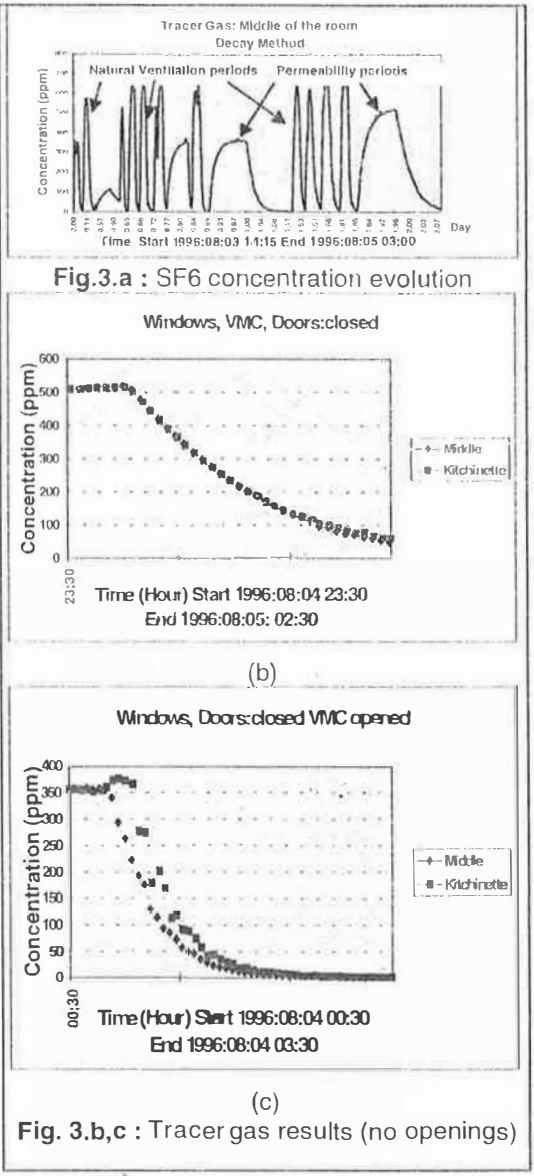

Fig.3.a : SF6 concentration evolution

Fig. 3.b,c : Tracer gas results (no openings)

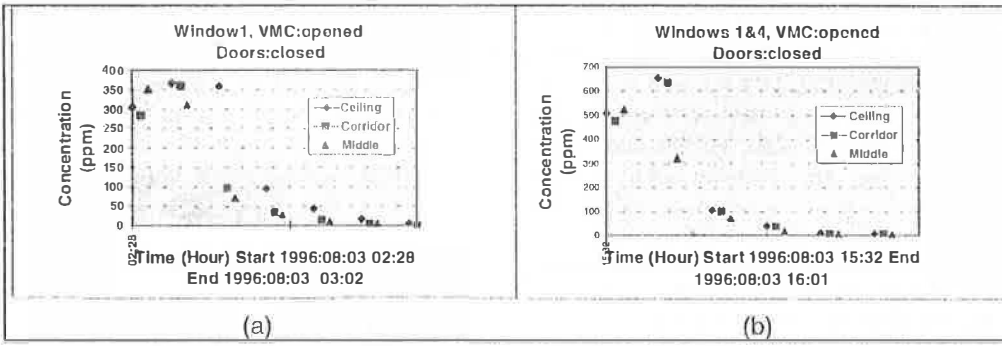

Fig. 4 : Tracer gas results (openings)

The geometrical average is calculated averaging on the 6 points which are uniformly distributed in the room. Several remarks can be done : Firstly, the CMV impact is very weak, it represents only 1 or 2% modification of the efficiency coefficient. Secondly, the fact of opening two windows is better than opening one window but it's striking to notice that, when the lateral windows are opened, the efficiency is 18% higher. This can be explained by the fact that when the lateral windows are opened, a draught appears and permits a better mixing of inside air.

	Bathroom & WC doors	Experiment	Geometrical average (%)
Window 1 opened	closed	1	68,34
	opened	2	69,21
		11	71,63
Window 1&4 opened	closed	3	87,45
Window 2&3 opened	closed	6	71,7
		12	69,67
	opened	8	71,34

Tab.2 : Efficiency coefficients

The efficiency is calculated by : $$\varepsilon = \frac{\tau p}{2 < \tau >} \quad (1)$$

with : τ_p is the local mean age $$\tau_p = \int_0^\infty \frac{C(t)}{C(0)} dt \quad (2)$$

$<\tau>$ is the room mean age $$<\tau> = \frac{\int_0^\infty t C(t) dt}{\int_0^\infty C(t) dt} \quad (3)$$

C(t) : SF6 concentration at the measurement point. Finally, comparing the efficiency coefficients of experiments 6 and 12, we can see that these two coefficients are similar. Nevertheless the wind velocities are different (6 m/s during experiment 6 and 2 m/s during experiment 12). So the conclusion is that, when the wind velocity reaches a certain threshold, the ventilation efficiency stays on the same level even if the wind velocity is still increasing.

. The scale model in the Hydraulic channel

he aim of this study is to define an experimental protocol in order to visualize air flow atterns in naturally ventilated building.

rom a fluid mechanics point of view, there is a direct similitude between two flows with ıe same Reynolds number. Around 20°C, there is a ratio of 20 between the viscosity of vater and air, which means that, for the same characteristic velocity between the reality nd the model, the geometrical dimensions can be reduced by an order of 20 times.

he facility is a 20 m long water channel of 1m² section and a 7 Watt laser equipped ith 30 m of optical fibre with different kinds of lenses [2]. The model, represents the Porte Ocean » apartment and moves automatically along the channel (fig. 6).

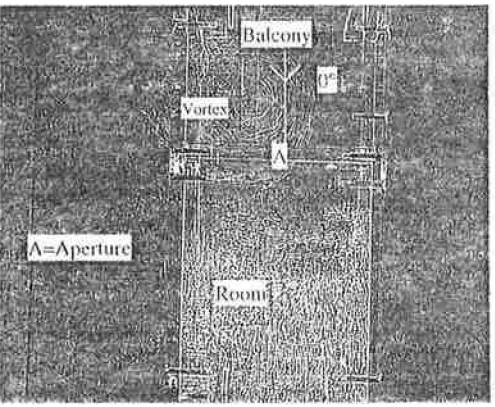

Fig. 5 : V=0.5 m/s, θ = 0°, balcony zoom

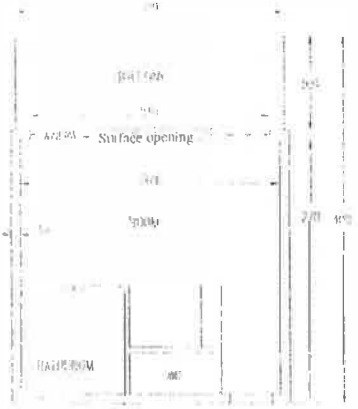

Fig. 6 : floor plan view of the scale model

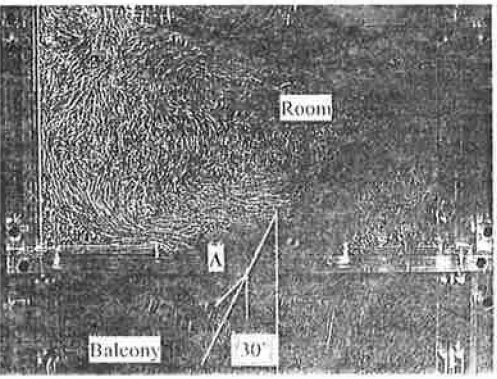

Fig. 7 : V= 0.5 m/s, θ = 30°, aperture zoom

Fig. 8 : The Balcony characteristics (mm)

The velocity covers a range from 0 to 7 m/s, representing external winds of the same characteristics. The data acquisition consists of photographs and video.

The aim of these experiments is to study single-side ventilation in a full scale building, under real climatic conditions, in order to: better understand the related phenomena, collect data for the validation of existing models (theoretical models and computational network models), and develop more accurate methodologies for the calculation of the air flow patterns in this specific case of natural ventilation. A scale model is conceived to provide the flow visualisation by Reynolds analogy in water channel. Indeed, we are interested in the velocity field of air, generated by an external wind in an apartment. The visualisation technique used Rilsan particles (density 1.06) which is very close to water density and leads to a very good transport in the flows (fig. 5).

The results consist of a video showing different configurations of air flow patterns in single sided ventilation with various angles of incidence upon the opening (fig. 5 and 7). It shows very clearly the different flow patterns that can be found in these configurations : inertial flow in room with a small circulation in aperture zone (the incidence value with respect to the normal of the opening in a single sided ventilation case is 0° induced a piston flow phenomena (fig. 5); and for case $\theta = 30°$ (Fig. 7) the concentration of particles localised in left of the room. This video is obviously a very good demonstration tool, but it is not sufficient to obtain quantitative data. There are also still photographs with different exposure times in order to obtain trajectory elements of the particles. These elements represent in fact velocity vector fields for different configurations.

Conclusion : In this study, through the experiments occurred during the last July and August, natural ventilation effects have been thrown into relief. The cooling effect induced by natural ventilation has been shown by the resultant temperature results and the efficiency coefficients enable us to show clearly the quality of natural ventilation in relation with the opening strategy. These results obtained by flow visualisation in a water channel demonstrate the suitability of this method to characterise the flow patterns. This methodology offers good perspectives to obtain a very detailed information about velocity fields.

Référence :

[1] ALTENER/AIOLOS CEC Research Programme. Programme, which was partly financed by the Commission of the European Union, DG XII for Science, Research and Development.
[2] Single Sided Ventilation, F. Allard and K. Limam (ed.) (1995), PASCOOL, Research Project, MDS/VTL Final Report, Ch. 2, EC DG XII, Brussels.

Acknowledgements :

The present study was carried out within the frame of ALTENER/AIOLOS CEC Research Programme, which was partly financed by the Commission of the European Union, DG XII for Science, Research and Development.

THE EFFECT OF THE INNER SURFACE MATERIAL ON THE INDOOR RELATIVE HUMIDITY

Oľga Koronthályová

Institute of Construction and Architecture, Slovak Academy of Sciences
Dúbravská cesta 9, 842 20 Bratislava, Slovakia

Abstract

The indoor air relative humidity is an important parameter influencing the human comfort and hygrothermal performance of a building. From the comfort aspect not only time averaged relative humidity but also its actual courses are important. With the aim to evaluate the effect of interior surface materials with different hygroscopicity on the resulting daily courses of indoor relative humidity the non-steady numerical calculations of the indoor relative humidity, considering time variable outdoor climatic conditions, indoor moisture production and ventilation rate were done.

1. Introduction

The value of indoor relative humidity is a result of the simultaneous effect of the following factors: outdoor climatic conditions, ventilation rate, indoor moisture production, indoor air temperature and the release or uptake of moisture by interior surface materials. The numerical model used in this study enables to evaluate the effect of the particular factors on indoor relative humidity. The presented calculations were focused on the effect of the interior surface material hygroscopic properties on the courses of the indoor relative humidity in the cases of constant or time variable ventilation rates.

2. Numerical model

On the assumption of the well-mixed air in the room the mass balance equation for indoor water vapour may be written as follows (ref. (1)):

$$\frac{\partial p_i}{\partial t} = \frac{462 \cdot T_i \cdot \left\{ G_p + \sum G_{sk} - \sum \left[\beta_j \cdot A_j \cdot (p_i - p_{sat,sj}) \right] \right\}}{V} + n \cdot (p_e - p_i) \qquad (1)$$

where p_i is the indoor vapour pressure [Pa], p_e is the outdoor vapour pressure [Pa], t is time [s], T_i is the indoor air temperature [K], G_p is the indoor vapour production [kg.s^{-1}], ΣG_{sk} is the sum of the moisture flows from or into the room construction surfaces, V is volume of the room [m^3], β_j is the diffusion surface film coefficient [s.m^{-1}], A_j is the area of the surface where condensation or drying takes place [m^2], $p_{sat,sj}$ is the saturation vapour pressure on that surface [Pa], n is the ventilation rate [s^{-1}].

According to the equation (1), the indoor vapour pressure after small time increment Δt can be written as:

$$p_i(t+\Delta t) = p_i(t) + \frac{\Delta t \cdot 462.5 \cdot T_i(t) \cdot \left\{ G_{in} + \sum G_{ak} - \sum \left[\beta_j \cdot A_j \cdot (p_i(t) - p_{sat,j}(t)) \right] \right\}}{V} +$$

$$+ \Delta t \cdot n \cdot (p_e(t) - p_i(t)) \qquad (2)$$

The presented numerical model for calculation of the indoor air relative humidity consists in the solution of the equation (2) coupled with 1-D numerical simulation the heat and moisture transport through the room constructions. On the base of that simulation the moisture flow from or into the hygroscopic surface of the room is calculated for each time step:

$$G_{sk} = \beta_k \cdot (p_{sk} - p_i) \cdot A_k \qquad (3)$$

where p_{sk} is the vapour pressure on the wall surface [Pa], A_k is area of the surface [m^2].

The numerical simulation of the heat and moisture transport through the room constructions was done using the program NEV 3, based on numerical solution of two coupled partial differential equations for heat and moisture balance. The more detailed description of the model used in program NEV 3 is in ref.(2).

The used numerical model for the calculation of the indoor air relative humidity was verified by comparing the calculated courses of the indoor relative humidity with the measured results. The experimental data were taken from ref. (1). The experiment was done for two rooms with volume 40 m^3 and total wall area 50 m^2. The walls and ceiling of the first room were covered with aluminium plates, the walls and ceiling of the second room were finished by gypsum board with textured paper. The plastic flooring was used in both of the rooms. The considered water vapour production was 0.2 kg per hour during the first 3.5 hours and the ventilation rate was time variable. The courses of the vapour production and ventilation rate are shown in Fig. (1). The material properties used in calculation were taken from ref. (3). The time step Δt = 300 s was used in numerical calculation. The comparison between the measured indoor relative humidity courses and the courses calculated by the numerical model is in Fig. (2). The calculated data coincide sufficiently with the measured ones.

3. Results of the numerical simulation

With the aim to evaluate the effect of the interior surface material hygroscopic properties on the indoor relative humidity the numerical calculations of its daily course for three rooms with different wall surface materials and for two different ventilation strategies were done. The volume of the each of the rooms was 81 m^3, the area of the possible hygroscopic surfaces was 55 m^2. In the first room the cellular concrete walls were finished with 15 mm of gypsum plaster (vapour resistance factor μ = 8), in the second room the concrete walls were covered with 0.3 mm thick vinyl wall paper (vapour diffusion thickness μd = 2.1m) and in the third room the concrete walls were

finished with 12 mm gypsum board (μ = 11) covered with 0.3 mm paper wall paper (vapour diffusion thickness μd = 0.027 m).
The considered daily course of vapour production is shown in Fig. (3).Two different ventilation strategies were considered :
- the constant ventilation rate
- basic air change rate with the additional ventilation by the window opening during the water vapour production periods (Fig. (3)).
The daily mean ventilation rate was the same in both of the cases: $n = 0.4\ h^{-1}$.
The considered indoor air temperature was constant t_i = 20°C. The daily courses of the outdoor temperature and relative humidities were used correspond to January in Bratislava with the daily mean temperature -1.3°C and the daily mean relative humidity 78 % (Ref. (4)). The solar radiation was not taken into the account. The calculations were done for one week period with the time step Δt = 300 s.

The calculated daily courses of indoor relative humidity for the all considered cases are shown in Fig. (4). As can be seen from the figure the ventilation strategy was very important as for the daily course of the indoor relative humidity as for its mean value. The hygroscopicity of the interior surface material decreased significantly the amplitude of the indoor relative humidity variation. The effect of the interior surface material hygroscopic properties was more significant in the cases when the constant ventilation rate was considered. The 'active thickness' that means the thickness of the surface material moisture content of which was changing daily as a result of the release or uptake the moisture into or from the indoor air was about 10 mm as in the case of gypsum plaster as in the case of gypsum board with paper wall paper.

4. Conclusions

The numerical model enabling the evaluation of the effect of the particular factors on the indoor relative humidity was presented.

The examples of calculation confirmed that as mean value of the ventilation rate as the ventilation strategy are important for the actual course of indoor relative humidity. The presented calculations confirmed the importance of the interior surface hygroscopicity on the daily course of the indoor relative humidity. It is more signifficant in the cases with constant ventilation rate.

A lot of further calculations for various ventilation and moisture production strategies, geometry of the room and longer time periods are necessary for more general conclusions regarding the global effect of the particular factors influencing the actual relative humidity courses.

Acknowledgment
The autor is grateful to VEGA (Grant No. 2/1263/96) for the supporting of this work.

5. References

(1) IEA-Annex XIV : Condensation and Energy, Source Book, 1991
(2) Hens H. : Task 1 : Modelling. IEA-Annex 24 Final Report, 1996
(3) Catalogue of Material Properties. Upgraded version. IEA - Annex 14 Report, 1994.
(4) Končok M: Climate and Bioclimate of Bratislava, Veda, Bratislava 1979 (in Slovak)

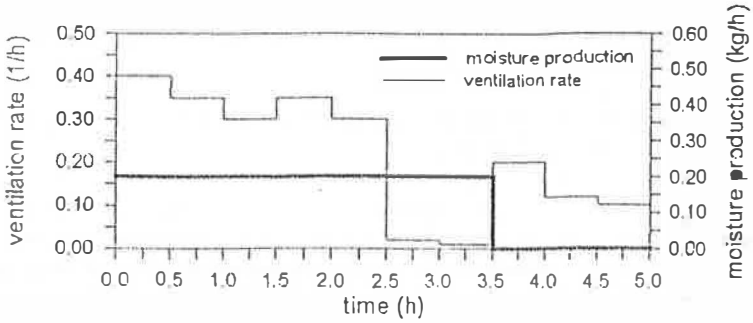

Fig. 1 The courses of the vapour production and the ventilation rate used in compariso between the measured and calculated data

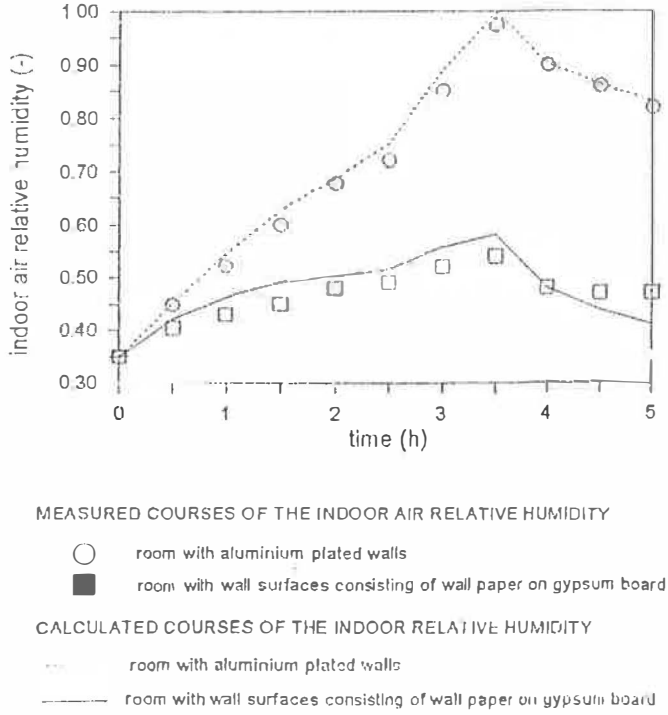

Fig. 2 The comparison between the measured indoor relative humidity courses and the courses calculated by the developed numerical model

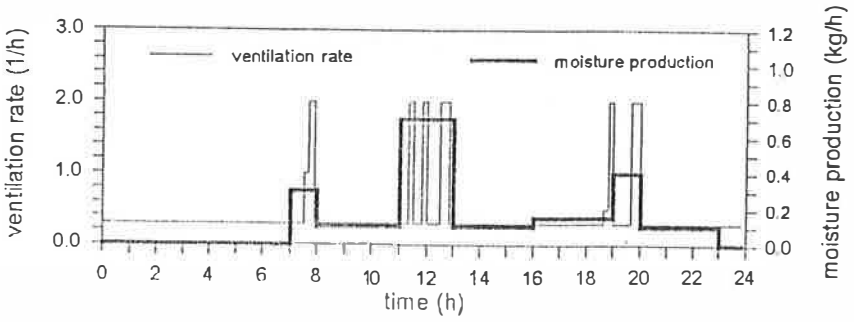

Fig. 3 Daily courses of the vapour production and the ventilation rate used in calculation

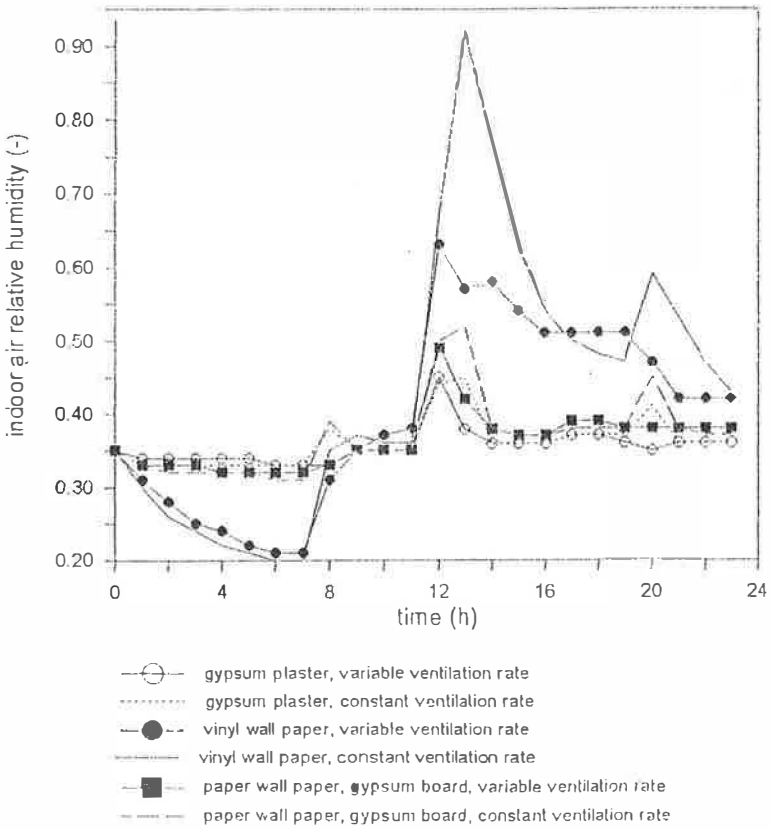

Fig. 4 Calculated courses of the indoor realtive humidity for different wall surface materials and ways of ventilation

ENERGY CONSERVATION MEASURES FOR RENOVATION OF OFFICE-BUILDING

Dahlsveen, T.[1], Petráš D.[2], Magyar J.[2]

[1]*ENSI*
P.O.Box 4257 Torshov
0401 Oslo, Norway

[2]*Slovak Technical University*
Department of Building Services
Radlinského 11, 813 68 Bratislava, Slovak Republic

ABSTRACT

Every building is unique. Therefore each project must be treated separately to find individual energy conservation possibilities. On the other hand the building owners might also have various plans for renovation and different requirements for the profit of ENCON measures.

The process of evaluating and implementing profitable energy conservation measures in a building is often described as "the ENCON process". The total ENCON-process has been derived to five main steps: Project Identification, Scanning, Energy Audit, Implementation and Operation.

The aim of energy audit of office building is to define energy conservation measures. The paper describes the existing state of building construction and HVAC-system, which ENCON measures to implement and how, investment costs and profitability. Based on building state description and the actual construction parameters, the energy consumption was calculated by the Key Number Method and compared with the measured energy consumption. Then the energy savings from relevant ENCON measures were calculated and described, before the investment costs and profitability for each measure were found.

The summary of these calculations: energy savings, investment costs and profitability makes up the ENCON potential of the office building.

INTRODUCTION

The aim of Energy Audits is to make an Energy Audit Report to be used as a platform for carrying out ENCON measures. The paper describes the existing building construction and the technical systems of office VVA building:

- Heating system
- Domestic hot water preparation
- Ventilation
- Lighting
- Various equipement
- Cooling / Air conditioning,

which measures to implement and how, invesment costs, profitability and proposal for time schedule for implementation of the measures.

Building State Description

Building envelope characteristics

The VVA building consists of two buildings joined together; The main office building is L-shaped with basement and three floors, the wall construction is made of bricks, with a flat roof. The second building - "Semerek" - is also made of bricks. Is has no basement, but two floors and a partially used wooden attic. The double glazed windows have wooden frames without sealing, the main stair case has double glazed walls with wooden frames. The entrance door is also of wood, with double glass. There are metal gate in the building. Thermal gains are stopped only by some light coloured (mostly white) curtains in the offices, there are no shading obstacles in other spaces of the building. Some windows are permanently shaded of the other building. Building envelope characteristics are defined by parameters:

Table 1. Building characteristics and parameters

Heated area:	5.200 m^2	**Heated volume:**	17.500 m^2
U - walls	1,3 $W.m^{-2}.K^{-1}$	**U - windows, average**	2,9 $W.m^{-2}.K^{-1}$
U - roof	0,9 $W.m^{-2}.K^{-1}$	**U - doors**	4,1 $W.m^{-2}.K^{-1}$
U - floor	0,5 $W.m^{-2}.K^{-1}$	**U - gate**	7,0 $W.m^{-2}.K^{-1}$

Average room temperature:	21 °C
Heating season:	15 October - 30 April
Energy supply efficiency:	88 %
Infiltration:	0,8 h^{-1}

HVAC-systems

The heating central for low-pressure gas boilers contains two SLATINA gas boilers with APH 50 PZ burners. Each boiler has a capacity of 440 kW, totally 880 kW. The installed power of pumps is 3 kW. There is a two-pipe distribution system with forced water circulation and a closed expansion vessel installed in the building. The horizontal part of the pipe line is installed below the cealing of the ground floor, no insulation. The rooms are heated by steel radiators with manual closing valves. Some thermostatic valves are also installed, but they seem to be broken. There is a gas meter installed, measuring the total gas consumption in the building. The operation of the boilers is controlled manually. Heating is continuous, with manual set back during nights and in the weekends, but with no outdoor compensation. The present construction of the heat distribution system is not suitable for zone control.

The **hot water preparation** is done by one standing storage-heater OVS 21, volume 1000 l . Two electric hot water heaters with a volume of 2 x 160 l are operated all year, installed

power is 3 kW. All of the tanks are insulated with appr. 100 mm mineral wool. The hot water preparation is manually controlled for a maximum temperature of 55 °C. The horizontal part of the distribution pipes are installed under the ceiling of the ground floor, no insulation. The main domestic hot water consumers in the building: 48 kitchen and toilet taps, there is no water saving sanitary equipment. The floors in common spaces such as corridors and halls are being cleaned regularily.

The computer room has an air conditioning unit (without humidifier) supplying cooled or heated air at a rate of 3.600 m^3/h. The air rate is controlled manually. Operation period: 8 hours per day, 5 days per week. The heating coil is electrically heated. All other rooms are naturally ventilated by the windows.

Estimated simultaneous fan power: 0,3 W/m^2. Operation period: 40 hours per week. The installed power of the 3 pumps is 3 kW (1 back up), estimated simultaneous power: 0,4 W/m^2, operation period: 24 hours per day during the heating season.

The light fittings consist mainly of illuminaries. Estimated installed power: 50 kW. Estimated simultaneous power: 5 W/m^2, 40 hours per week.

There is appr. 80 computers in the building, installed power appr. 200 W per computer. In addition there are some copy machines and oher electrical equipment. Estimated simultaneous power: 2,5 W/m^2, 40 hours per week

Appr. 300 persons have their work in the building, 250 of them are in average present. Estimated normal occupancy period is set to 9 hours per day, 5 days per week. Heat load: 100 W per person.

Energy Consumption

Measured energy consumption

The following energy data have been supplied by NAFTA:

Table 2. Measured energy consumption

Year: 1992 - 94	Electricity	Gas	Total
Energy demand	'92: 243 745	'92: 706 130	949 875
before ENCON [kWh/yr]	'93: 274 045	'93: 797 930	1 071 975
	'94: 263 566	'94: 814 650	1 078 216
Energy cost	'92: 425 963	'92: 222 432	648 395
before ENCON [Sk/yr]	'93 439 175	'93: 257 979	697 154
	'94: 688 512	'94: 272 909	961 421
Present energy prices		3,35	
Energy price unit	Sk/kWh	Sk/m^3	

- The measured gas flow values (m^3) have been multiplied by the normal gas efficiency to find the gross gas consumption in kWh/yr, and the gross energy demand for heating and domestic hot water. The efficiency of the energy production process (boiler) has been accounted for in the Key Number calculations.

Calculated vs. measured energy consumption

The most important variables which will influence upon the energy consumption of an existing building are climatic conditions and operation and use of the technical installations and equipment.

Without any registration routines regarding operation and maintenance of the building, it is impossible to know how the building and the technical installations have been operated previously: In which way has the manual control of the heating system been done? Has there been any leakages in the systems the last period? Actual room temperature the last years? Etc.

To obtain a reference for evaluation of ENCON measures, the Energy Audit always should include a calculation of the existing energy consumption, based on:

- a standard "climatic year"
- the existing building condition
- "normal" operation conditions.

Table 2. Adjusted energy consumption

Energy Budget, VVA NAFTA			
Budget Item	Calculated kWh/m²year	Measured kWh/m²year	Adjusted, measured kWh/m²year
1 Heating	210		+ 20
Sum 1 (gas)	**210**	**150**	**170**
2 Ventilation	5		
3 Domestic Hot Water	10		
4 Fans/Pumps	3		
5 Lighting	10		
6 Various	5		
7 Cooling	5		
Sum, 2 - 7 (electricity)	**38**	**50**	**38**
Total 1 - 7	**248**	**200**	**208**

This calculated energy consumption is the basis for the calculation of savings of the ENCON measures. Therefore will the measured savings never be equal to the calculated savings, and the measured savings will be higher or lower than the calculated savings depending on the outdoor climatic conditions and the previous operational conditions.

The energy consumption for 1994 has been used as a basis for the measured energy consumption and for the adjustment made.

Energy consumption before and after ENCON implementations

The table below shows the energy consumption per budget item before implementation of ENCON measures compared to the energy consumption after implementation, with or without non-profitable measures. From an energy point of view, appr. 40 % of the ENCON potential is connected to non-profitable measures.

Table 3. Energy consumption before and after ENCON implementations

Energy Budget			
Budget Item	Calculated consumption before ENCON kWh/m²year	After ENCON, profitable measures kWh/m²year	After ENCON, incl. non-profitable measures kWh/m²year
1 Heating	210	143	96
2 Ventilation	5	5	5
3 Domestic Hot Water	10	7	7
4 Fans/Pumps	3	3	3
5 Lighting	10	10	10
6 Various	5	5	5
7 Cooling	5	5	5
Total	**248**	**178**	**131**

CONCLUSION

This paper presents us the ENCON Potential - a considerable energy saving potential in the VVA building:

- Profitable energy savings 362.000 kWh/year (= 28 %)
- Economical savings 132.800 Sk/year
- Total investments 700.000 Sk
- Total profitability (Pay Back) 5,3 years

If the non-profitable measures are implemented because of need for renovation, the total energy savings will be 47 % of the total energy consumption.

The measures are ranked according to profitability; all of the profitable ENCON measures are assumed to be implemented simultaneously as one project in order for the investment to be valid. The figures have an accuracy of ± 10 - 15 %.

Table 4. ENCON potential of office VVA building

	Energy conservation measure	Investment [Sk]	Saving		Pay Back [years]
			[kWh/yr]	[Sk/yr]	
1	Water saving nozzles, kitchen and bathroom	20. 000	17.000	10.000	1,7
2	New automatic control system	60. 000	62.500	21.900	2,7
3	Energy Control System	65. 000	54.500	19.100	3,4
4	Sealing of windows	125. 000	99.000	34.600	3,6
5	Replacement of burner	80. 000	41.000	14.400	5,6
6	Balancing of the heating system	30. 000	9.000	3.100	9,7
7	Thermostatic radiator valves	320. 000	79.000	27.700	11,6
Total (Measure 1 - 7)		700. 000	362.000	132.800	5,3
Non-profitable measures:					
8	Replacement of windows	812. 000	68.000	23 800	340
9	Insulation of external walls	5 670. 000	106.000	37 100	152
10	Insulation of roof	2 520. 000	68.000	23 800	106

REFERENCES

[1] Energy audit report VVA Nafta Gbely a.s., ENSI / STU, Oslo / Bratislava 1995, p. 50

[2] Dahlsveen,T., Petráš, D.: Energetický audit budov - ENCON proces. TZB Haustechnik, 1/1995, Alfa konti s.r.o., Bratislava

[3] Dahlsveen,T., Petráš, D., Magyar, J.: Výsledky energetických auditov administratívnych budov - pilotné projekty a.s. Nafta Gbely. TZB Haustechnik, 5/1996, Alfa konti s.r.o., Bratislava

OCCUPANT INTERACTION WITH A MIXED MEDIA THERMAL CLIMATE CONTROL SYSTEM IMPROVES COMFORT AND SAVES ENERGY.

D. M. Rowe, B. Forwood, C. T. Dinh and W. G. Julian
Department of Architectural and Design Science
The University of Sydney, New South Wales 2006, Australia

Occupants of a suite of seven offices intervene to adjust their thermal environments by manipulation of ventilation through doors and windows and by operation of supplementary cooling and heating equipment when considered necessary. Intervention actions, space temperatures and energy consumption have been monitored continuously for twelve months. Energy simulation models have been used to compare the energy consumption with an estimate of what might be expected with a conventional ducted air conditioning system for the same space. It is reported that the recorded energy consumption is approximately one quarter of that estimated for the alternative system. Occupants rate the space highly for satisfaction with the thermal environment and air quality.

1.0 Introduction

Sydney, Australia, enjoys a mild climate with benign winters, mild spring and autumn weather and warm to hot summers. It is possible to be thermally comfortable indoors for much of the year without resorting to mechanical intervention when buildings are designed for passive control of energy flows and windows and doors can be operated to trim conditions as required. More or less similar conditions prevail in the heavily populated regions in Australia and de Dear ref.(1) has demonstrated that this is so for some seasons in many other parts of the world. In most places, however, there will be occasions when indoor conditions will move above or below acceptable comfort limits unless they can be modified by the operation of some form of supplementary cooling and heating equipment.

Despite the frequent availability of favourable outdoor conditions it has become customary in many parts of the world over the last thirty years or so to enclose buildings with fixed windows and to rely on mechanical cooling, heating and ventilation year round to maintain habitable conditions indoors. This is made possible by the expenditure of large quantities of cheap energy to the extent that about half the energy consumed in a typical office building is used by the climate control system.

It is now becoming evident, however, that these arrangements do not satisfy a substantial part of the occupant population. Duffy ref.(2) has suggested that *"The obvious preference for the natural environment, and the hatred of air conditioning, is increasing and is even beginning to be clearly seen in North America.* He goes on to say *"The North American idea that the building is separated from nature, hermetically controlled and engineered in such a way that it provides a stable internal environment, is not a sustainable idea."*

Rowe ref.(3) has presented scores for thermal comfort in twelve suites of offices which were studied in the period from 1992 to 1995. The sample included two in more or less free running spaces, eight that are air conditioned and two that are ventilated through doors and windows and have occupant controlled, on-demand supplementary cooling and heating. As indicated in Fig. 1 the best scores for thermal comfort were achieved in the latter two suites (numbers 1 and 11).

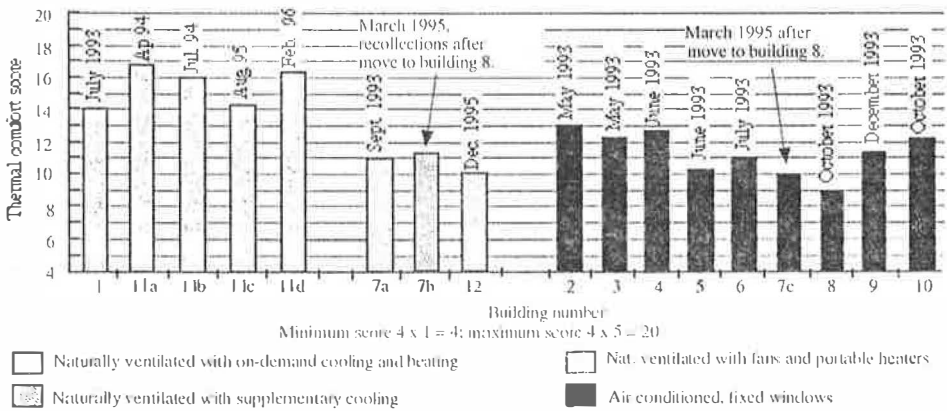

Fig. 1. Thermal comfort scores in twelve buildings. Rowe ref.(3)

This paper presents the results of continuously monitoring occupant interactions with control elements in the suite identified as number 11 in Fig. 1 over the period of twelve months from 1 August 1995 to 31 July 1996. It is reported that energy consumption is approximately a quarter of what would be expected if climate control were provided in the same space by ducted air conditioning with fixed windows. It is concluded that this very considerable saving is due to the intermittent use of the supplementary cooling and heating equipment. It seems probable that a large proportion of the occupants use passive controls by preference to maintain their comfort condition and only resort to mechanical intervention when this is not successful.

As reported in the Sydney Morning Herald ref.(4) Australia has recently come under international criticism for its reluctance to accept firm targets for the reduction of greenhouse gas emissions. In a world where opinion is moving steadily toward an understanding of the need for a the more sustainable relationship with the environment, a mixed media strategy for indoor climate control such as this paper describes represents a reasonable compromise between sustainability and comfort in buildings.

2.0 About the Project

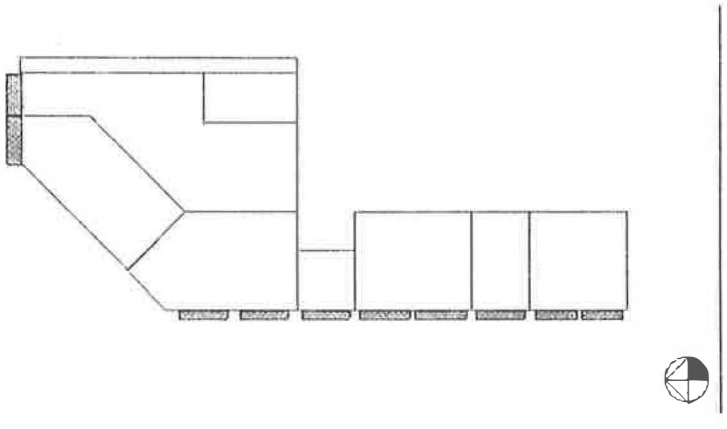

Fig. 2. The project site.

Twelve people occupy a suite of seven rooms used as offices in the architecture building at Sydney University. Total area is 210 m^2. The rooms are ventilated through windows and doors which can be adjusted as required by the occupants. The rooms have been equipped with reverse cycle refrigerated fancoil units which are available for supplementary cooling and heating under direct occupant control. Temperature set point, fan speed and direction of air supply are independently adjustable in each room. Background heating is available during the three winter months of June, July and August from the original installation of hot water panel radiators, also under direct control of occupants. The area under investigation is shown in Fig. 2.

It will be observed that all spaces are located in perimeter zones and are subject to direct influence of outdoor conditions. Main orientation is to the west with lesser exposures to north and east. External sunshades give some protection from solar heat gains. Ceilings at 3,500 mm. above the floor allow warm air to rise above the occupied zone. Heavy weight masonry construction provides thermal inertia to damp outdoor temperature swings.

Sensors on windows, external doors, fancoil units and panel heaters and temperature sensors in each room were monitored continuously to record status throughout a year of operation from 31 July 1995 till 1 August 1996. Energy consumed by the refrigeration system has been recorded from kWh meters on the supply at weekly intervals throughout the period. For comparison the energy that would be consumed by a ducted air conditioning system for the same suite of rooms was estimated using the energy simulation package ESPII ref.(5). The model operated an air cooled packaged unit with variable volume air distribution and an outdoor air economiser cycle on an hour by hour file of Sydney weather data for the test reference year 1981. As a check a simulation using the same weather data was run independently using the American simulation package DOE-2. Occupants were asked to indicate their satisfaction with thermal comfort over time on four occasions in April 1994, July 1994, August 1995 and February 1996 and the results were reported previously by Rowe ref.(3) as illustrated in Fig. 1.

3.0 Results

Mean indoor temperature was maintained on working days throughout the year in the range from 20 to 25°C. During this period outdoor temperatures varied between a low of 12°C in winter and a high of 37°C in summer. A strong tendency was observed toward selection of indoor temperatures that were higher on warm days and lower on cool days. Temperatures in individual rooms regularly showed variations up to 2°C on either side of the mean. The daily temperature range at 3 pm is illustrated in Fig. 3.

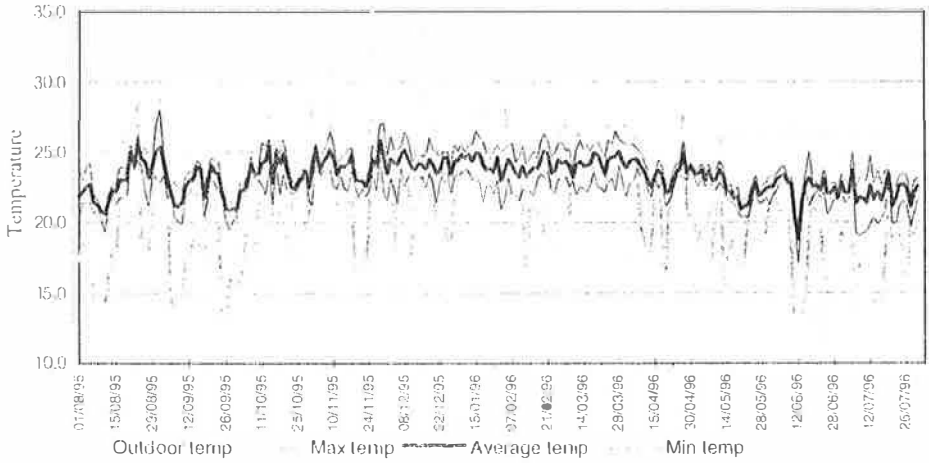

Fig. 3. Daily range of indoor and outdoor temperatures at 3 pm.

Use of the fancoil units is illustrated in figure 4 which indicates the number of units in operation on each work day at 3 pm with the concurrent outdoor temperature. It is observed that on 72 of 236 days (31 percent) no units were in operation at this time of day and on another 74 days (also 31 percent) only one was in use. Figure 4 shows that all units were in use at this time of day on only two days in mid January with four or more units used on 26 days (11 percent) in the period between early November and the end of March. This pattern suggests a tendency to turn units on only when it is necessary to modify conditions that are considered unsatisfactory.

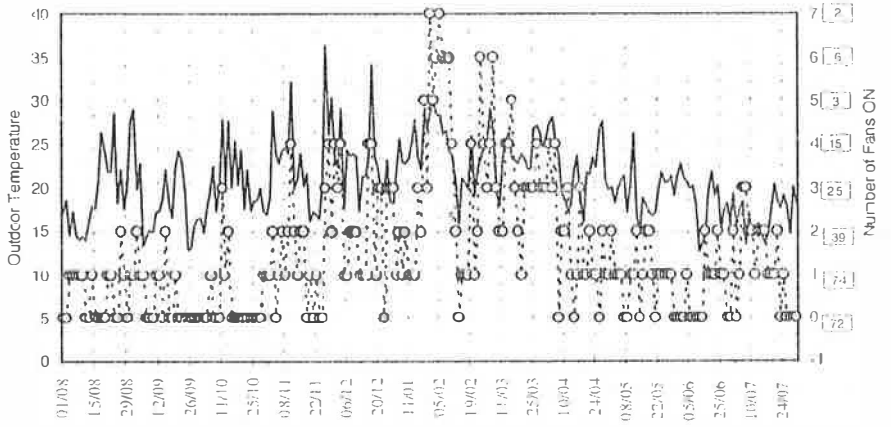

Fig. 4. Number of fancoil units operating at 3 pm on work days between 1 August 1995 and 31 July 1996.

Use of windows and external doors at the same time of day is illustrated in Fig. 5. Five of the rooms have wo operable windows with one in each of the remaining two. It is noted that more than half of the windows are opened on only four occasions during the year. The relationship between outdoor temperature and number of open windows is not as distinct as that observed with fancoil units although there is a discernible tendency for more windows to be open on the milder days. These rooms are provided with adjustable glass louvres above the main window sets and infiltration is sufficient for adequate ventilation even when both windows and louvres are closed.

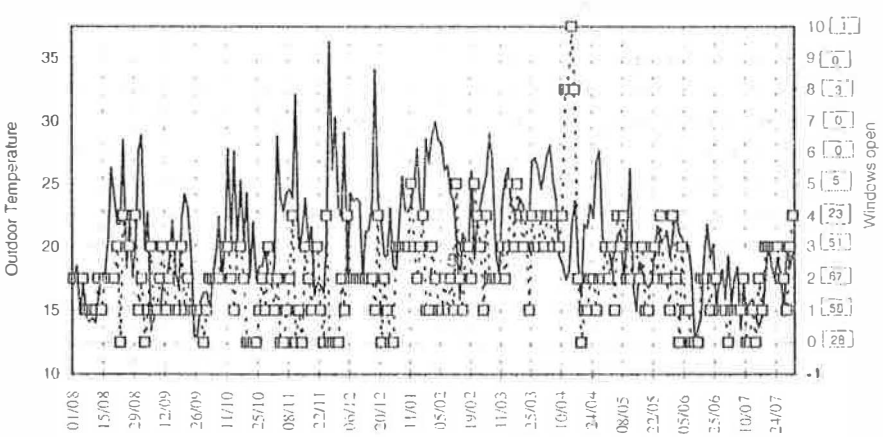

Fig. 5. Number of windows open at 3 pm on each work day between 1 August 1995 and 31 July 1996.

A total of 4115 kWh of energy was consumed by the supplementary refrigeration system in the year. Some of this was used during winter months when the system was operated in reverse cycle mode to augment the heating provided by the hotwater panel radiators. Direct comparison with the estimated total energy consumption by the alternative packaged air conditioning system is not possible because the input to the hotwater radiators could not be isolated. Compensation for this was introduced by accumulating only cooling energy in the energy simulations. The simulation with the package ESPII indicated an expected annual consumption for cooling of 15,519 kWh. The DOE-2 simulation yielded an estimate of 15,760 kWh. Figure 6 shows the monthly distribution of actual energy consumption and a comparison with estimated monthly consumption by the packaged air conditioning system as simulated by the ESPII software model.

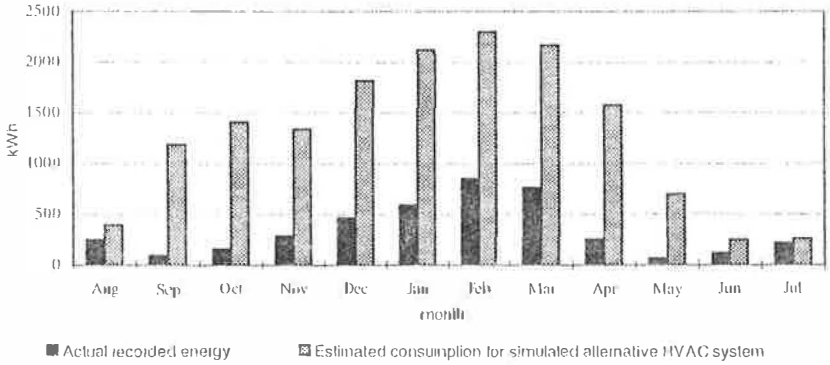

Fig. 6. Actual monthly energy consumption compared with estimated requirements for a conventional air conditioning system.

4.0 Discussion

The thermal comfort satisfaction score for this group of four men and eight women, although high, is not perfect. This is probably due, at least in part, to the shared occupancy of two rooms by three people in each and another by two with resultant compromises that are not necessary when a room has a sole occupant. A perfect score may never be achieved even without these compromises. Nevertheless scores for thermal comfort in this building are higher than those found in eight conventionally air conditioned and two free running naturally ventilated buildings.

The results are the more exciting in the light of the very low consumption of energy in comparison with what would be expected from a conventional air conditioning system. No doubt this result is to some extent due to the passive design of the building with external shading, high ceilings and heavyweight construction. However most buildings would provide occupants with opportunity for passive thermal control for part of the annual weather cycle. There is also little doubt that high comfort scores would not be recorded without the availability of supplementary mechanical control elements for use when the need is perceived.

The results reported above accord well with the findings of Bordass, Bromley and Leaman ref.(6) that building occupants are better satisfied with the indoor environment, and use less energy to achieve the desired result, when adequate control options are available to them and they can take action to rapidly correct a condition that is perceived as unsatisfactory.

5.0 Conclusions

The need to use energy in a more sustainable way and to reduce greenhouse gas emissions is being recognised widely around the world as it becomes more certain that global warming is a reality. Concurrently many people are realising that the artificial climates provided by air conditioning in modern commercial buildings are less than completely satisfactory.

This study of a mixed media office environment has shown that the occupants can achieve high levels of thermal comfort by manipulation of passive control elements with mechanical supplementation when necessary. Indoor temperatures were maintained within the range from 19 to 26°C, while outdoor temperatures ranged annually between 12 and 37°C. This was accomplished by opening windows and doors when conditions were judged to be favourable; or by the use of refrigerated cooling and reverse cycle heating when they were considered necessary. The result was achieved with an annual energy consumption estimated to be about a quarter of what would have been used by a well designed conventional air conditioning system.

Although the scale of this experiment is small and the building construction favours passive climate control the results suggest that a wider application of mixed media technology is likely to produce a more satisfactory thermal environment for the expenditure of a fraction of the energy used for full scale air conditioning, at least in the many small scale buildings that make up a large part of the urban commercial building stock and which tend to be the most wasteful of energy and the least comfortable.

It is even possible to suggest that the technique might be applied to tall buildings if those concerned could be persuaded to take a different approach to design. Mention of the idea that occupants of these structures might be allowed to open windows commonly draws negative responses. Yet early tall buildings at the end of the nineteenth century were naturally ventilated. And in the last few years a number of former tall office buildings in Sydney have been converted to residential use and, guess what! they now have operable windows and doors onto balconies because, one suspects, buyers would reject a sealed envelope.

Much is said these days about "the intelligent building". In this example sophisticated intelligence in the refrigeration equipment permits operation over a wide range of loads. Thus individuals can use their intelligence to establish conditions to their liking. If personal liking is for a gentle breeze through an open window then so much the better for personal comfort and the good of the environment.

6.0 Acknowledgements

This work was supported by funding from the Australian Department of Employment, Education, Training and Youth Affairs through the Australian Research Council. Daikin Australia Pty. Ltd. donated variable refrigerant volume equipment for the supplementary cooling and heating system; and Honeywell Ltd. donated the monitoring equipment. Colleagues participated patiently and with goodwill in the experiment; and Phil Granger and Ric Moss carried out the installation among their many other tasks.

7.0 References

(1) de Dear, R. J. (1994): *"Outdoor climatic influences on indoor thermal comfort requirements"* in Oseland, N. A. and M. A Humphreys Eds., Thermal comfort: past, present and future, Building Research Establishment, Watford, p. 207.

(2) Duffy, F. (1994): *"Designing comfortable working environments based on user and client priorities"* in Oseland, N. A. and M. A. Humphreys Eds., Thermal comfort: past, present and future, Building Research Establishment, Watford, p. 207.

(3) Rowe, D. M. (1996): *"Does HVAC work?"* in Cowan, H. J Ed., Architectural Science Review 39.3, Department of Architectural and Design Science, University of Sydney, Sydney, p. 128.

(4) Woodford, J. and C. Skehan (1996): *"Hill defends bid for greenhouse gas exemptions"*. The Sydney Morning Herald, 6 June 1996, p. 8.

(5) Australian Department of Housing and Construction/Australian Institute of Refrigeration Airconditioning and Heating (1985): User Guide for the APEC simulation computer programme ESPII: Mechanical Engineering Design Aids No. DA12. Australian Government Publishing Service.

(6) Bordass, W. K., K. Bromley and A. J. Leaman (1993): "User and occupant controls in buildings" in Sterling, E., C. Bevia and C. Collett, Eds. Proc. Int. Conference on Building Design, Technology and Occupant Well-being in Temperate Climates, Brussels 17 - 19 Feb. 1993. The American Society of Heating Refrigeration and Air Conditioning Engineers Inc., Atlanta, GA. pp. 12 - 15.

A Comparison Between the Laboratory and On-Site Testing on the New Ventilation System Proposed to be Used in the Ship Hull of an VLCC During the Repairing Process

H Sun, Kong HC, Xu WQ, Koh CN
Singapore Productivity & Standards Board
1 Science Park Drive, Singapore 118221

ABSTRACT

A new ventilation system was proposed to remove the smoke, heat and harmful gases generated during the repairing process of the ship hull of a very large crude carrier (VLCC). It basically transfers fresh air from the deck (top) to the bottom of the ship-hull via an air duct and then spread to the entire ship hull by an air distributor before being sucked out together with the smoke and dust via the suction at the deck. Laboratory experiments were performed using a scaled-down model of a ship-hull. The ventilation efficiency of the new system was determined as compared to the existing system. On-site testing using the prototype air distributor was also performed to measure the actual ventilation efficiency and to compare with the laboratory experiments. The main advantage of this new system is that it is easy to assemble and dismantle making it suitable when large scale, temporary ventilation is required.

1. INTRODUCTION

Laboratory experiments were performed using a scaled-down (≈1:12) model of a ship hull. The ventilation efficiency of the new system was determined as compared to the existing system. An on-site testing of the new system in an actual ship hull was performed to look into the effectiveness of the new system.

2. BRIEF DESCRIPTION OF THE TWO VENTILATION SYSTEMS

2.1 The new system basically supplies fresh air by fans installed on the deck of the VLCC and deliver this fresh air to the air distributors at the bottom of the ship hull via flexible plastic ducts. The air distributor will then distribute the fresh air throughout the entire hull, forming an upward-flowing, general displacement type of ventilation. Finally, the air suction fans, installed over various deck openings, will suck the air out of the hull and vent into the atmosphere.

2.2 The old system comprises only of air supply with attached flexible plastic ducting to deliver fresh air to the work zones. There were neither proper air distributing apparatus at the terminus of the duct nor any air suction fans mounted on the deck. The flow patterns in the ship hull are therefore random and the dust and smoke generated are circulated within the hull.

3. EXPERIMENTAL SETUP

3.1 The dimensions of the scaled-down ship hull were 4.17m(l) x 2.10m(w) x 2.50m(h) giving a volume of 22m^3. The experimental set up for this scaled-down model is shown in

Fig.(1) with two air distributors and three suctions at the top (ref.(1)). The old system was simulated using a smaller suction flow rate.

3.2 The dimensions of the ship hull (central tank) used for the on-site testing were 55.7m(l) x 20.8m(w) x 26.9m(h) giving a volume of 31165m^3. The experimental setup for the new system had four sets of air supply fans on the deck connected to the four air distributors at the bottom of the hull via flexible ducts (see Fig.(2)). Six air suction fans were installed at the deck for exhaust and to balance the air flow rate. The setup for the old system was similar to that of the new system setup. The only difference was that the air distributors were removed.

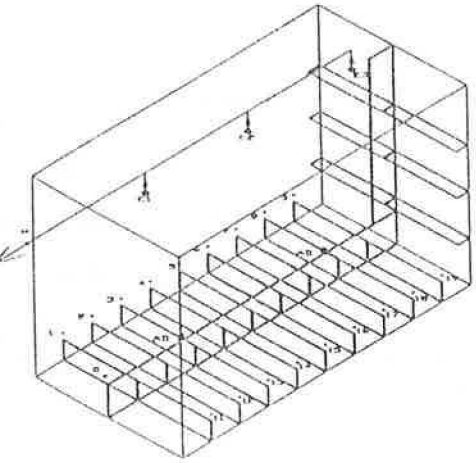

Figure 1: Experimental setup for scaled-down model

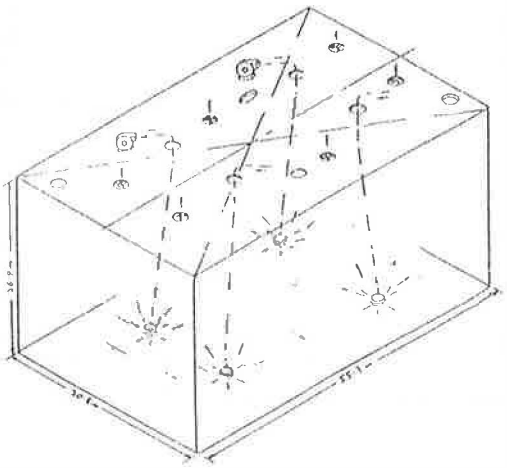

Figure 2: Experimental setup for on-site testing

4. EXPERIMENTAL RESULTS AND DISCUSSIONS

4.1 Air flow rate/Air-exchange rate

The total air supply and suction rates in the scaled-down experiment were 88m^3/h giving an air-exchange rate of 88/22 = 4 times/hr. As for the real-size on-site testing, the total flow rate was approximately 46,000m^3/h giving an air exchange rate of 46000/31165 = 1.5 times/hr.

4.2 Velocity at different distance from air distributor

4.2.1 The jets for both the scaled-down model and actual prototype air distributors were designed to be circular jets governed by Eq.(1). (see ref.(2)).

$$\frac{v_x}{v_o} = \frac{0.48}{\frac{ax}{d} + 0.145} \quad \text{.....Equation (1)}$$

where d is the diameter of the nozzle
x is the distance from the nozzle
v_o is the velocity at the nozzle
v_x is the velocity at a distance x from the nozzle

From Table (1), it was observed that the turbulence coefficient, $a_{prototype}$, for the prototype was about twice that of the model. The higher the coefficient, a, implied that the distance reached by the jet was shorter because it had a wider angle of spread.

Table 1: Velocity at different distances from the air distributor

Prototype air distributor			Scaled-down air distributor (1/10)		
Distance from air-distributor (m)	Velocity (m/s)	Turbulence coefficient, a	Distance from air-distributor (m)	Velocity (m/s)	Turbulence coefficient, a
0	30.0	-	0.0	12.8	-
1	11.0	0.1047	0.5	2.1	0.0445
2	6.0	0.1015	1.0	1.0	0.0480
3	4.5	0.0917	1.5	0.7	0.0460
4	3.5	0.0893	0.0	20.0	-
5	2.6	0.0971	0.5	3.5	0.0416
6	2.5	0.0842	1.0	1.6	0.0468
7	1.8	0.1010	1.5	1.1	0.0458
8	1.5	0.1064	0.0	15.8	-
9	1.5	0.0946	0.5	2.5	0.0462
-	-	-	1.0	1.3	0.0455
-	-	-	1.5	0.9	0.0442
Average, a	-	0.0967	-	-	0.0454

4.3 Comparison of Using Concentration-Decay Method

4.3.1 Scaled-down Laboratory Experiment (refer to ref.(1) for more details)

Tracer-gas technique and concentration-decay method were used to determine the ventilation efficiency. The monitoring point for tracer gas (CO_2) concentration, in the common pipe at M (see Fig.(1)) where complete mixing was assumed, would measure the average room concentration of CO_2. CO_2 was emitted at a constant rate until steady state concentration was reached before it was shut off and the decay monitored. This was done to ensure uniform mixing of the CO_2 in the scaled-down testing chamber while not affecting the air flow pattern.

From Table (2), it was observed that the efficiency of the new system was double that of the old system (ref.(1)). It should be noted that the simulated old system still had flow rate while the actual old system had no suction at all. Therefore, the improvement over the existing old system should be reasonably more than double.

Table 2: Results on measurement of ventilation efficiency in scaled-down chamber

	Room Average Ventilation Efficiency, η_d
Flow rates at suction hoods (E1, E2, E3) m^3/h	2 air distributors at (44, 0, 44) m^3/h
3 suction hoods at (10, 10, 10) m^3/h	0.294
3 suction hoods at (29.3, 29.3, 29.3) m^3/h	0.575

4.3.2 On-site Testing (Real-size)

The dust monitor was set up at a location about 10m above the hull bottom, and near to the wall to simulate a typical working zone. Dust was released using smoke machines placed at the hull bottom and supplied through the flexible ducts till suitable amount of smoke was emitted before switching them off and the dust concentration was monitored. The decay of the dust concentration was the main concern and the units of measurement was number of particles-per-litre (p/l) for particles sizes >0.7μm and >1.0μm, averaged over time intervals of one (1) minute.

The normal atmospheric concentration of dust particle of size >0.7μm was 20,000 p/l and for size >1.0μm was 7,000 p/l. These figures were taken on an average of about 20 minutes when no work was being carried out.

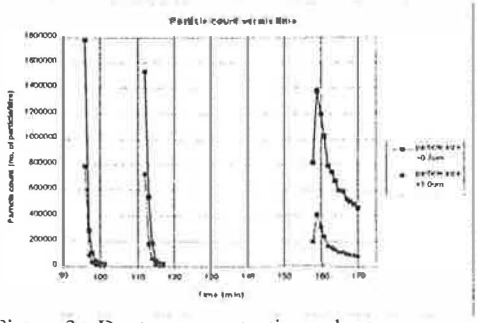

Figure 3: Dust concentration decay versus time for new (96th to 101st mins and 112th to 117th mins) and old (158th to 170th mins) systems

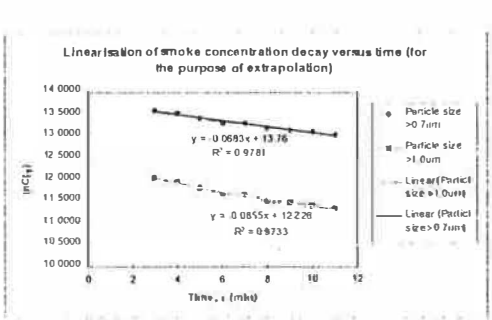

Figure 4: Linearisation of smoke concentration decay (of the old system for 162nd to 170th mins) by natural logarithmic method for extrapolation purposes.

Table 3: Three (3) minutes smoke concentration decay comparison

	Particle size >0.7μm			Particle size >1.0μm		
	Particle count (p/l)	C_2/C_1 (%)	No. of times above atm. conc. (20,000p/l)	Particle count (p/l)	C_2/C_1 (%)	No. of times above atm. conc. (7,000p/l)
$C_{1\,new}$	1,523,816	100.00	76.2	727,749	100.00	104.0
$C_{2\,new}$	40,545	2.66	2.03	13,065	1.80	1.87
$C_{1\,old}$	1,372,811	100.00	68.6	412,567	100.00	58.9
$C_{2\,old}$	790212	57.56	39.5	164,144	39.79	23.4

i. Comparison of smoke concentration decay after a fixed time of three (3) minutes

From Table (3), it was therefore evident that the new system could remove the smoke at an astonishing rapid rate comparatively with the simulated old system. A percentage decay of 2.66% (new system) against 57.56% (old system) for particle size >0.7μm and 1.8% (new system) against 39.79% (old system) for particle size >1.0μm were observed. It would thus be inferred that the new system could **remove about twenty (20) times as much of the dust concentration** as compared to the old system in a time span of 3 minutes.

Also, within this 3-minute span, the new system could bring the dust concentration level to only about two times (2.03 and 1.87 for particle sizes >0.7μm and >1.0μm respectively) that of the normal atmospheric concentration (see Table (3)). As for the old system, the dust concentration was still at a high 39.5 and 23.4 times, for dust particle sizes >0.7μm and >1.0μm respectively, that of the normal atmospheric concentration.

b. Comparison of time required for concentration to reach back to original atmospheric concentration

Table 4: Dust Concentration Decay for New System (112th to 117th minutes)

	Particle size >0.7μm		Particle size >1.0μm	
time (min)	concentration (particle/litre)	% of initial concentration	concentration (particle/litre)	% of initial concentration
112	1523816	100.00	727749	100.00
113	543421	35.66	174271	23.95
114	183868	12.07	64297	8.84
115	40545	2.66	13065	1.80
116	24847	1.63	7167	0.98
117	18984	1.25	5812	0.80

From Table (4), it took only 5 minutes for the new system to bring the concentration to fall below 20,000 p/l and approximately 4.2 minutes for the concentration to fall below 7,000 p/l for particle sizes >0.7μm and >1.0μm respectively.

For the old system, due to the long duration that was required for a full decay, a linear extrapolation of the natural logarithm of the concentration decay was employed using the last few readings obtained (Fig. (3) & (4)). This was extrapolated to predict the time required for the concentration to fall back to the normal atmospheric condition. It was predicted to require more than 56 minutes and more than 39 minutes, for particle sizes >0.7μm and >1.0μm respectively. Thus, by comparing the time duration for the dust concentration level to fall back to the normal atmospheric level, it could be seen that the time required was generally on the average of about **ten (10) times faster** using the new system as compared with the old system.

4.3.3 Some comments

There were some differences in the scaled-down experiment and the on-site testing:

a. The scaled-down experiment measured the global ventilation efficiency while the actual size test measured the local ventilation efficiency. Although local ventilation efficiency would be different for different location, a typical work zone was chosen. Also, global ventilation efficiency (as in the scaled-down experiment) would generally be lower than a well ventilated local area (on-site testing).

b. There were 4 air distributors, 4 supply and 6 suction fans for the on-site testing while only 2 air distributors and 3 suction hoods were used for the scaled-down experiment. Although

here were this proportionate differences in the number of air distributors, supply and suction ans, the flow rates for the two hull sizes were in accordance with the dimensionless analysis, i.e.

$$C_l = 1/12 \qquad \text{(for length)}$$

$$C_L = C_l^{5/2} = 0.002 \quad \text{(for flow rate)}$$

The turbulence coefficient, a, for the scaled-down air distributor was half that of the real-ize prototype air distributor. This would mean that, given everything else constant, the distance hat the jet of the scaled-down air distributor could reach would be doubled. This would also hean that although fewer air distributors were used in the scaled-down experiment, the jet would till be able to reach the wall as in the on-site testing.

CONCLUSIONS

.1 The construction of the scaled-down and real-size air distributor using dimensional nalysis was generally useful. The only difficulty was the construction of the nozzle which vould affect the turbulence coefficient, a, which in turn affect the distance reach by the jet.

.2 Although two different methods, global and local ventilation efficiency, were used for the caled-down and on-site testing respectively, both the results still demonstrated the effectiveness f the new system. This improvement was based on the respective simulated old system.

RECOMMENDATIONS

.1 Further on-site tests and monitoring should be carried out with the new system.

.2 Scaled-down experiments should be carried out to measure the local ventilation fficiency at the similar location as in the on-site testing for a better result comparison.

ACKNOWLEDGEMENT

We would like to take this opportunity to express our greatest appreciation and thanks to Jational Science & Technology Board of Singapore (NSTB) to have supported this project inancially, Jurong Shipyards Limited (JSL) management and staff and all those who have elped in one way or another to the success of this project.

REFERENCES

1) Xu WQ, H Sun, Sun QQ, etc. "Investigation of Air Flow Pattern of the Ventilation System in the Repair Process of VLCC", The 7th Int'l Conf. on Indoor Air Quality and Climate, Indoor Air '96, Nagoya, Japan. 21-26 July 1996.

2) V.V. Baturin, "Fundamentals of Industrial Ventilation", Pergamon Press Ltd, Headington Hill Hall, Oxford U.K. (1972).

Architecture and Aerodynamics, Passive downdraught evaporative cooling (PDEC) in non-domestic buildings Wind Tunnel Tests for the Experimental Building design.

Mario Cucinella, Elizabeth Francis, Edoardo Badano

Prof. Gianni Cesini*

MCA Mario Cucinella Architects, (JOULE III Partner)
26 bis bd Massena 75013 Paris France Tel: +33 1 45 83 92 78 Fax: +33 1 45 83 93 07
e-mail: mca@easynet.fr Web: http://www.easynet.fr/bal201/mca/

* Dipartimento di Energetica, University of Ancona, Via Brecce Bianche, 1-60100 Italy

ABSTRACT MCA is a partner in a research group which is being funded by the European Commissions JOULE program to explore the application of passive downdraught evaporative cooling (PDEC) in non-domestic buildings (1). As part of MCA's task to design a full scale experimental building, special components were designed to catch the wind and distribute through the building spaces. To determine the most efficient form for these components, a series of wind tunnel tests was undertaken at the University of Ancona, Italy. The following abstract describes the objectives methods and results of these tests.

1. Introduction

The efficient functioning of passive cooling systems in buildings depends largely on our ability to control internal air flows. The direction, speed and turbulence of the wind changes constantly thus creating unwanted fluctuations in the air-flow. It is possible to overcome this difficulty by careful design of the building components.

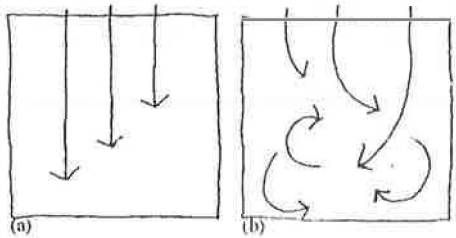

Fig 1 (a) uniform air flow (b) turbulent air flow

A full scale experimental building, designed by MCA, has been constructed in Catania in Sicily. The building consists of a tower and two test cells in which we can observe the functioning of the PDEC system and the induced air movement. A uniform stream of air of low turbulence is best for the evaporative cooling system. For this reason components were designed, a wind catcher and a wind straightener, to optimise the control of the air flow in the tower.

Quanlitative tests on scale models of the Experimental Building were carried out to assess the performance of the different components both individually and in combination. These visualisation studies seeked to inform the design of a system that

can be adapted to different situations, climates and building typologies. An important consideration in doing these experiments was to explore practical instruments and methods for designers to inform their designs at an early stage of the project within acceptable costs and with valid results.

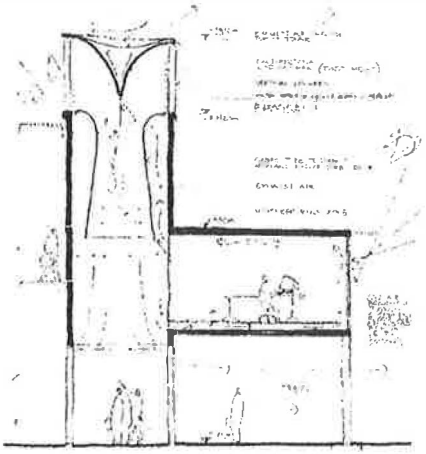

Fig.2 The Experimental Building Sketch design

2. The Wind Tunnel

The wind tunnel that was used is located in the laboratory of the Faculty of Mechanical Engineering in the University of Ancona in Italy. It was created to test aeroplane wing sections and spoilers, but its dimensions and capacity allow us to use it with architectural scale models. In the wind tunnel we can measure local wind speed and direction (mean velocity), turbulence intensity and do visualisation studies.

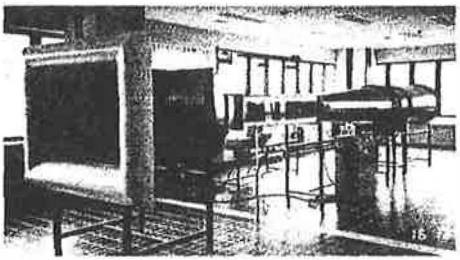

Fig.3 The wind tunnel in Ancona University

The different measuring tools are:
mean velocity: an axial flow vane anemometer, a Pitot tube
turbulence intensity-: a rapid sampling anemometer
visualisations: smoke: helium bubbles, paraffin and talcum powder

The visualisation studies undertaken at Ancona involved letting wisps of vapourised oil into the tunnel which shows clearly the airflow patterns. This gives information about the capacity of the prototype to reduce turbulences and to optimise the air flow

3. Models for testing

To retain similarity of flow patterns at a reduced scale it is neccessary to increase the velocity. The key parameter is the Reynolds number:

$$\frac{L \times v}{V}$$

length x velocity / Kinetic viscosity

Ideally this should be the same at model scale as at full scale i.e. if the scale is reduced the wind speed is increased. The models used in the wind tunnel must therefore be solid enough to resist very high wind speeds. We prepared 1:20 scale plexiglass prototype models of the experimental building. The models consisted of one tower onto which different components could be fixed. This gave us the flexibility to easily test different configurations. As the plexiglass models we built are at scale 1: 20, using the Reynold's number, we could simulate an air speed of 4/5 m/sec running the machine at a real speed up to 200 Km/h.

4. Building Components

The components to be tested were wind catchers, air straighteners and louvres.

4.1 Wind Catchers

The function of the wind catcher is, as its name suggests, to bring as much air as neccessary into the building. An ideal wind catcher should function well even when there is very little wind. The choice of which type of wind catcher to use in the building depends on:

- Efficiency
- Suitability for the site (i.e if there is a strong prevailing wind)
- Cost and materials

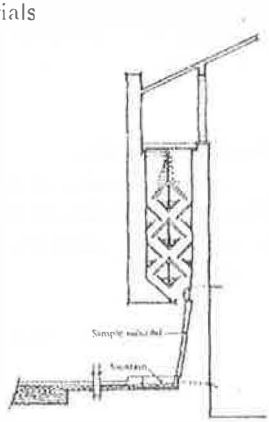

Fig.4 Malqaf (dowdraught cooling tower) designed by Hassan Fathy (Source H. Fathy)

We examined three different shapes for the wind catcher to test in the wind tunnel:

- Mono directional

These can catch wind only from one direction but give quite a uniform flow.

- Two directional

The wind is caught from two directions but causes an uneven flow.

- Multi directional

The wind is caught from all directions but the flow is much less uniform.

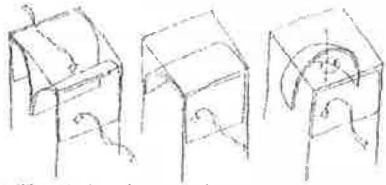

Fig.5 The wind catchers tested

The disadvantage of the mono directional catchers is that it catches the wind from one direction only. It would be costly and involve additional machines to develop a rotating wind catcher. The advantage of the multi-directional catcher is that it has a large opening area and is tolerant of all wind directions but it causes an uneven airflow within the tower. It is therefore our objective to make the multi directional catchers work. To do this we need a straightening device

4.2 Straighteners

The simplest devices for straightening the air flow are a grid or honeycomb. These are quite effective for reducing turbulence but are not effective for making the flow even. They would work well with the mono directional catchers but would be less successful with the multi directional catchers. Another way of straightening the air is to have a constriction followed by gentle dilation. This is a classical technique for producing a uniform low turbulence flow which gives the shape to the wind tunnel. We felt that this was the right technique to smooth the flow from the multi directional wind catchers.

The parameters for this device are:

1. the constriction ratio, which is the ratio of the throat area to the area of the tower plan. (a/b-see fig.6)
2. The dilation angle. This angle should be as shallow as possible (around 10° would be best).
3. A smoothly shaped inlet.

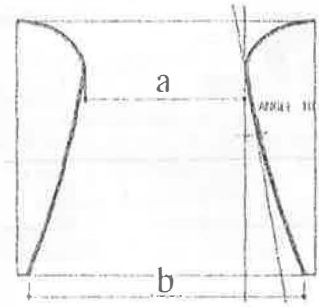

Fig.6 The air straightener

5. Experimental Protocol

Before commencing the wind tunnel tests we established an experimental protocol. It was decided to evaluate the efficiency of each component individually and then in combinations of catchers and straighteners.

6. Wind Tunnel Test Visualisations June 1996

Different wind catchers were tested first:

Wind catcher N° 1: asymmetrical mono directional.
Wind catcher N° 2: symmetrical which catches the wind from two directions.
Wind catcher N° 3: a quarter sphere which simulates a rotating device.

The second series of tests involved testing the different wind catchers in conjunction with the different straighteners. Two types of straightener were tested:

Straightener N° 1: Narrow constriction
Straightener N° 2: Wide constriction

7. Results of the visualisation tests

The results of the tests involving the different wind catchers and wind straighteners are outlined here.

7.1 Wind catcher n° 1- asymmetrical mono directional

This is an asymmetrical catcher that has been designed for prevailing wind conditions. The test indicates a small area of turbulence below the windward opening. This turbulence gradually disappears and the air flow seems to be slightly asymetrical at the bottom of the tower. (See fig.8)

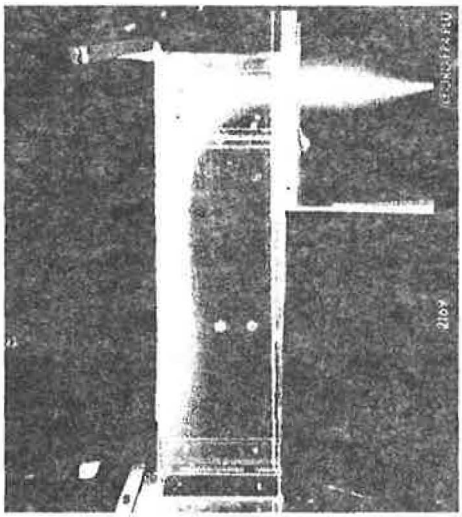

Fig.8 Visualisation of wind catcher n°1

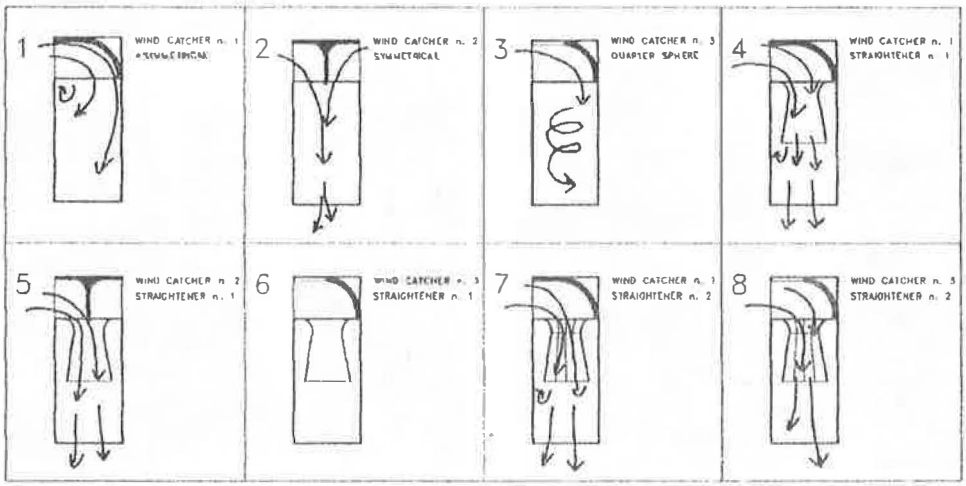

Fig.7 Experimental Protocol

7.2 Wind catcher n° 2 - symmetrical bi-directional

This catcher is bi-symmetrical and allows the wind in from two opposite directions. An even air flow is concentrated towards the middle of the tower's section.

7.3 Wind catcher n° 3 - quarter sphere

This catcher aims to simulate a revolving system that can follow the wind coming from any direction. The model simplifies this system by using a fixed quarter of a sphere on one side of the tower. The visualisation shows how this particular geometry tends to create a rotation of the flow around the vertical axis, with a spiral-like shape. A major area of turbulence appears under the windward opening and a minor one on the opposite face. The outlet flow is less uniform than in case 1. (See fig.9)

7.4 Wind catcher n° 1 with Straightener n° 1

The straightener is a Venturi tube whith a constriction ratio of 50%.

Its effect is quite evident, especially if compared with the efficiency of the head alone. The flow is very diffused and uniform inside the tower.

A small zone of turbulence appears immediately after the straightener, on the windward face. The outlet flow is uniform.

7.5 Wind catcher n° 2 with Straightener n° 1

This configuration seemed to be the most successful. The flow is quite central and uniform.

7.6 Wind catcher n° 3 + Straightener n° 1

The effect of the straightener seems to be very similar to the case n° 4.

Any difference in the outlet flow has not been visualised.

7.7 Wind catcher n° 1 + Straightener n° 2

The straightener is a Venturi tube with a constriction ratio of 80%.

The straightening effect is similar to that of case 4, giving quite a uniform flow.

7.8 Wind catcher n° 3 + Straightener n° 2

Here again the air flow is more uniform using the straightener which has an 80% constriction

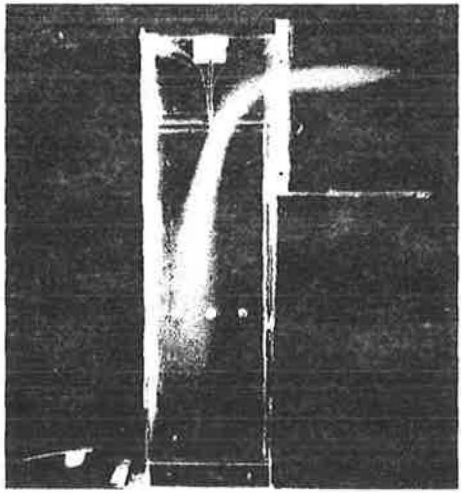

Fig.9 Visualisation of wind catcher n°2 with straightener n° 1

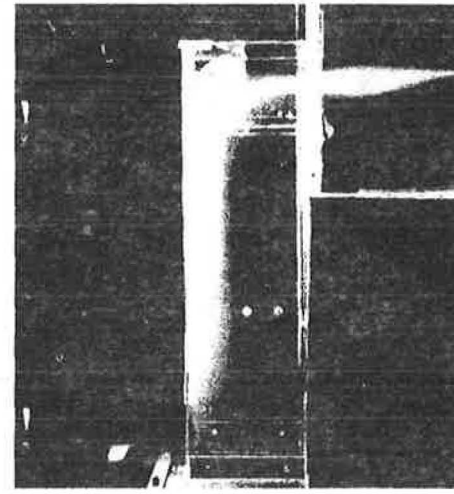

Fig. 10 Visualisation of wind catcher n°3

8. Conclusions

The visualisation tests showed quite clearly the effectiveness of each component. The heads alone, although efficient at catching the wind, give quite a turbulent air flow. The air straighteners have proved to work well at reducing this turbulence.

For the Experimental Building in Catania, given that the prevailing wind is east-west, it appears that the most efficient combination is the symmetrical head as with a straightener with a narrow constriction. The components have been constructed and installed in the Experimental building and their performance will be tested and moonitored this summer. The design of this type will be developed in more detail as part of a full scale building design project.

The next step is to revise the experimental protocol and measure pressure differences in a second series of tests.

Acknowledgements

The partners involved in this research project are: De Montfort university, UK, Short Ford & Associates, UK, Microlide, France, Conphoebus, Italy and University of Malaga, Spain.

This project is funded in part by the EUROPEAN COMMISSION in the framework of the Non Nuclear Energy Programme JOULE III.

The wind tunnel tests were carried out with Professor Gianni Cesini of the Dipartimento di Energetica, University of Ancona, Via Brecce Bianche, 1-60100 Italy

The aerodynamics consultant was Peter Heppel Engineer.

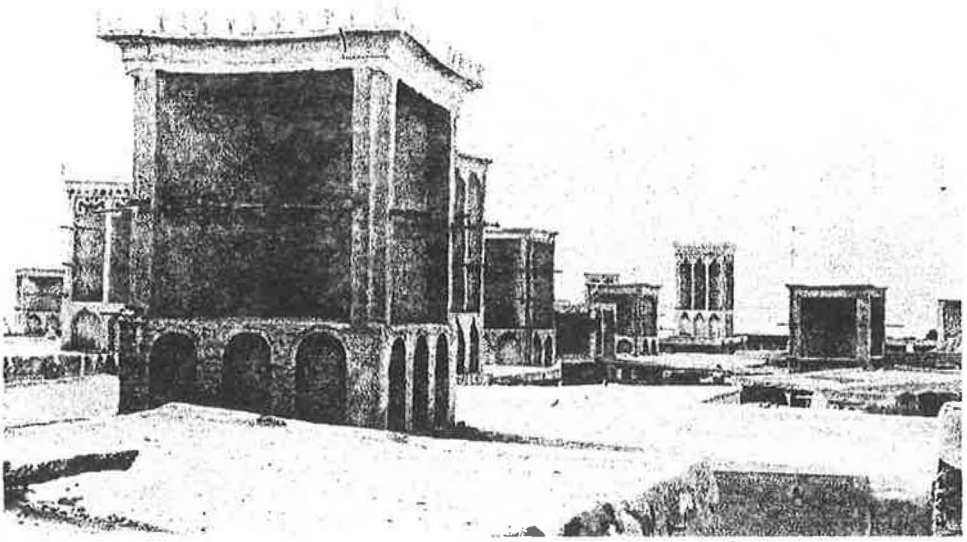

Fig.11 Traditional persian wind turret in Làft (Source: Khansari, Yavari- 1984, *Espace Persan* - P. Mardaga Editeur, Liège)

HEAT TRANSFER THROUGH A HOLLOW TILE WITH TWO CELLS

A. Abdelbaki, Z. Zrikem

LMFE, Department of Physics, Faculty of Sciences Semlalia,
BP. S - 15, Marrakesh, MOROCCO.

ABSTRACT The aim of this study is to calculate numerically the heat transfer through a hollow tile with two air cells in the direction of heat flow. The top and the bottom sides of the block are adiabatic while the vertical ones are isothermal. Equations of conservation governing the convective flow in internal cavities and the conductive heat transfer in the surrounding walls are solved using the SIMPLE algorithm. Radiation heat exchanges between surfaces of the internal cavities are also accounted for. Parameters that characterize the fluid flow in the cavities and the heat transfer through the block are evaluated for Rayleigh numbers between 10^3 and 5.10^5.

1. Introduction

Hollow concrete blocks or clay tiles are often used in the construction of the building walls and roofs. However, there are few studies that have processed numerically the problem of heat transfer through these structures. Most methods used are based on simplified models that suppose that the heat transfer is linear and can be predicted by using overall conductances whose values are determined experimentally [1,2]. This approximation is not always valid especially in the case of high differences between the outside and the inside temperatures. To contribute to the resolution of this problem, a numerical study has been presented by coupling between the conductive and the convective thermal transfers in a hollow tile with one cell deep [3]. The calculation program has been tested by comparing its results with those obtained by De Vahl Davis in the case of a differentially heated square cavity using the Bench Mark solution [4]. The integration of the radiative heat exchanges between the inner cavity surfaces in the simulation program of heat transfer through the block has been the subject of a recent study [5]. However, hollow tiles used in practice are based on two or several air cells in the direction of heat flow. In the present work we extend the preceding study [5] to the case of a hollow tile with two cells deep. Stream lines in the internal cavities, isotherms in the block, average Nusselt number and heat flux are predicted for a range of Rayleigh numbers. Effect of the tepmeratures of the block vertical sides on the heat transfer is also discussed.

2. Mathematical model

A schematic diagram of the studied configuration is shown in Fig. 1. It represents a hollow tile of width L and height H with two rectangular cells surrounded by conducting

walls whose thiknesses are indicated in Fig. 1. The horizontal sides of the block are adiabatic while the vertical ones are isothermal but at different temperatures T_h and T_c. In formulating governing equations it is assumed that the fluid and the walls properties are independent of temperature except for the density in the buoyancy term. The fluid is Newtonian, incompressible and the Boussinesq approximation is valid. Viscous heat dissipation in the fluid is assumed to be negligible. The fluid motion and the heat transfer are considered to be two-dimensional and laminar. The fluid inside the cavities is assumed to be nonparticipating and the cells surfaces are considered to be gray, diffuse emitters and diffuse reflectors. Dimensionless equations governing the conservation of mass, momentum and energy in the internal cavities are given by:

$$\frac{\partial U}{\partial X} + \frac{\partial V}{\partial Y} = 0 \tag{1}$$

$$\frac{\partial U}{\partial \tau} + U\frac{\partial U}{\partial X} + V\frac{\partial U}{\partial Y} = -\frac{\partial P}{\partial X} + Pr\frac{\partial^2 U}{\partial X^2} + Pr\frac{\partial^2 U}{\partial Y^2} \tag{2}$$

$$\frac{\partial V}{\partial \tau} + U\frac{\partial V}{\partial X} + V\frac{\partial V}{\partial Y} = -\frac{\partial P}{\partial Y} + Pr\frac{\partial^2 V}{\partial X^2} + Pr\frac{\partial^2 V}{\partial Y^2} + Pr\,Ra\theta_f \tag{3}$$

$$\frac{\partial \theta_f}{\partial \tau} + U\frac{\partial \theta_f}{\partial X} + V\frac{\partial \theta_f}{\partial Y} = \frac{\partial^2 \theta_f}{\partial X^2} + \frac{\partial^2 \theta_f}{\partial Y^2} \tag{4}$$

where U, V, P and θ_f are the dimensionless variables associated respectively with the velocity components, the pressure, and the fluid temperature, Pr is the Prandlt number, Ra is the Rayleigh number $Prg\beta(T_h-T_c)L^3/\nu^2$, and ν is the fluid kinematic viscosity. The dimensionless eqution of heat conduction in the walls is:

$$\frac{\alpha_f}{\alpha_s}\frac{\partial \theta_s}{\partial \tau} = \frac{\partial^2 \theta_s}{\partial X^2} + \frac{\partial^2 \theta_s}{\partial Y^2} \tag{5}$$

where α_f and α_s are respectively the fluid and the solid thermal diffusivities. The boundary conditions of the problem are:

* $U = V = 0$ on the walls of cavities

* $\theta_s(0,Y) = 1$ and $\theta_s(1,Y) = 0$ $\quad (0 \le Y \le H/L)$.

* $\partial\theta_s/\partial Y = 0$ for $Y = 0$ and $Y = H/L$ $\quad (0 \le X \le L)$.

The continuity of temperatures and heat fluxes at the fluid-wall interface gives:

$$-\frac{\partial \theta_s}{\partial \eta} = -N_k\frac{\partial \theta_f}{\partial \eta} + N_r Q_r \tag{6}$$

where η represents the dimensionless co-ordinate normal to the wall, N_k is the thermal conductivity ratio k_f/k_w, N_r is the dimensionless radiation to conduction parameter

$\sigma T_h^4 L/k_w(T_h-T_c)$, σ is the Stefan-Boltzman constant and Q_r is the dimensionless radiative heat flux which can be expressed at any surface i as:

$$Qr_i(r_i) = \varepsilon_i(1-\frac{1}{\gamma})^4(\theta_i(r_i)+\frac{1}{\gamma-1})^4 - \varepsilon_i\sum_{j=1}^{4}\int J_j(r_j)dF_{d\Lambda i-d\Lambda j} \qquad (7)$$

where ε_i is the emissivity of the surface i, γ is the temperature ratio T_h/T_c, $J_j(r_j)$ is the dimensionless radiosity at the position r_j on surface j and $dF_{d\Lambda i-d\Lambda j}$ is the configuration factor between the finite surfaces $d\Lambda_i$ and $d\Lambda_j$ located at r_i and r_j respectively. By dividing the walls of the internal cavities into finite isothermal surfaces equation (7) leads to a set of algebric equations where the unknowns are the dimensionless radiosities $J_j(r_j)$.

The average Nusselt number and heat flux at the hot surface of the block are given respectively by:

$$\overline{Nu} = \frac{L}{H}\int_0^{\frac{H}{L}}\frac{\partial\theta}{\partial Y}(0,Y)dY \qquad (8)$$

$$\overline{Q} = \frac{k_s(T_h-T_c)}{H}\int_0^{\frac{H}{L}}\frac{\partial\theta}{\partial Y}(0,Y)dY \qquad (9)$$

Equations (1) to (9) are solved by the SIMPLE algorithm using 58×32 nonuniform grid with 23×23 grid in each cavity. It has been found that the use of 76×42 grid leads to a relative difference in the Nusselt number about 0.025 percent for $Ra = 10^5$ and 0.4 percent for $Ra = 5.10^6$. The time step used in the simulation is 10^{-4}. Convergence is obtained when the relative difference on all variables calculated in two successive iterations becomes lower than 10^{-3}.

3. Results

Results presented in this study are carried out for a hollow clay tile characterized by: L= 10cm, H= 4,5cm, $ex_1 = ex_2 = ex_3 = 1cm$, $ey_1 = ey_2 = 0.5cm$, $\varepsilon_i = 0.8$, $k_w = 1W/mK$ and Pr= 0.71. The simulation is conducted by varying Ra, γ, N_r and T_c but their variation should be restricted within the ranges of practical values corresponding to the processed situation.

Fig. 2 shows the contours of the streamlines and isotherms obtained for $Ra=5.10^6$. It can be noted that the flow structures in the cavities are similar to those in a hollow tile with one cell deep [3]. Near the adiabatic horizontal sides the temperature decreases almost linearly from the hot vertical side to the cold one. The distortion of isotherms in the central region ($ey_1 < y < H-ey_2$) shows the two-dimensional nature of heat transfer which is due to the convection in the cavities.

To account for the radiative heat exchanges between surfaces of the internal cavities for a given Rayleigh number, it is necessary to specify one of the two temperatures of the block vertical sides. So, for different values of T_c, figures 3 and 4 show the variations of the average Nusselt number $\overline{Nu}$ and heat flux $\overline{Q}$ as functions of the Rayleigh number Ra and the temperature difference $\Delta T = (T_h-T_c)$ respectively. It can be seen that the heat

transfer through the block increases with the Ra number (i.e. with ΔT) as expected. The increase of $\overline{Nu}$ and $\overline{Q}$ with T_c is due to the radiative heat exchanges between the surfaces of the internal cavities. However, one can note that the variation of T_c has no significant effect on the heat transfer for the range of practical temperatures ($0 \leq \Delta T \leq 40°C$ and $283 \leq T_c \leq 323K$). The use of a reference temperature T_c of 300K in the simulation constitute a good approximation. In fact, the maximum relative difference in the average heat flux predicted using other reference temperature between 283K and 323K is less than 5 percent. It can also be noted from Fig. 4 that the variation of the heat flux as a function of the temperature difference is almost linear.

Fig. 5 gives the variation of the average heat flux as a function of the radiation to conduction number N_r. One can observe that for lower values of N_r, the heat transfer is important and decreases rapidly as N_r increases. For $N_r > 4$, the heat flux is weak and decreases slowly to become negligible for $N_r > 20$. The variation of heat flux against the temperature ratio γ given in Fig. 6 is almost linear. This is due to the linear relationship between γ and ΔT ($\gamma = 1 + \Delta T/T_c$).

4. Conclusion

Heat transfer across a hollow clay tile with two cells has been predicted for various parameters of physical interest. Simulation results have shown that the heat transfer is not only a function of the temperature difference between the vertical surfaces of the block but it depends also upon the temperature of these surfaces. However, the effects of these temperatures is not significant enough in the range of practical values. Therefore, the use of a cold surface temperature of 300K in the simulation of heat transfer through the hollow block constitutes a good approximation. The heat transfer through the block increases almost linearly as the temperature difference between the external surfaces increases. Then, based on the established results, it is possible to generate, by identification, the transfer function coefficients that permit to predict easily the transient heat transfer through the considered hollow block.

References

[1]. Abdelbaki, A. : Contribution à la modélisation des transferts thermiques à travers le plancher d'un habitat sur terre-plein. D.E.S. Thesis, Faculty of sciences Semlalia, Marrakesh, Morocco, (1993).

[2]. EL Biyâali, A., Roux, J.J., Yezou, R. and Ayaichia, H.: Application de la réduction de modèles aux singularités thermiques de bâtiments, Rev. Gen. Ther., n° 394, pp. 571-579, (1994).

[3]. Abdelbaki, A., and Zrikem, Z. : Couplage conduction-convection dans un bloc creux différentiellement chauffé, CMM, Ghardaia, Algeria, (1996).

[4]. De Vahl Davis, G. : Natural convection of air in a square cavity: a Bench Mark numerical solution, Int. J. for Numerical Methods in Fluids, Vol. 3, pp. 249-264, (1983).

[5]. Abdelbaki, A., and Zrikem, Z. : Effet du rayonnement sur le transfert de chaleur dans un bloc creux, COMPLES, pp. 116-121, Agadir, Morocco, (1996).

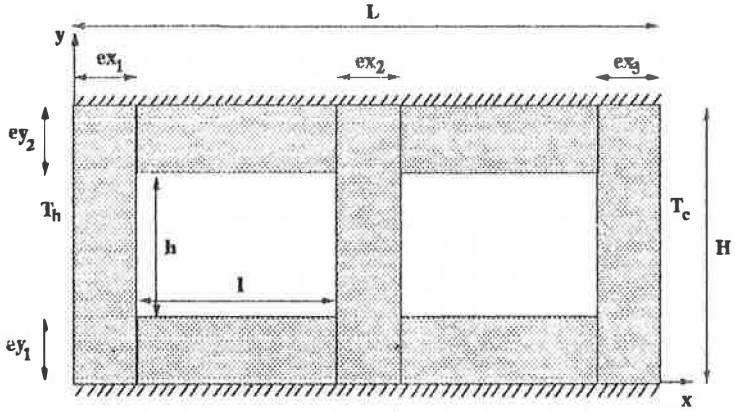

Fig. 1 Schematic diagram of the studied configuration.

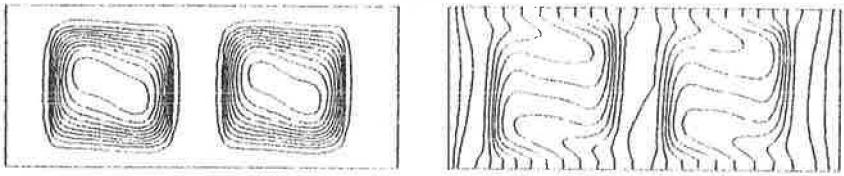

(a) (b)

Fig. 2 (a) stream lines; (b) isotherms.

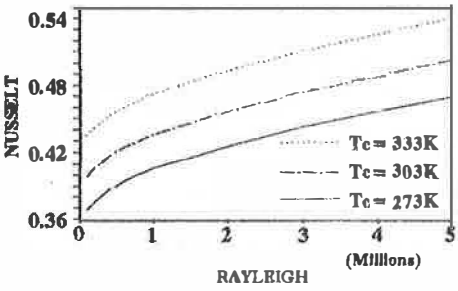

Fig. 3 Average Nusselt number as a function of the Raylelgh number.

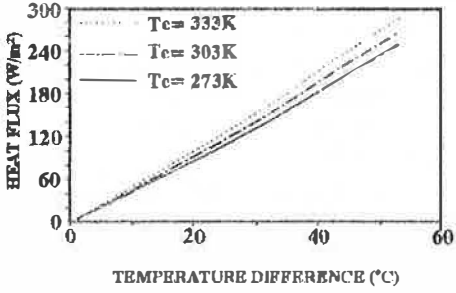

Fig. 4 Heat flux as a function of the temperature difference.

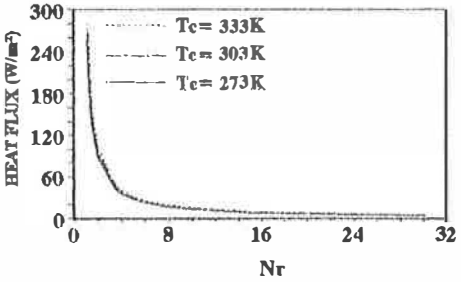

Fig. 5 Heat flux as a function of the conduction to radiation number.

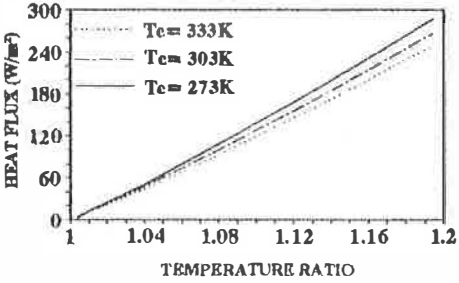

Fig. 6 Heat flux as a function of the temperature ratio.

THE TWO-DIMENSIONAL MULTI-LAYER TRANSFER FUNCTION FOR AN EARTH-SHELTERED BUILDING

S. Amjad, A. Abdelbaki, Z. Zrikem

L.M.F.E., Faculty of Science Semlalia, Cadi Ayyad University, B.P. S-15, Marrakesh, Morocco

ABSTRACT This paper describes the use of the bidimensional multi-layer transfer functions method for predicting the time-varying heat transfer from an earth-sheltered building to the ground. This method is based on the decomposition of the studied system into different rectangular regions in the (x, y) directions. Each region is characterized by its inputs and outputs and by its appropriate transfer function coefficients. This technique permits a significant reduction in the computation time required to generate the transfer function coefficients of the building coupled to the soil. The procedure is tested by comparing its results with those of the ADI method for various situations.

1. Introduction

Transfer function methods are generally used to predict transient heat conduction through opaque walls of the building envelope. However, the application of this procedure in solving the ground coupling problems is rather limited. Based upon the Seem's multi-dimensional algorithm [1], transfer function coefficients have been derived recently for two underground structures: a shallow-basement [2] and an earth-sheltered building [3]. It has been found that the transfer functions method results agree well with those of the ITPE and the ADI methods. To reduce significantly the computational effort to generate transfer function coefficients for buildings coupled to the soil, an efficient technique called the multi-layer transfer functions method has been developed [4]. This procedure is based on the decomposition of the system formed by the building and the soil into superposed layers following the y direction.

In this study, the multi-layer transfer functions method is applied to predict the two-dimensional heat transfer between an earth-sheltered building and the soil by decomposing the system into different rectangular regions in the (x, y) directions. This technique permits an important reduction of the calculation time required in the generation of the transfer function coefficients. Comparison of the results obtained using this procedure with those of the ADI method is made in two typical climates for a range of parameters of physical interest.

2. Mathematical model

The studied two-dimensional configuration is shown in figure 1. It represents an earth-heltered building of width $2a$ having a roof of thickness e_r situated at a depth b below he soil surface. The vertical wall height and thickness are respectively H_w and e_w. The lab-below-grade floor thickness and depth are respectively e_f and c. A water table at the emperature T_W is assumed to be at a depth d below-grade. The soil surface and the interior ir temperatures are respectively $T_1(t)$ and $T_{int}(t)$. The calculation domain is limited by $= -L$ and $+L$. Taking into account the symmetry of the problem, only one half of the alculation domain is considered.

The equation governing the transient heat conduction in the soil, the building walls, the oof and the floor is expressed as:

$$\frac{\partial^2 T_k}{\partial x^2}(x,y,t) + \frac{\partial^2 T_k}{\partial y^2}(x,y,t) = \frac{1}{\alpha_k}\frac{\partial T_k}{\partial t}(x,y,t) \tag{1}$$

where α_k is the thermal diffusivity of the considered medium. The boundary conditions of he problem are given by:

$$\lambda_r \left.\frac{\partial T_r}{\partial y}(x,y,t)\right|_{y=b+e_r} = h_r(T_r(x,b+e_r,t) - T_{int})$$

$$\lambda_w \left.\frac{\partial T_w}{\partial x}(x,y,t)\right|_{x=-a} = h_w(T_w(-a,y,t) - T_{int})$$

$$\lambda_f \left.\frac{\partial T_f}{\partial y}(x,y,t)\right|_{y=c} = h_f(T_f(x,c,t) - T_{int})$$

$$T_S(x,0,t) = T_1 \text{ and } T_S(x,d,t) = T_W\,, \qquad -L \le x \le 0$$

$$\frac{\partial T_S}{\partial x}(x,y,t)_{x=-L} = 0\,,\ 0 \le y \le d \text{ and } \frac{\partial T_k}{\partial x}(x,y,t)_{x=0} = 0$$

$$T_r(x,b,t) = T_S(x,b,t) \text{ and } T_f(x,c+e_f,t) = T_S(x,c+e_f,t)$$

$$T_w(-(a+e_w),y,t) = T_S(-(a+e_w),y,t)$$

$$\lambda_r \frac{\partial T_r}{\partial y}(x,y,t)_{y=b} = \lambda_S \frac{\partial T_S}{\partial x}(x,y,t)_{y=b}$$

$$\lambda_w \frac{\partial T_w}{\partial x}(x,y,t)_{x=-(a+e_w)} = \lambda_S \frac{\partial T_S}{\partial x}(x,y,t)_{x=-(a+e_w)}$$

$$\lambda_f \frac{\partial T_f}{\partial y}(x,y,t)_{y=c+e_f} = \lambda_S \frac{\partial T_S}{\partial y}(x,y,t)_{y=c+e_f}$$

where h_w, h_f and h_r are the heat transfer coefficients at the vertical wall, the floor and the roof surfaces respectively. λ_w, λ_f and λ_r are respectively the thermal conductivity of the wall, the floor and the roof.

As shown in figure 1, the system formed by the earth-sheltered building and the soil is decomposed into rectangular blocks obtained by decomposing the system into Ny layers in the y direction and Nx layers in the x direction. Each block n is characterized by its inputs $[U]^n$ and outputs $[\varphi]^n$ and by its appropriate transfer function coefficients witch are generated separately using the Seem's multidimensional algorithm [1]. We note that for each block, the inputs and outputs are respectively the temperatures and the heat fluxes at nodes located on the external sides of the block.

It is known that the transfer function relates current outputs to current inputs and also to previous outputs and inputs. Then, we obtain:

$$\varphi_k^n(t) = \sum_{j=0}^{Nn} \sum_{i=1}^{m_n} S_{k,i}^{j,n} U_i^n(t \quad j\Delta) \quad \sum_{j=1}^{Nn} c_j^n \varphi_k^n(t \quad j\Delta) \tag{2}$$

where Δ is the time step used to sample inputs which are assumed to be continuous and linear between time t and $t+\Delta$. $S_{k,i}^{j,n}$ is the transfer function coefficient corresponding to the n^{th} block, the k^{th} output, the i^{th} input and the time $t - j\Delta$. c_j^n is the transfer function coefficient corresponding to the block n and the time $t - j\Delta$.

The continuity of the temperature and the heat flux at the node k located at the interface between two adjacent blocks p and q gives:

$$U_k^p = U_k^q \tag{3}$$

$$\varphi_k^p = \varphi_k^q \tag{4}$$

If the node k is located at the interior surface of the building then:

$$\varphi_k = h(U_k - T_{int}) \tag{5}$$

where h is equal to either h_r, h_w or h_f.

Substituting equation (2) into equations (3) to (5) leads to a system of equations where the unknowns are the temperatures at the surfaces separating two adjacent blocks and those

of the nodes located at the roof, the wall and the floor surfaces. This system is solved by the Gauss-Seidel iterative method.

3. Results

The results presented here are obtained in two typical climates : a hot climate with $T_1(t) = 20 + 7\cos wt$ $(°C)$ where w is the angular frequency of the annual cycle, $T_W = 20$ $°C$ and $d = 13$ m and a cold climate with $T_1(t) = 8 + 7\cos wt$ $(°C)$, $T_W = 10$ $°C$ and $d = 6$ m. $T_{int} = 20$ $°C$, $a = 3$ m, $b = 0.6$ m, $c = 4$ m, $H_w = 3$ m, $e_r = e_w = e_f = 0.4$ m, $L = 9$ m, $\lambda_k = 1$ W/mK and $\alpha_k = 6.45\ 10^{-7}$ m^2/s. h is taken as 8.3 W/m^2K if the building is uninsulated and 0.41 W/m^2K if it is strongly insulated. The time step used is $\Delta = 864000$ s for the transfer functions method and $\Delta = 86400$ s for the ADI one. The grid spacing used in the simulation ranges from 0.025 m to 1 m for the two methods.

For an uninsulated building envelope, figure 2 shows the temperature distributions as a function of the x distance at the depth $y = 1$ m and $y = 4$ m while figure 3 gives the temperature distributions as a function of the y distance at $x = -3.4$ m. These temperature profiles are obtained for two representative days: January 15 when the soil surface temperature $T_1(t)$ is minimum and July 15 when $T_1(t)$ is maximum. It can be seen that there is a very good agreement between the ADI and the multi-layer transfer function results (TF). In fact, the maximum relative difference on the temperatures predicted by the two methods is less than 1 percent. The temperature profiles show that, in both climates, the heat transfer is important near the building and has a two-dimensional nature but it decreases as the x and/or the y distances increase.

Figure 4 gives the annual variations of the monthly heat flux through the envelope of an uninsulated building ($h = 8.3$ W/m^2K) and a strongly insulated one ($h = 0.41$ W/m^2K). It can be observed that there is a very good agreement between the predictions of the two methods and that the heat exchanged between the building and the soil is reduced significantly when the building envelope is strongly insulated. Other results (not presented here) show that only the insulation of the earth-sheltered building roof plays an important role in the hot climate.

4. Conclusion

A numerical prediction of heat transfer from an earth-sheltered building to the ground has been carried out by applying the multi-layer transfer functions technique following the x and y directions. The comparison of the temperature and the heat flux distributions obtained by the transfer functions and the ADI methods shows a very good agreement between the predictions of the two methods in the different processed cases. This procedure has reduced considerably the calculation time required to generate the transfer function coefficients in comparison with the multi-layer transfer functions following only the y direction.

References

[1] Seem, J.E.: Modeling in heat transfer in buildings, Ph. D. thesis, University of Wisconsin, Madison, USA, (1987).

[2] Abdelbaki, A., Amjad, S., and Zrikem, Z.: Prediction of heat transfer from shallow basements to the soil by the two-dimensional transfer functions method, 3th Renewable Energy Congress, Reading, UK, (1994).

[3] Amjad, S., Abdelbaki, A., and Zrikem, Z.: Adaptation de la méthode des fonctions de transfert à une cavité enterrée, 3ème Congré de Mécanique, pp. 497-502, Tétouan, Maroc, (1997).

[4] Amjad, S., Abdelbaki, A., and Zrikem, Z.: Calcul du transfert de chaleur entre un habitat semi-enterré et le sol par la méthode des fonctions de transfert multicouches, Comples, pp. 122-127, Agadir, Maroc, (1996).

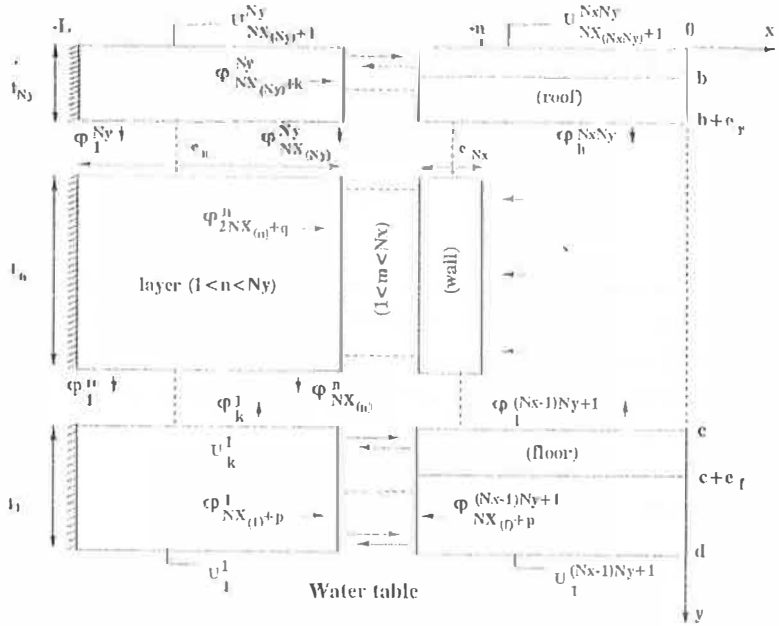

Fig. 1 The studied configuration.

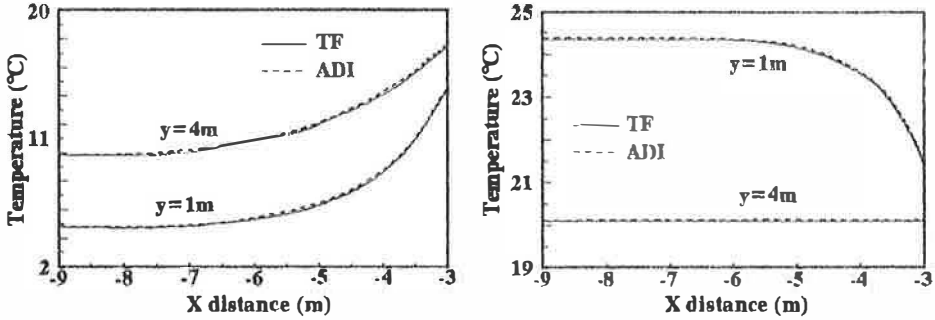

Fig. 2 Temperature distribution at various depth below-grade: a) cold climate (January 15); b) hot climate (July 15).

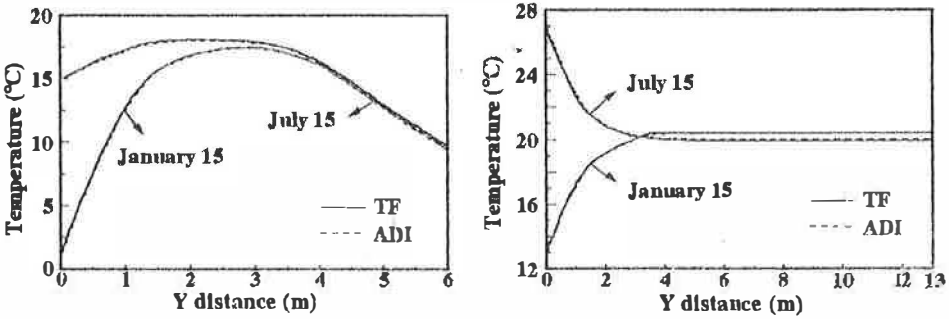

Fig. 3 Temperature distribution at x = -3.4m : a) cold climate; b) hot climate.

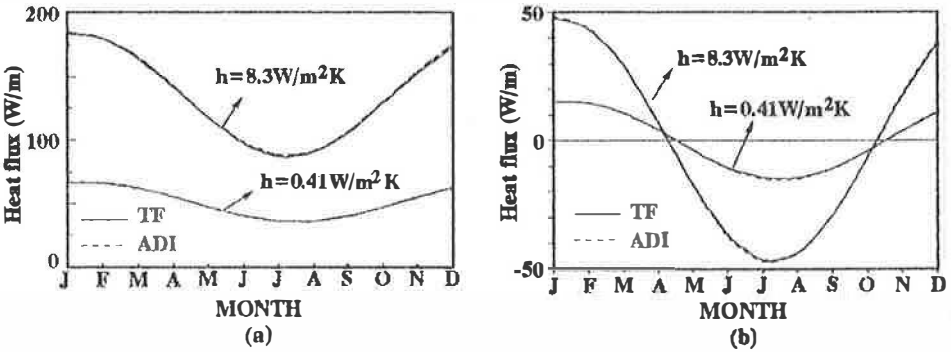

Fig.4 Annual variations of the monthly heat flux: a) cold climate; b) hot climate.

SYMPOSIUM ON ENVIRONMENT

INFLUENCE OF WATER DROPLET SIZE ON THE CHEMICAL REACTIVITY IN A SUPERSATURATED MOIST AIR.

A. Sanfeld[+,*] and P. Carlier[++]

[+]L.I.S.A., Paris 7 University, 2, place Jussieu,
75251 Paris Cedex 05

[*]L.M.M.T., Aix - Marseille III University, Saint-Jérôme Faculty,
Bd, Escadrille Normandie-Niemen,
13397 Marseille Cedex 20

Abstract

A new thermodynamic approach is presented giving relations between water droplet size in a supersaturated air and chemical reactivity. Different realistic examples show an increase or a decrease of the chemical affinity with the size of the droplet. Supersaturation versus radius curves show stable and unstable domains. Finally, a generalized supersaturation formula is given for charged droplets.

1. Introduction

The purpose of our work is to show the relations between the curvature of droplets and the chemical affinites of reactions taking place in vapour and aqueous phases and then to analyse the consequences on the physical chemistry of the atmosphere. In this first theoretical approach, we consider no surface-active compounds.

The atmosphere is a very complex system covering injection, transport, chemical reactions, phase transfer and deposition of minor species. All these processes induce a rich and fascinating chemistry involving numerous components generally at extremely weak concentrations. In the beginning of the studies on tropospheric physico-chemistry, scientists were only interested in homogeneous gas-phase reactions. Moreover, mass transfers from air or solid phase to hydrometeors also lead to a complex chemistry in the aqueous phase. There is now a tendency to develop multiphasic mechanisms taking simultaneously into account chemical transformations in interstitial air, matter transfer across the gas water interface and chemical reactions in the aqueous phase, ref. (1.5). Except for nucleation phenomena, none of these studies allow for capillary effects. Using an *a priori* approach, our goal was to discover whether this gap could lead to uncertainty in the results on the tropospheric mechanism. Therefore we use the thermodynamic approach in order to find the relations between the concentration of the reactive species, the size of the droplets and the chemical affinites, ref. (6).

This new approach is based on the thermodynamic capillarity of macroscopic systems, ref. (7.8). The system considered is composed of a mist of aqueous droplets (phase β) comprising a solvent and one or several solutes. The supersaturated vapour (phase α) also contains several species. Transfer of matter and chemical reactions take place in both phases. Three processes studied using simplified examples are proposed involving chemical reactions in the vapour and aqueous phases, respectively. Moreover as a general rule, at equilibrium, the partial vapour pressures, p_w^{α}, of the solvent w (in our case water) is larger than the vapour pressure, $p_w^{0\alpha}$, corresponding to a plane interface. We define the supersaturation as the quantity $\ln\left(p_w^{\alpha} / p_w^{0\alpha}\right)$, and we assume here that the droplet has to accommodate itself in order to maintain constant the partial pressure of the solvent.

2. Basic equations.

For uncharged components in an equilibrium partition between the α and β bulk phases, we can write the variation of the chemical affinity $A_\rho^\varphi \left(= -\Delta G_\rho^\varphi\right)$, of a reaction ρ in each phase $\varphi(\varphi \equiv \alpha, \beta)$ in terms of the variations of the chemical potentials

$$dA_\rho^\varphi = -\sum_\gamma \nu_{\gamma\rho}^\varphi d\mu_\gamma^\varphi \tag{1}$$

where $\nu_{\gamma\rho}^\varphi$ is the stoichiometric coefficient and μ_γ^φ is the chemical potential of component γ. Considering the vapour phase (α) as an infinite reservoir at constant T, the Gibbs-Duhem equation reduces, as a first approximation, to

$$\sum_i c_i^\alpha d\mu_i^\alpha + \sum_{\gamma \neq w} c_\gamma^\alpha d\mu_\gamma^\alpha = 0 \tag{2}$$

where the concentration of the inert component i varies during the reactions in order to maintain a constant pressure in the atmosphere.

Considering the atmosphere as perfect gas, we get from Eqs. (1), and (2)

$$\frac{dA_\rho^\alpha}{RT} = \sum_{\gamma \neq \delta, w} \left\{ \left[-\frac{\nu_{\gamma\rho}^\alpha}{c_\gamma^\alpha} + \frac{\nu_{\delta\rho}^\alpha}{c_\delta^\alpha} \right] dc_\gamma^\alpha \right\} + \nu_{\delta\rho}^\alpha \sum_i \frac{dc_i^\alpha}{c_\delta^\alpha} \tag{3}$$

where δ refer to one particular component $(\delta \neq w, \gamma)$.

From the classical Laplace equation, we obtain

$$dp^\beta = d(2\sigma\kappa) \tag{4}$$

where δ is the surface tension and κ the curvature of the droplet.

Using now the Gibbs-Duhem equation for the liquid droplet phase and assuming very low solubility of the inert components, Eq. (4) reads

$$d(2\sigma\kappa) = \sum_\gamma c_\gamma^\beta d\mu_\gamma^\beta = \sum_\lambda c_\lambda^\beta \, d\mu_\lambda^\beta + \sum_{\gamma \neq \lambda} c_\gamma^\beta d\mu_\gamma^\beta \tag{5}$$

where among all the species γ, we consider the component λ in thermodynamic equilibrium between α and β and

$$d\mu_\lambda^* = RT \frac{dc_\lambda^\alpha}{c_\lambda^\alpha} \tag{6}$$

From Eq. (1) the variation of the chemical affinity in the liquid phase (β) reads

$$dA_\rho^\beta = \sum_{\gamma \neq \theta, w} \left\{ \left[-\nu_{\gamma\rho}^\beta + \frac{\nu_{\theta\rho}^\beta c_\gamma^\beta}{c_\theta^\beta} \right] d\mu_\gamma^\beta \right\} - \frac{\nu_{\theta\rho}^\beta}{c_\theta^\beta} d(2\sigma\kappa) \tag{7}$$

where (θ) is one component in the aqueous phase (β).

where (θ) is one component in the aqueous phase (β).

For ideal solutions of non surfactants (s) the supersaturation is given by the relation, ref. (8.10),

$$\frac{1}{v_w^\beta} \ln \frac{p_w^\alpha}{p_w^{0\alpha}} = \frac{2\sigma\kappa}{RT} - \sum_s c_s^\beta \qquad (8)$$

where v_w^β is the partial molar volume of the solvent.

3. Applications to semi-realistic models for atmosphere

The three simplified models are :

(a) quasi-insoluble chemical species precursor in vapour phase of an ionizable soluble species ;

(b) soluble chemical species precursor in vapour and / or in aqueous phases of an ionizable soluble species ;

(c) oxidation of a soluble product leading to a less soluble product.

The mechanism (a), (b) and (b') can be schematized respectively by

(a) air water

$$\nu_P P^\alpha \longrightarrow \nu_S S^\alpha \Leftrightarrow \nu_S S^\beta \Leftrightarrow \nu_S \left(\nu_{C^+} C^+ + \nu_{A^-} A^-\right)$$

$\downarrow$ Red^α

(b) and (b')

air water

$$\nu_P P^\alpha \Leftrightarrow \nu_P P^\beta$$

$$OX^\alpha \longrightarrow \mathrm{Red}^\alpha \text{ (b) } OX^\beta \dashrightarrow \mathrm{Red}^\beta \text{ (b')}$$

$\downarrow$ $\downarrow$

$$\nu_S S^\alpha \Leftrightarrow \nu_S S^\beta \Leftrightarrow \nu_S \left(\nu_{C^+} C^+ + \nu_{A^-} A^-\right)$$

(c) water air

$$OX^\alpha$$

$$\nu_P \left(\nu_{C^+} C^+ + \nu_{A^-} A^-\right) \Leftrightarrow \nu_P P^\beta \Leftrightarrow \nu_P P^\alpha \longrightarrow \nu_S S^\alpha$$

$\downarrow$

Red^α

For the three cases, components OX and Red are assumed to be in a steady state. Furthermore one assumes that C^+ and A^- are only ionic components existing in the solution. It means among others that we neglect the self-ionization of the solvent.

Although very simplified, these three schemes represent reasonably well actual atmospheric cases. The hypothesis that the OX and Red species are in steady state is generally well verified. Indeed, one often has a system as follows : $OX \equiv OH + O_2$ and $\mathrm{Red} \equiv HO_2$. In such cases, a steady state is maintained by the recycling of HO_2 into OH by NO. One can then give some examples following more or less these schemes.

For (a) :

$$CO + OH \xrightarrow{+O_2} CO_2 + HO_2$$

$$NO_2 + OH \longrightarrow HNO_3$$

For (b) :

$$CH_3CHO + OH \xrightarrow{+O_2} CH_3 + CO_2H + HO_2 \text{ (only in liquid phase)}$$

$$SO_2 + OH \xrightarrow{+O_2+H_2O} H_2SO_4 + HO_2 \text{ (In both phases)}$$

For (c), it seems that it is much harder to find actual cases corresponding to the last mechanism. Indeed, the atmospheric oxidations products are mostly more polar and thus more soluble than their precursors. Nevertheless an example is the oxidation of formic acid (very soluble) into carbon dioxide (less soluble).

$$HCO_2H + OH \xrightarrow{+O_2} CO_2 + HO_2 + H_2O$$

4. Analysis of the mechanisms

4.1. Mechanism (a)

By using the previous equations (2) - (8), we obtain an integration from a constant curvature κ^* corresponding to the concentration c_s^* to κ

$$\frac{A^{*\alpha} - A^{\alpha}}{RT} = \nu_s^{\alpha} \nu^{\beta} \ln \frac{2\sigma\kappa + aRT}{2\sigma^* \kappa^* + aRT} \tag{9}$$

The chemical affinity in the vapour decreases with increasing curvature of the droplet. It is interesting to note that the variation of A in the vapour phase is not only a function of the curvature, but also of the nature of the two phases through the physical quantities σ and ν^{β}.

For the case $a \approx 0$ (i.e. $p_w^{\alpha} \approx p_w^{0\alpha}$), $\nu_s^{\alpha} = 1, \nu^{\beta} = 3$ and $2\Gamma\kappa^* \leq c_w^{\beta}$, Eq. (9) then reads

$$\frac{\Delta G^{\alpha} - \Delta G^{*\alpha}}{RT} = 3 \ln \frac{\kappa}{\kappa^*} \left(\frac{c_w^{\beta}}{c_w^{\beta} + 2\Gamma\kappa} \right)$$

At 25°C for

$\kappa^* = 10^5 cm^{-1}, \kappa = 2 \times 10^6 cm^{-1}, 2\Gamma = 1.8 \times 10^9$ mol $cm^{-2}, c_w^{\beta} = 5.55 \times 10^9$ mol cm^{-3}, we obtain

$$\Delta G^{\alpha} - \Delta G^{*\alpha} = 22 kJ \text{ mol}^{-1}$$

4.2. Mechanism (b)

For the mechanism (b) all the other components ($\neq$ P, S, Ox, Red) are supposed to be in partition equilibrium (for example w) between the two phases. Moreover the vapour phase contains inert components i slightly soluble in the droplets (mainly N_2 and O_2).

The chemical affinity in the droplet becomes then

(i) strong electrolytes

$$\frac{A^{*\beta} - A^{\beta}}{RT} = \nu_S \nu \ln\left[1 + \frac{2\sigma\Delta\kappa}{B\nu RT}\left(K_S c_S^{*\alpha}\right)^{-1/\nu}\right] \tag{10}$$

(ii) weak electrolytes

$$\frac{A^{*\beta} - A^{\beta}}{RT} = \nu_S \ln\left[1 + \frac{2\sigma\Delta\kappa}{RT}\left(K_S c_S^{*\alpha}\right)^{-1}\right] \tag{11}$$

where

$$B = \frac{1}{\nu_{C^+}}\left[K_d\left(\frac{\nu_{C^+}}{\nu_{A^-}}\right)^{\nu_{A^-}}\right]^{1/\nu} ; K_d = \frac{c_{C^+}^{\nu_{C^+}} c_{A^-}^{\nu_{A^-}}}{c_S^{\beta}}$$

$$\nu = \nu_{C^+} + \nu_{A^-} ; K_S = \frac{c_S^{\beta}}{c_S^{\alpha}}$$

For both cases the chemical affinity in the droplet increases with its radius. It also depends on the surface tension, on the concentration, $c_r^{*\alpha}$, of the gaseous phase and on the chemistry in the aqueous phase (K_r).

Let us give two examples :

(i) $SO_2 \rightarrow H_2SO_4 \rightarrow 2H^+ + SO_4^{--}$

For
$2\sigma = 144$ erg cm^{-2}, $\Delta\kappa = 2 \times 10^6$ cm^{-1}, $\nu = 3$, $\nu_S = 1$, $K_S = 10^3$, $K_d = 1$ mol^{2}cm^{-6}, $T = 300$°K,
$c_S^{*\alpha} = 10^{-12}$ mol cm^{-3}

we obtain

$$\frac{\Delta G^{\beta} - \Delta G^{*\beta}}{RT} = 6$$

or

$$\Delta G^{\beta} - \Delta G^{*\beta} = 15 \text{ kJ mol}^{-1}$$

(ii) $CH_3CHO \rightarrow CH_3CO_2H$

(For very large dilution, we neglect the surface activity of the solute). For
$2\sigma = 144$ erg cm^{-2}, $\Delta\kappa = 2 \times 10^6$ cm^{-1}, $\nu_S = 1$, $K_S = 10^2$, $T = 300$°K, $c_S^{*\alpha} = 10^{-10}$ mol cm^{-3},
one has

$$\frac{\Delta G^{\beta} - \Delta G^{*\beta}}{RT} = 14 \quad \text{or}$$

$$\Delta G^{\beta} - \Delta G^{*\beta} = 35 \text{ kJ mol}^{-1}$$

The analysis of the first two models, (a) and (b) shows that the larger the droplet size the larger the chemical affinity. This result depends on the solubility of the reaction products.

4.3. Mechanism (c)

For the mechanism (c) the oxidation of a soluble product leads to a less soluble product and

$$\frac{A^{\alpha} - A^{\gamma\alpha}}{RT} = \nu_p^{\alpha} \ln \frac{c_p^{\alpha}}{c_p^{\gamma\alpha}} = \nu_p^{\alpha} \nu^{\beta} \ln \frac{2\sigma\kappa + aRT}{2\sigma^{*}\kappa^{*} + aRT} \tag{12}$$

For this case, a decrease in the droplet size induces an increase in the chemical affinity.

5. Supersaturation for charged droplets

Charged droplets induce in the vapour phase (α) a diffuse layer so that the previous relations must be replaced by expressions taking into account the local electric field. Instead of the chemical potentials, and the chemical affinity we have to use the electrochemical potentials and the electrochemical affinity. Recently A. Sanfeld, ref. (11), has shown that the influence of curvature on the saturation pressure of a charged droplet reads

$$\frac{1}{\nu_w^{\beta}} \ln \frac{p_w^{\alpha}}{p_w^{0\alpha}} = \frac{2\sigma\kappa}{RT} - \sum_s c_s^{\beta} + \frac{1}{2\nu_w^{\beta} RT} \left(\frac{\partial \varepsilon}{\partial c_w} \right)^{\alpha} \left(E_r^2 \right)^{\alpha} \tag{13}$$

where $\partial c / \partial c_w$ is the derivative of the dielectric constant with the concentration of the solvent and E_r is the radial component of the electric field. The last term, called polarization effect, ref. (12), is taken at the surface of the droplet. Therefore

$$E_r^{\alpha 2} = \frac{Q^2 \kappa^4}{16\pi^2 \varepsilon^2} \tag{14}$$

with Q the charge of the droplet.

Finally, for a simple dissociation reaction in the droplet, we find the relation $\tilde{A}_p(\kappa, Q)$.

Acknowledgments

This work was supported by the European Union Contract ERBCRHXCT 0940481 and GDR 1185 CNRS / CNES.

References

(1) Schwartz, S.E.,. Mass transport considerations pertinent to aqueous phase reactions of gases in liquid-water clouds, in [W. Jaeschke (ed.)], Chemistry of Multiphase Atmospheric Systems, NATO ASI series G6, 414., 1986

(2) Graedel, T.E. and Weschler, C.J., Chemistry within aqueous atmospheric aerosols and raindrops, Rev. Geophys. Space Phys., 19 , 505, 1981.

(3) Warneck, P., The equilibrium distribution of atmospheric gases between the two phases of liquid water clouds, in [W. Jaeschke (ed.)], Chemistry of Multiphase Atmospheric Systems, NATO ASI series G6, 473, 1986.

(4) Wexler, A.S. and Seinfeld, J.H., Second generation inorganic aerosol model, Atmos. Environ., 25A , 2731, 1991.

(5) Pandis, S.N. and Seinfeld, J.H., Should bulk cloudwater or fogwater samples obey Henry's law ?, J. Geophys. Res., 96 , 10791, 1991.

(6) Sanfeld, A., Carlier, P. and Mouvier, G., Influence of water droplet size on the chemical affinity, Fluid Phase Equilibria, 107, 75, 1995.

(7) Koehler, H., On the problem of condensation in the atmosphere, Nova Acta Regiae Soc. Sci. Ups., 4(14) , 9, 1950.

(8) Dufour, L. And Defay, R., Thermodynamics of Clouds, Academic Press, New York, Ch. 8-10, pp 67-129, 1963.

(9) Defay, R., Prigogine, I. and Bellemans, A., Surface Tension and Adsorption. Longman-Green, Bristol, Ch. 16, 1966.
(10) Perrault, G., Contribution à l'étude du comportement des gouttes volatiles en atmosphère contrôlée. Thèse de doctorat des Sciences, Paris, 1971.
(11) Sanfeld, A., Supersaturation for charged droplets 1997, Private Com. Un. Paris 7. LISA., Febuary 5.
(12) Sanfeld, A., Introduction to the Thermodynamics of charged and polarized layers, Wiley Interscience, London, Ch. 8, 1988.

METHANOL SYNTHESIS FROM CO_2 AND H_2 OVER Cu/ZnO-BASED MULTICOMPONENT CATALYSTS

Masahiro SAITO*, Tadahiro FUJITANI, Masami TAKEUCHI+, Jamil TOYIR++, Shengcheng LUO++, Jingang WU++ and Taiki WATANABE+

National Institute for Resources and Environment (NIRE)
16-3 Onogawa, Tsukuba-shi, Ibaraki 305, Japan
+ Research Institute for Innovative Technology for the Earth (RITE)
9-2 kizukawadai, kizu-cho, Soraku-gun, Kyoto 619-02, Japan
++ RITE (NEDO Industrial Technology Researcher)
16-3 Onogawa, Tsukuba-shi, Ibaraki 305, Japan

Abstract : Methanol synthesis from CO_2 and H_2 has been investigated for establishing a global system for the conversion and transportation of hydrogen energy produced from natural energy such as solar energy, hydropower and so on. First, the authors elucidated the role of metal oxides contained in Cu/ZnO-based ternary catalysts prepared by a coprecipitation method and developed Cu/ZnO-based multicomponent catalysts containing two or three metal oxides. Then, the operation conditions for preparing a Cu/ZnO-based multicomponent catalyst were optimized. In the following step, a long-term (> 2000 h) stability of the catalyst developed was examined in a continuous methanol synthesis test at 523 K with a total pressure of 5 MPa using a fixed bed flow reactor. Furthermore, the methanol synthesis over the multicomponent catalyst was investigated using a recycle reactor serving as a model reactor for a practical methanol synthesis process.

1. INTRODUCTION

The greenhouse effect of carbon dioxide has been recognized to be one of the most serious problems in the world, and a number of countermeasures have been proposed so far. Catalytic hydrogenation of CO_2 to produce various kinds of chemicals and fuels has received much attention as one of the most promising mitigation options. In particular, methanol synthesis by CO_2 hydrogenation has been considered to play an important role in the conversion and transportation of hydrogen energy produced from natural energy such as solar energy, hydropower and so on, as shown in Fig. (1) (ref.(1)). According to some estimations (ref.(2)), if H_2 is produced by electrolysis of water using an electric power of 1000 MWh and then methanol synthesized from CO_2 and H_2 is transported to Japan through the system shown in Fig. (1), an electric power of 300 MWh could be obtained from a methanol fired power plant in Japan.

A practical methanol synthesis process greatly requires a high performance catalyst, which must be highly active and selective for methanol synthesis and also stable for a long period in a continuous operation. NIRE and RITE have been jointly implicated in the development of high performance methanol synthesis catalysts since 1990. The authors elucidated the role of metal oxides contained in Cu/ZnO-based ternary catalysts prepared by a coprecipitation method, and then developed Cu/ZnO-based multicomponent catalysts containing two or three metal oxides (ref.(3)). After the development of the catalyst, the operation conditions for preparing a Cu/ZnO-based multicomponent catalyst were optimized by investigating the effects of various preparation conditions on the activity of the catalyst. In the following step, the change in the activity was examined for the multicomponent catalyst prepared under the optimum preparation conditions during a long-term (> 2000 h) methanol synthesis test at 523 K with a total pressure of 5 MPa using a conventional fixed bed flow reactor. Furthermore, we investigated the methanol synthesis over the multicomponent catalyst using a recycle reactor serving as a model reactor for a practical methanol synthesis process.

* To whom correspondence should be addressed.

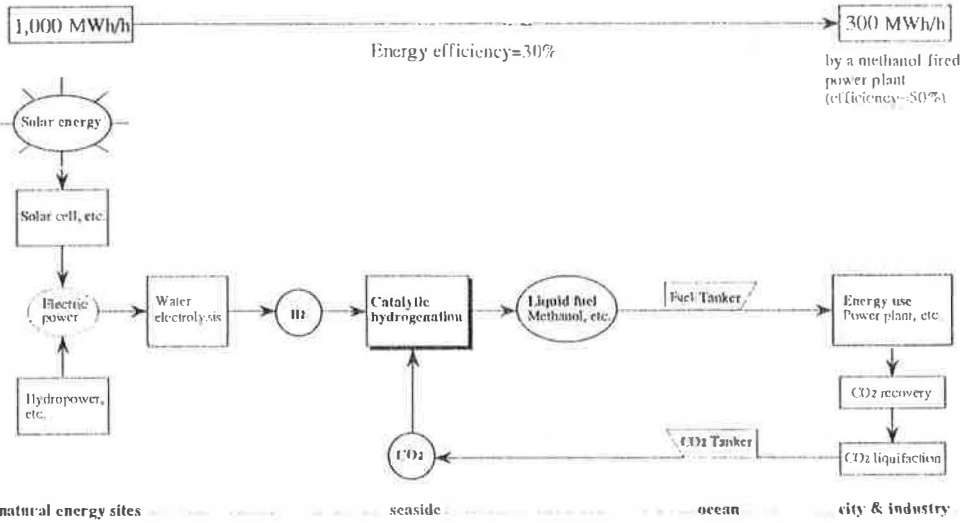

Fig. 1 Global energy network combined with catalytic hydrogenation of CO_2.

. EXPERIMENTAL

All Cu/ZnO-based catalysts were prepared by a coprecipitation method. A mixed aqueous olution of metal nitrates and an aqueous solution of Na_2CO_3 were added dropwise to distilled vater. Subsequently, the precipitate was filtered out, washed with distilled water, dried in air at 83 K overnight, and calcined in air at 623 K for 2 h. The operation conditions for preparing the atalyst such as the temperature during coprecipitation, the concentration of an aqueous solution of ixed metal nitrate, the time of aging precipitate, the extent of washing precipitate with distilled vater and so on were varied.

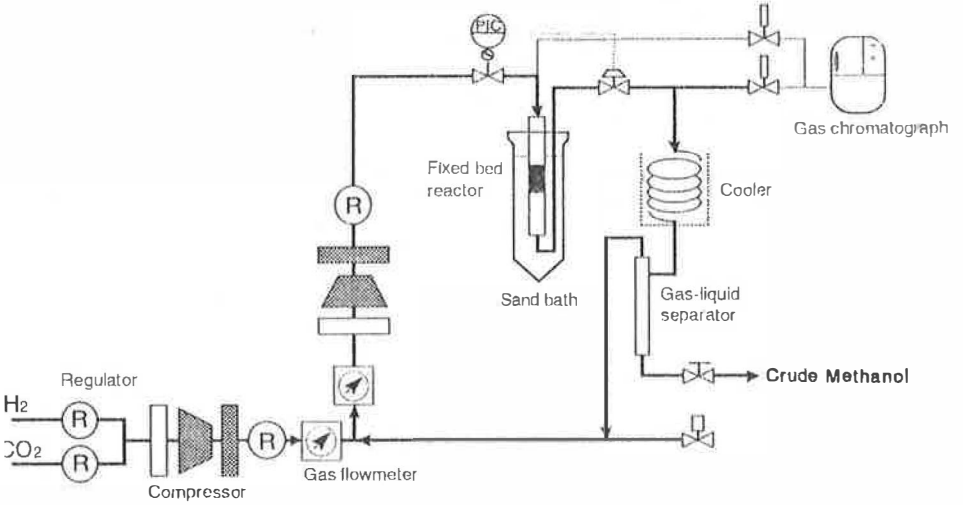

Fig. 2 Schematic diagram of a recycle reactor with a catalyst volume of 50 ml.

A conventional fixed bed flow reactor was used both for short-term and long-term methanol ynthesis tests. A commercial catalyst ($Cu/ZnO/Al_2O_3$) for methanol synthesis from syngas was

used for comparison. Furthermore, a recycle reactor equipped with a compressor for recycling unreacted gases was used for investigating practical methanol synthesis operations, as shown in Fig. (2). The catalyst fixed in a reactor was reduced in a gas mixture of H_2 (10%) and He (90%) at 573 K with a total pressure 5 MPa. The hydrogenation of CO_2 was then carried out at 523 K with a total pressure of 5 MPa in a fixed bed flow reactor by feeding a gas mixture of H_2 and CO_2 with a mole ratio of $H_2/CO_2=3$. The reaction products were analyzed by means of gas chromatographs directly connected to the reactor. The main products of CO_2 hydrogenation over Cu/ZnO-based catalysts were methanol, CO and water. Methane, dimethyl ether and methyl formate were also detected in the reaction products, but the selectivities for the by-products were less than 0.1%. The catalyst activity was measured 2h after supplying the feed gas to the reactor except for a long- term test and for a test using the recycle reactor.

The total copper surface area of the catalyst after the reaction (Cu_{total}) was determined by the technique of N_2O reactive frontal chromatography (RFC) after re-reducing the post-reaction catalyst with H_2 at 523 K (ref.(4)). X-ray diffraction measurements were performed for analyzing the structure of the catalyst.

3. RESULTS AND DISCUSSION

3.1 Development of Cu/ZnO-based multicomponent catalysts

The methanol synthesis activities of Cu/ZnO-based ternary catalysts ($Cu/ZnO/M_XO_Y$) containing various metal oxides were examined. Ga_2O_3, Al_2O_3, ZrO_2 and Cr_2O_3 exhibited promoting effects for methanol synthesis. Figure (3) shows the methanol synthesis activity of Cu/ZnO-based ternary catalysts containing Ga_2O_3, Al_2O_3, ZrO_2 and Cr_2O_3 on varying the content from 5 to 40 wt% as a function of total Cu surface area (Cu_{total}). For each metal oxide contained in the Cu/ZnO-based catalysts, a linear relationship between MTY and Cu_{total} was obtained, indicating that the specific activity is identical for each metal oxide even if the content of a metal oxide in a Cu/ZnO-based catalyst is varied. The specific activities for the Cu/ZnO-based catalysts containing Ga_2O_3 and Cr_2O_3 were greater than that of a Cu/ZnO catalyst by factor of 40% and 30%, respectively. On the other hand, the specific activity was not altered by the addition of Al_2O_3 or ZrO_2, though these metal oxides play a role in increasing Cu surface area. This indicates that the addition of Al_2O_3 or ZrO_2 improves the dispersion of Cu particles without changing the specific activity of a Cu/ZnO catalyst, while Ga_2O_3 and Cr_2O_3 are not effective for improving the dispersion of Cu, but are effective for increasing the specific activity of a Cu/ZnO catalyst.

In the following step, two kinds of Cu/ZnO-based multicomponent catalysts named MCA ($Cu/ZnO/ZrO_2/Al_2O_3$) and MCB ($Cu/ZnO/ZrO_2/Al_2O_3/Ga_2O_3$) were prepared by selecting metal oxides on the basis of the role of metal oxide described above. Figure (4) shows the activities of the multicomponent catalysts, Cu(50)/ZnO(45)/Al_2O_3(5) and Cu(50)/ZnO(50) as a function of the temperature of pretreatment in H_2 ranging from 523 K to 723K. The activities of all the catalysts decreased with increasing pretreatment temperature mainly due to the decrease in Cu surface area by the sintering of Cu particles. However, the activities of MCB and MCA decreased only 10% and 15% even in pretreatment at 723 K, respectively. while the activities of the ternary catalyst and the binary catalyst decreased 30% and 85%, respectively. This suggests that the sintering of Cu particles can be suppressed by the addition of several metal oxides to Cu/ZnO.

3.2 Optimization of Operation Conditions for Preparing the Catalyst

The various operation conditions for preparing the precipitate except the temperature during coprecipitation had no significant effect on the activity of the multicomponent catalyst. This finding is very favorable for preparing a practical catalyst.

No significant difference among the activities of the catalysts prepared at temperatures between 273 K and 313 K has been observed, whereas the activity of the catalyst prepared at 333 K was slightly (only 7%) lower. XRD measurements showed that the crystallite size of the precipitate prepared at 333 K was slightly larger than those of the precipitates prepared at temperatures ranging from 273 K to 313 K. This finding suggests that the activity of the catalyst depends on the crystallite size of the precipitate.

In the next step, the effect of extent of washing the precipitate with distilled water to remove Na coming from Na_2CO_3 on the methanol synthesis activity of the catalyst was investigated. The amount of Na remaining in the catalyst decreased with an increase in the number of washing the

precipitate. The activity of the catalyst and the Cu surface area of the catalyst greatly increased with a decrease in the amount of Na in the catalyst. The precipitates after different number of washings gave almost the same XRD patterns, whereas the XRD pattern for the catalyst calcined at 623 K became sharper with an increase in the amount of Na in the catalyst. This finding clearly indicates that the Na remaining in the catalyst crystallizes the components of the catalyst, and thus decreases the surface area, the Cu surface area and the activity of the catalyst.

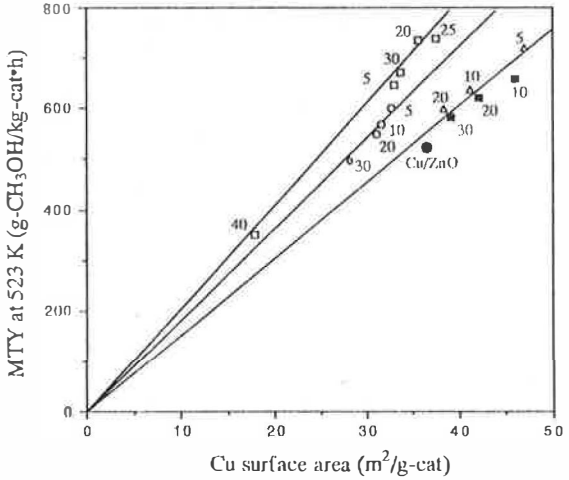

Fig. 3 Methanol synthesis activity (MTY) as a function of Cu surface area. The contents (wt%) of metal oxides in the catalysts are indicated in the figure. Cu content of the catalysts was 50 wt%. Reaction conditions: weight of catalyst = 1 g, feed gas = $CO_2(25)/H_2(75)$, feed gas rate = 300 ml/min, temperature =523 K, total pressure = 5 MPa. □:Cu/ZnO/Ga_2O_3, ○:Cu/ZnO/Cr_2O_3, △:Cu/ZnO/Al_2O_3, ■:Cu/ZnO/ZrO_2, ●:Cu/ZnO (50/50).

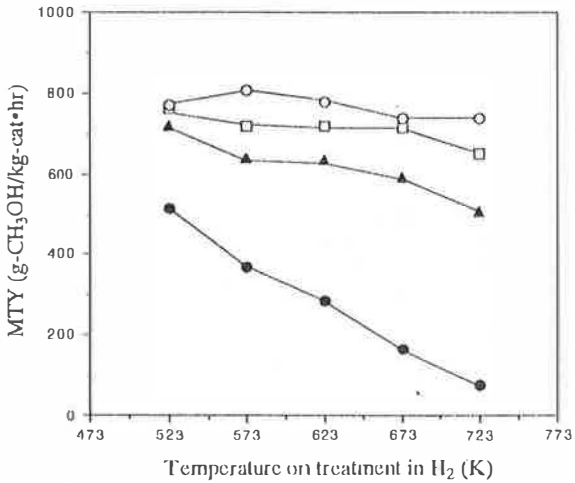

Fig. 4 Activities of various Cu/ZnO-based catalysts as a function of temperature on treatment in a stream of H_2. Reaction conditions were the same as shown in Fig. 3.
○: MCB (Cu/ZnO/ZrO_2/Al_2O_3/Ga_2O_3), □: MCA (Cu/ZnO/ZrO_2/Al_2O_3),
▲:Cu(50)/ZnO(45)/Al_2O_3(5), ●: Cu(50)/ZnO(50)

3.3 Long-term Stability of the Catalyst

A methanol synthesis catalyst for a practical process is highly required to have a stable activity for a long period in a continuous operation. A long-term methanol synthesis test was performed at 523 K with a total pressure of 5 MPa by using a gas mixture of CO_2, CO and H_2, because unreacted gases and CO must be recycled to the reactor in a practical process. Figure 5 shows the change in the activity with time on stream of the multicomponent catalyst compared with a commercial catalyst used for methanol synthesis from syngas. The activity of the multicomponent catalyst decreased only by 17% in 1000 h during the test, but unchanged from 1000 h to 3400 h. On the other hand, the activity of the commercial catalyst decreased by 20% in 1000 h, and still decreased to 75% of the initial activity in 2100 h. The Cu particle size of the multicomponent catalyst increased by 50% after the methanol synthesis for 3400 h, whereas that of the commercial catalyst increased by 75% in 2100 h. Therefore, one explanation for the deactivation could be related to the decrease in the Cu surface area of the catalyst. These findings described above clearly indicate that the multicomponent catalyst developed in the joint research is very stable for a long period in a continuous methanol synthesis operation.

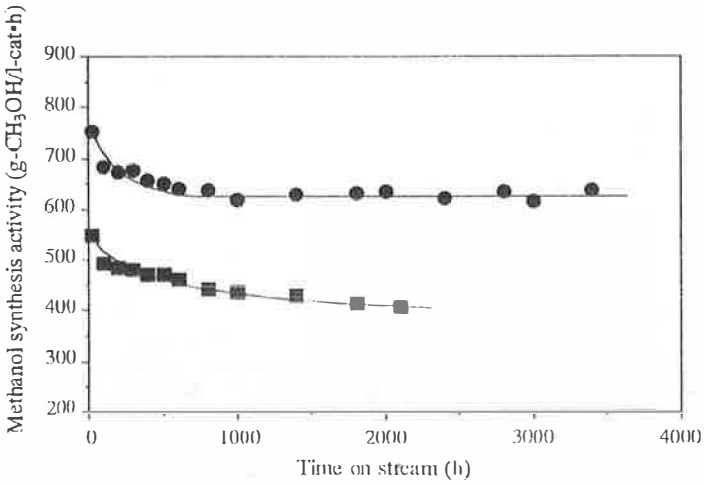

Fig. 5 Change in the activities of the multicomponent catalyst ($Cu/ZnO/ZrO_2/Al_2O_3/Ga_2O_3$, ●) and a commercial catalyst used for methanol synthesis from syngas($Cu/ZnO/Al_2O_3$, ■) during a long term methanol synthesis. Reaction conditions: temperature =523 K, total pressure = 5 MPa, SV = 10,000, feed gas composition = CO_2 (22)/CO(3)/H_2 (75).

3.4 Methanol Synthesis using a Recycle Reactor

Practical methanol synthesis must be performed by using a reactor with recycling equipments for unreacted gases, because the conversion of CO_2 to methanol at reaction equilibrium is very low under ordinary reaction conditions, for example, 17% at 523 K and 5 MPa. Therefore, methanol synthesis using a recycle reactor was also investigated. The products of CO_2 hydrogenation at 473 K to 548 K with a total pressure of 5 MPa in the recycle reactor were methanol, CO, water, methane, ethane, dimethyl ether, methyl formate, ethanol, propanol and butanol, but the yields of the products other than methanol, CO and water were very small. The selectivity for methanol in the products except CO and water was more than 99.8%. The reaction products were cooled to 270 K in a gas-liquid separator connected to the reactor. Liquid products collected in the gas-liquid separator were taken out of the reactor, and unreacted gases as well as gaseous products such as CO, methane, ethane and dimethyl ether were recycled back to the reactor. The concentrations of methane, ethane and dimethyl ether in a recycled gas mixture remained constant after some initial period in CO_2 hydrogenation without purging unreacted gases. Table 1 shows the composition of liquid products except H_2O taken out of the recycle

reactor. The purity of the crude methanol produced in the present work was 99.96 wt%, and higher than that of the crude methanol produced in a commercial methanol synthesis from syngas. The CO concentration of the feed gas to the reactor in the methanol synthesis from CO_2 and H_2 is much lower than that in the methanol synthesis from syngas. It is well known that CO is much more reactive with H_2 to produce higher alcohols and higher hydrocarbons than CO_2. Therefore, this finding suggests that the lower CO concentration in the feed gas to the reactor should result in the lower yield of by-products and thus the higher methanol purity.

Table 1 The composition of liquid products (except water) from a recycle reactor in this work[a], compared with that from a commercial plant for methanol synthesis from syngas[b]

Compound		Composition	
		This work	A commercial plant
Methanol	**CH_3OH**	**99.96 wt%**	**99.59 wt%**
Methyl formate	$HCOOCH_3$	330 ppm	700 ppm
Higher alcohols (C_2-C_4)	ROH	30 ppm	530 ppm
Hydrocarbons (C_6-C_{10})	C_nH_m	-	50 ppm
Dimethyl ether	$(CH_3)_2O$	-	230 ppm

a) Reaction conditions : catalyst=Cu/ZnO/ZrO_2/Al_2O_3/Ga_2O_3, temperature=517K, total pressure=5 MPa, H_2/CO_2 ratio in the make-up gas=3.
b) cited from a booklet on ICI methanol synthesis catalyst.

In conclusion, the presented results clearly indicate that the Cu/ZnO-basec multicomponent catalysts developed in the joint research are highly effective for a practical methanol synthesis from CO_2 and H_2.

ACKNOWLEDGEMENT

The present work was partly supported by New Energy and Industrial Technology Development Organization (NEDO).

REFERENCES

(1) H. Sano, *Proc. Int. Symp. on CO_2 Fixation & Efficient Utilization of Energy*, Tokyo, Japan, 117-122(1993).
(2) Y. Kubo, private communication.
(3) M. Saito, T. Fujitani, M. Takeuchi and T. Watanabe, *Appl. Catal. A: General*, **138**(1996), 311
(4) G. C.Chinchen, K. C. Waugh and D. A. Whan, *Appl. Catal.*, **25**(1986), 101.

DEVELOPMENT OF HIGH PERFORMANCE RANEY COPPER BASED CATALYSTS FOR METHANOL SYNTHESIS FROM CO_2 AND H_2

Jamil TOYIR, Masahiro SAITO+*, Isamu YAMAUCHI++, Shengcheng LUO+++, Jingang WU+++, Isao TAKAHARA+, Masami TAKEUCHI++++

Research Institute for Innovative Technology for the Earth (RITE),
(NEDO Industrial Technology Researcher), 16-3 Onogawa, Tsukuba-shi,
Ibaraki 305, Japan
+ National Institute for Resources and Environment (NIRE), 16-3 Onogawa,
Tsukuba-shi, Ibaraki 305, Japan
++ Department of Material Science and Processing, Faculty of Engineering, Osaka
University, 2-1 Yamadagaoka, Suita-shi, Osaka 565, Japan
+++ RITE, (NEDO Industrial Technology Researcher), 16-3 Onogawa,
Tsukuba-shi, Ibaraki 305, Japan
++++ RITE, 9-2 Kizukawadai, Kizu-cho, Soraku-gun, Kyoto 619-02, Japan

Abstract : Catalytic hydrogenation of CO_2 into methanol, considered as a serious option for the conversion and transportation of hydrogen energy produced from natural energy such as solar energy, hydropower and so on, has been investigated with Raney Cu based catalysts. Raney Cu catalysts have been prepared by leaching of various metallic alloys in NaOH or NaOH/Sodium zincate aqueous solutions. The catalysts leached in NaOH/zincate aqueous solutions and tested in CO_2 hydrogenation at 523 K and 5 MPa, showed high activities and selectivities for methanol synthesis. The deposition of Zn on the surface of Cu particles increased the surface area and the specific activity of Raney Cu-M examined. Raney Cu-Zr developed were significantly more active than a commercial catalyst.

1. Introduction

The increase of carbon dioxide in the atmosphere over the past 50 years has been the most dramatic in the history of the earth. Understanding the ecological implications of this increase and finding the effective ways of mitigating "greenhouse" gas emissions is of the most prominent concern. Catalytic hydrogenation of carbone dioxide is one of the crucial issues and processes to present a serious option for the global warming control. In particular, methanol synthesis has been considered to play an important role in the transportation of hydrogen energy derived from natural energy such as solar energy, hydropower and so on.

Recently, RITE started a joint research program on methanol synthesis via the catalytic hydrogenation of carbone dioxide. It has been widely reported that Cu/ZnO based catalysts are among the interesting systems for this reaction (ref.(1)-ref.(7)). Since this project has began our laboratory has developed Cu/ZnO-based multicomponent catalysts containing from two to five metal oxides on the basis of the role of metal oxides (ref.(8), ref.(9)) . In our previous studies we have reported that metals oxides such as Ga_2O_3, Al_2O_3, ZrO_2 and Cr_2O_3 contained in Cu/ZnO-based ternary catalysts for methanol synthesis from CO_2 and H_2 have been classified into two categories (ref.(10)) : to improve the Cu dispersion and to increase the specific activity . The addition of Al_2O_3 and ZrO_2 to Cu/ZnO improves the surface area of Cu, i.e, the dispersion of Cu particles on the surface while the association of Ga_2O_3 and Cr_2O_3 to the bicomponent catalyst Cu/ZnO enhances the specific activity by optimising the ratio Cu^+/Cu on the surface of Cu particles.

The association of the promoting metal oxides with Copper has an important role to improve simultaneously the activity and the selectivity for methanol synthesis . In order to develop a new

* To whom correspondence should be adressed

/pe of catalyst with high performance for methanol synthesis, the authors started to investigate :aney Cu-based catalysts .

So far, Raney Copper catalysts have not been widely reported in the literature as practical atalysts for methanol synthesis. However, 20 years ago Wainwright and co-workers have been ie first to report the potentiel use of Raney Cu and Raney Cu-Zn as catalysts to produce methanol rom syngas to use as synthetic liquid fuel (ref.(11)). Recently Wainghright et al. published an xcellent review about their results in the last decade and related studies in the literature on Raney Cu catalysts as catalysts for methanol synthesis and WGS reactions from syngas (ref.(12)). This tudy showed that the alkaline leaching of Copper/Zinc/Aluminium alloy to produce Zinc-romoted Raney Cu leads to an exeellent mixing of the components and consequently allows a igh activity for methanol synthesis by improving the surface area and the porosity of the catalyst. n this work also, it has been demonstrated that the production of MeOH is promoted by Copper nd the major role of Zinc oxide. The resulting catalysts have been found to be at least as active as ommercial co-precipitated catalysts for methanol synthesis from syngas. This work showed also hat the carbon dioxide is the major reactant forming methanol under the industrial conditions.

Starting from these works it is completly legitimate to envisage the methanol synthesis directly rom CO_2 and H_2 over an adequat Raney Cu catalyst. In this conference, we report an inprecendented high catalytic performance for methanol synthesis from CO_2 and H_2 over new netal-promoted Raney Cu catalysts developed on the basis of the nature of the precursor alloy.

2. Experimental

Various kinds of Raney Cu-M catalysts (M=Metal added to Cu/Al alloy; Ti, V, Cr, Zn, Ga, Zr, Nb, Mo, Pd, La, Ce) for methanol synthesis reaction were prepared by leaching of the metal alloys in moderately stirring a NaOH aqueous solution and/or a sodium zincate ($Na_2Zn(OH)_4$)/NaOH solution which was prepared by adding ZnO to a NaOH aqueous solution. The concentrations of NaOH were respectively 250 (g-NaOH in 1 kg-H_2O) for NaOH leaching solution and 300 (g-NaOH in 1 kg-H_2O) for NaOH-Zincate leaching solution. The Raney-Cu catalysts prepared after leaching were washed with distilled water until the complete removing of the NaOH excess and then stored in distilled water. The storage in distilled water has been the best way to avoid the re-oxidation of the metallic particles in Raney -Cu catalysts. The total specific surface area of the catalysts after reaction was determined by BET technique. The total copper surface area of each catalyst after reaction was determined by the technique of N_2O reactive frontal chromatography (RFC) after re-reducing the post-reaction catalyst with hydrogen at 523 K (ref.(13)). The catalytic measurements were conducted as follows : the catalyst fixed in a flow reactor was reduced in a gas mixture of pure H_2 at 523 K and 573 K during 2 hrs with a total pressure 5 MPa. After reduction the catalyst was exposed to a feeding mixture of CO_2 and H_2 with a molar ratio of CO_2 /H_2 = 1/3 (ref.(11), ref.(14)). The analysis of reactions products was realized by adequate gas chromatographs connected on line of the reactor.

3. Results and discussion

When a mixture of CO_2/H_2 passes over Raney-Cu-M catalysts at the operating conditions described above (*vide supra*) two major reactions occur. The formation of methanol and water from carbone dioxide and hydrogen. the second reaction is giving carbone monoxide with water. These equilidriums are the main competitive reactions on the surface of Raney Cu-M catalysts. There is also a presence of by reactions producing dimethyl ether, methane and methyl formate but the selectivities of the by-products were less than 0.1 %.

Raney Cu-M (1atomic %) catalysts leached in a NaOH or a NaOH/Zincate aqueous solution have been tested for methanol synthesis under the same reaction conditions (Fig.(1)).

Raney Cu-Zr have exhibited the best activity among the catalysts tested. For every catalyst tested, the presence of zincate in the leaching solution leads to the deposition of Zn on the surface of Cu particles and had a strong effect to improve the activity and the Cu surface area (respectively by 95% and 50% for Raney Cu-Zr). The highest activity due to the presence of zincate seems to be partially related to the increase of Cu surface area.

It has also been observed that the zincate doping leads to better specific activity (Fig. (2)). As it was reported in others works (ref.(15)), the increase in Copper surface area could be related to

the formation of smaller copper particles on the surface of raney copper due to the slower rate of leaching when the zincate is present.

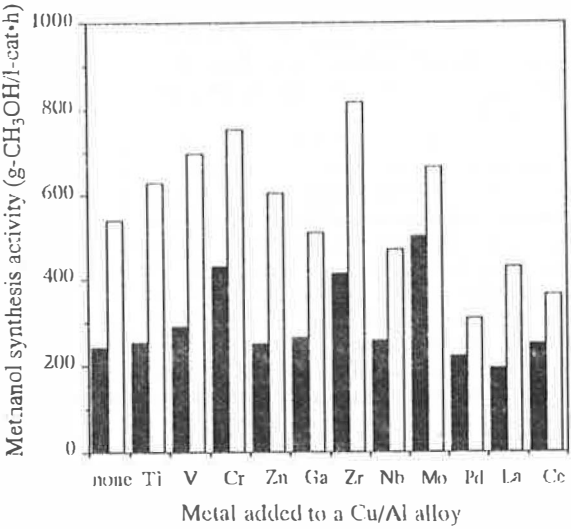

Fig.1 Effect of metal added to a Cu/Al alloy on the activity of Raney Cu catalysts leached with aqueous solutions of NaOH(20%, ■) and Zincate (NaOH + ZnO, □).
Conditions for leaching alloys : 313 K in N_2
Reaction conditions : 523 K, 5 MPa, SV=18,000, H_2/CO_2=3

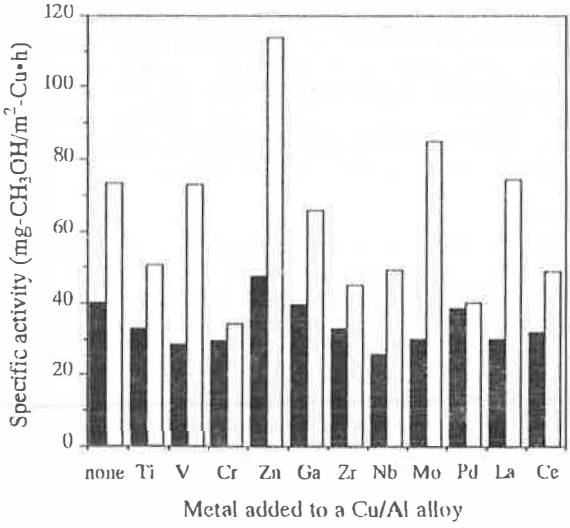

Fig.2 Effect of metal added to a Cu/Al alloy on the specific activity of Raney Cu catalysts leached with aqueous solutions of NaOH(20%, ■) and Zincate (NaOH + ZnO, □).
Conditions for leaching alloys : 313 K in N_2
Reaction conditions : 523 K, 5 MPa, SV=18,000, H_2/CO_2=3

However, in order to have more informations about the role of zincate, we have examined the chemical composition of the raney copper catalysts after reaction by analysing the samples at the atomic level. Table (1) shows the atomic composition of Raney-Cu and Raney Cu-Zr 1% leached in NaOH and NaOH-Zincate solutions and after reaction. For both catalysts the presence of zincate leads to a significant deposition of metallic Zinc . The amounts of metallic Zinc deposited on the surface were 1.1 % for Raney-Cu and 1.9% for Raney Cu-Zr (1atomic%).

Table 1 Compositions and activities of Raney Cu catalysts leached with aqueous solutions of NaOH and Zincate

Catalyst (alloy)	Leaching solution	Composition of catalyst leached (atomic %)	Cu surface area (m^2/ml)	Activity (g-CH_3OH/l-cat•h)	Specific activity (mg-CH_3OH/m^2-Cu•h)
Cu/Al (1/2)	NaOH	Cu/Al=98.6/1.4	6.0	239	39.8
	Zincate	Cu/Al/Zn=98.4/0.5/1.1	7.4	540	73.0
Cu/Al+Zr(1 at%)	NaOH	Cu/Al/Zr=89.5/7.6/2.9	12.7	415	32.7
	Zincate	Cu/Al/Zr/Zn=89.9/5.0/2.9/1.9	18.2	814	44.7

a) Leaching conditions : 313K in N_2

b) Reaction conditions : 523 K, 5 MPa, SV=18,000, H_2/CO_2=3

Table (2) displays the influence of ZnO concentration in the leaching solution on the composition of Raney Cu-Zr (1 atomic %) and its activity has been examined by varying the concentration of ZnO from 0 g to 91 g in 1kg-H_2O (which corresponds to maximum concentration of ZnO). It is clearly shown in this table that the content of zinc metal in the catalyst after reaction increased with ZnO concentration. On the other hand, the Cu surface area and the activity of Raney Cu-Zr (1 atomic %) are significantly improved by increasing the ZnO concentration. Therefore, the chemical composition and the texture of Raney copper tested changed by the addition of zincate and increasing the content of metallic zinc deposed on the surface of Cu particles had an important role to improve both the activity and the Cu surface area of Raney Cu catalyst.

Table 2. Effect of the ZnO concentration on the composition and the activity of Raney Cu/Zr [1] leached with an aqueous solution of NaOH and Zincate

[ZnO] in a leaching solution [1] (g-ZnO/kg-H_2O)	Composition of the catalyst after the reaction (Cu/Al/Zr/Zn atomic %)	Surface area [3] (m^2/ml-cat)	Cu-Surface area [3] (m^2/ml-cat)	Methanol activity [4] (g-CH_3OH/l-cat•h)		Specific activity [5] (mg-CH_3OH/m^2-Cu•h)
91[a]	94.6/1.5/1.8/2.1	26.1	18.8	931[a]	842[b]	44.7
84[b]	92.5/3.2/2.3/2.0	29.2	19.1	936	838	43.7
67[c]	93.4/2.5/2.2/1.9	28.1	19.5	939	836	43.6
51[d]	93.3/2.7/2.3/1.5	31.4	20.9	923	809	38.7
34[e]	-	23.5	16.5	881	798	48.4
27[f]	94.3/2.6/2.1/1.2	12.6	9.4	721	738	78.6

(1) Zr content in $CuAl_2$ alloy was 1 atomic %

(2) Conditions of preparation : Leaching in an aqueous solution of NaOH/ZnO in the stream of N_2 at 323K for 1hr before fixing the temperature at 333 K. The concentrations of NaOH were (a) 341, (b) 333, (c) 316, (d) 300, (e) 283, (f) 276 g in 1kg-H_2O.

(3) Surface area and Cu surface area were measured after the reaction at 523 K following the reduction at 573 K.

(4) Conditions : reduction : (a) 523 K, (b) 573 K, 2 hrs in pure H_2
reaction : 523 K, 5 MPa, SV=18,000, H_2/CO_2=3

(5) Specific activity was calculated by dividing the activity (4-b) by Cu surface area (3).

Catalytic performances of the best Raney Cu obtained (Raney Cu-Zr 1%) were compared with those of the optimum multicomponent catalyst developed in our laboratory and the commercial catalyst tested in the same conditions for methanol synthesis from CO_2 and H_2 (Table (3)). The initial activity (with the calyst reduced at 523K) of Raney Cu was (30%) higher than commercial catalyst and 10% higher than the multicomponent catalyst. In addition, the Raney Cu-Zr (1 atomic%) showed a higher specific activity which was 57% higher than the commercial catalyst and 25% higher than that of the multicomponent catalyst. These findings clearly indicated that the synergetic alloying between Copper and the metallic components is more exerted in the case of Raney Cu catalyst than in the case of mixture oxides catalysts.

Table 3 Catalytic performances of a typical Raney Cu based catalyst compared with those of an optimal Cu/ZnO-based catalyst and a commercial catalyst

Catalyst	Surface area [3] (m^2/ml-cat)	Cu- surface area [3] (m^2/ml-cat)	Methanol activity [4] (mg-MeOH/ml-cat·h)		Specific activity [5] (mg-MeOH/m^2-cat·h)
Raney Cu/Zr [1]	31.2	20.6	941[a]	853[b]	41.4
Cu/ZnO/ZrO_2/Al_2O_3	90.7	26.4	845	839	31.8
Commercial catalyst [2]	72.5	34.5	626	591	17.1

(1) Conditions of preparation : Leaching of an alloy $CuAl_2$/Zr containing 1.5 atomic % of Zr in an aqueous solution of NaOH(341 g)/ZnO (91 g) in 1kg-H_2O in the steam of N_2 at 333K .
(2) Cu/ZnO/Al_2O_3
(3) Surface area and Cu surface area were measured after the reaction at 523 K following the reduction at 573 K.
(4) Conditions : reduction : (a)523 K, (b) 573 K,
reaction : 523 K, 5 MPa, SV=18,000, H_2/CO_2=3
(5) Specific activity was calculated by dividing the activity (4)-b by Cu surface area (3).

In summary, this study clearly showed that Raney Cu catalyst prepared in the optimal conditions determined was highly active for methanol synthesis from CO_2 and H_2. For every Raney Cu-M catalyst, the presence of zincate with NaOH in the leaching aqueous solution leads to the deposition of Zn on the surface of Cu particles. The degree of Zinc deposition was improved by increasing ZnO concentration in the leaching solution. The presence of Zn matal along with Cu on the surface of Raney Cu catalyst had a strong double effect: to increase the surface area and to enhance the specific activity. Raney Cu-Zr (1 atomic %) was the most active catalyst among Raney Cu-M catalysts tested. The initial activity of the present catalyst was significantly higher than that of a commercial catalyst tested in the same reaction conditions.

Acknowledgement

This work was supported in part by New Energy and Industrial Technology Development Organization (NEDO).

References

(1) E. Ramaroson, R. Kieffer, and A. Kinnemann. Appl. Catal, 4 (1982) 281.
(2) T. Tagawa, G. Pleizier, and Y. Amenomiya, Appl. Catal., 4 (1985) 285.
(3) B. Denise and R. P. A. Sneeden, Appl. Catal., 28 (1986), 235.
(4) R. Kieffer, "Proc. Int. Symp. Chem. Fix. Carbon Dioxide", Nagoya, (1991). p.151.
(5) T. Inui, T. Takeguchi, A. Kobama and K. Tanida, Energy Convers. Mgmt, 33 (1992), 513.
(6) H. Arakawa, J.-L. Dubois and K. Sayama, Energy Convers. Mgmt, 33 (1992), 521.
(7) M. Fujiwara, H. Ando, M. Tanaka and Y. Souma, Bull. Chem. Soc. Jpn., 67 (1994), 546.
(8) M. Saito, Shokubai(catalysis),35 (1993) 485.
(9) M. Saito, T. Fujitani, I. Takahara, T. Watanabe, M. Takeuchi, Y. Kanai, K. Moriya, T. Kakumoto, Energy Convers. Mgmt. 36, 577 (1995).
(10) M. Saito, T. Fujitani, M. Takeuchi, T. Watanabe, Appl.Catal. A: General 138 (1996) 311-318.
(11) M.S. Wainwright, Proc. Alcohol Fuels, sydney, Aug. 1978, p.8.
(12) M. S. Wainwright, D. L. Trimm., *Catalysis Today*, 23 (1995), 29.
(13) G. C. Chinchen, K. C. Waugh and D. A. Whan, Appl. Catal. , 251(1986), 101.
(14) T. Fujitani, M.Saito, Y. Kanai, T. Kakumoto, T. Watanabe, J. Nakamura and T. Uchijima, Chem. Lett. (1994), 1877.
(15) H.E. Curry, M.S. Wainwright and D.J. Young, in D. Bibby and C.C. Chang (Editors) Methane Conversion, Stud. Surf. Sci. Catal., Vol. 36, Elsevier, Amsterdam, 1988, pp. 239-244.

MINERALIZATION OF XENOBIOTIC ORGANIC COMPOUNDS IN SOIL

I. Scheunert

GSF-Institute of Soil Ecology,
D-85764 Neuherberg, Federal Republic of Germany

ABSTRACT The mineralization rates of ^{14}C-labelled xenobiotic organic compounds in soils were determined by measuring $^{14}CO_2$ output. For the chemicals studied, aerobic and anaerobic mineralization in suspended soil did not differ very much. The kinetics of aerobic mineralization in soil was represented by a 3/2-order function, and the dependence of kinetic parameters on soil properties and environmental conditions was studied. For two herbicides, in some soils a positive linear correlation between mineralized amounts and microbial biomass was found. Fresh organic material added to the soil influenced the mineralization rates also.

1. Introduction

Organic xenobiotic chemicals reach the soil, either intentionally by the application of pesticides or other agricultural chemicals, or unintentionally by solid waste, waste water, or atmospheric dry or wet deposition. Their mineralization, resulting in carbon dioxide, water, and other small inorganic molecules, is the only pathway for a final elimination of the xenobiotic from the environment. Therefore, information on this process is indispensable for an ecotoxicological evaluation of organic chemicals in the environment. The determination of the disappearance of the xenobiotic parent compound in soil is not an appropriate way to quantify mineralization in soil because this decrease may be caused by various processes other than mineralization.

Mineralization is best described by quantification of CO_2 released by total degradation. This is feasible only after labeling the xenobiotic with ^{14}C, which allows discrimination between CO_2 derived from the xenobiotic and that from normal soil respiration.

2. Methods

In our laboratory, a closed aerated apparatus has been developed to measure $^{14}CO_2$ evolving from ^{14}C-labelled chemicals directly.

In order to discriminate between aerobic and anaerobic mineralization, soil containing the ^{14}C-labelled chemical is suspended in water and agitated for an incubation period between 5 days and several weeks. Either oxygen or nitrogen is drawn through the apparatus daily (or every two days) for 1 hr, and the volatile ^{14}C is trapped in a system of absorption tubes. In order to exclude a misinterpretation of volatile parent compound or its organic metabolites for $^{14}CO_2$, the first tube is filled with ethyleneglycolmonomethylether to absorb volatile organic substances; the following tubes are filled with scintillation liquid containing an organic base for the absorption of $^{14}CO_2$. Cumulative $^{14}CO_2$ in percentage of ^{14}C applied is plotted as a function of time (1).

For studying aerobic mineralization in soil, natural soil samples treated with ^{14}C-chemical are placed in the apparatus and incubated without agitation. In daily intervals, the samples are flushed with air, and $^{14}CO_2$ is determined as described above (2-3).

3. Mineralization in suspended soil under aerobic or anaerobic conditions

The mineralization rates of various ^{14}C-labelled chemicals after 5 days, in % of ^{14}C applied, under either aerobic or anaerobic conditions, are presented in Table 1.

The table reveals that the differences in mineralization between aerobic and anaerobic conditions in general were small. The detergent n-dodecylbenzene-sulphonate (LAS) was mineralized better under anaerobic conditions, whereas the plasticizer di-(2ethylhexyl)phthalate (DEHP) was mineralized better under aerobic conditions. The mineralization of organochlorine compounds such as lindane, DDT, 2,4-D, 2,6-dichlorobenzonitrile, and hexachlorobenzene was very low; the rates seemed to be slightly higher under anaerobic conditions. This might be due to reductive dechlorination which often represents the first step in the degradation of organochlorine compounds and which occurs preferably under anaerobic conditions.

Table 1. Mineralization of ^{14}C-labelled organic chemicals in a soil-water suspension under aerobic or anaerobic conditions ($^{14}CO_2$ after 5 days in % of ^{14}C applied) (1)

^{14}C-Chemical	$^{14}CO_2$, aerobic	$^{14}CO_2$, anaerobic
Urea	66.3	70.1
Methanol	53.4	46.3
Aniline	17.4	n.m.
n-Dodecylbenzene-sulphonate	13.8	26.0
Di-(2ethylhexyl)-phthalate	5.6	2.9
Phenanthrene	3.0	4.2
4-Chloroaniline	1.5	n.m.
Lindane	0.4	0.4
DDT	0.1	0.3
Anthracene	0.1	0.3
2,4-D	0.1	0.2
2,6-Dichlorobenzonitrile	< 0.01	< 0.01
Hexachlorobenzene	< 0.01	< 0.01

n.m. = not measured

4. Mineralization in soil under aerobic conditions

4.1 Mineralization kinetics

The characterization of mineralization of xenobiotics is often attempted by using their half-lives. However, this presumes that degradation follows first-order kinetics. In this case, the degradation rate is proportional to the concentration of residual substrate, which has been reported for the decomposition of bromacil, diuron, chlortoluron (4), and of some other compounds in soil (5). However, this simple model must not be extrapolated to all soil situations. First-order kinetics require that neither growth nor decrease of degrading populations occur, that substrate concentrations are very low, and that the pesticide is the sole source of carbon of the degrading organisms (6). These conditions are rare in normal soils under natural conditions. Thus, normally first-order kinetics apply only to part of the degradation curve.

In mineralization experiments measuring $^{14}CO_2$ evolution, time curves often indicate an apparent lag phase at the beginning followed by an exponential second phase and a third phase in which mineralization decreases continuously until a complete stop is reached; complete

mineralization is not achieved. This sigmoid curve course of $^{14}CO_2$ release from ^{14}C-labelled organic compounds is reported frequently in the literature (7-9). It is a characteristic of biological systems involving growth and/or adaptation in soil. Scow *et al.* (8) found that the lag phase accounts for an adaptation of soil microflora to the foreign compound. The third phase may represent the stage in which a substrate level is reached that is too low to sustain the metabolizing microbial fraction. Irreversible binding of substrate may also reduce the availability. The third phase might also represent the mineralization of formerly assimilated carbon from the xenobiotic either by normal respiration or by decay after the death of the microorganisms. This evolution of carbon dioxide also continues after the degradation of the original xenobiotic has discontinued (10).

In our laboratory, the mineralization kinetics was studied with ^{14}C-LAS and ^{14}C-DEHP. $^{14}CO_2$-evolution was determined in three soils discontinuously flushed with air, as described above. Soils EF and BB were sampled fresh in two forest sites, whereas soil GSF was a rendzina taken from a greenland (2). The time course of mineralization is shown in Figs. 1 and 2.

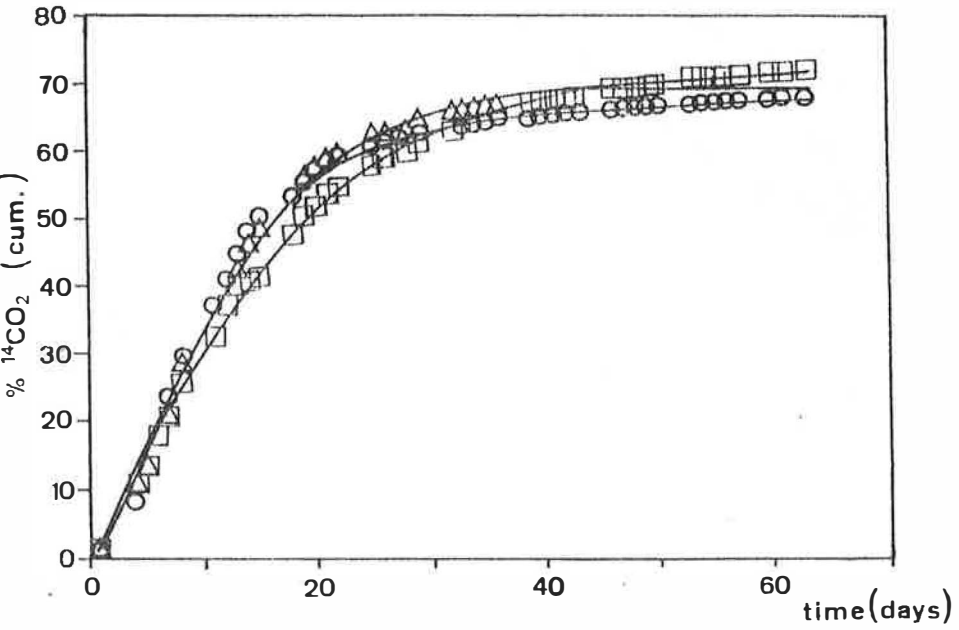

Fig. 1. Time course of mineralization of [^{14}C]LAS in three soils (cumulative $^{14}CO_2$ in percentage of ^{14}C applied; dose, 10 mg/kg). □, Experimental points, soil BB; △, experimental points, soil EF; ○, experimental points, soil GSF, and — fitted curves.

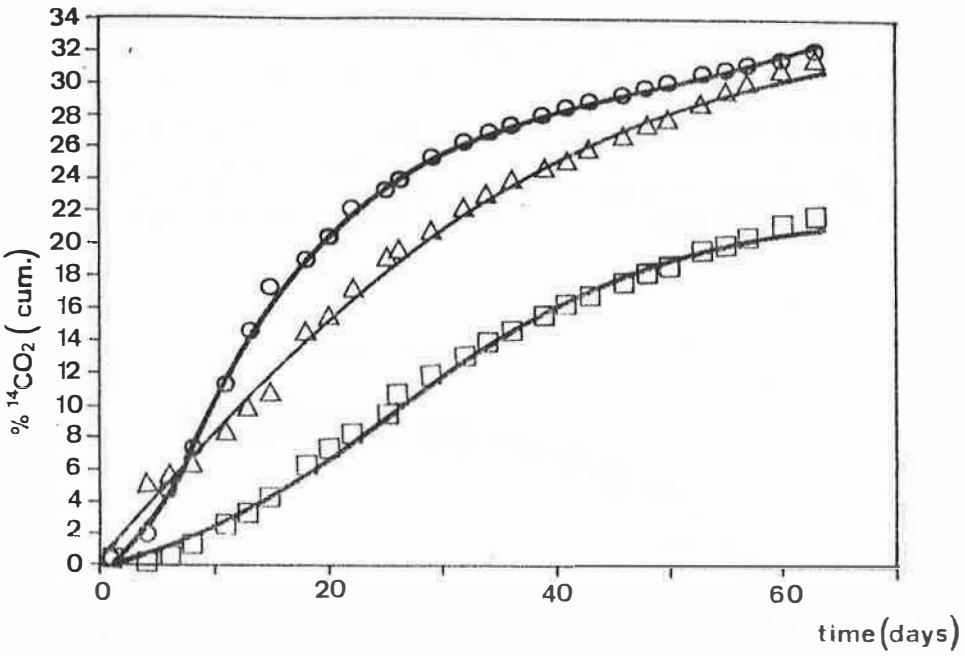

Fig. 2. Time course of mineralization of [^{14}C]DEHP in three soils (cumulative $^{14}CO_2$ in percentage of ^{14}C applied; dose, 10 mg/kg). □, Experimental points, soil BB; △, experimental points, soil EF; ○, experimental points, soil GSF; and —, fitted curves.

The curves were adapted to 3/2-order kinetics with linear adaptation, described by the following equation (2).

$$P = S_0 \cdot x_3 \cdot \left\{ 1 - e^{\left[- x_1 \cdot t - 0.5 \cdot \left(x_2 \cdot t \right)^2 \right]} \right\}$$

where P is the percentage amount of carbon dioxide formed and the regression coefficients x the kinetic model parameters. x_1 ($1/t$) describes the gradient of the exponential part of the curve. x_2 ($1/t^2$) characterizes the lag phase. It determines the sigmoid course of the curve by giving it a turning point and fixes the beginning of the exponential part of the curve. x_3 (dimensionless) describes the last, asymptotic part of the curve. $S_0 \cdot x_3 = A$ is the final value of the asymptote. It represents the total degraded amount and is given in percentage of dose initially applied. S_0 is the last data point. Thus, $x_3 = A/S_0$ gives the degree of correspondence between the asymptotic value

and the last data point. $x_3 > 1$ means that the asymptote is not reached at the end of the experiment; $x_3 < 1$ indicates that $^{14}CO_2$ is still evolving from the soil.

4.2 Correlation of maximal degraded amounts and of kinetic parameters of ^{14}C-LAS and ^{14}C-DEHP with soil properties and environmental conditions

For ^{14}C-LAS, the maximal degraded amount A was similar in all three soils and was positively related to pH in two soils and to humidity in one soil (rendzina). The parameters x_1-x_3 were positively influenced by soil humidity in all three soils. The degraded amounts A, expressed as percentage of added dose, were independent of initial concentration. Both A and the parameters x_1-x_3 increased with increasing temperature. Degradation was negligible below 3°C.

For DEHP, the mineralization was much slower than for LAS and was most rapid and most complete in the rendzina soil. Relative degradation A was lower for higher initial application rates. Temperature influenced both A and the lag phase. Degradation was not significant below 10°C (2).

4.3 Correlation of maximal degraded amounts of ^{14}C-herbicides with soil microbial biomass.

The mineralization of the ^{14}C-labelled herbicides isoproturon and glyphosate was determined in four soils for 67 or 26 days, respectively, and compared with total soil microbial biomass, as estimated by microcalorimetry (3, 11). The first soil was sampled from a field with biological cropping since 15 years, i.e., without mineral fertilizer and pesticide application since that time. This soil had a relatively high microbial biomass. The second soil was taken from a neighbouring field and had physico-chemical properties similar to those of the first soil, but a much lower biomass. The third and fourth soil came from a site with biological cropping for 2 years; their history, however, was different. Soil 4 came from a field which in the past had been used for hop cultivation and had a copper content of nearly 200 mg/kg dry soil, originating from previous fungicide applications.

The $^{14}CO_2$-production from both ^{14}C-labelled herbicides was positively correlated with total microbial biomass for soils 1-3. Soil 4 did not fit this correlation. Its capacity to degrade these herbicides was - in relation to its microbial biomass - significantly higher than that of the other soils. This might be caused by physiological stress of the microflora due to the high copper content. In addition, copper may affect the composition of soil microbial communities (12).

When ^{14}C-isoproturon and ^{14}C-glyphosate were applied to the same soils as residues incorporated in plant cell-walls, $^{14}CO_2$ production could not be correlated with soil microbial biomass.

4.4 Influence of fresh organic material on biomineralization of ^{14}C-isoproturon

Mineralization experiments were performed with ^{14}C-isoproturon in soil with and without addition of wheat straw, lucerne, or farmyard manure. Among these variants, wheat straw effected the highest mineralization of the herbicide (13). Maize straw also stimulates the mineralization of pesticides (^{14}C-methabenzthiazuron, 14). The promotion of oxidative metabolic reactions during the degradation and humification of straw is documented also by the increase in oxidized metabolites and in soil-bound residues (13-14).

5. Conclusion

The biological mineralization of xenobiotic organic chemicals in soils depends on a large number of physico-chemical and biological parameters. More research is needed to get a better insight into this process which is most important for the toxicological and ecotoxicological evaluation of environmental chemicals.

6. References

(1) Scheunert, I., Vockel, D., Schmitzer, J., and Korte, F.: Chemosphere, 16, 1031-1041 (1987)

(2) Dörfler, U., Haala, R., Matthies, M., and Scheunert, I.: Ecotoxicol. Environ. Saf., 34, 216-222 (1996)

(3) Lehr, S., Scheunert, I., and Beese, F.: Soil Biol. Biochem., 28, 1-8 (1996)

(4) Madhum, Y.A., and Freed, V.H.: Chemosphere, 16, 1003-1011 (1987)

(5) Alexander, M.: Environ. Sci. Technol., 19, 106-111 (1985)

(6) Vasseur, P., Kuenemann, P., and Devillers, J.: In Chemical Exposure Predictions (D. Calamari, Ed.), pp. 47-61, Lewis, Boca Raton, FL (1993)

(7) Simkins, S., and Alexander, M.: Appl. Environ. Microbiol., 47, 1299-1306 (1984)

(8) Scow, K.M., Simkins, S., and Alexander, M.: Appl. Environ. Microbiol., 51, 1028-1035 (1986)

(9) Brunner, W., and Focht, D.D.: Appl. Environ. Microbiol., 47, 167-172 (1984)

(10) Scheunert, I.: In Chemistry of Plant Protection (W. Ebing, Ed.), Vol. 8, pp. 23-75, Springer Verlag, Berlin (1992)

(11) Lehr, S., Scheunert, I., and Gläßgen, W.E.: Paper presented at the 6th International Workshop: Pesticides in Soil and the Environment, Stratford-upon-Avon, U.K. (1996)

(12) Zelles, L., Bai, Q.Y., Ma, R.X., Rackwitz, R., Winter, K., and Beese, F.: Soil Biol. Biochem., 26, 439-446 (1994)

(13) Reuter, S.: Doctoral Thesis, Technical University of Munich, FRG, in preparation (1997)

(14) Printz, H., Burauel, P., and Fuhr, F.: J. Environ. Sci. Health, B30, 435-456 (1995)

Phototransformation of aromatic pollutants in aqueous solution

P. BOULE and C. RICHARD
Laboratoire de Photochimie Moléculaire et Macromoléculaire
UMR 6505 CNRS - Université Blaise Pascal (Clermont-Ferrand)
F - 63177 AUBIERE Cedex (France)

Abstract

Direct and induced photolyses are important ways for elimination of pollutants from surface waters. Direct phototransformation of halogenated organic pollutants is highly dependent on the position of halogen on the ring, but the most common reaction is photohydrolysis *i.e.* hydroxylation with the release of halide ion and proton.
When the pollutant does not absorb solar light, the phototransformation can be induced in various ways. Nitrates, nitrites, iron (III) and humic substances are important sources of oxidizing species such as $^{\bullet}OH$, $HO_2^{\bullet}/O_2^{\bullet-}$, $^1O_2$. Iron (III) is also able to induce oxidations by formation of intermolecular complexes, and humic substances can transfer energy. With nitrate and nitrite ions nitration or nitrosation were observed in laboratory conditions.

1. Direct photolysis

Direct photolysis occurs if the compound absorbs solar-light *i.e.* wavelengths longer than *c.a.* 290 nm in summer and *c.a.* 300 nm in winter. The kinetics of transformation is characterized by its quantum yield, ϕ, *i.e.* the ratio between the number of molecules transformed and the number of photons absorbed during the same time. From the quantum yield and the solar spectrum in local geographic conditions it is possible to estimate the photochemical half-life in surface waters.
A special attention was focussed on chloroaromatic derivatives and halophenols since they absorb in UV range, are often toxic and give typical reactions.
It was observed with halophenols that the reactivity is highly dependent on the position of the halogen on the ring, but it is not significantly influenced by the nature of the halogen : the same reactions can be observed with chloro-, fluoro- and bromo derivatives (1,2).

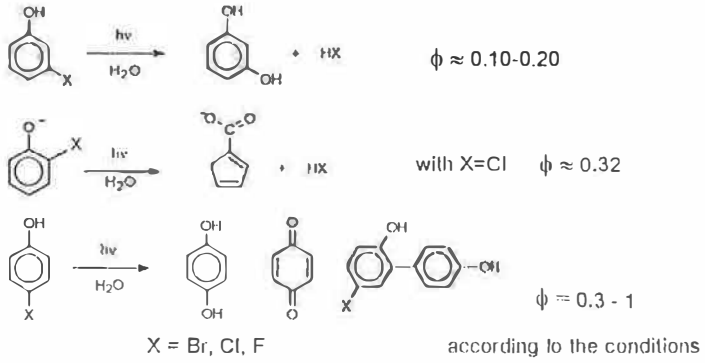

The reaction most commonly observed with haloaromatic derivatives is the heterolytic substitution of the halogen by OH. It is almost specific with 3-halophenols, chloro- and polychlorobenzenes, 3-chloroaniline, chlorophenylureas and chlorophenylcarbamates. It involves a molecule of water and the release of halogenated acid. For this reason it was called « photohydrolysis ». The specificity of the reaction is unconsistent with a radical scission of C-halogen bond, and on the other hand the fact that the quantum yield is not significantly different with Br, Cl and F is consistent with a heterolytic mechanism. The quantum yield is generally lower for polyhalogenated derivatives than with monohalogenated compounds.
With 3,4-dichlorophenol the main reaction is the *meta*photohydrolysis. The same behaviour was observed with diuron irradiated at $\lambda \leq 310$ nm, but *para* hydroxylated derivative was the main product obtained at longer wavelengths (3).

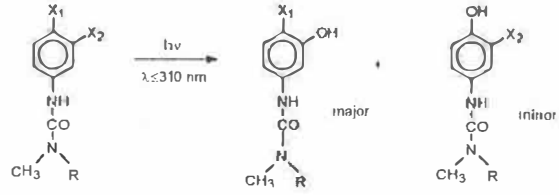

Diuron : $X_1 = X_2 = Cl$, $R = CH_3$

Linuron ($X_1 = X_2 = Cl$, $R = OCH_3$) and chlorbromuron ($X_1 = Br$, $X_2 = Cl$, $R = OCH_3$) have a more complex behaviour : photohydrolysis competes with elimination of the methoxy group and reduction (elimination of Br).
Photocontraction of the ring leading to cyclopentadiene carboxylic acid is a specific reaction of the anionic form of 2-halophenols, but it was also observed with nitrophenols. It was proved by laser flash photolysis that the reaction involves the initial formation of a cetene (4).

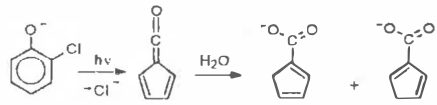

The phototransformation of 4-halophenols is more complex. It was elucidated only recently by means of laser flash photolysis (5). It involves the initial formation of a carbene which leads to various reactions according to the conditions.

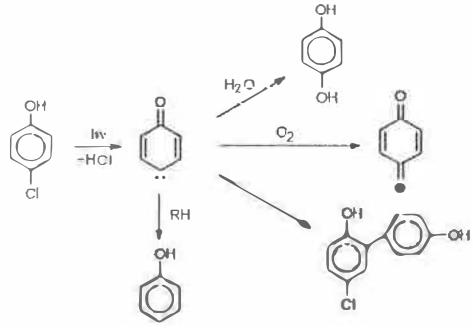

These phototransformations of haloaromatic derivatives are typical reactions of pure aqueous solutions. When the solutions contain a few percent of alcohol or surfactant commonly used to increase the solubility, the major reaction pathway is the substitution of the halogen by H.
Some herbicides such as diuron were also irradiated in the absence of water, dispersed on silica or clay used as a model of dry soil. In these conditions reactivity can be completely different. With diuron given as an example, the main phototransformation is the oxidation or the elimination of a methyl group.

2. Indirect phototransformation.

When a pollutant does not absorb sunlight, the phototransformation can be induced through various ways such as photosensitization, photocatalysis, reactions induced by excitation of H_2O_2, O_3, NO_3^-, NO_2^-, Fe^{III}, humic substances, etc... Photocatalysis, excitation of O_3 or H_2O_2 are quite efficient techniques for the elimination of organic pollutants. They play a minor role in environmental conditions and they are not the purpose of the present work.

2.1 Reactions induced by nitrate and nitrite ions.
Nitrate ions absorb near 300 nm with a low absorption coefficient (about 7.2 $mol.l^{-1}.cm^{-1}$) but they are often present in natural waters (10-30 $\mu mol.l^{-1}$ in sea water) and they are a significant source of hydroxyl radicals in surface waters. Actually two processes compete :

$$NO_3^- \xrightarrow{h\nu} NO_2^- + O(^3P)$$
$$NO_3^- \rightarrow NO_2^{\bullet} + O^{\bullet -}$$
$$O^{\bullet -} + H^+ \rightarrow {}^{\bullet}OH$$

In sunlight range the quantum yield of the first process ($\approx 1.1 \times 10^{-3}$) is about one tenth of the quantum yield of the second one. Moreover hydroxyl radicals are more efficient oxidants than atomic oxygen and they accounts for induced oxidations.
Nitrogen dioxide disproportionates into nitrate and nitrite ions. Most often the concentration of the latter is very low but they absorb a larger proportion of sunlight than nitrate ions and their excitation leads to the formation of hydroxyl radical with more efficiency.

$$NO_2^- \xrightarrow{h\nu} NO^{\bullet} + {}^{\bullet}OH$$

Thus nitrate and nitrite ions contribute to the photooxidation of organic substances present in water (6,7). But in some cases the formation of nitrogen oxides can induce nitrations or nitrosation. Fortunately these reactions were only observed in laboratory conditions and probably they play a minor role in environmental dilute conditions.

2.2. Reactions induced by $Fe^{(III)}$.
Iron (III) is present in the aquatic compartment and in sediments at relatively high concentration. Two main reactions involving iron (III) are able to induce the degradation of pollutants :
- a complex between iron (III) and the pollutant is formed that causes the onset of an absorption up to the visible domain. An intramolecular photoredox process is usually observed leading to iron (II) and to a radical arising from the pollutant.

$$R{-}COO\ Fe(III) \xrightarrow{h\nu} Fe(II) + RCOO^{\bullet} \dashrightarrow \boxed{\text{degradation}}$$

This process is particularly efficient with complexing agents such as ethylene diaminetetraacetic acid (EDTA), nitrilotriacetic acid (NTA) or ethylene diaminetetramethylene phosphonic acid (EDTMP) (8).

- there is no interaction between iron (III) and the pollutant. Aquocomplexes of iron (III) absorb solar light and undergo a photoredox process leading to iron (II) and $^{\bullet}OH$ radicals which are known to be very efficient oxidizing agents :

$$Fe(OH)^{2+} \xrightarrow{h\nu} Fe^{2+} + {}^{\bullet}OH$$

$^{\bullet}OH$ initiates the degradation of the pollutant (9).

2.3 Reactions induced by humic substances

Humic substances (HS) are naturally-occuring macromolecules present in soils and in the aquatic environment. They absorb solar-light and play a role in the photochemical processes occuring in surface waters.The nature of the reactive species produced upon excitation of HS depends on the wavelength of irradiation.

At short wavelength (254 nm) solvated electrons are formed. In the presence of oxygen they are converted into the highly reactive hydroxyl radicals. As a consequence, depending on the experimental conditions, reduction or oxidation reactions can be observed. When CH_2Cl_2 is irradiated at 254 nm in the presence of HS, Cl^- is released showing that CH_2Cl_2 is reduced. On the other hand oxidation of fenuron into hydroxylated compounds is observed in oxygenated medium.

Excitation of humic substances at wavelengths longer than 300 nm yields singlet oxygen, oxidant triplet states, $HO_2^{\bullet}/O_2^{\bullet-}$ and hydroxyl radicals in acidic medium. These species are capable of oxidizing a great variety of organic pollutants. When fenuron is irradiated at 365 nm in the presence of HS, its degradation is observed again. The photoproducts are not the same as those produced at 254 nm.

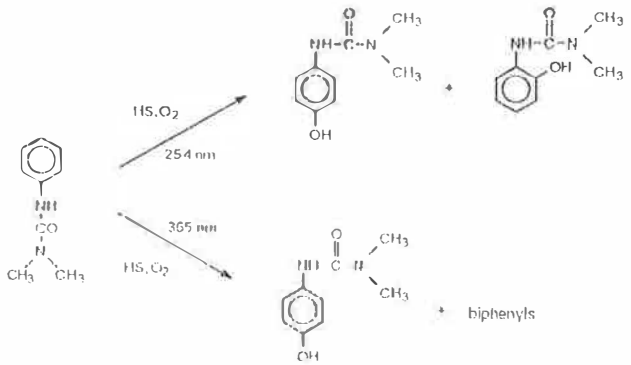

References

(1) P. Boule, C. Guyon and J. Lemaire, Chemosphere 1982, **11**, 1179.
(2) K. David-Oudjehani and P. Boule, New J. Chem. 1995, **19**, 199.
(3) J. Jirkovský, V. Faure and P. Boule, Pestic. Sci. *in press*.
(4) C. Richard and G. Grabner, publication submitted.
(5) G. Grabner, C. Richard and G. Köhler, J. Am. Chem. Soc. 1994, **116**, 11476.
(6) D. Kotzias, H. Parlar and F. Korte, Naturwissenschaften 1982, **69**, 444.
(7) R.G. Zepp, J. Hoigné and H. Bader, Environ. Sci. Technol. 1987, **21**, 443.
(8) S. Andrianirinaharivelo, G. Mailhot and M. Bolte, Solar Energy Materials and Solar Cells 1995, **38**, 459.
(9) P. Mazellier, J. Jirkovský and M. Bolte, Pesticide Science 1997, *in press*.
(10) J.P. Aguer, C. Richard and F. Andreux, J. Photochem. Photobiol. A, *in press*.

A STUDY OF ISOPROTURON PHOTODEGRADATION KINETICS

A. BOUDINA, A. BAALIOUAMER*, B-Y MEKLATI & M. MANSOUR**

*Laboratoire d'Analyse Organique Fonctionnelle, Institut de Chimie, USTHB-CRAPC, BP 248 Alger RP, 16004, Algérie.

**GSF-Institut für Okologische Chemie Neuherberg, Postfach 1129 D-85758 Oberchleissheim, Germany.

The great difference between the persistence of the herbicide isoproturon (3-(4-isopropylphenyl)-1,1-dimethylurea) under field conditions in temperate and tropical climates shows the possible role of light as a contributory factor in degradation.

The aim of this study reports a photodegradation kinetics of isoproturon in water, water + humic acid and water + soil sediment, under sunlight irradiation condition

UV light (λ>290 nm). High performance liquid chromatography with diode array detector is used.

The results showed that the presence of soil sediment accelerate the degradation speed GC/MS and MS/MS were investigated to caracterize some photoproducts.

Introduction:

Isoproturon is a phenyl urea herbicide widely used for pre - and post-emergence control of annual grasses and broad-leaved weeds in winter cereals [1].

Because of its widespread use and its properties of moderate persistance and relatively low adsorption , isoproturon has become an occasional water contaminant [2] .

Recognition of possible non - biological, chemical or photochemical transformation routes, provides a better understanding of pesticide behaviour and possible ways of protecting the environment [3] .

The aim of this work is to compare the photostability in water, water + humic acid and water + soil sediment under UV light irradiation ($\lambda \geq 290$nm) and to identify some photoproducts.

Experimental:

-Reagents :

Isoproturon (99,9 %) was obtained from Reidel-de Haen (Germany) , humic acid Mr 600-1000 from Fluka, soil sediment : (probenstelle-hamburg) Germany : Acetonitrile , Dichloromethan were used as analytical grade solvents

-Photodegradation experiments:

The isoproturon solution to be irradiated was prepared at a concentration of 65 mg.litre^{-1} in distilled water .

Photolyse experiments were conducted with philips lamps (125w) and pyrex filter ($\lambda \geq 290$nm).

-The concentration of isoproturon after : (0, 24, 48, 72, 96 and 120 hours) of irradiation is determined by HPLC (HP series 1090) using a 250mm x 4.6 i.d C_{18} octadecyl column (5μ). The mobile phase was a mixture of water and acetonitrile (50/50 v/v), and the detection was realised at 245nm with diode array detector.

-GC/MS spectra of isoproturon extracted with CH_2Cl_2 after 24 & 48 hours of irradiation were obtained with a HP 5992 A chromatographe/mass spectrometer at 70ev using electron

impact ionization equipped with DB5 60mx0.25mm. GC conditions were: initial oven temperature = 80°c, rate 10°c/min, final temperature 180°C/min (20min), carrier gas helium.

- MS/MS analysis were conducted by API 300 LC/MS/MS system in conventionel positive ion chemical ionization.

Results and discussion:

- Photostability study of isoproturon: In order to study a kinetic of isoproturon in distilled water (DW), water + humic acid (WHA) and water + soil sediment (WSD), the photodegradation of isoproturon has been reported to be faster in (WSD) and (WHA) as compared to distilled water. In figure 1 it can be observed that the half-life value demonstrate that photodegradation of isoproturon in WHA and WSD (24 h) is about three times faster than in distilled water (72 h).

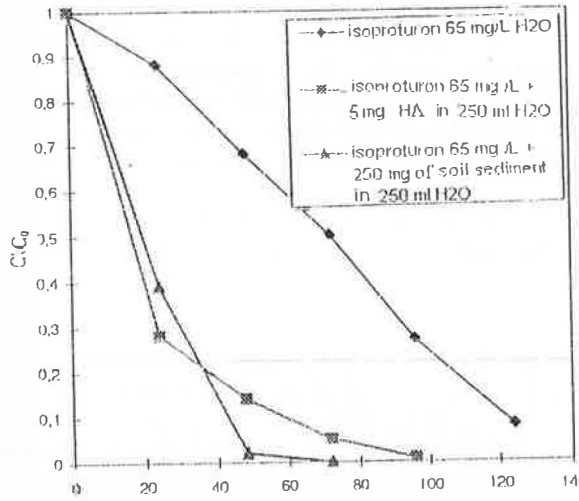

Fig.1 :Photodegradation of isoproturon in water under different conditions with λ≥290 nm.

-GC/MS spectra data: GC/MS analysis of isoproturon in (DW) after 24 and 48 hours of irradiation showed two different base peaks at m/z 135 and 148 , corresponding respectively to para isopropyl phenyl urea and para isopropyl, N,N-dimethylaniline (fig. 2) .

-MS/MS analysis of isoproturon in (DW) after 48 hours of UV light irradiation (λ≥290nm) showed different photoproducts at molecular weight: 135, 149, 163, 178 (fig. 3).

After the results obtained by GC/MS & MS/MS, a photodegradation pathway of isoproturon in distilled water under UV light is proposed (fig. 4).

Fig.2: GC/MS spectra of isoproturon in distilled water after 48 h of irradiation

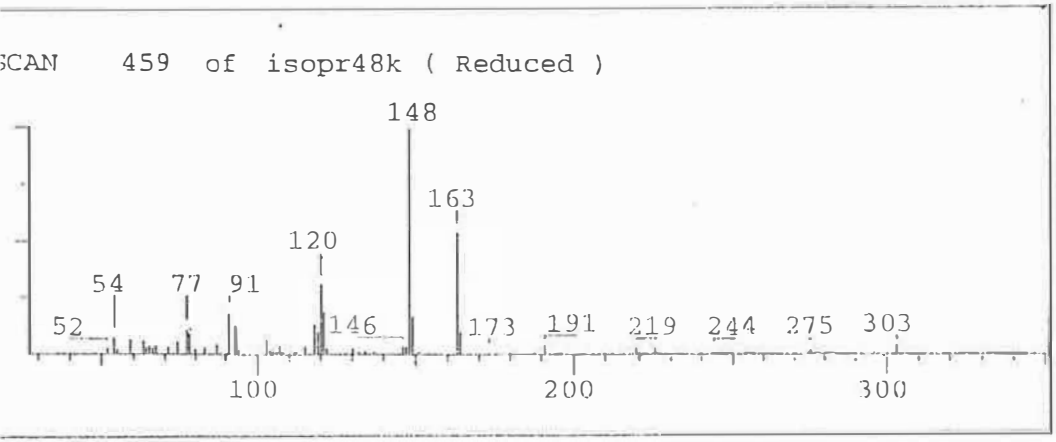

Fig.3: MS/MS total ion current of isoproturon in distilled water after 48h of irradiation

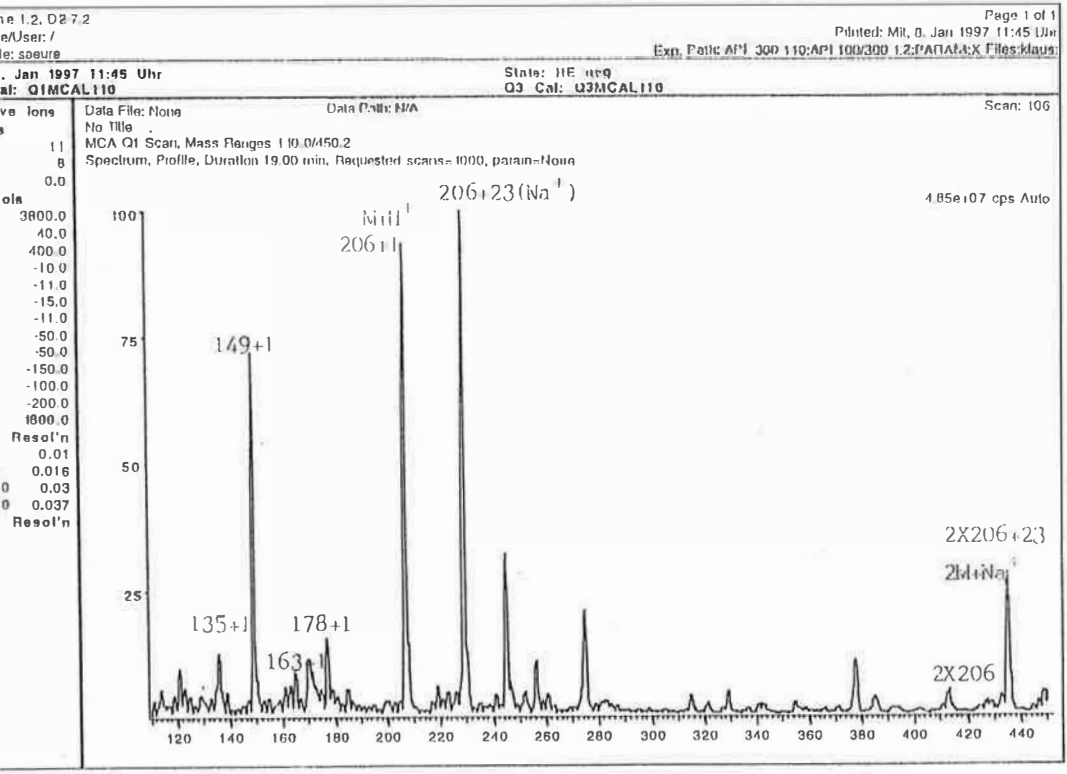

Fig.4

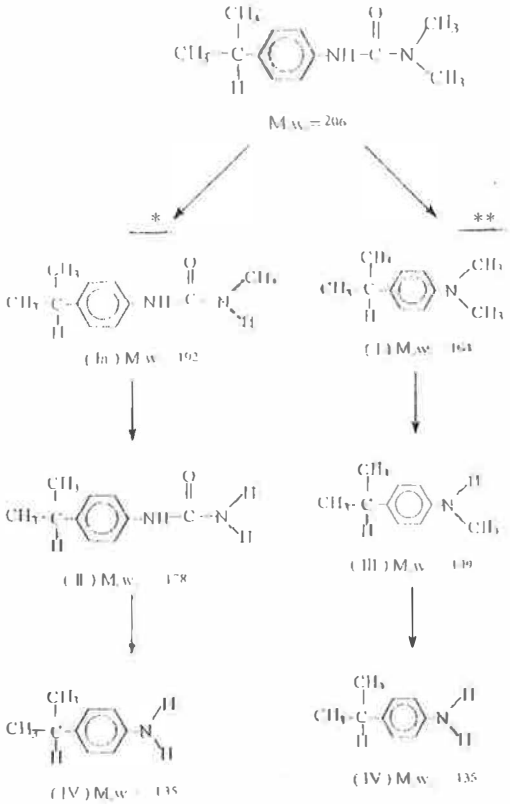

*Ref . 4
**Our work.

References:

(1) Tomlin, C., The Pesticide Manual, 10 th Edition . BCPC, Farnham, Surrey, UK, (1994)
(2) Lucia Cox, A. Walker & S.J. Welch: Pest. Sci., 48 , 253-260 (1996).
(3) E. Romero, P. Schmitt & M. Mansour: Pest. Sci., 41 , 21-26 (1994)
(4) G. Kulshrestha & S. K. Mukerjee: Pest. Sci., 17 , 489-494 (1986)

ADSORPTION OF SOME ORGANOPHOSPHORIC PESTICIDES BY ORGANO-INORGANO-PILLARED BENTONITE

O.BOURAS, H.KHALAF, S.BENAÏ et D. FERRAH
Department of chemical engineering, University of Blida, P.O. Box 270, 09000 Blida-Algeria

ABSTRACT

Owing to the increasing use of pesticides in agriculture the possibility of contamination of both surface and ground waters by these compounds is also increased.

In fact, the clay minerals are the most active soil components towards the organic molecules. Thus, the fate and the movements pesticides in soil depends in large part of their adsorption on clay minerals.

In this study, the adsorption from aqueous solution of organophosphoric pesticides, as malathion, méthylparathion and Fénitrothion, on surfactant modified Fe-pillared bentonites was investigated.

It is well known that the pillared clays (PILC) exhibit interesting properties as adsorbent. Furthermore, the introduction of organic cations into interlamellar space offers the possibility to convert the hydrophilic properties of the surface into organophilic ones.

Mixed organo-inorgano clays were prepared by exchanging a pillaring solution of iron with Na-montmorillonite. Then, the obtained products were treated with cation surfactant solutions (CTAB).

Adsorption test were carried out onto these new class adsorbents. The influence of CTAB/solid on adsorption uptake was investigated between 1 and 10 mmol/g solid. Products prepared with 5 mmol/g CTAB/g showed a higher adsorption capacity.

1. INTRODUCTION

The contamination of rivers and ground water by organic chemicals, applied to soils as pesticides or dispersed in industrial waste, as phenols or PCB, has promoted numerous investigation in various scientific fields (chemistry, agronomy, ...etc.).

One recent study published by « Association Française pour l'Etude des Eaux) shows that a 30% of accidental pollution in the world concern the pesticides and particulary the herbicides.

organophosphoric compounds as malathion and méthylparathion represent a group of pesticides used for the destruction of living organisms considered as hazardous for agriculture and industry.

Introducing of these pesticides into rivers and ground water accidentally or volontary may cause a considerable damage for environment. This phenomenon turn in fixation of these pollutants by sediments of lacks and rivers and might be reached a concentration greater than that is found in water.

Among the methods used for treatment of water containing organic pollutants as organophosphoric pesticides, one can quote a chemical oxidation, floculation, decantation and particulary adsorption onto microporous solids such as activated carbon or clay based adsorbents. However, it is known that a fraction of carbon is lost with each regeneration cycle. This is a major disadvantage the current research efforts have been made to design new based clay adsorbents.

In this perspective, a new bentonite based adsorbents designed s Fe-pillared bentonite with surface modified by coadsorption of cationic surfactant cetyltrimethyl ammonium bromide which yield the surface hydrophobic and organophilic.

These adsorbents were characterized by XRD, BET and IR spectroscopy. The conditions of preparation were optimized in our previous works [4,5,6].

In this study our objective was to investigate the adsorption affinity of bentonite based adsorbents from a deposite in western algeria (Maghnia) toward two organophosphoric pesticides (malathion and méthylparathion).

2. EXPERIMENTAL

2.1. PURIFICATION OF BENTONITE

The bentonite of Maghnia supplied by ENOF was purified by following procedure:

- sodium homoionisation by treatment with NaCl
- Removal of impurities by sedimentation
- Removal of excess NaCl by dialyse

2.2. PREPARATION OF PILLARING SOLUTIONS

a/ The polycations hydroxy-Fe solution designed as PCHF was prepared according to following conditions optimized in our previous work [4].

- OH/Fe molar ratio = 2
- Fe concentration of 0.2M
- Aging period of 10 days

b/ Surfactant solution of CTAB of 0.2% W/W was prepared by dissolution an appropriate amount of CTAB 99% purity in distilled water.

2.3. INTERCALATION OF BENTONITE

2.3.1. INORGANO CLAY COMPLEXES type Fe(OH)-MONT.

These complexes were prepared by dropwise addition of 0.2M solution of PCHF to a bentonite suspension of 0.1% W/W with vigorous stirring during 30mn.

A Fe/Mont ratio of 5 mmol Fe/g mont stirring was continued for more than two hours. After which the solids were separated by filtration and dried at 40°C for minimum of three days.

2.3.2. ORGANO-INORGANO COMPLEXES type Fe(OH)-CTAB-MONT

An appropriate of Fe(OH) mont, was redispersed in distillated water for preparation of a 0.1% (W/W) suspension. After which a solution of 0.2% was slowly added with vigorous stirring. stirring was continued for 30 mn. more solid were separated by filtration and washed with distillated water until disappearence of foaming . These solids were dried at 40°C for three days.

2.3.3. POLLUTANTS SOLUTION

Aqueous solution of malathion and methylparathion were prepared by dissolution of appropriate amount of each polltant in distillated water. The initial concentration of pollutant solution was 40µmol.dm-3.

2.3.4. METHOD OF ANALYSIS

The concentration of both pesticides was determined by spectrophotometric in UV-VIS. using a SPECORD M40 spectrophotometer.

Maximum wavelength was obtained by scanning the solution between 200 and 800nm.

Table 1: characteristic of two organophosphoric pollutants.

Product	λ (nm)	Solubility in water (mg/l)
Malathion	277	145
Methylparathion	275	60

3. RESULTS AND DISCUSSION

Complexes were characterized by XRD, BET surface area, IR spectroscopy (not shown) and CEC prior and after the modification of the surface by cationic surfactant. Results obtained are summarized in table 2.

Table 2: Results of XRD, textural and CEC measurements.

PRODUCT	XRD d001 (nm)	BET (m2/g)	CEC meq/100 g
Untreated bentonite	14	54	50
Na-montmorillonite	14	91	96
Fe(OH)-montmorillonite	26	270	6
CTAB-Fe(OH)-montmorillonite	21	-	-

3.1 ADSORPTION MEASUREMENTS

In order to check the adsorption capacity of these adsorbents, it is important to determin their pH dependance. Besides, it might be of interest to compar the capacity of such microporous materials with activated carbon which represent the most used sorbent at present.

3.1.1. ADSORPTION ISOTHERMS OF MALATHION

Figure 1 shows the adsorption isotherm of malathion obtained with following conditions:

-CTAB/Fe(OH)-mont. = 5mmol/g

- contacting time = 24 hours

From the results depicted in figure 1, it can be easily seen that the greater adsorption uptake took place in acidic medium (pH=2) and in all cases it was greater than that onto activated carbon.

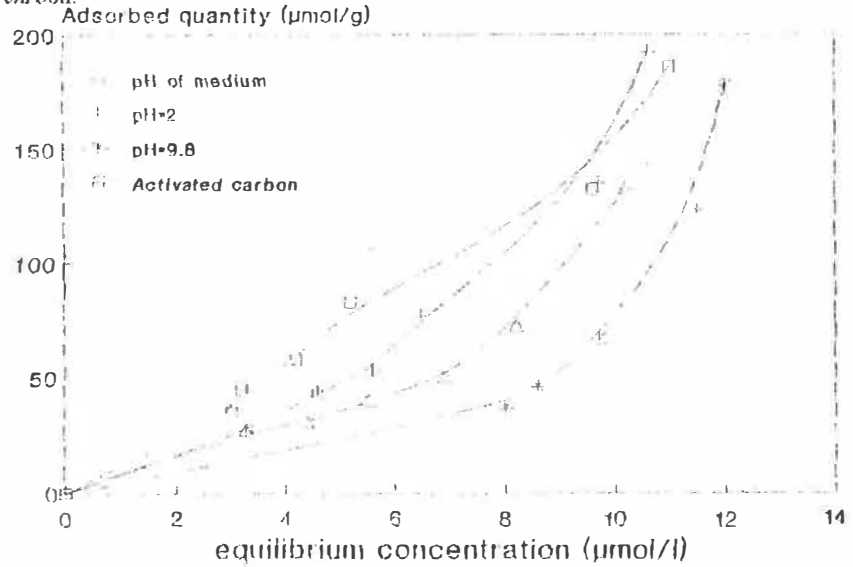

Fig. 1 : Adsorption isotherms of malathion

3.1.2. ADSORPTION ISOTHERMS OF METHYL PARATHION

Adsorption isotherms of methyl parathion were showed in figure 2. It was determined at pH of about 7. CTAB-Fe(OH)-montmorillonite complexes show a good affinity for this toxic organic pollutant.

The adsorption uptake was about 100 µmol/g for an equilibrium concentration of about 5 µmol.dm-3. The adsorption capacity of these complexes was found superior to that obtained by activated carbon.

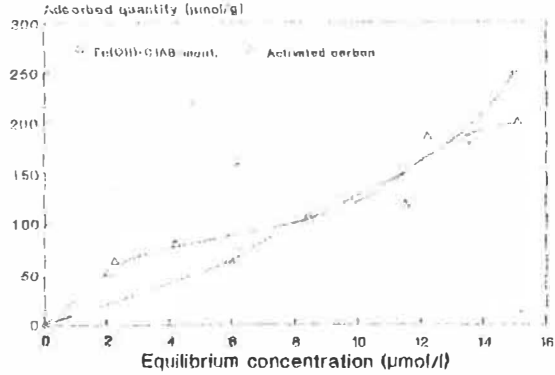

Fig.2: Adsorption isotherms of methyl parathion

4. CONCLUSION

The study of adsorption of organophosphoric pesticides (Malathion and méthylparathion) in batch type experiments onto inorgano-organo clay based complexes schows an important adsorption uptake of these toxic micropollutants even at low concentration.

The greater adsorption uptake as compared with that obtained with activated carbon and the low price point to the possible reuse of these new based adsorbent suggest their application as valuable materials for removal some organic pollutants such the pesticides from aqueous phase.

REFERENCES

[1] Mortland, M.M. (1975), Interaction between clays and organic pollutants. In proc. Inter. Clay Conf., Mexico City, S.W. Bailey Ed., Applied Publishing, Wilmett, Illinois, 469-475.

[2] F.Andreux, M. Shiavon, C. Munier-Lamy, M.Mansour and I. Scheunert, (1995), Factors affecting the movements, reactions and biotransformations of xenobiotics in environmental impact of soil component interactions, Vol.I, Lewis publishers.

[3] Michot J.L. and Pinnavaia, (1991), Adsorption of chlorinated phenols from aqueous solution by surfactant modified pillared clays, Clays and Clay Minerals, 39, 634-641.